

Aus dem Bereich Molekular Biophysik

Theoretische Medizin und Biowissenschaften der Medizinischen Fakultät

der Universität des Saarlandes, Homburg/Saar

A novel Splice Variant of Stim1 – Stim1B differentially regulates Store Operated Calcium Entry

Dissertation zur Erlangung des Grades eines Doktors der Naturwissenschaften der
Medizinischen Fakultät

der UNIVERSITÄT DES SAARLANDES

2023

vorgelegt von: Girish Ramesh

geb. am: 19.06.1989 in Chennai, India.

Supervisor: Univ Prof. Dr. Barbara Niemeyer

Tag der Promotion: 22.04.2024

Dekan: Prof. Dr. med. Michael D. Menger

Berichterstatter: Prof. Dr. rer. nat. Barbara Niemeyer-Hoth

Prof. Dr. med. Frank Schmitz

Table of Contents

Summary	1
Zusammenfassung	3
1. Introduction.....	5
1.1 Calcium signaling and calcium homeostasis:	5
1.2 Store Operated Ca ²⁺ Influx (SOCE):.....	8
1.3 Orai proteins:	11
1.4 STIM proteins:.....	12
1.5 STIM splicing and their variants:.....	15
1.6 Pathophysiology of Stim and Orai:	17
1.7 Role of Stim and Orai in Neuronal SOCE:	19
1.8 Aim & Objectives of the Ph.D Thesis	23
2. Materials.....	25
2.1 Chemicals & Reagents	25
2.2 Commercial Kits	26
2.3 Antibodies.....	27
2.3.1 Primary antibodies	27
2.3.2 Secondary Antibodies	27
2.4 Bacterial strain	28
2.5 Protein Markers / Standards.....	28
2.6 Lab Equipments	28
2.6.1 Lab Equipments for Patch clamp Electrophysiology	28
2.6.2 Lab Equipments for TIRF Microscopy Imaging	28
2.6.3 Other Basic Equipments used in this study	28
2.7 Solutions / Buffer Compositions	29
2.8 SDS Page / Western blot buffer.....	30
2.9 Enzymes	32
2.9.1 Modified enzymes.....	32
2.9.2 Restriction enzymes	32

2.10 Primers for cloning & qRT-PCR primers	33
2.11 Vectors & Constructs.....	34
2.12 Cell culture	35
2.12.1 Cell culture medium.....	35
2.12.2 Cell lines	35
2.12.3 Transfection reagents & Kits.....	36
2.13 Experimental Model / Strain	36
2.14 Softwares	36
3. Methods	37
3.1 Generation of genetically modified recombinant DNA.....	37
3.1.1 Polymerase chain reaction (PCR)	37
3.1.2 RNA isolation & cDNA synthesis.....	38
3.1.3 Analytical PCR	38
3.1.4 Site-directed mutagenesis	38
3.2 Cloning & restriction digestion.....	39
3.2.1 Dephosphorylation of vector DNA	40
3.2.2 Gel electrophoresis:	40
3.2.3 Agarose / GTQ gel	41
3.2.4 Gel extraction.....	41
3.2.5 Phosphorylation & Ligation.....	41
3.3 Bacterial transformation.....	42
3.3.1 Colony PCR.....	42
3.3.3 Sequencing.....	43
3.3.4 Preparation of plasmid constructs – Minis & Maxis	43
3.4 Cell culture	44
3.4.1 Cell transfection.....	44
3.4.2 Electroporation	45
3.4.3 Lipofection.....	45
3.5 Protein biochemistry	45
3.5.1 Cell lysis	45
3.5.2 Determination of protein concentration (BCA Assay).....	46

3.5.3 SDS PAGE Electrophoresis & Western blotting	46
3.5.4 Western blotting transfer and detection:.....	47
3.5.5 Immunoprecipitation.....	48
3.5.6 Coomassie staining	49
3.5.7 Silver staining	49
3.6 Electrophysiology.....	49
3.7 Recordings of autaptic synaptic currents.....	50
3.8 Behavioural Tests.....	50
3.8.1 Elevated plus maze	50
3.8.2 Open field test.....	51
3.8.3 Erasmus ladder.....	51
3.9 Immunostaining	53
3.11 Data Analysis & Statistics.....	54
4. Results.....	55
4.1 Expression analysis of new splice variant of Stim1 - Stim1B.....	55
4.1.1 Detection of a new mammalian-specific splice variant of Stim1 - Stim1B.....	55
4.1.1 Stim1 B forms clusters upon store depletion and strongly co-localizes with Stim1	59
4.2 Functional Characterization of Stim1B.....	60
4.2.1 STIM1B differentially activates ORAI channels	60
4.2.2 Murine Stim1B also differentially activates Orai channels	64
4.2.3 Stim1B showed significantly reduced Orai1 CRAC and does not exhibit SCDI under low buffering conditions.....	66
4.2.4 STIM1B also significantly reduced Orai1 I _{CRAC} and reduced SCDI, but not as strong as murine Stim1B.....	67
4.2.5 Fast Ca ²⁺ dependent inactivation (FCDI) is not altered by Stim1B	68
4.3 Investigation of Molecular mechanism regulating Stim1B's phenotype	69
4.3.1 Reduced SCDI function mediated by STIM1B is not altered by SARAF	69
4.3.2 Mutation of Negatively Charged Residues Modifies CDI, but the STIM1B Phenotype Remains Unchanged.....	71
4.3.3 Cloning of genetically modified constructs of Stim1B	72
4.3.4 Stim1 phenotype is still retained despite the missing C-terminal domain of Stim1.....	74
4.3.5 Insertion of Domain B determines the Stim1B phenotype.....	76
4.3.6 Cloning of genetically modified constructs of Stim1B	78

4.3.7 A specific motif in domain B determines the STIM1B phenotype	79
4.4. Function of Stim1B in regulating synaptic plasticity and maintaining neuronal calcium homeostasis.....	80
4.4.1 Neither quantal signaling nor basal synaptic signaling is affected by Stim1B expression.....	80
4.4.2 Stim1B but not Stim1 turns synaptic depression into short-term enhancement at high-frequency stimulation (HFS).....	82
4.4.3 Stim1B's STE phenotype requires a rise in presynaptic Ca ²⁺ levels.....	85
4.4.4 Presynaptic localization corroborates the synaptic physiology of Stim1B	86
4.5 Validation of Splice-deficient mice (10A mice)	89
4.6 The absence of Stim1B suggests reduced levels of Synapsin.....	89
4.7 Behavioral studies.....	91
4.7.1 Assessment of motor performance and motor learning in mice lacking Stim1B	91
4.7.2 Both Motor performance and Adaptive cerebellar learning were impaired in splice-deficient mice	91
4.7.3 Assessment of anxiety behavior in mice lacking Stim1B.....	100
4.7.4 Anxiety-related behavior was unaffected in splice-deficient mice	100
4.7.4.1 Elevated plus maze	100
4.7.4.2 Open field test.....	101
4.8 Proteomics	102
4.8.1 To identify potential interacting partners of Stim1B – Mass spectrometry approach	102
5. Discussion	106
5.1 Splice variants of Stim1	106
5.1.1 Stim1B is a new Stim1 splice variant.....	106
5.2 STIM1B is a differential activator of SOCE with distinct characteristics	107
5.2 Calcium-dependent inactivation (CDI) is significantly altered by Stim1B	111
5.3 Insertion of Domain B and not the missing C terminal determines the Stim1B phenotype.....	114
5.4 Domain B-specific motif KANR is responsible for Stim1B's phenotype	115
5.5 Presynaptic localization of Stim1B, but not Stim1 reinforced the synaptic physiology of Stim1B.....	116
5.6 Stim1B expression might promote the facilitation through enhanced Synapsin levels	122
5.7 Stim1B's absence leads to an impairment in motor performance and adaptive cerebellar learning.....	122
5.8 Identification of interacting partner of new splice variant - Stim1B	124

5.9 Outlook:.....	125
References.....	126
Publications & Conferences	151
Abbreviations	152
Appendix	154
Acknowledgments	157

Summary

Calcium (Ca^{2+}) acts as a second messenger orchestrating various intracellular processes. Store-operated calcium entry (SOCE) is known for its role in regulating Ca^{2+} homeostasis, gene expression, metabolism, cytokine release, and proliferation in immune cells. This mechanism depends on the calcium concentration in the Endoplasmic Reticulum (ER) and the Stim protein family residing in the ER acts as a sensor promptly responding to ER Ca^{2+} store depletion and facilitates the entry of calcium from extracellular through gating of plasma membrane residing Orai family of proteins. Recent advances have shown that SOCE not only plays a mediator role in immune cells but also in electrically excitable cells such as neurons and skeletal muscle cells. Yet, the intricate mechanisms governing how SOCE adapts to diverse cellular needs, cellular architectural complexities, and metabolic demands remain less clear. Alternative splicing of the STIM family encompassing Stim1 & Stim2 yielded several functionally distinct variants.

In this work, a new splice variant of Stim1- Stim1B is identified and characterized. Insertion of Exon B between exon 12 and 14 led to a frameshift and terminated early resulting in a significantly short protein variant lacking 170 amino acids, but incorporates an additional 26 residues encoded by exon B and those translated due to the frameshift. RNA and protein expression studies showed that Stim1B is exclusively expressed in the brain with expression levels surpassing conventional Stim1 in the cerebellum and varying levels of expression in other regions of the brain. Functionally, patch clamp electrophysiology experiments with heterologous overexpression of Stim1B were able to demonstrate that Stim1B is able to activate both murine and human ORAI homologs, albeit with reduced kinetics, I_{CRAC} as well as reduced inactivation and that Domain B, but not the missing C terminal residues of Stim1 or the additional translated residues encoded by Stim1B was responsible for it. Additional patch clamp experiments with mutants identify a specific motif KANR within domain B as the key determinant behind Stim1B's unique properties. Immunoprecipitation with self-made antibody against Stim1B indicated that Stim1B exhibited a stronger interaction with Stim2 than Stim1. Immunohistological investigations in wild-type neurons provide insight into Stim1B's distinct localization. Unlike Stim1, Stim1B is targeted to presynaptic terminals. Functionally, neuronal patch clamp experiments underscore the pivotal role of domain B in modulating synaptic

transmission where Stim1B was able to convert classic synaptic depression into short-term synaptic enhancement (STE) at high-frequency stimulation (HFS) which is dependent on Ca²⁺ and Orai-dependent Ca²⁺ release. Lastly, behavioral analysis involving mice lacking Stim1B strongly indicated an impairment in motor performance and adaptive cerebellar learning.

Overall, the findings from this work broaden our understanding of the mechanism of Ca²⁺ regulation, highlighting the relevance of STIM1 splicing on neuronal calcium homeostasis and synaptic plasticity, thereby shaping cellular adaptations in response to varying metabolic demands. Most importantly, the observed behavioral impairments in mice lacking Stim1B emphasize the physiological relevance of Stim1B in neurological processes.

Zusammenfassung

Calcium (Ca^{2+}) fungiert als zweiter Botenstoff und orchestriert verschiedene intrazelluläre Prozesse. Die Calciumeintragung über speicherabhängige Mechanismen (Store-operated calcium entry, SOCE) spielt eine wichtige Rolle bei der Regulation der Ca^{2+} -Homöostase, der Genexpression, dem Stoffwechsel, der Freisetzung von Zytokinen und der Proliferation in Immunzellen. Dieser Mechanismus hängt von der Calciumkonzentration im endoplasmatischen Retikulum (ER) ab, und die Stim-Proteinfamilie im ER fungiert als Sensor, der rasch auf die Erschöpfung des ER- Ca^{2+} -Speichers reagiert und den Eintritt von Calcium aus dem extrazellulären Raum durch die Steuerung von Orai-Proteinen an der Plasmamembran ermöglicht. Neuere Fortschritte haben gezeigt, dass SOCE nicht nur in Immunzellen eine Rolle spielt, sondern auch in elektrisch erregbaren Zellen wie Neuronen und Skelettmuskelzellen. Dennoch bleiben die komplexen Mechanismen, die regeln, wie SOCE sich an verschiedene zelluläre Anforderungen, zelluläre architektonische Komplexitäten und metabolische Anforderungen anpasst, weniger klar.

Die alternative Spleißung der STIM-Familie, zu der Stim1 und Stim2 gehören, hat mehrere funktionell unterschiedliche Varianten hervorgebracht. In dieser Arbeit wurde eine neue Spleißvariante von Stim1, Stim1B, identifiziert und charakterisiert. Die Insertion von Exon B zwischen Exon 12 und 14 führte zu einer Rahmenverschiebung und einer vorzeitigen Beendigung, was zu einer erheblich verkürzten Proteinvariante führte, die 170 Aminosäuren fehlt, aber zusätzlich 26 Aminosäuren aus Exon B und aufgrund der Rahmenverschiebung übersetzte Aminosäuren enthält. RNA- und Proteinexpressionsstudien zeigten, dass Stim1B ausschließlich im Gehirn exprimiert wird, wobei die Expression in der Kleinhirnrinde die von herkömmlichem Stim1 übertrifft und in anderen Regionen des Gehirns variierende Expressionsniveaus aufweist.

Funktionell konnten Patch-Clamp-Elektrophysiologie-Experimente mit heterologer Überexpression von Stim1B zeigen, dass Stim1B in der Lage ist, sowohl murine als auch humane ORAI-Homologe zu aktivieren, wenn auch mit reduzierter Kinetik, I_{CRAC} und reduzierter Inaktivierung. Dabei war es das Domänen-B, und nicht die fehlenden C-terminale Aminosäuren von Stim1 oder die zusätzlich übersetzten Aminosäuren von Stim1B, das dafür

verantwortlich war. Zusätzliche Patch-Clamp-Experimente mit Mutanten identifizierten ein spezifisches Motiv, KANR innerhalb von Domäne B, als das entscheidende Merkmal hinter den einzigartigen Eigenschaften von Stim1B. Immunopräzipitationen mit einem selbst hergestellten Antikörper gegen Stim1B zeigten, dass Stim1B eine stärkere Wechselwirkung mit Stim2 aufwies als mit Stim1.

Immunohistologische Untersuchungen an Neuronen in Wildtyp-Mäusen gaben Aufschluss über die besondere Lokalisation von Stim1B. Im Gegensatz zu Stim1 wurde Stim1B an präsynaptischen Enden gezielt. Funktionell unterstrichen neuronale Patch-Clamp-Experimente die wichtige Rolle von Domäne B bei der Modulation der synaptischen Übertragung, wobei Stim1B klassische synaptische Depression in eine kurzfristige synaptische Verstärkung (STE) bei Hochfrequenzstimulation (HFS) umwandeln konnte, was von Ca^{2+} und Orai-abhängiger Ca^{2+} -Freisetzung abhängig war.

Schließlich deuteten Verhaltensanalysen an Mäusen, die Stim1B fehlte, stark auf Beeinträchtigungen in der motorischen Leistung und dem adaptiven Lernen im Kleinhirn hin. Insgesamt erweitern die Ergebnisse dieser Arbeit unser Verständnis des Mechanismus der Ca^{2+} -Regulation und betonen die Bedeutung des STIM1-Spleißens für die neuronale Calciumhomöostase und die synaptische Plastizität, wodurch zelluläre Anpassungen an unterschiedliche metabolische Anforderungen geformt werden. Am wichtigsten ist jedoch, dass die beobachteten Verhaltensstörungen bei Mäusen ohne Stim1B die physiologische Bedeutung von Stim1B für neurologische Prozesse unterstreichen.

1. Introduction

1.1 Calcium signaling and calcium homeostasis:

In all eukaryotic or multicellular organisms, a prime feature of the cell is to adapt to changing environments by transmitting signals and those signals are regulated by messengers. Calcium is a divalent cation, which acts as a universal & versatile second messenger responsible for various cellular processes beginning with the origin of new life (fertilization), gene transcription, muscle contraction or relaxation, mediating enzyme production/release, regulating metabolic pathways, and ultimately in the termination of life by programmed cell death (Clapham et al., 2007, Carafoli et al., 2001, Brini & Carafoli et al., 2009).

Diverse events governed by Ca^{2+} include conformational changes in protein structure based on the strength, effectiveness, and affinity of Ca^{2+} signals and it is achieved by establishing a steep Ca^{2+} gradient app. 20000-fold across the membrane between the extracellular and intracellular, with cytosolic Ca^{2+} lowered to submicromolar concentration (nM) and luminal Ca^{2+} in the range of micromolar to millimolar levels (Carafoli, 1987, Antebi et al., 1992, Clapham et al., 2007). The reason for lower levels of cytosolic Ca^{2+} could be due to the less binding affinity of Ca^{2+} to water molecules than other ions like Mg^{2+} and evolutionarily cells have managed to find ways to keep the low cytosolic Ca^{2+} levels by chelation, utilizing its binding capacity for signal transduction, compartmentalization and eliminate it. Several hundreds of proteins have been identified to perform this task with great specificity and affinity to maintain homeostasis.

These proteins can be categorized into two broad classes; those that are intrinsic to membranes that contains one or more transmembrane domains and has hydrophobic or hydrophilic or amphipathic properties, for eg. Receptors that mediate the Ca^{2+} mobilization from the extracellular space or from the ER into the cytosol and are termed Ca^{2+} buffers. Unlike intrinsic membrane proteins, proteins that are extrinsic to membrane do not contain hydrophobic transmembrane domains and are loosely bound. They can interact with the membranes through non-covalent interactions. These category of proteins apart from buffering Ca^{2+} , also signals the targeting protein and are termed as Ca^{2+} sensors (Brini & Carafoli 2009). Buffering of Ca^{2+} to nM range is mediated by transport mechanisms across membranes (plasma membrane and ER membranes among others). The classical plasma membrane Ca^{2+} extruding systems necessary to maintain low cytosolic concentrations and to restore these after sustained increases

by triggered Ca^{2+} influx is through Plasma Membrane Ca^{2+} ATPases (PMCA) (Guerini et al., 1999). PMCA can also be activated by Ca^{2+} - Calmodulin complexes, by limited proteolysis, or by acidic phospholipids and long-chain polyunsaturated fatty acids with each having nonidentical effects on Ca^{2+} regulation. The binding of Ca^{2+} - Calmodulin to PMCA is highly dependent on free Ca^{2+} concentration in cytoplasm while activation by phospholipids is Ca^{2+} independent (Enyedi et al., 1987, Scharff et al., 1983, Carafoli. E 1982). The other plasma membrane Ca^{2+} ejection system are $\text{Na}^+/\text{Ca}^{2+}$ exchangers (NCX) as well as $\text{Na}/\text{K}/\text{Ca}$ exchangers, which are mostly active in excitable cells complementing the action of ATPases and thereby transporting the bulk of ions with low affinity for Ca^{2+} . It exchanges 3Na^+ ions for 1 Ca^{2+} ion thereby establishing an electrochemical gradient across the membrane and also responding to transmembrane potential and maintaining the level of these ions outside the cell (Reviewed in Carafoli E et al., 2016). The third Ca^{2+} transport that regulates the Ca^{2+} ions in the cytosol are the $\text{Na}^+/\text{Ca}^{2+}/\text{K}^+$ exchangers (NCKX; SLC24A1-5) which transports one K^+ ion with one Ca^{2+} ion in exchange for 4 Na^+ ions which functions in feed-forward mechanism. The PMCAs and NCX/NCKX complement each other as the former is efficient in maintaining low internal Ca^{2+} over a long period of time while the latter does with a substantial influx that is necessary during the action potential in nerve cells (Clapham et al., 2007, Hilgemann et al., 2006).

Apart from the extrusion mechanism of transporting Ca^{2+} out of the cell, there are other pump systems that pump Ca^{2+} into the intercellular compartments which takes place at the expense of ATP hydrolysis (PMCA also needs ATP). It is termed as Sarcoplasm/Endoplasmic reticulum Ca^{2+} ATPase, a member of Ptype ATPase pump and first identified in skeletal muscle fraction in the year 1961-62 which pumps the released Ca^{2+} into the SR during muscle contraction (Ebashi F et al., 1962). Crystallographic structure studies of SERCA in skeletal muscle revealed that SERCA has a transmembrane domain comprising 10 alpha helices bound by 2 Ca^{2+} ions on either side (Reviewed in Brini M et al., 2009, Toyoshima et al., 2000). Although the endoplasmic reticulum is considered a major intracellular store, other organelles like the Golgi apparatus and Mitochondria also play a vital role in Ca^{2+} regulation (Berridge et al., 2002). The Golgi apparatus, apart from the SERCA pump, has the secretory pathway Ca^{2+} - ATPases (SPCAs) which pump Ca^{2+} & Mn^{2+} into the Golgi lumen (Reviewed in Missiaen L et al., 2007). Mutations in SERCA2 and SPCA1 protein which resulted in abnormal protein folding, thus no

longer transport ions are seen in Hailey-Hailey disease (HHD) (Fairclough et al., 2003, Reviewed in Dhitavat et al., 2004, & Missiaen L et al., 2007).

The molecular machinery of mitochondrial Ca^{2+} transport plays a crucial role in ATP production, shaping calcium transients and cell death. Mitochondrial Ca^{2+} buffering is mediated among other mechanisms by a 40kDa protein of the mitochondrial inner membrane, namely the mitochondrial calcium uniporter (MCU) which shapes the spatiotemporal patterns of cytosolic Ca^{2+} concentration (Rizzuto et al., 1998, De Stefani et al., 2011). Also, IP3R-mediated increases of Ca^{2+} by ER release into the cytosol can trigger mitochondrial calcium uptake. The Ca^{2+} signal transmission gets stronger between the ER and Mitochondria contact sites upon local transfer of Ca^{2+} from ER (Hajno' czky et al., 1994, Rizzuto et al., 1998).

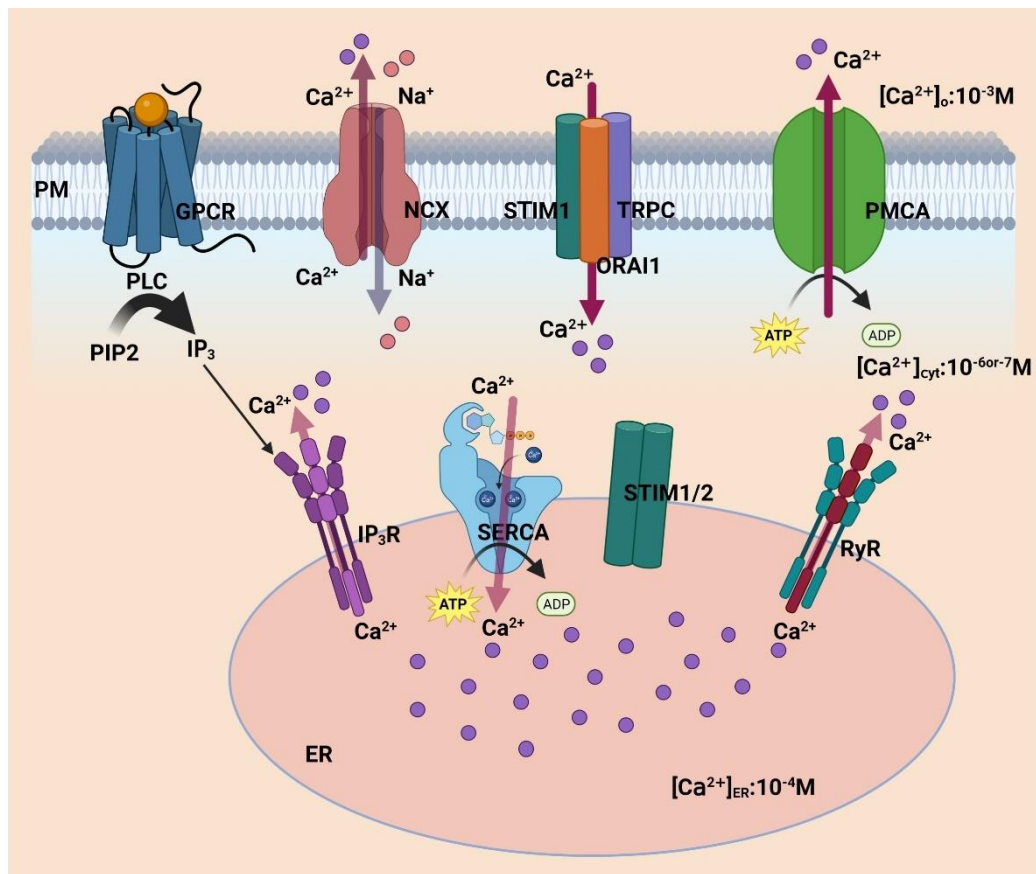


Figure 1 Intracellular Ca²⁺ Homeostasis: Ca²⁺ influx into the cell through Plasma Membrane (PM) channels (Store Operated Orai channels & voltage-gated calcium channels) and efflux of calcium through the plasma membrane (Ca²⁺-Mg²⁺)-ATPase (PMCA) and Na⁺/Ca²⁺ exchangers. Ca²⁺ release triggered by the GPCR signaling pathway and release of calcium from ER modulated by ER residents including inositol-1,4,5-trisphosphate receptor (IP₃R) and the ryanodine receptor. Ca²⁺ is transported to ER by sarco/endoplasmic reticulum Ca²⁺ ATPase (SERCA) and ER resident Stromal Interaction molecule (STIM) activate Store Operated Ca²⁺ entry via ORAI or TRPC interaction resided in the PM. (Modified from Mei et al., 2013).

Mitochondrial Ca^{2+} efflux is mediated by NCLX, a mitochondrial $\text{Na}^+/\text{Ca}^{2+}$ exchanger localized on the cristae which exchange Na^+/Li^+ ions for Ca^{2+} ions (Palty et al., 2010). In addition to these, endosomes, lysosomes, secretory granules, and melanosomes which are single membrane-bound compartments are also considered as Ca^{2+} storing organelles and thereby may function as release sites (Reviewed in Rizzuto et al., 2006, Clapham et al., 2007).

In excitable cells such as neurons, the electrical activity including action potentials or receptor-mediated depolarizations triggers the activation of voltage-gated- calcium channels (VGCCs) (L, P/Q, T type), and transmitter release triggers receptor-gated channels (ROCs) such as N-methyl-D-Aspartate receptor (NMDAR) that requires ligand gating and also results in substantial Ca^{2+} influx (Reviewed in Berridge M et al., 1998). In general, proteins modulated by Ca^{2+} , termed Calcium modulators or Ca^{2+} sensors, often possess EF-hand motifs that can bind to Ca^{2+} to decipher the Ca^{2+} signals directly or indirectly (i.e., by binding calmodulin) and that cells have evolved positively with new mechanisms to regulate calcium (Carafoli E et al., 2001, Clapham et al., 2007). The importance of Ca^{2+} signaling and its role in intracellular Ca^{2+} homeostasis is shown in Figure 1. Diffusion of Ca^{2+} from internal stores like ER is sensed by a few Ca^{2+} binding proteins and act together with membrane channels has led to the discovery of an entirely new mechanism of Ca^{2+} regulation, which is discussed in the next chapter.

1.2 Store Operated Ca^{2+} Influx (SOCE):

In the year 1986, James Putney and his colleagues proposed a new mechanism of Ca^{2+} influx in non-excitabile cells when they observed a sustained Ca^{2+} entry by imaging experiments across the plasma membrane following a receptor-mediated Ca^{2+} release from intracellular stores and they termed it as Capacitative Ca^{2+} entry (CCE) with a hypothesis that Ca^{2+} entry was regulated by the state of refilling of Ca^{2+} stores (Berridge et al., 1995, Putney 1986). Later in 1995, it was renamed as Store Operated Ca^{2+} entry (SOCE) to more clearly define its mode of activation. A universal mechanism of Ca^{2+} signalling is the release of Ca^{2+} from intracellular compartments which is mediated by activation of G protein-coupled receptor (GPCR) through several extracellular stimuli like hormones, growth factors, neurotransmitter release, neutrophins, odorant or light stimuli which in turn activate phospholipase C (PLC) and thereby cleaving membrane phosphatidylinositol 4,5 bisphosphate (PIP2) into soluble 1,4,5-inositol triphosphate (IP3) and diacyl glycerol (DAG) by hydrolysis (Streb et al., 1983, Berridge & Irvine, 1984, Berridge et al., 1993). IP3 released in this process binds to the IP3 receptor (IP3R)

which is localized at ER membranes and thereby triggers the diffusion of Ca^{2+} from ER to increase cytosolic Ca^{2+} levels (Streb et al., 1983, Thorn P et al., 1993, Rebecchi M.J et al., 2000, Reviewed in Rizzuto et al., 2009).

The use of pharmacological inhibitors in particular SERCA inhibitors like Thapsigargin (Tg), which is a plant-derived lactone (Thastrup et al., 1989), and other inhibitors like cyclopiazonic acid (CPA), or BHQ that are specific inhibitors of SERCA in the endoplasmic reticulum, the use of certain Ca^{2+} sensitive dyes like Fura2 and use of calcium chelators like BAPTA/EGTA have made it possible to measure the Ca^{2+} release in response to depletion of Ca^{2+} stores from ER (Grynkiewicz G et al, 1985). Using a combination of patch-clamp electrophysiology and Fura2-based Ca^{2+} imaging, Hoth & Penner in 1992 and Zweifach & Lewis in 1993 have shown that the depletion of intracellular Ca^{2+} pool under different independent mechanisms (IP_3 /ionomycin/EGTA) led to activation of Ca^{2+} currents which was measured in mast cells and Jurkat T Cells respectively and they named this current as Calcium release-activated Calcium currents (CRAC/ I_{CRAC}). This CRAC is not voltage-activated and is characterized by high selectivity for Ca^{2+} in comparison to other mono/divalent cations, very low unitary conductance of app.10-24 fS, and a strong inward rectifying current (Hoth & Penner, 1992 and Zweifach & Lewis, 1993, Fasolato et al., 1998).

After numerous candidates were screened that were speculated to be involved in ER Ca^{2+} refilling to understand the physiological relevance and molecular mechanism (reviewed in Prakriya & Lewis 2015), Stromal Interaction Molecule (STIM) was identified as an essential component for the activation of SOCE based on genome-wide RNA interference screening methods (Liou et al., 2005, Roos et al., 2005, Zhang et al., 2006). This protein resides on the endoplasmic reticulum and has a single spanning transmembrane domain with N terminal EF-hand motif, present inside the ER lumen which senses the Ca^{2+} concentration inside the ER lumen (Roos et al., 2005, Liou et al., 2005). A plasma membrane docking protein for STIM, named CRAC modulators (CRACM1&2, also named as Orai channels) is highly selective for Ca^{2+} ions is the missing molecular component identified to take part in SOCE as previous reports suggested that fully activated STIM was not sufficient to mediate Ca^{2+} influx via SOCE mechanism in patients suffering from severe combined immune deficiency (SCID) although they possess normal STIM expression levels (Vig M et al., 2006, Feske et al., 2005).

Upon store depletion in the ER through physiological stimulation of IP₃ release, STIM1 molecule undergoes a conformational change upon Ca²⁺ dissociation from the EF-hand, oligomerizes via EF-SAM (Sterile alpha Motif) region in the N terminus (Stathopoulos et al., 2006, 2008, Liou et al., 2007). The oligomerized STIM1 is then translocated to ER-PM junctions where it forms punctate / clusters, where it traps and recruits Orai (Liou et al., 2007, Wu et al., 2006, Luik et al., 2008, Stathopoulos et al., 2008). CRAC channels are opened via direct binding of STIM1 with N and C termini of Orai1 thereby mediating Ca²⁺ influx from the extracellular matrix (Luik et al., 2008, Park et al., 2009, Wu et al., 2014). Cytoplasmic Ca²⁺ levels determine the disassembly of STIM1 oligomers, bringing them back to a resting state independent of the state of ER Ca²⁺ refilling, thereby protecting the cells from SOCE overload (Malli et al., 2008). SOCE, apart from Ca²⁺ refilling into ER, plays a major role in mast cell degranulation, cytotoxic killing mediated by T cells, Ca²⁺ dependent translocation of NFAT into the nucleus mediated by Calcineurin (Feske et al., 2001, Feske et al., 2006, Gwack et al., 2007). The mechanism of SOCE activation mediated by Stim and Orai proteins has been depicted in Figure 2.

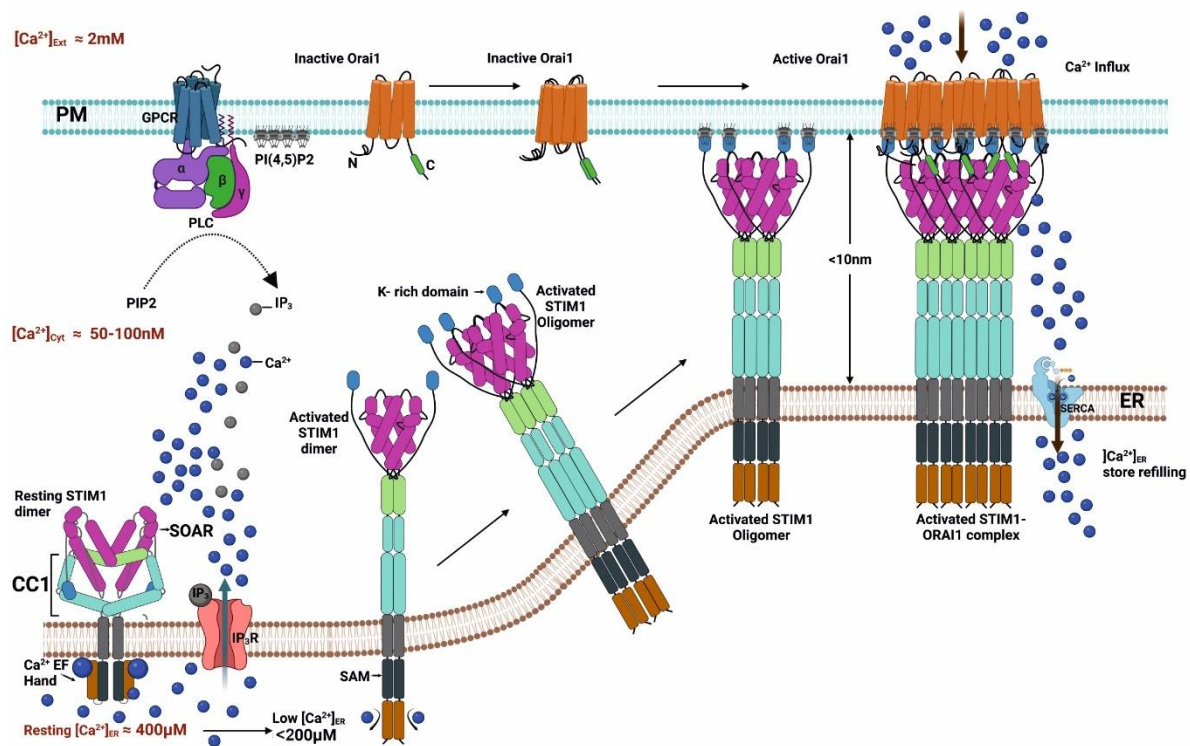


Figure 2 Store-Operated Ca²⁺ Entry (SOCE) activation process: STIM1 and ORAI1 form homodimers at resting ER Ca²⁺ levels. Agonist-induced stimulation of G-protein coupled receptors (GPCRs) or tyrosine kinase receptors (RTKs) leads to hydrolysis of phosphatidylinositol 4,5-bisphosphate [PI (4,5) P₂] and release IP₃ and

diffuses into the cytosol. IP₃ binds to the IP₃ receptor on the ER membrane causing ER Ca²⁺ release from IP₃R. STIM1/2 senses the ER Ca²⁺ drop loses Ca²⁺ bound to their EF-hand, undergoes oligomerization, and translocates to the ER-PM junction. Oligomerized STIM1 binds to PI (4,5) P₂ at the inner leaflet of PM via their K-rich domains. Activated STIM1 oligomers activate the ORAI1 channel, facilitating the influx of extracellular Ca²⁺ into the cytosol and filling the ER Ca²⁺. (Modified from Bhardwaj et al., 2016).

1.3 Orai proteins:

The Orai protein family, which are the constituents of the highly Ca²⁺ selective plasma membrane channels, comprise three conserved homologs Orai1, Orai2, and Orai3; with Orai3 the evolutionary newest addition which would probably be evolved from Orai1 in mammals (Mercer et al., 2006, Vig et al., 2006, Zhang et al., 2006, Gwack et al., 2007, Rothberg et al., 2013, Cai et al., 2007). Structurally, all three Orai homologs contain four transmembrane domains with N – and C- termini exposed to the cytosolic region and linked by 2 extracellular and 1 intracellular loop (Penna A et al., 2008, Mignen et al., 2008). While they share 87% sequence identity between the TM 1-4 regions, the TM1 region is conserved between the Orai homologs (Reviewed in Derler et al., 2016). The first extracellular loop is 60-80% conserved while the second extracellular loop is only 20-30% conserved among the Orai isoforms. The intracellular loop connecting TM2 and TM3 of Orai1 and Orai3 are identical, however, loop 2 of Orai1, but not Orai3 caused significant inhibition of Stim1 mediated currents with N terminus truncated Orai1 mutants and MD simulations studies indicated a shorter cytosolic extension of TM2 in Orai1 than in Orai3 (Reviewed in Fahrner et al., 2018). Both N – and C-termini of the Orai channels are required for gating STIM1 (Muik et al., 2009, Park et al., 2009, Derler et al., 2013, Palty et al., 2015, Frischauf et al., 2009, 2015), although the C-Terminal region is the dominant site gated by STIM proteins.

All three Orai homologs display a highly inward rectified Ca²⁺ current with a low unitary conductance and form either homo or heteromultimers (Gross et al., 2007, Gwack et al., 2007, Lis et al., 2007). The Orai channels were previously thought to form only tetrameric assemblies (Gwack et al., 2007, Zhou et al., 2010). However, the crystal structure of *Drosophila melanogaster* Orai (dOrai) revealed a hexameric Orai stoichiometry as a functional channel arranged around the central ion pore which forms the Ca²⁺ selective ion pore of the CRAC that traverses the membrane and extends into the cytosol (Prakriya et al., 2006, Hou et al., 2012, Cai et al., 2016). The ion pore is located at the hexamer's center, including 6 TM1 domains and the extended Orai1 N terminal region (ETON aa 74-90), which contributes to STIM1 binding

(reviewed in Rosado et al., 2016). TM1 residue E106 extends into the pore towards the outer part of the PM and comprises the ion selectivity filter. A hydrophobic cavity is formed by residues (aa V102, F99, and L95) and a very basic region (aa R91, K87, R83) at the cytoplasmic junction regulates the channel to be in a closed state or allowing Ca^{2+} permeation upon gating STIM proteins (Hou et al., 2012, Vig et al., 2006, Derler et al., 2013, Zhou et al., 2010, McNally et al., 2009, McNally et al., 2012, Reviewed in Yeung et al., 2020, Tiffner et al., 2021, & Humer et al., 2022). The extracellular loop of Orai1 contains a glycosylation site at N223, modulation of which can attenuate SOCE in a cell type-specific manner (Dorr et al., 2016). The cysteine residues at C195 at the extracellular site of the third transmembrane domain of Orai1 contribute to the redox regulation of Orai1, residue lacking in Orai3, making Orai3 redox insensitive (Bogeski et al., 2010). Interestingly in a heteromeric complex, one Orai3 subunit is sufficient to render the heteromeric complex redox insensitive, which suggests that Orai3 proteins facilitate the fine-tuning of efficient STIM1 gating and redox regulation (Alansary et al., 2015, Alansary et al., 2016; Saul et al., 2016).

The average CRAC amplitudes of native Orai2 and Orai3 are approximately 3-fold smaller in comparison to native Orai1 (Lis et al., 2007, Lis et al., 2010). In the murine Orai2 gene, two splice isoforms were identified that differ in their N termini and functionally expressed in a cell-specific manner, namely Orai2L and Orai2s that lacks 14 aa of Orai2L and functionally, Orai2s is more sensitive to inactivation by internal Ca^{2+} when compared to Orai2L and Orai1 (Gross et al., 2007).

1.4 STIM proteins:

The members of STIM family, comprising STIM1 and STIM2 are type 1 transmembrane proteins residing within the ER membrane (Roos et al., 2005, Zhang et al., 2005), also located in acidic stores (Zbidi et al., 2011). STIM1 was initially described as a phosphoprotein before its role in SOCE was established (Manji et al., 2000, reviewed in Frischauf et al., 2008). The N terminal region of STIM is inside the intraluminal compartment of the ER and after cleavage of its signal peptide, which is much longer and rather atypical in Stim2. Following a short linker domain, both homologs have an active canonical and a hidden EF-hand domain (aa 63-128) (Liou et al., 2005, Roos et al., 2005) followed by a sterile alpha motif (SAM) domain (Stathopoulos et al., 2008). Ca^{2+} is bound to the canonical EF-hand forming the luminal Ca^{2+} sensor. Mutations within the EF-hand domain trigger constitutive Ca^{2+} entry (Spasova et al.,

2006). Followed by is the SAM domain (aa 132-200) that interacts with EF-hand to keep the Ca^{2+} bound domain in stable condition and they exhibit distinctive properties in Stim1 and Stim2 (Stathopoulos et al., 2008, Zheng et al., 2011). Downstream of the SAM domain is the transmembrane domain (TM) (aa214-343) which can undergo reorganizational changes thereby initiating the conformational changes in the SOAR to promote the gating of Orai channels (Ma et al., 2015). The STIM C terminus region is localized in the cytosol and starts with 3 conserved coiled-coiled (CC) domains. Coiled-coil domains are further divided into CC1 (aa238-343), CC2 (aa 363-389), and CC3 (389-444). Following those is the CRAC modulatory domain (aa 448-530). Within the CRAC modulatory domain lies the Inactivation domain (ID) (aa 470-491) which is responsible for promoting Ca^{2+} -dependent inactivation of the Orai channel possibly by direct interaction with 3 Aspartic residues present in the Orai channel pore (Mullins et al., 2009, Mullins and Lewis 2016). The minimal amino acid residues required for the activation of the Orai channel localize between the CC2 and CC3 domain and are termed as Channel activation domain (CAD) or Store Operated Activation Region (SOAR) (aa 342-444) (Park et al., 2009, Yuan et al., 2009, Kawasaki et al., 2009, Yang et al., 2012, Wang et al., 2014). The serine/proline-rich region (aa 600-629) and lysine-rich region (aa 671-685) / polybasic K-domain at the end of C terminus mediates the binding of phospholipids at the plasma membrane and helps anchoring of Stim1 towards the ER-PM junction (Liou et al., 2005, Liou et al., 2007). Although the CC regions are nearly identical between Stim1 and Stim2, distinct Orai coupling sites in Stim1 and Stim2 showed notable differences in Orai1 gating and activation (Wang et al., 2014). Some studies have found that besides the role of the polybasic lysine-rich region in binding to Plasma membrane phospholipids, Calcium bound Calmodulin could bind to the polybasic domain of Stim1 which is essential for regulating the entry of Ca^{2+} by STIM1 (Jardin et al., 2009, 2013, Mullins et al., 2009). The TRIP motif at the C terminus region of STIM1 harbours the binding site for end binding protein, EB1 that tracks along the microtubule ends, traps the oligomerized STIM1 and delays the translocation of STIM1 to the ER –PM junction, thereby tuning the kinetics of SOCE (Chang et al., 2018, Wang et al., 2018, reviewed in Poth et al., 2020). However, another study shows that inhibition of EB1 binding to Stim1 could only abolish the microtubule tracking of Stim1, but does not affect SOCE (Grigoriev et al., 2008). Calmodulin (CaM) whose role in maintaining Ca^{2+} homeostasis is well reported, also regulates SOCE by disrupting the interaction of the SOAR domain of

Stim1 with Orai1 thereby disassembling the active complex as well as Stim1 oligomers and contributes to the slow Ca^{2+} dependent inactivation (SCDI) of Orai1 (Li et al., 2017).

Upon ER store depletion, the stimulus prompts the displacement of Ca^{2+} from the EF hand and numerous conformation changes happen within the N terminus. Upon Ca^{2+} dissociation, EF-hand mediates the conformation of the SAM domain exposing the hydrophobic domains and initiating the oligomerization of STIM1 (Stathopoulos et al., 2006, 2008). The signals are then transferred to the TM region which controls the active/inactive state of STIM (Ma et al., 2015). Ultimately, the signals are transferred to the cytosolic region into the CC1 domain which releases the closed state of the C terminus to the open state and exposes the STIM1 activating region to the N- and C- termini of Orai (Stathopoulos et al., 2013, Derler et al., 2013, Fahrner et al., 2014). It has been suggested that STIM1 forms homo or heterodimers via the coiled-coil domain also in the resting state (Baba et al, 2006; Covington et al, 2010; Muik et al, 2008; Penna et al, 2008; Williams et al, 2002). The interaction between the C terminal domains of STIM1 and Orai1 has also been studied by NMR and pointing towards critical positive residues such as K382, K284, K385 and K386 of Stim1 interacts with non-polar residues L273,276,286, and polar residues R281,289 of Orai1 thus forming a Stim1-Orai1 Association pocket (SOAP) (Stathopoulos et al., 2013). Regulation of SOCE can also be mediated by several phosphorylation sites of Stim1 where Y361 phosphorylation via proline-rich kinase 2 facilitates the recruitment of Orai1 to the Stim1 puncta thereby triggering Ca^{2+} entry (Yazbeck et al., 2017); S486/S668 phosphorylation mediates mitosis (Reviewed in Guisado et al., 2013).

Stim2 has a sequence similarity of 76%, although its N – and C- termini are distinguishable making them exhibit differential biophysical properties in terms of SOCE activation and gating of Orai channels (Hooper et al., 2013, Prakriya and Lewis, 2015, Nguyen et al., 2018). Although Stim1 and Stim2 are ubiquitously expressed in almost all cell types, Stim2 expression is highest in most brain regions especially in hippocampus and dendritic cells (Berna Erro et al., 2009, Bandyopadhyay et al., 2011). Stim2 EF-SAM domain has a low binding affinity to Ca^{2+} (K_d :600-800 $\mu\text{mol/L}$) in comparison to Stim1 which has a 2-fold lower affinity, making Stim2 more sensitive to small fluctuations of ER Ca^{2+} levels (Brandman et al., 2007., Kar et al., 2012) and thereby plays an important role in maintaining basal Ca^{2+} as well as Ca^{2+} oscillations. Stim2 mediated I_{CRAC} exhibits slower activation kinetics of Orai channels due to structural differences in N term luminal region (Wang et al., 2014). EF-SAM domain of

Stim2 is much more stable than Stim1 and decreases the tendency of oligomerization (Zheng et al., 2008, Stathopoulos et al., 2008, Zheng et al., 2011). Stim2 also exhibits low efficacy in Orai coupling due to differences in the Stim2 SOAR domain (Wang et al., 2014). Stim2 has a consensus sequence for di-lysine ER retention motif (K(X)KXX) at the end of the C terminus which makes their expression restricted more exclusively to the ER, while STIM1 is still sparsely located at the plasma membrane (Reviewed in Soboloff et al., 2012). Stim2 has a higher affinity to PIP2 at the plasma membrane because of the differences in the poly-lysine region by forming an amphipathic alpha helix (Bhardwaj et al., 2013).

1.5 STIM splicing and their variants:

The process of intron removal and exon ligation is termed alternative splicing arising to various protein isoforms in a developmental, tissue-specific manner leading to distinctive functions (Nilson et al., 2010, Wang et al., 2014). The human genome consists of approximately 20,600 protein-coding genes, which is surprisingly low for the proteomic complexity in tissues, but with an average of 6.3 alternatively spliced transcripts (3.9 different protein-coding transcripts) per locus with more than 95% of human genes have been found to undergo splicing. (The ENCODE Project Consortium, 2012).

Both Stim1 and Stim2 genes are encoded by large genomic regions spanning app.180kbp and encoded in their conventional forms by 12 exons. The first ever identified Stim1 splice variant is the Stim1L, which is a resultant of alternatively spliced-in, in-frame extension (318bp) of exon 11 that translates to a longer cytosolic C terminal tail (Darbellay et al., 2011). This protein is predominantly expressed in skeletal muscle, also detected in spleen, lungs, liver, and heart and the extended additional domain contains an actin-binding domain (aa 515-620) that is able to interact with actin fibers enabling the formation of permanent clusters without remodeling the cortical ER and triggers the fast repetitive release of Ca^{2+} within seconds as demanded in muscle cells (Darbellay et al., 2011, Saüc et al., 2015). Stim1L augments the Ca^{2+} entry through Orai1 than the conventional Stim1 and also suppresses the endothelin type A mediated Ca^{2+} entry via binding to TRPC3/6 than Stim1 (Horinouchi et al., 2012). While it was thought that Stim1L brought more Ca^{2+} entry via Orai1 than Stim1, Dyrda A et al., 2020 reported a strong coupling of Stim1L to TRPC1 than Orai1 and the larger SOCE mediated by Stim1L is likely due to TRPC1 activation.

Later in 2015, it was found that alternative splice addition of a short exon that encodes for only 8 amino acids (VAASYLIQ) into the CAD domain of Stim2 led to the identification of a new splice variant, named Stim2.1/Stim2 β , which converted the protein from an activator to inhibitor of SOCE by preventing gating of Orai channels (Miederer et al., 2015; Rana et al., 2015.). Also, Stim2.1 has been shown to have a dominant negative effect on Stim1 and Stim2.2 (Miederer et al., 2015). Apart from the already reported Stim2 splice variant, database mining resulted in the prediction of an additional splice variant, Stim2.3 which arises from the retention of additional exon between conventional exons 11 and 12, which, upon translation results in a frame shift and has a premature stop codon lacking 157 C-terminal residues including Stim2's lysine rich region (Miederer et al., 2015, Reviewed in Berna Erro et al., 2017) and its function is currently explored in Niemeyer's group.

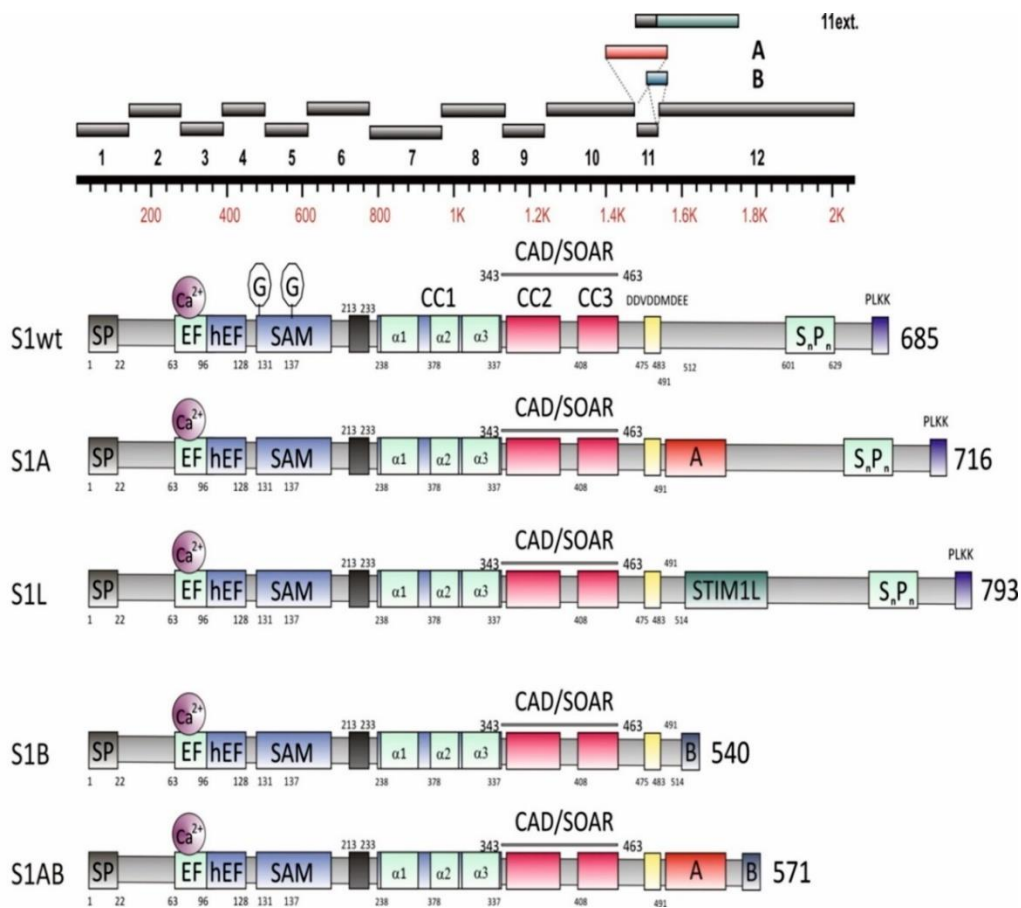


Figure 3 Schematic representation of the exon and domain structure of the STIM1 and its splice variants. The top panel shows the Exon structure of STIM1 with conventional exons shown in grey and spliced exons highlighted in blue (exon 13, 36bp long, named B), red (exon 11, 93 bp named A), and green (exon 13, L). The bottom panel shows the domain structure of STIM1 and the splice variants of STIM1 – STIM1A, STIM1L, STIM1B, and STIM1AB. Each domain is represented in different color codes. Image provided by Barbara. A. Niemeyer.

A new splice variant of Stim1 was recently identified as additional exon A (93bp) spliced between the conventional exons 10 and 11 which led to an additional 31 amino acids into the cytosolic domain of Stim1 upon translation and it is named Stim1A. It is found to be expressed in astrocytes, testes, heart, and kidney and plays a crucial role in increased NFAT translocation by modulating PDE8 although it imposes a dominant negative effect on SOCE by destabilizing the gating of Orai channels (Knapp et al., 2022). The Stim1 and its splice variants domain structure are shown in Figure 3.

1.6 Pathophysiology of Stim and Orai:

The role of Stim and Orai in regulating Ca^{2+} entry via SOCE mechanism in maintaining normal physiology/health was highlighted upon identifying the physiological consequences of loss or gain of function of these proteins in the immune system. A missense mutation in Orai 1 (R91W) leads to abrogation of SOCE which causes severe combined immunodeficiency (SCID) and is characterized by loss of immune cell function (Feske et al., 2006). Mouse lacking Orai1 developed eyelid irritation and sporadic hair loss and also showed defective T and B cell function which resulted in decreased Ca^{2+} influx and production of cytokines although it did not affect the development of immune cells (Gwack et al., 2008). Knockdown of STIM2 did not completely abolish I_{CRAC} in T cells compared to STIM1, however, STIM2 appears to be particularly involved in the longer-term maintenance of Ca^{2+} signaling, resulting in a greatly reduced translocation of NFAT and production of cytokines (Oh-Hora et al., 2008). Stimulation of fibroblasts from patients having LoF mutations in Orai1 (A103E/L194P) or for a frameshift nonsense mutation in Orai1 (A88SfsX25) or in Stim1 (E136X) failed to induce SOCE and it is associated to cause immunodeficiency, myopathy, and ectodermal dysplasia (McCarl et al., 2009, Picard et al., 2009). LoF mutation of Stim1 in the CAD domain at position R429C causes CRAC channelopathy by abolishing SOCE although Stim1 expression was only moderately reduced in B cells and fibroblasts. This residue is also important for stabilizing the α -helical folding of the CC3 domain of Stim1 and thereby mediating the intermolecular interactions with Orai1 (Maus M et al., 2015,). A novel gain of function mutation in Orai1 (S97C) leads to constitutive Ca^{2+} entry and causes tubular aggregate myopathy and congenital miosis (Garibaldi M et al., 2017). Gain of function mutation in Stim 1 (R304W) causes Stormorken-like syndrome associated with tubular myopathy, thrombocytopenia, bleeding diathesis, and congenital miosis as a result of constitutive activation of CRAC channels. A point mutation in

Orai 1 (P245L) is also associated with Stormorken syndrome of congenital miosis and tubular aggregate myopathy resulting in reduced slow Ca^{2+} -dependent activation but not constitutive Ca^{2+} entry (Nesin et al., 2014). Other forms of missense mutations in Orai 1 (G98S, V107M, T184M) lead to constitutive Ca^{2+} entry which is associated with tubular aggregate myopathy with hypocalcemia (Endo et al., 2015, Böhm et al., 2017). All of these mutations are located within the TM regions which play a crucial role in stabilizing the Stim1 –Orai1 gating and that Proline residue in TM4 is required for stabilizing the closed state of the channel which highlights the functions of these residues in channel regulation (Yueng et al., 2018, Palty et al., 2015, Lacruz and Feske, 2015). Another form of mutation in Stim1 at R426 resulted in impaired colocalization of Stim1 with Orai1 due to the tight holding of the C terminal region of Stim1 and preventing activation and associated with dental enamel defect (Wang et al., 2014).

Stim and Orai play an important role in platelet activation mediated by agonist-induced Ca^{2+} entry and are crucial in several thrombotic occlusive diseases as several reports highlighted the pathological effects of impaired platelet function due to mutations in these proteins (Grosse et al., 2007, Reviewed in Verga Szabo et al., 2008, Braun et al., 2009, Bergmerier et al., 2009, Reviewed in Münzer et al., 2022). Stim1, apart from Ca^{2+} signaling, also regulates the signaling of STING (Stimulation of Interferon genes) as a recent report suggests that patients with SCID or mice lacking Stim1 caused enhancement of IFN1 expression (Srikanth S et al., 2019).

Orai3, although not a dominant homolog of CRAC channels, plays a major role in cancer as reports suggested a higher Orai3 expression in various types of cancer such as lung adenocarcinoma, prostate cancer, and breast cancer (Motiani et al., 2010, Reviewed in Déliot et al., 2015, Chamlali et al., 2021, Ay et al., 2013, Dubois et al., 2014, Tiffner et al., 2021) while Holzmann et al., 2013 reported a decrease in Orai3 expression. Orai1 and Stim1 are considered to be essential for breast tumor cell migration and metastasis as silencing these proteins in breast cancer cells decreased the metastasis (Yang et al., 2009, Reviewed in White et al., 2017).

Although, in excitable cells like neurons, SOCE is not the major Ca^{2+} influx, dysfunction of Stim and Orai have been reported in several neurological diseases. Under acute conditions like cerebral ischemia or stroke, receptor-mediated Ca^{2+} exo-cytotoxicity and Ca^{2+} leak from intracellular organelles leads to neuronal death via ER stress (Reviewed in Secondo et al., 2018). As a result of Ca^{2+} leak, SOCE-mediated Ca^{2+} influx refills the ER to re-establish homeostasis and could protect neurons from ischemia or stroke (Parekh et al., 2010), and during

ischemia, Orai2 promotes Ca^{2+} overload as Orai2 deficient mice being protected from ischemia-induced neuronal death (Stegner et al., 2019). Stim2 has been reported to play an agonist role in reducing ischemia-induced neuronal death (Berna Erro et al., 2009, Reviewed in Serwach et al., 2020, & Tedeschi et al., 2021). High levels of Stim1 and Stim2 are reported in chronic epileptic rodents and pharmacological inhibition of SOCE suppressed the epileptic bursts (Steinbeck et al., 2011). In Parkinson's disease, the activity of dopaminergic neurons is regulated by Stim1 via interaction with TRPC1 which in turn inhibits the L-type Ca^{2+} channels (Selvaraj et al., 2012, Sun et al., 2017). The dominant negative effect of Orai1 on tyrosine hydroxylase regulation is also associated with Parkinson's disease (Pathak et al., 2015). In Huntington's disease, elevated Stim2 in the striatum was observed in a mouse model of HD causing elevated neuronal SOCE and spine loss in the striatum and, and TRPC1-mediated SOCE regulation could be a potential target to treat HD (Wu et al., 2011, 2016). Aberrant ER Ca^{2+} refilling is reported in motor neurodegenerative diseases like Amyotrophic lateral sclerosis and that, ER Ca^{2+} overload could be due to enhanced S glutathionylation of Stim1 (Cassina et al., 2008, Hawkins et al., 2010, Kawamata et al., 2014). Alzheimer's disease can be caused by mutations in amyloid precursor proteins (APP), presenilin 1 & 2 (Reviewed in Karch & Goate, 2015) and alterations of ER Ca^{2+} have been implicated to also contribute to AD (Reviewed in Secondo et al., 2018). Downregulation of Stim2 was observed in APP knock-in mice which affected neuronal SOCE. This affects the activation of Ca^{2+} /calmodulin-dependent kinase II (CaMKII) and causes destabilization of mushroom spines at the post-synapse (Sun et al., 2014, Zhang et al., 2015, 2016, Reviewed in Secondo et al., 2018).

1.7 Role of Stim and Orai in Neuronal SOCE:

Ca^{2+} signaling in excitable cells such as neurons has mostly been linked to the activity of voltage- or ligand-gated channels. In neurons, Ca^{2+} influx from the extracellular matrix is mediated majorly by voltage-gated calcium channels and glutamate receptors (ionotropic and metabotropic), while SOCE-mediated Ca^{2+} entry complements it and it is the main source while neurons are at rest (Berna Erro et al., 2009, Brini et al., 2014, Kraft et al., 2015). SOCE influences the frequency of spontaneous transmitter release at the synaptic boutons and modulates synaptic plasticity (Emptage et al., 2001). Stim1 and Stim2 homologs are ubiquitously expressed in all brain regions with Stim2 predominantly expressed in hippocampus & cortex and the highest expression of Stim1 in cerebellum (Berna Erro et al.,

2009, Skibinska Kijek et al., 2009, Klejman et al., 2009, Uhlénet al., 2015). All three Orai homologs are expressed in murine brain with Orai2 predominantly expressed in neurons, in particular hippocampus (Berna Erro et al., 2009, Gwack et al., 2007, <https://mouse.brain-map.org/>, RP_051214_03_B05).

Stim2 exerts its role in the regulation of AMPA receptor trafficking through the facilitation of synaptic delivery and removal thereby regulating the activity-dependent changes in synaptic strength (Yap et al., 2017). Stim2 plays a crucial role in mediating the phosphorylation of AMPAR subunit GluA1 in response to cAMP signaling and PKA activation and promotes its localization in dendritic spines and regulates the dendritic spine morphogenesis (Garcia-Alvarez et al., 2015). Mushroom-shaped dendritic spines that are associated with long-term synaptic stability and memory formation, are regulated by Stim2 by forming a complex with TRPC6-Orai2 that depends on neuronal SOCE (Sun et al., 2014, Zhang et al., 2016). Ca^{2+} influx through SOCE promotes the degradation of transcription factor Sp4 in cerebellar granule neurons and Sp4 is crucial for normal dendritic morphology in the hippocampus and cerebellum (Ramos et al., 2007, Zhou X et al., 2007, Lalonde et al., 2014). Orai1 also plays an important role in the formation of new synapses in cultured hippocampus and strongly colocalizes with Stim2 (Korkotian et al., 2017). These studies highlighted the role of Stim2 in neuronal SOCE through the regulation of LTP and LTD and receptor trafficking. Absence of Stim1 in Purkinje neurons resulted in attenuated SOCE, altered mGluR dependent EPSCs, delayed clearance of cytosolic Ca^{2+} in the soma, but not in dendrites during spike firing of Purkinje neurons, and thereby impairs motor behavior and memory consolidation (Hartman et al., 2014, Ryu et al., 2017). Recently published data suggest that Purkinje cell-specific Stim1KO led to impaired intrinsic plasticity which paved the way for the formation of aberrant neural plasticity in neurons of vestibular nucleus and was found to be impacted in memory consolidation of vestibule ocular reflex memory (Jang et al., 2020), however, this study did not address the long term effects of SOCE due to cell-specific Stim1KO as long term effects of KO might result in altered transcription of several essential genes.

Depletion of Ca^{2+} from internal stores contributes to action potential evoked Ca^{2+} transients at the presynaptic boutons thereby regulating the spontaneous miniature synaptic events (Emptage et al., 2001). In Purkinje cells, miniature inhibitory postsynaptic currents (mIPSCs) are regulated by ryanodine receptor-mediated Ca^{2+} release, and those intracellular Ca^{2+}

transients are concentrated at putative presynaptic terminals (Llano et al., 2000). On the other hand, Carter et al., 2002 controversially reported that at the excitatory synapses, plasticity is not due to the calcium-induced Ca^{2+} release as the store depletion or prevention did not have an effect on paired-pulse facilitation, delayed neurotransmitter release instead due to the residual Ca^{2+} influx through voltage-gated Ca^{2+} channels. ER extends along the axons and activation of Stim1 at the presynaptic terminal is controlled by Ca^{2+} concentration in ER thereby resulting in tuning of presynaptic function which in turn controls the neurotransmitter release (de Juan – Sanz et al., 2017). These reports addressed the role of SOCE in postsynaptic ER, the role of the ER for the presynaptic function is not well understood and controversial.

Synaptotagmin 1 (Syt1) and synaptotagmin 7 (Syt7) are essential calcium-binding proteins that modulate different aspects of presynaptic function. Syt1 functions as a calcium sensor for rapid synchronous neurotransmitter release, facilitating the fusion of synaptic vesicles (exocytosis) with the presynaptic membrane upon an action potential (Xu et al., 2009, Tagliatti et al., 2020, Courtney et al., 2019). In contrast, Syt7 is implicated in asynchronous neurotransmitter release, which occurs after the initial synchronous release and contributes to sustained neurotransmitter signaling (Bacaj et al., 2013). Additionally, Syt7 is thought to play a role in regulating synaptic vesicle trafficking and replenishment (Liu et al., 2014). Both Syt1 and Syt7 demonstrate distinct roles in shaping the temporal dynamics of neurotransmitter release, contributing to the complex and finely tuned processes of synaptic transmission. A recent study has revealed a novel function of the presynaptic endoplasmic reticulum (ER), connecting ER stress with increased spontaneous neurotransmission. This report proposes that chronic ER stress triggers an elevation in presynaptic calcium levels, resulting in the augmentation of spontaneous glutamate release. This process is found to be dependent on synaptotagmin 7 (Syt7), a calcium-binding protein implicated in asynchronous neurotransmitter release (Chanaday et al., 2021). In a parallel investigation, the conditional knockout of Stim2, a regulator of store-operated calcium entry (SOCE), in neurons lacking synaptotagmin 1 (Syt1) was found to rescue the observed Syt1 phenotype. This finding underscores the mechanistic link between Syt1-mediated regulation of SOCE and the modulation of spontaneous neurotransmitter release, highlighting the importance of Stim2 in this process (Chanaday et al., 2021).

Several studies have highlighted the involvement of Stim1 in the regulation of Voltage-gated Calcium channels. A study from Park et al., 2010 demonstrated that Stim1 has a direct

inhibitory effect on $\text{Ca}_v1.2$ through direct binding to the C terminus of $\text{Ca}_v1.2$ and acutely suppresses its opening upon membrane depolarization and leads to long-term internalization of $\text{Ca}_v1.2$ channels from the membrane (Park et al., 2010). Adding to Park et al., 2010's finding, Wang et al., 2010 further demonstrated that Stim1 plays a mediator role in activating $\text{Ca}_v1.2$ and Orai1 channels, and the SOAR domain of Stim1 is required for both actions. Another study by Dittmer et al., 2017 demonstrated that inhibition of L-type Voltage-gated Ca^{2+} channels by Stim1 influences dendritic spine ER structure and restricts NFATc3 transcription factor nuclear translocation. A recent study by Erdogmus et al., 2022 demonstrated the contrasting role of Ca^{2+} signaling in T cells and the involvement of VGCCs. The study suggests that TCR stimulation triggers the critical Ca^{2+} signals in T cells and $\text{Ca}_v\beta1$, encoded by *Cacnb1* is involved in the regulation of T cell function, but its effects are independent of functional VGCC activity (Erdogmus et al., 2022). Collectively, these studies highlight the diversity of calcium signaling in various cellular processes involving Stim1 and Ca_v channels, while Stim1 emerges as a central player in regulating calcium channels, the role of VGCCs appears to vary between the cell types with their functional significance being doubted in T cells.

Forebrain-specific condition knockout of Stim1/2 led to impaired spatial memory and LTP was remarkably enhanced with a marked increase in phosphorylation of AMPAR GluA1, LTCC on protein kinase A (PKA) sites (Garcia Alvarez et al., 2015b). Knocking out Orai1 selectively in forebrain excitatory neurons has been demonstrated to lead to deficits in both working and associative memory, along with impaired neuronal excitability (Manishi et al., 2020). Ca^{2+} influx via SOCE contributes to ischemia-induced Ca^{2+} influx and, Orai2 is involved in this calcium overload as Orai2 deficient mice reversed the ischemia/ oxygen deprivation-induced changes in neuronal excitability (Stegner et al., 2019). In neurons, ER is dynamic and can extend along the axons and dendritic boutons. Release of Ca^{2+} from the ER stores occurs via ryanodine receptor (RyR) and inositol 1,4,5 triphosphate 3 (IP_3) receptor-mediated responses and it was assumed to share the same Ca^{2+} pool in neurons. However recent study suggests that hippocampal CA1 pyramidal neurons consist of functionally distinct two intracellular Ca^{2+} pools: IP_3 -sensitive Ca^{2+} store refilling which is mediated by Orai2 and RyR-sensitive Ca^{2+} store refilling is activated by VGCC (Chen Engerer et al., 2019).

1.8 Aim & Objectives of the Ph.D Thesis

In this work, another splice variant of Stim1 was identified, named Stim1B, where insertion of short exon B which is 36bp long between exon 12 and 14 of Stim1 led to frameshift and termination of translation after aa 571 (including signal peptide) and resulted in a significantly shorter protein lacking 170 aa but contains additional 26 residues encoded by exon B and the translated residues due to the frameshift. As a result, the C terminal region of Stim1B lacks the serine/proline-rich region, EB1 binding motif (TRIP), and the polybasic domain.

Aim:

The primary aim of this Ph.D. thesis was to comprehensively characterize a newly identified splice variant of Stim1, termed Stim1B, and investigate its role in regulating Store-Operated Calcium Entry (SOCE).

Objectives:

1. Expression and Localization of Stim1B:

Objective: To determine the expression pattern of Stim1B at both RNA and protein levels in various murine tissues and cell types. Additionally, to investigate the subcellular localization of Stim1B compared to the canonical Stim1.

2. Functional Properties of Stim1B in SOCE Activation:

Objective: To assess the biophysical properties of Stim1B and examine its impact on SOCE activation using patch-clamp electrophysiology.

3. Effect of Exon B Insertion and Translated Residues on Stim1B Phenotype:

Objective: To investigate whether the insertion of exon B, additional translated residues, or C-Terminal residues affect the functional characteristics of Stim1B. This will be accomplished through site-directed mutagenesis and subsequent functional analysis.

4. Localization of Stim1B and Its Influence on Synaptic Transmission:

Objective: To study the localization patterns of Stim1B in neuronal cells, particularly in hippocampal cultures, and compare them to canonical Stim1. Additionally, to evaluate the

impact of Stim1B on synaptic transmission through neuronal patch-clamp experiments. This aim was carried out in collaboration with Dr. Yvonne Schwarz (AG Burns).

5. Identification of Stim1B Binding Partners:

Objective: To identify potential binding partners of Stim1B that may influence its phenotype. This will involve immunoprecipitation experiments in specific cell lines lacking Stim1/2 and using brain lysates from mice. Analysis of pull-downs using Mass Spectrometry was done in collaboration with Prof. Dr. Vera Jankowski, Universitätsklinikum Aachen.

6. Assessment of the Physiological Relevance of Stim1B:

Objective: To determine the physiological significance of Stim1B by conducting behavioral experiments on splice-deficient mouse models (10A mice). Behavioral experiments were performed in collaboration with Dr. Wenhui Huang (AG Kirchoff). The assessments will include evaluations of anxiety levels, cerebellar motor performance, and learning capabilities.

This comprehensive investigation aims to elucidate the role and functional significance of Stim1B in calcium signaling and its potential impact on neuronal function and behavior.

Majority of the results presented in this thesis have been published in Ramesh, G., Jarzemboski, L., Schwarz, Y., Poth, V., Konrad, M., Knapp, M., Schwär, G., Lauer, A.A., Grimm, M.O.W., Alansary, D., Bruns, D. and Niemeyer, B.A. (2021). A short isoform of STIM1 confers frequency-dependent synaptic enhancement. *Cell Reports*, 34: 108844. The dissertation author is the shared first author of this publication and responsible for Western blot analysis, patch-clamp analysis in heterologous overexpression in cell lines, most of the cloning of mutants and constructs. Figure legends within the results indicate if data is also shown in the publication. The publication is attached at the end of the appendix.

2. Materials

2.1 Chemicals & Reagents

Table1 List of Chemical reagents used in this study

Chemical reagents	Manufacturer	Catalog number / Order Number
2 – Mercaptoethanol	Acros Organics	125472500
2- Propanol	Sigma	19516
Acrylamide – Bisacrylamide	Sigma	A7168
Select Agar	Sigma	A5054
Agarose Broad range	Roth	T846.3
Agarose GTQ	Roth	6352.4
Albumin from Bovine Serum	Sigma	A3294
Ampicillin	Sigma	A9393
Ammonium persulfate	Sigma	248614
L-Aspartic acid	Sigma Aldrich	A9256
BAPTA - Tetracesium	Fisher Scientific	B1212
Bissulfosuccinimidyl suberate (BS3)	Thermofisher Scientific	21580
Bromophenol blue	Roth	A512.1
Boric acid	Sigma	B0394
Calcium Chloride Dihydrate	Merck Scientific	102382
Glucose	Merck Scientific	108337
Cesium hydroxide, hydrate	Sigma Aldrich	C8518-50G
Chloroform	Sigma	288306
cOmplete mini, EDTA-free Protease Inhibitor	Sigma Aldrich	5892791001
Cocktail tablets		
Dodecylsulphate Na-salt (SDS)	Acrosorganics	3272315000
DMSO	Sigma	D8418
DTT	Sigma	D9779
Dynabeads™ Protein A for Immunoprecipitation	Thermofisher Scientific	10001D
Dynabeads™ Protein G for Immunoprecipitation	Thermofisher Scientific	10003D
EDTA	Sigma	ED2SS
EGTA	Sigma	E4378.2506
L-Glutamic acid	Sigma Aldrich	49450-250G
Glycine	Applichem	R030
Hydrogen Per oxide	Fisher Scientific	H325-500
HEPES	Difco	212750

D-myo-Inositol-1,4,5-Triphosphate trisodium salt	Sigma Aldrich	407137-1
Kanamycin	Sigma Aldrich	K0254-20ML
Magnesium Chloride	Merck	105833025
Methanol	Fisher Chemicals	M3950
OptiMEM	Thermofisher	31985088
Paraformaldehyde	Polysciences	00380-250
PeqGold dNTP Mix	Peqlab	20-3011
PeqGreen DNA / RNA Dye	Peqlab	37-500
Phenylmethylsulfonyl fluoride (PMSF)	Sigma Aldrich	10837091001
Poly-L-ornithine	Sigma	P3655
Potassium Chloride	Calbiochem	407950
Sigma Cote	Sigma Aldrich	SL2-25ML
Skimmed milk powder	Sucofin	-
Sodium Ascorbate	Sigma	
Sodium Azide	Sigma	S8032
Sodium Chloride	Sigma	S9888
Thapsigargin	Invitrogen	T7458
TEMED	Sigma	T9281
Tetraethyl Ammonium Chloride (TEA-Cl)	Sigma Aldrich	T2265-25G
Triton X 100	Eurobio	18774
Trizma Base	Sigma	T1503
TRIZol	Life Technologies	15596018
Trypsin	Fisher Scientific	25300-062
Tryptone / peptone	Sigma	T9140
Tween-20	Sigma	P1379
Urea	Sigma	U5378
Yeast extract	Difco	212750

2.2 Commercial Kits

Table 2 List of commercial kits used in this study

Name of the Kit	Manufacturer	Catalog / Order Number
Dream Taq Green PCR Master Mix	Thermo Scientific	K1081
Phusion High-Fidelity PCR kit	NEB	F553S
QIA Quick Gel Extraction Kit	Qiagen	28706
QIA-Spin miniprep	Qiagen	27106
QIAGEN Plasmid Maxi Kit	Qiagen	12662
Quantitect SYBRgreen kit	Qiagen	204145
T4 DNA Ligase kit	Life Technologies	EL0012
BCA-Protein Assay Kit	Thermo Scientific	23225
Clarity Western ECL	Biorad	1705060

2.3 Antibodies

2.3.1 Primary antibodies

Table 3 List of Primary antibodies

Name of the Antibody	Manufacturer	Catalog / Order Number	Species & Clonality	Dilution
Anti STIM1 / GOK	Acris GmbH	AM20946PU-N,RRID:AB_10849514	Mouse monoclonal	1:500
GOK / STIM1 aa 25-139	BD Biosciences	610954, RRID:AB_398267	Mouse monoclonal (aa 25-139)	1:500
STIM1	Proteintech	11565-1-AP, RRID:AB_2302808	Rabbit polyclonal aa 2-350	1:1000
STIM1B	Dr. Martin Jung (Self made)	This study	Rabbit polyclonal	1:500
STIM2	Proteintech	21192-1-AP, RRID:AB_10734322	Rabbit Polyclonal, 525-674aa	1:1000
Beta-Actin	Sigma Aldrich	A1978, RRID:AB_476692	Mouse monoclonal, Clone AC-15	1:2000
Anti GAPDH	Cell Signaling Technology	2118, RRID:AB_561053	Rabbit monoclonal, Clone 14C10	1:2000
mCherry	Biorbyt	orb11618, RRID:AB_2687829	Rabbit polyclonal	1:1000
RFP /mKate2	Evrogen	AB233, RRID:AB_2571743	Rabbit polyclonal	1:1000
Synapsin	Synaptic Systems	106 011	Mouse monoclonal	1:2000
Anti Bassoon	Synaptic Systems	141011, RRID:AB_2619827	Mouse monoclonal	1:2000

2.3.2 Secondary Antibodies

Table 4 List of Secondary antibodies

Name of the Antibody	Manufacturer	Catalog / Order Number	Dilution
Anti Rabbit -HRP	GE Healthcare Amersham	NA9340	1:25000
Anti mouse – HRP	Amersham Bioscience	NA931	1:5000
Goat anti-Mouse IgG Alexa Fluor 555	Invitrogen	A-21422	1:2500
Goat anti-Rabbit IgG Alexa Fluor 488	Invitrogen	A32731	1:2000
Goat anti-Guinea Pig IgG Alexa Fluor 643	Invitrogen	A21450	1:2500

2.4 Bacterial strain

Table 5 List of Bacterial competent cells used in this study

Bacterial strain	Manufacturer	Catalog / Order Number
XL-1 blue Subclone grade	Agilent Technologies	200249

2.5 Protein Markers / Standards

Table 6 List of Protein markers / Standards

Protein / DNA Marker	Manufacturer	Catalog / Order number
1 Kb plus ladder	Invitrogen	10787-018
100 bp Ladder	NEB Biolabs	N3231S
Precision Plus Protein dual color standard	BioRad	161-0374

2.6 Lab Equipments

2.6.1 Lab Equipments for Patch clamp Electrophysiology

Equipment name	Manufacturer
Inverted Microscope	Olympus
YFP-Filter (F36-528)	Analysetechnik AG
mCherry-Filter (F20-451)	Analysetechnik AG
Pipette puller	HEKA Electronics

2.6.2 Lab Equipments for TIRF Microscopy Imaging

Equipment name	Manufacturer
Leica AM TIRF MC	Leica
HCX Plan Apo (100x; 1.46 NA)	Leica

2.6.3 Other Basic Equipments used in this study

Lab Equipments	Manufacturer
4D Nucleofactor	Lonza
Infinite M200 pro Plate-Reader	TECAN
FLoid Cell Imaging Station	Life Technologies
Cell Observer	Zeiss
Nucleofactor Iib Amaxa	Lonza
ChemiDoc TM XRS	Bio Rad

CO2 Incubator	Thermofisher Scientific
Gel Electrophoresis	Bio-Rad
Heat Block	Bioer
Centrifuge 5415 C	Eppendorf
Centrifuge 5418	Eppendorf
Centrifuge micro 220R	Hettich
Centrifuge mini spin 5452	Eppendorf
Centrifuge Universal 32R	Hettich
Semi-Dry Blotter	Tyler Research
Vortexer	Peqlab
Bio Photometer	Eppendorf
NanoDrop UV- Spectrophotometer	Thernofisher Scientific

2.7 Solutions / Buffer Compositions

Patch Clamp Electrophysiology

ICRAC Ca²⁺-Containing Bath Solution

120mM	NaCl
10mM	Tetraethylammonium Chloride
10mM	CaCl ₂
2mM	MgCl ₂
30mM	Glucose
10mM	HEPES

Adjust pH to 7.2 with NaOH, Osm adjusted to 320-330mOsm

ICRAC Pipette / Internal Solution with BAPTA

120mM	Cesium Glutamate
10mM	HEPES
3mM	MgCl ₂
10mM	NaCl
20mM	BAPTA
0.05mM	IP ₃

Adjust pH to 7.2 with CsOH, Osm adjusted to app. 300mOsm

Internal Solution – EGTA

140 mM	Cesium aspartate
10mM	HEPES
3mM	MgCl ₂
10mM	NaCl
2mM	EGTA
0.05mM	IP ₃

pH adjusted to 7.2 with CsOH, Osmolality adjusted to around 300mOsm

2.8 SDS Page / Western blot buffer

Lamelli buffer 2X

20% Glycerine
8% SDS
0.1% Bromophenol blue
0.1% Beta- Mercaptoethanol
120mM Tris pH 6.8

Lamelli buffer 5X

60% Glycerine
2.5% SDS
0.1% Bromophenol blue
0.1% Beta- Mercaptoethanol
125mM Tris pH 6.8

Primary antibody solution

Primary antibody diluted in below freshly prepared solution

1% BSA
0.02% Sodium Azide

Secondary Antibody Solution

Secondary antibody diluted in freshly prepared solution

5% Skimmed milk in TBST

RIPA Lysis Buffer

PBS pH 7.4
150mM NaCl
10mM Tris pH 7.4
1% Triton X-100
0.5% NP-40

Stacking gel buffer

0.5M Tris HCl
0.4% SDS
Dissolved in H₂O pH 6.8

SDS Electrophoresis buffer 10X, pH 8.3

250mM Tris HCl
1.92M Glycine
1% SDS

TBE, 10x, pH 8.3

89mM Tris Base
89mM Boric Acid
10mM EDTA

TBS, 10x pH 7.5

500mM Tris Base
1.5M NaCl

TBST, 10X

10% 10X TBS
0.1% Tween20

Separating gel buffer

1.6M Tris-HCl
0.4% SDS
Dissolved in H₂O pH 8.8

Bacterial culture / medium

LB medium

1% Peptone / Tryptone
0.5% Yeast extract
1% NaCl

Antibiotics

100µg/mL From stock Ampicillin (50mg/mL)
60µg/mL From stock Kanamycin (50mg/mL)

Bacterial agar medium

50.7%	K ₂ HPO ₄
0.3%	KH ₂ HPO ₄
0.05%	Sodium Citrate
0.01%	MgSO ₄
50%	Glycerine

LB Agar plates

LB	+
Medium	
1.5%	Agar + Antibiotic selection (Ampicillin / Kanamycin)

2.9 Enzymes

2.9.1 Modified enzymes

Table 7 List of modified enzymes used in this study

Modified Enzymes	Manufacturer	Catalog / Order Number
Antarctic Phosphatase	NEB	M0289S
Phusion Polymerase	NEB	M0530S
T4 DNA Ligase	NEB	M0202S
Superscript II RT	Life Technologies	18064
T4 Polynucleotide Kinase	NEB	M0201S

2.9.2 Restriction enzymes

Table 8 List of restriction enzymes used in this study

Restriction Enzymes	Manufacturer	Buffer	Catalog / Order Number
EcoRI-HF	NEB	Cut smart	R3101S
EcoRV-HF	NEB	Cut smart	R3195S
DpnI	NEB	Cut smart	R0176S
BamHI HF	NEB	Cut smart	R3136S
XhoI	NEB	Cut smart	R0146S
SpeI-HF	NEB	Cut Smart	R3133S

2.10 Primers for cloning & qRT-PCR primers

Table 9 List of Primers used for this study

Primer Name	Sequence (5'- 3') or Catalog number
Stim1, mouse (Qiagen Quantitect)	QT00105119
Stim1, human (Qiagen Quantitect)	QT00083538
Stim2 (Qiagen Quantitect)	QT00289009
Orai1 (Qiagen Quantitect)	QT00285775
Orai2 (Qiagen Quantitect)	QT01533441
Orai3 (Qiagen Quantitect)	QT00255598
Hprt1 (Qiagen Quantitect)	PPM03559F-200
Tbp1 (Qiagen Quantitect)	PPM03560F-200
Stim1B for	CTCTAAAGGCAAACAGGCTC
Stim1_nonB for	GATCTCAGAGGGATTTGAC
Stim1_all rev	ATTGGAAGGCATGGCATTG
STIM1_all rev II	CCATTGGAAGTCATGGCATTG
½ exon STIM1B for	AAACAGGCTCTCTAGTAAGGGATTTGACCCATTCCGATTC
½ exon STIM1B rev	GCCTTTAGAGATGATCCTCTCTGAGATCCCAGGCCATG
STIM1_514* for	TGGCCTGGGATCTCAGAGGTAGTAAGATTTGACCCATTCCGATTCG
STIM1_514* for	CGAATCGGAATGGGTCAAATCTTACTACCTCTGAGATCCCAGGCCA
Stim1_514* rev	CTACCTCTGAGATCCCAGGCCA
Stim1BØStop for	GAGTCCTCCCTCCACATGAGGACCGCCAGCGTGTGGC
Stim1BØStop rev	GCCACACGCTGGCGGTCCCTCATGTGGAGGGAGGACTC
mKate2 for	ATGGTGAGCGAGCTGATTAAG
mKate rev	TCTGTGCCCCAGTTTGCTAG
Stim1 rev	ACTCTGGCCCTGATGCAGA
Stim1 for	CTCAGCCATAGTCACAGTGAA
Stim1B_CADm (L373S&A376S) for	CAAAATGCAGAGAGGCAGAGCCTGGTGAGCAAGGAGGGGGCTGAGAA
Stim1B_CADm (L373S&A376S) rev	TTCTCAGCCCCCTCCTTGCTCACCAGGCTCTGCCTCTCTGCATTTG
SARAF for	GCCGCCACCATGGGCGCAGCCTGC
SARAF rev	CAGGATATCATTTGCCAGATC
Stim1B GSSL>AAAA for	CCTGGGATCTCAGAGAGCCGCCGCCAAGGCAAACAGGCTCTCTCTAGTAAGGG
Stim1B GSSL>AAAA rev	CCCTTACTAGAGAGAGCCTGTTTGCCTTGGCGGGCGGCGGCTCTCTGAGATCCCAGG

Primer name	Sequence (5'- 3') or Catalog number
Stim1B KANR>AAAA for	GGATCTCAGAGAGGATCATCTCTAGCCGCCGCCCTCTCT AGTAAGGGATTTGACC
Stim1B KANR>AAAA rev	GGTCAAATCCCTTACTAGAGAGGGCGGGCGGCTAGAGAT GATCCTCTCTGAGATCC
Stim1B_526* for	CAGGCTCTCTAGTAAGTGAGGATTTGACCCATTCCG
Stim1B_526* rev	CGGAATGGGTCAAATCCTCACTTACTAGAGAGCCTG
Amaxa for II (pMax)	GATTGGTGCGCCGTTTTAG
pMax rev	GATAATTCCTGCAGCCCG
STIM1/STIM1B_7A for	ATGGCCGCCGCCATTGTGTGTCGCCCTTGTCCATGC
STIM1_7A rev	GGCGGCCACGGCGGCAGTCATGATGAAGTGAGCAGG
STIM1B_7A rev	GGCGGCCACGGCGGCAGTCATGATGAAGTGGGCGG
5' UTR Stim1 for	TCTGGGATTTGCTTCTGGGA
5' UTR Alt exon for	GGCCCCTAGACAACATTTCA
5' UTR Alt exon for (II)	TGCCACAGTGAGGATGAGAA
5' UTR Alt exon rev	TCCTCCACGCTGATAAGCTT
Exon 2 rev	TCACTGTGACTATGGCTGAGA

2.11 Vectors & Constructs

Table 10 List of plasmid constructs used in this study

Name of the construct	Gene of Interest	Tag	Vector
YFP_hSTIM1_pEX	STIM1	YFP	pEX
YFP_hSTIM1B_pEX	STIM1B	YFP	pEX
YFP-hSTIM1Δ515_pEX	STIM1_514*	YFP	pEX
YFP-hSTIM1B Delta STOP_pEX	STIM1BØSTOP	YFP	pEX
YFP-hSTIM1 ID Mutant-pEX	STIM1_7A	YFP	pEX
YFP-hSTIM1B ID Mutant-pEX	STIM1B_7A	YFP	pEX
mSTIM1_pmax_IRES_mcherry	Stim1	IRES-mCherry	pMax
mSTIM1B_pmax_IRES_mcherry	Stim1B	IRES-mCherry	pMax
SP_mKate2_Stim1_pmax	Stim1	mKate2	pMax
SP_mKate2_mStim1B_pmax	Stim1B	mKate2	pMax
mSTIM1D515_IRESmcherry_pmax	Stim1_514*	IRES-mCherry	pMax
SP_mKate2_mSTIM1B Delta STOP_pMax	Stim1BØ*	mKate2	pMax
mSTIM1B Delta STOP_IRESmCherry_pMax	Stim1BØStop	IRES-mCherry	pMax
SP_mKate2_mSTIM1B CAD mutant_pMax	Stim1B_CADm	mKate2	pMax
mKate2-mSTIM1B STOP after Exon B_pMax	Stim1B_526*	mKate2	pMax

Name of the construct	Gene of Interest	Tag	Vector
mStim1B_GSSL>AAAA_IRES mCherry_pMax	Stim1B_GSSL>AAAA	IRES-mCherry	pMax
mStim1B_KANR>AAAA_IRES mCherry_pMax	Stim1B_KANR>AAAA	IRES-mCherry	pMax
mOrai1_IRES_GFP_pMax	Orai1	IRES-GFP	pMax
mOrai2s_IRES_GFP_pMax	Orai2	IRES-GFP	pMax
mOrai3_IRES_GFP_pMax	Orai3	IRES-GFP	pMax
hORAI1_IRES RFP_pCAGGS	ORAI1	IRES-RFP	pCAGGS
hORAI2_IRES RFP_pCAGGS	ORAI2	IRES-RFP	pCAGGS
hORAI3_IRES RFP_pCAGGS	ORAI3	IRES-RFP	pCAGGS
hSARAF_IRES_mCherry_pMax	SARAF	IRES-mCherry	pMax
SP_mKate2_Stim1_pWPXL	Stim1	mKate2	pWPXL
SP_mKate2_Stim1B_pWPXL	Stim1B	mKate2	pWPXL
SP_mKate2_Stim1BØStop_pWPXL	Stim1BØ*	mKate2	pWPXL
SP_mKate2_Stim1BCADm_pWPXL	Stim1B_CADm	mKate2	pWPXL

2.12 Cell culture

2.12.1 Cell culture medium

Table 11 List of media used for cell culture

Name of the Media	Manufacturer	Catalog number
GIBCO's Minimum Essential Medium (MEM)	Thermo Fisher Scientific	31095029
GIBCO's Dulbecco's modified eagle's medium (DMEM)	Thermo Fisher Scientific	41966029
GIBCO's Fetal Calf serum (FCS)	Thermo Fisher Scientific	10270106
GIBCO's Non-Essential amino acids (NEAA)	Thermo Fisher Scientific	11140050

2.12.2 Cell lines

Table 12 List of different cell lines & primary cells used in this study

Cell lines	Primary cells
MEF STIM1/ STIM2 -/- HEK 293 Wt HEK STIM1 / STIM2 -/- HEK ORAI/ORAI2 -/- HEK O1 SHSY5Y STIM1 / STIM2 -/- HEK O2	Hippocampal Neuronal culture

2.12.3 Transfection reagents & Kits

Table 13 List of Transfection kits used in this study

Name of the Kit	Manufacturer	Catalog Number
JetPRIME	Polyplus	114-15
JetOptimus	Polyplus	117-07
Opti-MEM	ThermoFisher Scientific	31985062

2.13 Experimental Model / Strain

Table 14 Animal model used in this study

Experimental model	Source	Strain code
C56BL/6N	Charles River	Strain code 027
C56BL/6 (10A Splice deificient mice)	Prof. Dr. Khaled Machaca	-

2.14 Softwares

Table 15 List of different software tools used for data analysis

Name of the Software component	Manufacturer
Patchmaster / Pulse	HEKA Electronik
GraphPad Prism 9	Graphpad
Igor Pro 7	WaveMetrics
CorelDRAW Graphic Suit 21	Corel
Image Lab	BioRad
ImageJ	National Institute of Health (NIH)

3. Methods

3.1 Generation of genetically modified recombinant DNA

3.1.1 Polymerase chain reaction (PCR)

Polymerase chain reaction, abbreviated as PCR, is enzyme-driven DNA replication, using an enzyme called DNA polymerase which amplifies the specific region of DNA from a template DNA using specific primer pairs that anchor to the region of interest. Each PCR cycle consists of three steps. The PCR steps include denaturation at a temperature of 94-98°C, also called as DNA melting step, through which the double-stranded DNA is denatured into two single-stranded DNA. Followed by, is the annealing step which mediates the binding of primers to each of the single-stranded DNA. The third step is the elongation step, where DNA polymerase acts on the DNA template and synthesizes new strands of DNA. Typically, 25 to 30 cycles have to be repeated to yield a new amplified product (DNA) from PCR. This principle was adapted to PCR protocol with program steps is shown below in the table.

Table 16 Pipetting Scheme for PCR reaction

Component	50 μ L reaction	Final concentration
H ₂ O	35.5 μ L	
5X Phusion HF buffer	10 μ L	1X
10mM dNTPs	1 μ L	200 μ M each
Forward primer	1 μ L	10 pmol/ μ l
Reverse primer	1 μ L	10 pmol/ μ l
Template DNA	1 μ L	50-100ng
Phusion DNA polymerase	0.5 μ L	0.02U/ μ L

Table 17 Reaction program of PCR amplification

Cycle step	Temperature	Time	Cycles
Initial denaturation	98°C	30s	1
Denaturation	98°C	30s	35
Annealing	60°C	30s	
Extension	72°C	1min/kb	
Final extension	72°C	10min	1
End	4°C	∞	

3.1.2 RNA isolation & cDNA synthesis

The freshly isolated tissues (cerebellum, hippocampus, cortex, olfactory bulb) or cells were homogenized in 800uL of TRIzol and RNA was isolated according to the manufacturer's instructions. The RNA purity and concentration were checked in a nanodrop one spectrophotometer. 0.8 µg of the isolated RNA was utilized to reverse transcribed into cDNA using Superscript II Reverse Transcriptase (Life Technologies) according to the manufacturer's instructions.

3.1.3 Analytical PCR

The Stim1 splice variants were detected from cDNA isolated from different brain regions by using splice-specific primers and an enzyme called Taq polymerase. The PCR protocol and program cycle are listed below.

Table 18 **Pipetting scheme for analytical PCR**

Component	20 µL reaction	Final concentration
dH2O	8 µL	
DreamTaq Green PCR Master MixTaq Green	10µL	1X
Forward primer	1µL	10 pmol/µl
Reverse primer	1µL	10 pmol/µl
cDNA	1-2µL	50-100ng

Table 19 **Reaction program for analytical PCR**

Cycle step	Temperature	Time	Cycles
Initial denaturation	98°C	30s	1
Denaturation	98°C	30s	35
Annealing	58-60°C	30s	
Extension	72°C	1min/kb	
Final extension	72°C	10min	1
End	4°C	∞	

3.1.4 Site-directed mutagenesis

Site-directed mutagenesis is a well-established method to introduce mutations (insertion, deletion, or substitution) within a plasmid DNA. Such mutations are achieved by quick change PCR using primer pairs of interest having a base exchange and a DNA polymerase. The PCR product, which is the methylated template plasmid, is then digested by a restriction enzyme called DpnI which cleaves the methylated DNA. The plasmid is re-ligated directly (if the

primers have 5' phosphate groups) or treated with phosphatase if the primer pairs have a blunt end. The PCR reaction protocol and the program conditions are shown below.

Table 20 **Pipetting scheme for PCR with Phusion DNA polymerase**

Component	50 μL reaction	Final concentration
H2O	35.5 μ L	
5X Phusion HF buffer	10 μ L	1X
10mM dNTPs	1 μ L	200 μ M each
Forward primer	1 μ L	10 pmol/ μ l
Reverse primer	1 μ L	10 pmol/ μ l
Template DNA	1 μ L	20-30ng
Phusion DNA polymerase	0.5 μ L	0.02U/ μ L

Table 21 **PCR reaction program with DpnI reaction**

Cycle step	Temperature	Time	Cycles
Initial denaturation	98°C	30s	1
Denaturation	98°C	30s	35
Annealing	58-60°C	30s	
Extension	72°C	1min/kb	
Final extension	72°C	10min	1
End	4°C	∞	
DpnI *1 μ L	37°C	2hr	1
End	4°C	∞	

3.2 Cloning & restriction digestion

The plasmid constructs used in this study were derived by molecular cloning using restriction enzyme digestion. Restriction enzymes, also known as restriction endonucleases cut the DNA at specific points that hydrolyze the phosphodiester backbone of DNA within or near the recognition sequence. The digested DNA fragments can be resolved by gel electrophoresis. The same restriction enzymes are used to cut the insert DNA and for the plasmid vector DNA (within multiple cloning sites). The resultant fragments could either be blunt end or sticky end depending on restriction enzymes. A template of the DNA cloning reaction scheme is shown below.

Table 22 **Pipetting scheme for cloning reaction**

Component	Volume
DNA	0.5-1 μ g
Restriction enzyme	0.5-1 μ L
Recommended restriction enzyme buffer	4 μ L
10X BSA	4 μ L
H ₂ O	Made up to 30 μ L reaction
Incubated at 37°C for 1.5-3 hrs	

3.2.1 Dephosphorylation of vector DNA

If a single restriction digestion is performed, the vector DNA could re-ligate on its own. Therefore, following the restriction digestion of vector DNA, phosphatase treatment has to be considered before setting up the ligation reaction. This step decreases the number of clones without the insert DNA and thereby reduces the number of colonies to be screened. Dephosphorylation reaction scheme is shown below and the reaction is incubated for 2 hours at 37°C

Table 23 **Pipetting scheme for dephosphorylation reaction**

Component	Volume
DNA following restriction digestion	30 μ L
Antarctic Phosphatase	2 μ L
Antarctic phosphatase buffer	4 μ L
H ₂ O	4 μ L

3.2.2 Gel electrophoresis:

Agarose gel electrophoresis is an effective and efficient method used to separate a mixed population of nucleic acids and works on the principle that the phosphate backbone of negatively charged DNA or RNA can be separated based on their size by applying an electric field. In general, the size of the pores generated by agarose determines the molecular sieving which retains DNA fragments of larger size compared to small DNA fragments resulting in the separation of DNA based on size. Agarose gels of higher percentage are more effective at separation of small DNA fragments between 100bp-500p. A standard marker is used to determine the size of each separated DNA fragment.

3.2.3 Agarose / GTQ gel

Agarose powder is dissolved in TAE buffer and boiled in a microwave for 30-45 sec until it is completely dissolved. The solution was allowed to cool down and DNA peqGREEN (1:20000) was added before casting the gel. The samples are mixed with loading buffer and loaded into the gel and set at a voltage of 90-120V for 30 minutes. When a screening of PCR reaction or a restriction digest, broad range agarose is used. When the separated DNA fragments have to be isolated and further used for ligation reaction, then GTQ agarose powder (Molecular Grade) is more effective as they have a low melting temperature and are free of DNAses and RNAses.

3.2.4 Gel extraction

After the separation of DNA fragments on a GTQ agarose gel, the desired DNA fragment is excised from the agarose gel with a clean scalpel and isolated under UV light. The DNA is extracted from the gel using the QIAquick Gel Extraction kit from Qiagen by following the manufacturer's protocol and finally eluted in 20-30 μ L of elution buffer.

3.2.5 Phosphorylation & Ligation

DNA ligation is the joining of two DNA fragments by forming two covalent phosphodiester bonds between 3' hydroxyl group of one nucleotide and 5' phosphate group of another driven by ATP dependent and catalysed by an enzyme called DNA ligase. While sticky end restriction digestion has 5' phosphate groups, blunt end ligation lacks them. Additionally, DNA amplified through PCR reaction also lacks 5' phosphate groups unless phosphorylated primers are used for the amplification reaction. In this regard, the insert DNA fragment must be phosphorylated by treatment with T4 polynucleotide Kinase before setting up the ligation reaction. To set up the ligation reaction, the molar ratio of insert and vector DNA is usually between 3:1 to 7:1 and incubated overnight at 16°C. The reaction scheme for kinase treatment and ligation reaction is shown below.

Table 24 **Pipetting scheme for ligation reaction**

Volume	Component
X μ L	Vector
Y μ L	Insert
4 μ L	10X T4 Ligase buffer
1 μ L	T4 Ligase
Made up 15 μ L	dH ₂ O

Volume	Component
X μ L	Eluted Insert DNA from the PCR reaction
3 μ L	10X T4 Ligase buffer
1 μ L	T4 PNK (Polynucleotide kinase)
Made up to 30 μ L	dH ₂ O
Incubated at 37°C for 30 min & heat inactivated at 60°C for 20 min, used this for further ligation step	
X μ L	Phosphorylated Insert DNA
Y μ L	Vector
1 μ L	10X T4 ligase buffer
1 μ L	T4 Ligase
Made up to 15 μ L	dH ₂ O

3.3 Bacterial transformation

The engineered recombinant plasmid containing the DNA insert of interest is introduced into a bacterium through a process called bacterial transformation where the bacterium can rapidly replicate the plasmid in large quantities upon adding the corresponding antibiotics. For this purpose, E. coli bacteria competent cells (DH-10, XL1 blue bacterial competent cells) were used.

The XL1 blue competent cells were thawed in ice for 15 minutes. 15 μ L of ligation mixture were added and mixed & incubated in ice for 25 minutes. Later, this mixture was briefly heat shocked at 42°C for 90 sec and kept in ice immediately for 5 minutes. Then, 1mL of LB medium is added and mixed. This mixture was incubated at 37°C for 1 hour. The mixture was centrifuged at 5000RPM for 5 minutes and the supernatant was decanted. The pellet is resuspended in 20-30 μ L LB medium and the bacterial suspension was spread out evenly on LB Agar plates with appropriate antibiotic selection and incubated overnight at 37°C.

3.3.1 Colony PCR

Colony PCR, similar to conventional PCR, is a method to rapidly screen the bacterial colonies that are allowed to grow on selective media following transformation and can be verified if the bacterial colonies contain the clones that carry the plasmid of interest with the desired insert. The bacterial colony is used directly as a template and a portion of the desired insert is amplified by using appropriate primer combinations to check the presence of the insert and also the orientation of the insert in the vector. The colony PCR reaction scheme and program conditions are shown below.

Table 25 Pipetting scheme for colony PCR reaction

Component	20 μ L reaction
H ₂ O	8 μ L
Forward primer (10pmol/ul)	1 μ L
Reverse primer (10pmol/ul)	1 μ L
Bacterial colony	1/2
Dream Taq green PCR master mix	10 μ L

Table 26 PCR reaction program for colony PCR

Cycle step	Temperature	Time	Cycles
Initial denaturation	98°C	3min	1
Denaturation	98°C	30s	35
Annealing	58-60°C	20-30s	
Extension	72°C	30-45s	
Final extension	72°C	10min	1
End	4°C	Infinite	

3.3.3 Sequencing

DNA sequence was confirmed by sending them to SEQLAB in Göttingen. The concentration of DNA (mini prep) was determined by Nanodrop one Spectrophotometer and the reaction scheme is shown below.

Table 27 Pipetting scheme for sequencing

Volume	Component
1-2 μ g	DNA
3-5 μ L	Primer of interest (10pmol/ul)
Made up to 15 μ L	dH ₂ O

3.3.4 Preparation of plasmid constructs – Minis & Maxis

Upon confirming with colony PCR, plasmid DNA is expanded from half the colony by inoculating in 5mL LB medium with appropriate antibiotics (100 μ g/ μ L for ampicillin, 60 μ g/ μ L for kanamycin) and incubated overnight at 37°C in an incubator shaker. The mini prep DNA is further processed from the bacterial culture using GeneJET plasmid miniprep kit (Thermo Scientific) and DNA is extracted from the bacterial culture according to kit instructions.

The isolation of plasmid DNA from the 200mL bacterial culture on a large scale is carried out using Qiagen plasmid Maxi kit (#12162) and it is termed as Maxi prep. The DNA is extracted from bacterial culture according to the kit instructions. The purity and concentration of DNA were measured using a Nanodrop one Spectrophotometer.

3.4 Cell culture

All the cell lines were maintained at 37 °C, 5% CO₂ in a humidified incubator with a humidity of 95% in their respective medium. Experiments with cell lines were performed under sterile conditions under a sterile bench with laminar airflow. All the adherent cells are detached and passaged by application of 0.05% trypsin-EDTA.

The following cell lines are utilized in this study and their specifications are given below.

HEK293 / HEK293-O1

Human Embryonic Kidney 293 (HEK293) cells are maintained in Minimum Essential Medium (MEM) supplemented with 10% FCS

MEF STIM1/STIM2-/- / HEK STIM1/STIM2-/-

Mouse Embryonic Fibroblast (MEF) STIM1/STIM2-/- & Human Kidney Fibroblast (HEK) STIM1/STIM2-/- cells were maintained in Dulbecco's Modified Eagle's Medium (DMEM) supplemented with 10% FCS.

SHSY5Y STIM1/STIM2-/-

SHSY5Y STIM1/STIM2-/- (cell line derived from human neuroblastoma) were maintained in DMEM medium supplemented with 1% non-essential amino acids (NEAA) & 10%FCS.

3.4.1 Cell transfection

Cell transfection is the process of introducing foreign nucleic acids like plasmid DNA or siRNA into the cytoplasm of a cell or transporting it to the nucleus allowing for transcription. This process allows for achieving overexpression of a protein of interest and investigating its function in an exogenous manner. Some of the common modes of transfection are calcium phosphate precipitation, lipofection, electroporation, and viral delivery. In this study, electroporation technique is adapted for electrophysiology experiments and lipofection is used for other experiments like TIRF, Immunostaining.

3.4.2 Electroporation

Uptake of plasmid DNA by application of an electric pulse which permeabilizes the cell membrane is the basis of transfection by electroporation. HEK 293 / HEK293T / HEK1 / HEK101 cells were trypsinized and 1×10^6 cells and were centrifuged at 1000RPM for 3minutes. The pellet was resuspended in 100 μ L transfection reagent (optiMEM or Nucleofactor kit V) and 2-4 μ g DNA was mixed gently. The mixture was then transferred to an electroporation cuvette and electroporation was carried out in Nucleofactor 2B using the program Q001. Following electroporation, mixture was resuspended in 600-650 μ L of prewarmed medium containing 50 μ M beta-mercaptoethanol. The cells were seeded dropwise in a 35mm dish with 1.5mL medium. Measurements were taken 24 hours after transfection. The Stim: Orai DNA concentration for all experiments was in the ratio of 3:1.

3.4.3 Lipofection

For Immunostaining experiments, immunoprecipitation experiments & screening of overexpression in western blotting, HEK, or MEF cells were lipofected using JetPRIME (Polyplus transfection) according to the manufacturer's protocol. Briefly, $1-1.5 \times 10^6$ cells were seeded on 100mm dishes with 9-10mL of the respective medium, the day before transfection. Transfection was carried out when the dish was 80% confluent. The volume of Jet prime buffer and jet prime reagent is calculated based on the amount of DNA to be transfected according to the kit instructions. The DNA-Jetprime reagent mixture is added to the dish dropwise and kept in an incubator. The medium is changed 4-6 hours after the transfection. Measurements were made 24 hours after transfection.

3.5 Protein biochemistry

3.5.1 Cell lysis

Mice brain tissues of different regions (cortex, cerebellum, olfactory bulb, hippocampus) were washed with PBS and homogenized with a 22 gauge needle 18x times in ice-cold lysis buffer (20mM Tris, pH 7.4, 100mM KCl, 10% glycerol (v/v), 1% n-dodecyl β -D-maltoside (DDM)) with 1X protease inhibitor complete (Sigma Aldrich). Usually, tissue: lysis buffer ratio is kept at 1:7 (100mg tissue lysed in 700 μ L lysis buffer). Later it was centrifuged at 18000 RPM, 4°C for 20 minutes. For the extraction of cell lysate from cultured cells, transfected cells were washed with PBS and detached with a cell scraper, and resuspended in 300-400 μ L of ice-cold

lysis buffer. Later it is centrifuged at 18000 RPM (4°C) for 20 minutes. The supernatant is transferred to a fresh tube and stored at -80°C until further use for the experiments.

3.5.2 Determination of protein concentration (BCA Assay)

Protein concentrations from cell lysates were determined using the Pierce BCA protein assay kit (Thermoscientific). Samples were diluted in three different concentrations (1:100, 1:200, 1:300). 25µl each of Protein standards in duplicates and samples in triplicates were prepared in 96 well plates and 200µL of freshly prepared BCA reaction solution was added to the wells and mixed thoroughly without bubble formation. The plate is incubated at 60°C for 45 minutes with gentle shaking. Absorbance is measured at 562nm in a plate reader and the protein concentration of the samples was extrapolated from the standard curve.

3.5.3 SDS PAGE Electrophoresis & Western blotting

SDS page is a vertical discontinuous electrophoresis-based separation method that separates the protein by molecular mass through the application of an electric field. Samples were boiled at 95°C for 5 minutes to initiate the denaturation. Heating mediates the disruption of secondary and tertiary structures of the protein by breaking the hydrogen bonds between them and thereby linearized protein is derived. For separation, a gel cassette is made with two different gel compositions of polyacrylamide – Stacking gel (top) and Separating gel (bottom). Denatured samples were loaded onto the casted gel placed in electrophoresis buffer connected with voltage. Application of voltage causes the migration of negatively charged molecules through the gel in the direction of positive charge. Stacking and separating gel differs in pore size, pH, and % of acrylamide. The stacking gel helps in stacking of protein and the separation of protein starts as they migrate into the separating gel which has basic pH.

In this study, protein samples of equal concentration (50-75µg) were taken for all groups and mixed with 2X Lamelli dye, and boiled at 95°C for 5 minutes to denature the protein. To detect the unglycosylated protein or native protein on the western blot, lysates were treated with Endoglycosidase H which reduced the glycosylation events. EndoH enzyme cleaves the entire glycan group from glycoprotein thereby deglycosylate the protein. Briefly, 10µL of denatured lysates were mixed with 2µL of 10X glycol buffer, and 2µL endoH enzyme and made up to 20µL with dH₂O and incubated for 10 minutes at 65°C before loading onto the SDS PAGE gel. Normally, 10% separating gel was cast with 4% stacking gel on top. When a clear separation

is required between two proteins that fall under small differences in their molecular weight range, 7% separating gel is preferred. Samples were loaded onto the gel and the chamber was filled with SDS running buffer. Initially, the voltage is set to 80V until the samples have migrated to the edge of the stacking gel. Then the voltage was increased to 120-140V and the samples were allowed to run till it reached the bottom of the gel. Along with the samples, 5 μ L of protein standard - Precision plus Protein dual color standard marker (Bio-Rad) is added to confirm the separation and subsequent detection of the protein of interest through antibodies. The stacking and separating gel composition are shown below.

Table 28 Composition of stacking & separating gel for western blot

Volume for 5mL		Component
1.25 mL		Stacking gel buffer
3.21 mL		H ₂ O
0.5mL		Acrylamide
37.5 μ L		10%APS
7.5 μ L		TEMED

Volume for 10mL	Volume for 10mL	Component
8% Gel	10% gel	
2.5mL	2.5mL	Separating gel buffer
2mL	2.5mL	Acrylamide
5.41mL	4.91mL	H ₂ O
75 μ L	75 μ L	10%APS
15 μ L	15 μ L	TEMED

3.5.4 Western blotting transfer and detection:

After the SDS PAGE electrophoresis step, protein from the gel is eluted and transferred onto Nitrocellulose (NC) or Polyvinylidene difluoride (PVDF) through electrophoretic transfer. This process is termed blotting. PVDF membranes were used while detecting hydrophobic proteins and it requires pre-soaking with methanol before the transfer. For the transfer process, the gel and membrane are prepared as sandwich between wet paper towels and packed in a cassette. The whole cassette is kept in a blotting transfer system and filled with 1X transfer buffer. A voltage of 0.35A was applied and a transfer time of 90 minutes was set and maintained at 4°C.

Following the transfer, the membrane was blocked with 5% skimmed milk prepared in 1X TBST and kept on a rocking shaker for 1 hour. The membranes were then incubated with

primary antibody solution (overnight at 4°C on a rotating shaker. The membrane is then washed 3 times with TBST. Later the membrane was incubated with a secondary antibody coupled with horseradish peroxidase for 1 hour at room temperature on a rocking shaker. The membrane is again washed 2 times with TBST and last washed with TBS

The detection of protein bands was performed using the Clarity Western ECL kit (Bio-Rad) by means of chemiluminescence. The kit contains the luminol or enhancer reagent and peroxide reagent. They were mixed in a ratio of 1:1 and prepared fresh for each use and spread over the membrane. The HRP linked to the secondary antibody activates the Luminol in the developing solution and produces a signal that is recorded digitally. The development of the blotting was carried out in the ChemiDoc XRS gel documentation unit (Bio-Rad) for 5-30 minutes with an exposure of 0.2-2s which can be optimized based on the antibody sensitivity and strength of the signal protein.

3.5.5 Immunoprecipitation

For immune precipitation experiments, mouse cerebellum tissues or Stim1/Stim1B overexpressed in MEF S1/S2 DKO cells were homogenized in ice-cold lysis buffer with freshly added protease inhibitors (1X protease inhibitor complete (Sigma Aldrich) and 1mM PMSF) and left in ice for 2 hours and later centrifuged for 20 minutes at 18000RPM, 4°C. The supernatant was collected in fresh tubes and protein concentration was determined using BCA assay. Immunoprecipitation of Stim1 or Stim1B or an unknown interacting partner is performed using Dyna A/G beads from Thermoscientific and performed according to the manufacturer's instructions. Briefly, lysates were diluted to 4mg/mL in ice-cold lysis buffer and precleared with Dyna A/G beads. 3µg of Stim1 antibody with N terminal epitope or C terminal epitope was mixed with Dyna A/G beads and incubated at 4°C for 4 hours. Later the precleared lysates were added to the antibody-beads mixture and incubated overnight in a hula mixer at 4°C. Beads were washed 5 times with lysis buffer and the crude protein mixture from the magnetic beads was eluted by mixing with 100µL 2X SDS-lamelli dye and incubated at 65°C for 15 minutes. Later the eluted samples were loaded onto the SDS PAGE gel and gel electrophoresis was performed. The gel is either stained with Coomassie or by silver staining. Additionally, western blotting was performed to screen the desired protein of interest in the eluted sample.

3.5.6 Coomassie staining

Coomassie Blue stain is efficient, quick, and easy to use and it stains the proteins separated by electrophoresis. The advantage of Coomassie stain is that it binds to basic and hydrophobic residues of proteins under acidic conditions and stains to blue color without protein modifications. After the electrophoresis, the gel is washed with distilled water and the gel is immersed in freshly prepared Coomassie stain and kept on a rocker with gentle shaking for 3-4 hours at room temperature. The Coomassie stain is decanted and rinsed the gel with distilled water for 30 minutes to 1 hour to reduce the background staining. The respective lanes were cut with a sterile scalpel to categorize based on molecular weights and the samples were sent to Dr. Vera Jankowski, Aachen University for MS analysis.

3.5.7 Silver staining

Although Coomassie staining is relatively easy, it is less sensitive to detect the low abundance of protein. In this case, silver staining is advantageous over Coomassie staining. Similar to Coomassie staining, silver staining is performed after SDS-PAGE electrophoresis using Pierce Silver staining kit from ThermoFisher Scientific (#24612) and the staining procedure is followed according to the kit instructions. Following the staining process, the respective lanes or bands were cut with a sterile scalpel to categorize based on molecular weights, and the samples were sent to Dr. Vera Jankowski, Aachen University for MS analysis.

3.6 Electrophysiology

Stim and Orai plasmids are co-expressed in HEK S1/2 DKO or HEK O1 cell lines using electroporation technique as described in the methods section. For electrophysiology experiments, the transfected cells were seeded on a 35mm culture dish in a low density with respective medium and kept in 37°C incubator for 18-24 hours before the recording. The recordings were obtained with an EPC-10 patch-clamp amplifier controlled by Patchmaster software (HEKA Electronics). The cells were gently washed twice with I_{CRAC} bath solution and 1mL of I_{CRAC} bath solution was added. Patch pipettes were pulled with a Micropipette puller (DMZ-universal puller) which has a resistance of 2-3 M Ω . The pipette was filled with I_{CRAC} internal solution (BAPTA or EGTA) and briefly dipped with coating solution (SigmaCote) before the recording, which can decrease the capacitance currents caused by pipette. A positive pressure was applied either by blowing or clamping the tube before approaching the cell to begin the whole-cell configuration. A transfected cell is selected and approached with the

pipette using coordinates while monitoring the pipette resistance. The positive pressure was released as soon as the tip of the pipette was in contact with the cell surface. The giga seal was achieved by applying negative pressure to the tube. Series resistance was compensated to 85%. All voltages were corrected for a liquid junction potential of 10 mV. Currents were filtered at 2.9 kHz (four-pole Bessel filter) and digitized at 10 kHz. Immediately after achieving the whole-cell configuration, linear voltage ramps from -150 mV to +150 mV (50ms duration) were applied every 2 s from a holding potential of 0 mV for the period of 150s /300s. For analysis of I_{CRAC} , currents were analyzed at -130 mV and for 300s after break-in using IgorPro 7 (Wavemetrics). The data was then imported into GraphPad 9 (Prism) for further statistical analysis and plotting.

3.7 Recordings of autaptic synaptic currents

Synaptic recordings were performed by our collaborator Dr. Yvonne Schwarz. The methods applied by the collaborating partners are described in the publication attached in the appendix section.

3.8 Behavioural Tests

The behavioural experiments were performed in collaboration with the AG Kirchhoff. The 10A control and Littermate animals were included in the animal licence 08/2021 (Mausverhaltenstests und Awake Imaging).

3.8.1 Elevated plus maze

The elevated plus maze test is used to measure anxiety-like behavior in rodents and the model helps us to assess the degree of aversion to spending time in open arms as the rodents tend to spend more time in the closed arms and correlate to anxiety-like symptoms. The elevated plus maze apparatus measuring 40 cm × 10 cm × 50 cm (lxbxh) (O'Hara & Co., Tokyo, Japan), consists of two open and two closed facing perpendicular to each other. The closed arms were enclosed by a black wall which is 20cm in height and provided with optimal lighting conditions (300 lux). The mice group that was used for this study was brought to the experimental room a day before the experiment to get accustomed to the environment. The mouse is placed in the central area facing toward one of the open arms. The number of entries into each of the arms

and its behavioral alterations were recorded for 5 minutes with a USB webcam connected to the computer which was placed above the apparatus. The time spent and distance traveled in the EPM and the number of entries into the open and closed arms were analyzed using the EthoVisionXT 11.5 video imaging system (Noldus Technology). The entry into the open arm is considered only when the center of the mouse's body is completely into the open arm. The maze was cleaned with 70% ethanol and dried up for 5 minutes after each test to prevent olfactory influence from the previously tested mouse.

3.8.2 Open field test

The open field test is another behavioral task to evaluate anxiety-like behavior in rodents. The mice were kept in the experimental room one day prior to the behavioral observation day. On the day of the experiment, the mice were put in the open field maze, which is made of a black square box measuring 50x50x38 (lxbxh). Mice were allowed to explore freely in the open field square after it was placed at the center of the square arena. The mice's behavior was recorded with a USB webcam connected to the computer and the video was analyzed using Ethovision CT11.5, Noldus technology. The total distance traveled and time spent in the central area of the square arena were determined. The maze was cleaned with 70% ethanol and dried up for 5 minutes after each test to prevent any olfactory influence from the previously tested mice.

3.8.3 Erasmus ladder

The Erasmus Ladder is a system to study motor performance and motor learning in rodents. Mice were allowed to run across a horizontal ladder from one goal box to another. Erasmus Ladder (ERLA-0010; Noldus Information Technology) was used for this experiment and Erasmus Ladder software (v1.1) was used to control the Ladder. A trial was considered complete when the mouse walked across the ladder to reach the goal box and each session consisted of 42 trials. The entire experimental paradigm was carried over 8 such sessions, of which the first 4 sessions were the training phase (Undisturbed) and the following 4 sessions were the perturbation phase where sudden challenges were imposed on the mice such as conditional stimulus (CS) for which a high-frequency tone was randomly presented to mice while walks across the ladder /unconditional stimulus (US) for which mice confronted a computer-controlled obstacle which would disturb their locomotion pattern / or paired stimulus for which a CS was presented followed by US with an interstimulus interval of 250 milliseconds which is programmed by the software in a randomized fashion. Each rung of the

ladder is connected to a sensor which enables measuring steps and step duration. The automated software enables us to understand the behavioral adaptation of the animal through several parameters such as step frequency, step type, back steps and jumps.

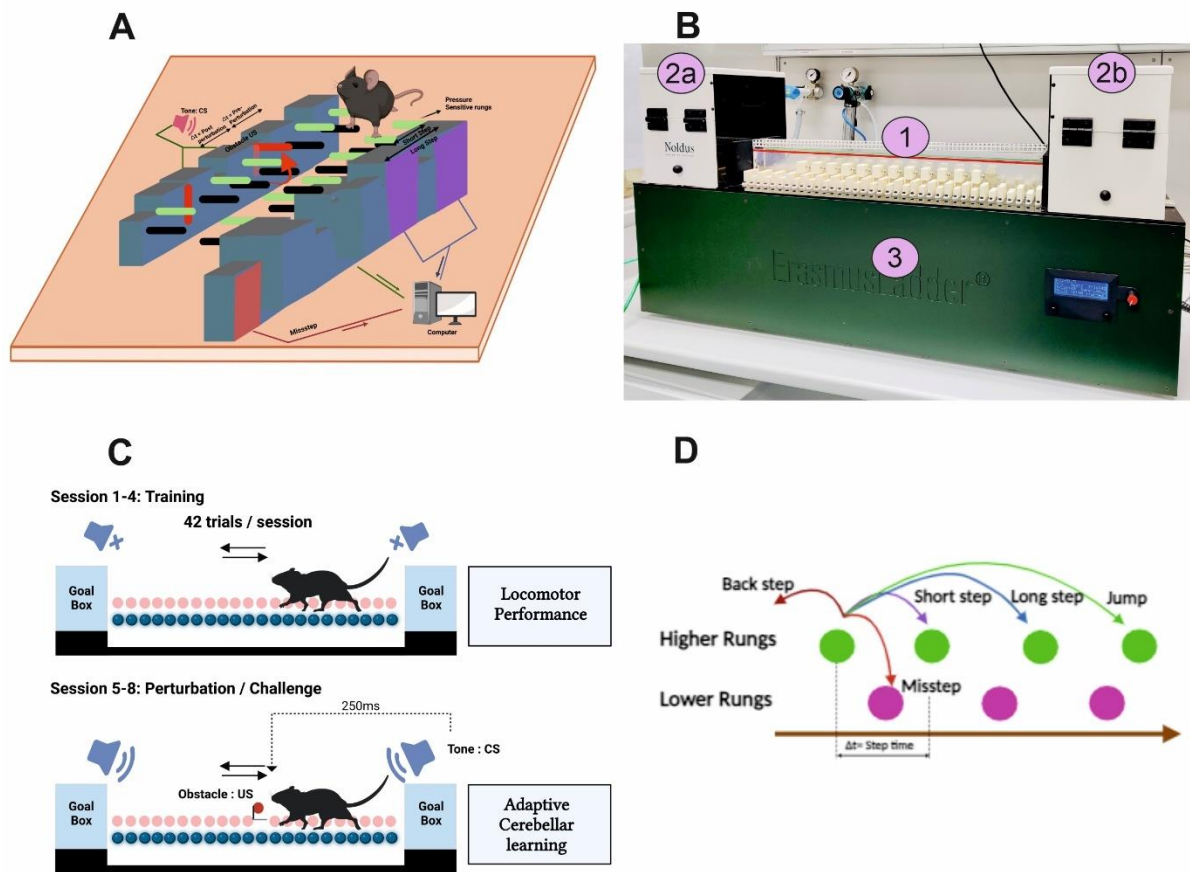


Figure 4 Cerebellar motor learning behavioral analysis using Erasmus Ladder. (A) A cartoon representation (not drawn to scale) showing mouse locomotor behavior on the Erasmus ladder setup. Step types are acquired using pressure-sensitive rungs (green) with step types categorized into short or long steps as shown in the cartoon. Locomotion performance is assessed by the percentage of missteps (black lower rung, marked light pink), Adaptive cerebellar learning is assessed by conditional paradigm involving a high pitch tone (conditional stimulus, CS) followed by activation of an obstacle (red, Unconditional stimulus, US). (B) The Front view of Erasmus ladder: 1- Ladder with pressure sensitive rungs, 2a&2b – goal boxes, 3- Base unit with LED display. (C) A side view representation of the Erasmus ladder showing default walking rungs (blue), missteps (grey), obstacles (red), goal boxes (light blue), and mouse (black). (D) Classification of steps assessment (Adapted from Sathyanesan et al., 2019).

Data from long or short steps that are classified as High-High (H-H), High-Low (H-L), Low-High (L-H), and Low-Low (L-L) and High – High (H-H) and High – Low (H-L) jumps during the undisturbed (no tone/obstacle), conditional stimulus (CS), unconditional stimulus (US) and paired stimulus were analyzed to observe the differences in the locomotive behavior between the groups. From these data, missteps were calculated by the ratio of cumulative long steps

(low) to all the long steps together and this is a critical measure to better understand reflexive motor learning and a reflection of cerebellar functioning. These experiments were started by myself and additional runs were performed by Christopher Farzenah and Wenhui Huang. The description of the Erasmus ladder experimental setup and procedure is described in Figure 4.

3.9 Immunostaining

Immunostaining in MEF STIM1^{-/-} STIM2^{-/-} cells was performed together with Maik Konrad. Briefly, MEF STIM1^{-/-} STIM2^{-/-} cells were seeded on 25 mm / 12 mm coverslips placed in 6 well cell culture plates and transfected with Stim1 / Stim1B pMax Ires-mCherry using Jet Prime transfection reagent. The medium changed 6 hours after the transfection and was maintained in an incubator at 37°C. 24 hours following the transfection, the medium was discarded and the cells were washed twice with 0.25mM Ca²⁺ Ringer solution. The cells were fixed with 3%PFA in 0.25mM Ca²⁺ Ringer solution and incubated at room temperature for 15 minutes. The cells were washed twice again with 0.25mM Ca²⁺ Ringer solution following fixation. The fixed cells were permeabilized with 0.1% TritonX100 in PBS for 15-20 minutes and washed briefly once with PBS. Unspecific epitope binding was blocked with freshly prepared 2% BSA in PBS and incubated for 30 minutes. Primary antibodies such as monoclonal Stim1 antibody (1:250) whose epitope is on the C terminus that detects conventional Stim1 and self-made B-specific antibody that detects Stim1B were prepared fresh in blocking solution and added to the coverslips and incubated overnight at 4°C. The cells were washed twice with PBS before adding the corresponding secondary antibody which was freshly prepared in blocking solution and incubated for 30 minutes at room temperature. The cells were washed thrice with PBS and the coverslip was dipped in distilled water. The coverslips were dried by gently pressing the edge to a paper towel. Finally, the coverslips were mounted on the slides with a DAPI mounting medium (Thermofisher Scientific). Images were acquired as z stacks on a confocal microscope LSM 700 (Zeiss) with a 3 63/1.4 NA oil objective.

Immunostaining in neuronal culture was performed by our collaborator Dr. Yvonne Schwarz. Briefly, mass hippocampal neurons were transfected with Stim1 / Stim1B – mKate2 cloned in pWPXL and maintained in culture for 10-14 days before the experiment. On the day of the experiment, the transfected neurons were washed with Ca²⁺ Ringer solution before fixing them in 4%PFA in PBS for 10 minutes at room temperature. Then the cells were quenched with 50mM NH₄Cl in PBS for 10 minutes. The fixed cells were permeabilized with 0.1%

TritonX100 in PBS for 15-20 minutes and washed briefly once with PBS. Unspecific epitope binding was blocked with freshly prepared 3% BSA in PBS and incubated for 30 minutes. Primary antibodies – Bassoon (1:500) and anti-RFP (1:500) were freshly prepared in blocking solution and added to the cells and incubated for 1.5 hours at room temperature. The cells were washed twice with PBS and incubated with the corresponding secondary antibody and incubated for 1.5 hours at room temperature. The neurons were washed thrice gently with PBS. Neurons were imaged either on a confocal microscope (LSM 710; Zeiss) using AxioVision 2008 software (Carl Zeiss) or an Axiovert200 (Zeiss), fluorescence was elicited with a Polychrome V monochromator (Till Photonics), and captured with an EMCCD camera (Evolve, Visitron, Germany).

3.11 Data Analysis & Statistics

The obtained data were analyzed using GraphPad PRISM version 8.0 and Microsoft Excel (Microsoft). Data consisting of two groups were analyzed using the student's t-test with Welch's correction for normal distribution and Mann-Whitney's correction for non-Gaussian distributed data sets. For the comparison of more than two groups, one-way ANOVA followed by Dunn's post hoc test. The data were obtained from more than 3 biological replicates. (*) represents data significant with $p < 0.05$, (**) represents data significant with $p < 0.01$ & (***) represents data significant with $p < 0.001$. The figures shown in this work were generated using CorelDRAW Graphic Suit 2021.

4. Results

4.1 Expression analysis of new splice variant of Stim1- Stim1B

4.1.1 Detection of a new mammalian-specific splice variant of Stim1 - Stim1B

Stim1 and Stim2 genes are encoded by a large genomic region which spans approximately 180Kbp and consists of 12 exons for both conventional variants (Williams et al., 2001). However, database mining has predicted multiple splice variants with alternatively inserted exons, and therefore a new exon nomenclature is shown in Figure 5A. The genomic region spanning exons 12 to exon 14 is a hotspot of mutually exclusive splice site except for exon A, due to which insertion of exon 13L (formerly named *exon III*, XM_006507533.3) resulted in muscle-specific expression of longer Stim1 protein, Stim1L which is already well characterized and described earlier in Darbellay et al., 2011, Saüc et al., 2015, Dyrda et al., 2020. Insertion of alternative exon A (new exon 11) between exons 10 and 12 resulted in an additional splice variant named Stim1A which is expressed predominantly in the testes, heart, and astrocytes and also partially present in lungs, kidney, intestine, and skeletal muscle. This variant was recently characterized and described by Knapp et al., 2022. Similarly, a variant of Stim2, Stim2.1 converted the SOCE from an activator to an inhibitor (Miederer et al., 2015). Predictions from the database show that insertion of the mutually exclusive alternative Stim1 exon 13B which encompasses only 36bp results in an mRNA codon frameshift and upon translation results in significantly shorter protein terminating at E540 thereby lacking 170 amino acids of conventional Stim1, but containing additional 26 residues as a resultant of translated exon B. Alina Gilson (B.Sc thesis 2016) was able to detect the presence of different splice variants of Stim1, namely Stim1A, Stim1B, and Stim1AB in mice using a diagnostic PCR strategy. Since several splice variants of Stim1 have been confirmed from database mining, with primer pairs it is expected to have multiple bands based on the size of exon A or B or L or AB, which are 310bp for Stim1 Wt, 346bp for exon13B splice variant, 402bp for Exon A, 438bp for exon AB and 613 bp for exon L. cDNA derived from cortex, cerebellum, hippocampus, and olfactory bulb along with lung, heart, liver, kidney, and intestine were used for diagnostic PCR using primer pairs BAN 1273 and 1274. All the samples displayed a prominent strong band of just over 300bp which corresponds to Stim1. Only the amplified products from the cortex, cerebellum, hippocampus, and olfactory bulb showed multiple bands

that run approximately above 340 bp which corresponds to the Stim1B band, Stim1A, and Stim1AB splice variants (Gilson's Bachelor thesis, 2016).

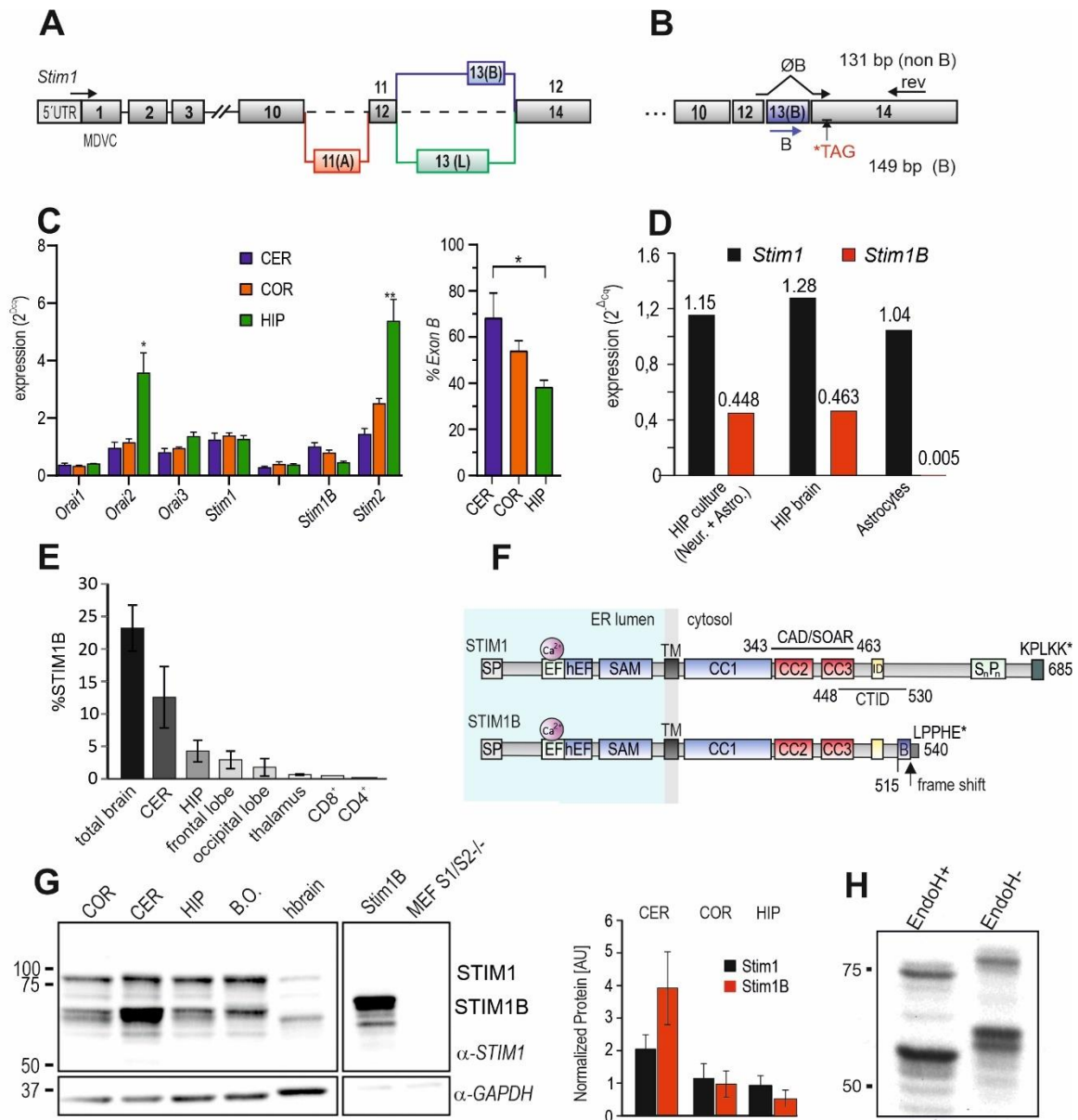


Figure 5 Expression of the alternative Stim1 exon 13B splice variant. (A) Schematic *Stim1* exon structure with conventional exons represented in grey. Highlighted in red is an alternative exon 11(A) and the mutually exclusive alternative splice variants exon 13 (B, blue) and exon 13(L, green). (B) Schematic representation of annealing sites of splice specific primers. (C) Quantitative expression levels normalized to TBP of *Orai1-3*, *Stim1*, *Stim2*, *Stim1B* and *Stim1 Δ B* in Cerebellum, Cortex and Hippocampus of mouse brain cDNA (left) and relative expression levels of *exon B* compared to total *Stim1* in mouse brain regions (\pm SD, n=3) (right panel). (D) Relative expression of *Stim1* and *Stim1B* in cDNA derived from hippocampal cultures, total hippocampus and astrocyte cultures, normalized to TBP. (E) Relative expression of *STIM1B* in cDNA derived from different brain regions of human post mortem brain (Cerebellum, hippocampus, frontal lobe, occipital lobe, thalamus and stimulated CD8⁺ and

CD4+ immune cells), normalized to TBP. **(F)** Schematic domain representation of Stim1 and Stim1B protein showing functional motives. Domain B in blue inserts downstream of residue 514 and adds 12 residues, resulting in a frame shift to terminate 14 residues downstream. **(G)** Western blot showing endogenous expression levels of Stim1 and Stim1B in lysates of Cortex, Cerebellum, Hippocampus, Olfactory bulb from mice, human post-mortem brain (n=3, left) and heterologous overexpression of Stim1B in HEKS1/2^{-/-} and MEFS1/2DKO (negative control) (right). Normalized expression level of Stim1 and Stim1B to GAPDH (house keeping gene) in different brain regions of mice (\pm SD, n=3), detected by an N-terminal Stim1 antibody. **(H)** Western blot showing expression levels of Stim1 and Stim1B in lysates of Cerebellum following PNGase treatment. qPCR data and analysis were done by Getrud Schwär and Kathrin Förderer. (Ramesh et al., 2021).

Using calibrated qRT PCR strategy, primer pairs that flank the regions between exons 12 and 14 were designed to be specific for Stim1B or the conventional variant, Stim1 ($\emptyset B$ = Wt) which skips Stim1B as shown in Figure 4 B.

To determine the expression levels of SOCE genes in the brain regions, a qRT PCR was performed with qRT PCR primers for Orai1, Orai2, Orai3, Stim1, and Stim2 along with splice-specific primer sets for Stim1B and the conventional variant Stim1 $\emptyset B$. The relative quantification of the expression of the SOCE genes is shown in Figure 5 C. Orai1 expression is relatively low in comparison to Orai2 and Orai3. Orai1 expression is same in Cerebellum, cortex, and hippocampus, while Orai2 expression is significantly higher in hippocampus when compared to cortex and cerebellum, which is in par with previously reported. Orai3 expression has a higher tendency in the hippocampus, however not significant when compared to other brain regions. Stim1 showed relatively equal expressions in all three brain regions; however, Stim2 expression varied in the brain regions with predominant expression shown in hippocampus. With cDNA samples performed with splice-specific primers, Stim1B showed dominant expression in cerebellum when compared to cortex and hippocampus. As the cumulative addition of individual $2^{\Delta Cq}$ values obtained for Stim1B and Stim1 $\emptyset B$ corresponded well with the $2^{\Delta Cq}$ value obtained for Stim1 calibrated quantitec primers, it is assumed to have equivalent primer efficiencies and therefore relative expression of Stim1B over Stim1 was calculated from these values. The calculated expression of Stim1B showed approximately 70% of total Stim1 in cerebellum, almost equal expression in cortex (54%), and 38% in hippocampus as shown in Figure 5C. These results are congruent with results obtained by diagnostic PCR performed by Gilson in 2016.

To further confirm that Stim1B is neuronal specific and not present in astrocytes as seen with qRT PCR results, cDNA was derived from cultures of astrocytes and hippocampal neuronal

cultures on astrocytic feeder layers and qRT PCR was performed to test the expression of Stim1B. While the astrocytes alone showed very minimal expression of Stim1B, the hippocampal neuronal cultures on the feeder cell layer showed prominent expression of Stim1B with $2^{\Delta Cq}$ of 0.448 which is more closely similar to $2^{\Delta Cq}$ value obtained with cDNA derived from murine hippocampus. From these results, it is clear that Stim1B is neuronal-specific and has a dominant expression of total Stim1 in cerebellum (Figure 5D).

In addition to the detection of Stim1B in murine brain regions, another diagnostic PCR with primer pairs of BAN 1269 and BAN 1345, and cDNA derived from human post-mortem brain as a template, additional band above Stim1 approximately around 510bp size which corresponds to the Stim1B as shown in the B.Sc thesis of Lukas in 2017. Following that cDNA derived different brain regions of the human post-mortem brain (Cerebellum, hippocampus, frontal lobe, occipital lobe, thalamus, and stimulated CD⁸⁺ and CD⁴⁺ immune cells) was used to perform qRT PCR and relative expression of Stim1B showed dominant expression in cerebellum as shown in Figure 5E. This confirms that Stim1B is also expressed in humans.

Following the confirmation of Stim1B in brain from mRNA expression analysis, Western blotting analysis was performed to confirm the presence of Stim1B at the protein level and correspond to the expected length of 540 amino acids as depicted in Figure 4F. The calculated molecular weight of Stim1 and Stim1B according to the length of the protein is 77kDa for Stim1 and 62kD for Stim1B. To confirm the presence of Stim1B at the protein level, protein lysates were made from murine brain tissue regions such as cortex, cerebellum, hippocampus, and olfactory bulb along with lysates obtained from human post-mortem brain samples and probed with Stim1 antibody from proteintech, whose antigenic epitope is located within the N terminus of Stim1 and therefore, detects both Stim1 and Stim1B variants. All the samples showed a prominent band at approximately above 75kDa which corresponds to the size of Stim1. In addition to that, below Stim1 is a band detected at a molecular mass approximately 15kDa lower, corresponding to the expected size of Stim1B (62kDa). To confirm that the lower band corresponds to the size of Stim1B, overexpression of Stim1B in MEF S1/2DKO cells also ran at the same size as the other sample lysates (Figure 5G). The detection of double bands for Stim1B could be due to an expected N-glycosylation event. To confirm this, lysates from Cerebellum were treated with EndoH from NEB before loading onto the gel and 1st lane in Figure 5H showed a marked reduction in the double band and also ran a little lower due to the

reduced glycosylation event. Additional bands are also detected between the Stim1 and Stim1B bands; these could be due to the Calpain/caspase cleaved Stim1. The bands below Stim1B could be from the degradation of the protein lysate. Human post-mortem brain lysates also show prominent bands for both Stim1 and Stim1B (Figure 5G). The band intensities corresponding to Stim1 and Stim1B from the different sample lysates were normalized over the housekeeping protein, GAPDH. The quantification analysis showed approximately 2-fold higher levels of Stim1B in cerebellum when compared to Stim1, while cortex, hippocampus, and olfactory bulb showed low levels of expression of Stim1B in comparison to Stim1, which is in good agreement with qPCR data. Overall, the mRNA expression analysis by quantitative PCR and protein analysis by Western blotting, confirms the existence of the splice isoform of Stim1 - Stim1B in mice and humans, with Stim1B being the predominant isoform in cerebellum but also showing significant protein levels in other brain regions.

Since the experiments were performed with both murine and human constructs, we adhere to the conventions, human constructs are mentioned as STIM & ORAI, and for murine constructs, it is denoted as Stim and Orai.

4.1.1 Stim1 B forms clusters upon store depletion and strongly co-localizes with Stim1

To test the localization and expression pattern of Stim1B, Stim1 and Stim1B cloned into pMax-IRES-mCherry were co-overexpressed in MEF S1/2 DKO cells using JetPRIME transfection method. The experiment was performed together with Maik Konrad. Cells were transferred to coverslips after 24 hours and activated with thapsigargin before being fixed with PFA. Fixed cells were immune stained with monoclonal C-terminal antibody and self-made B-specific rabbit polyclonal antibody (primary antibody) overnight and incubated with Alexa Fluor secondary antibody (Goat anti-rabbit Alexa fluor 488 and Goat anti-mouse Alexa Fluor 555) and mounted with DAPI. Images were acquired in LSM 700 (Zeiss). As shown in Figure 6A in the top panel without the addition of thapsigargin (Tg), both Stim1 and Stim1B show ER localization, and the signals extend along the ER. In the bottom panel of Figure 6C, upon the addition of Tg, an inhibitor of SERCA that induces the depletion of ER Ca²⁺ stores, both Stim1 and Stim1B were able to form clusters as seen along the ER extensions. The merged image along with the DAPI filter showed strong nuclear staining. Mander's coefficient was calculated to quantify the degree of colocalization of Stim1 and Stim1B. M1 denotes the measurement of

intensity of red over the green channel and M2 denotes the measurement of intensity of the green over the red channel. As seen in Figure 6 B and D, both Stim1 and Stim1B are strongly co-localized both in resting state and activated state with a co-efficient value approximately close to 1.

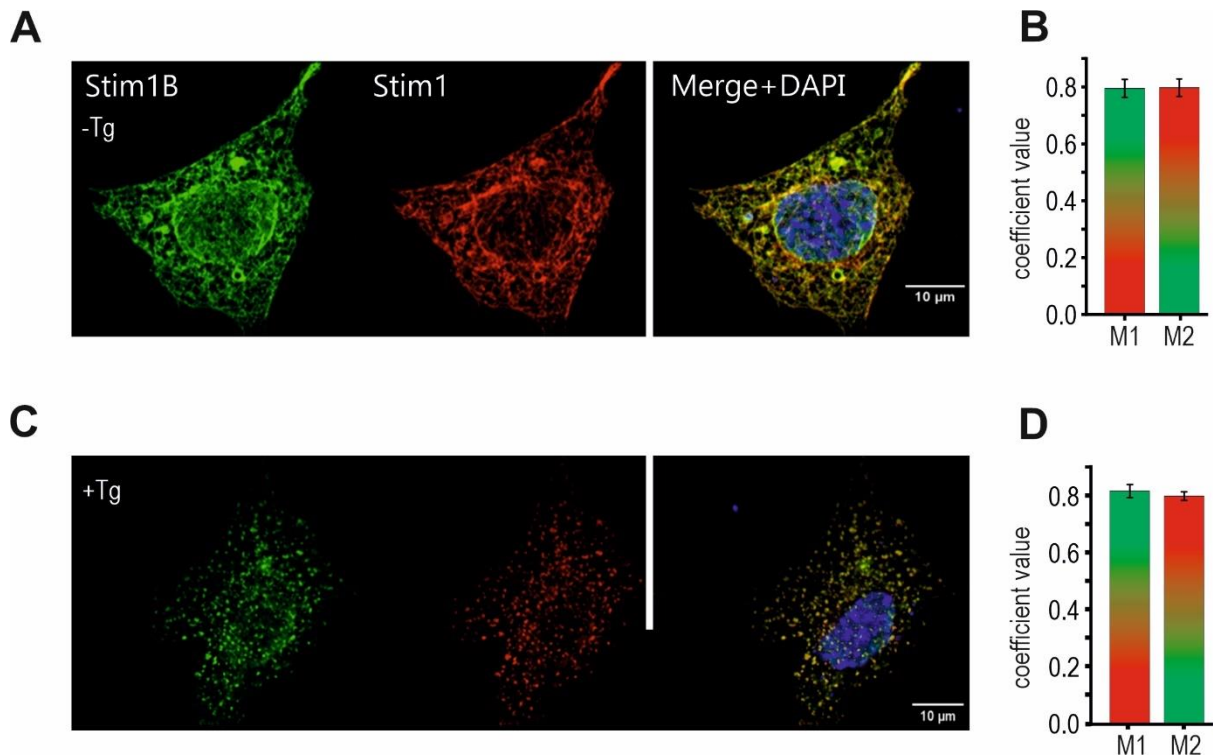


Figure 6 Colocalization analysis of Stim1B. (A) Exemplary images of STIM1B (green) and STIM1 (red) expressed in MEF S1/2 DKO before Tg application and merged images stained with DAPI (blue). (C) Images of activated STIM1B (green), STIM1 (red), and merged images with DAPI stained (blue) after Tg application. (B&D) The colocalization index is quantified using Manders' coefficients, where M1 represents the fraction of Stim1B overlapping with Stim1 and M2 is the fraction of Stim1 overlapping with Stim1B. Image & analysis made by Maik Konrad. (Ramesh et al., 2021).

4.2 Functional Characterization of Stim1B

4.2.1 STIM1B differentially activates ORAI channels

To understand the function of the new splice variant, Stim1B in activating SOCE, the STIM1/STIM1B was cloned into YFP tagged pEX vector (Maik Konrad). To begin with, YFP-STIM1 or YFP-STIM1B was co-transfected with ORAI1-pCAGGS-IRES-RFP in HEK 293 Wildtype cell line by electroporation in the ratio of 3:1 and 24 hours after transfection, cells were maintained in a bath solution containing 10mM Ca²⁺ and analyzed by patch-clamp

electrophysiology technique to record the ORAI1 mediated Ca^{2+} current induced by STIM1/STIM1B in the presence of 20mM BAPTA and 0.05mM IP3 in the pipette solution.

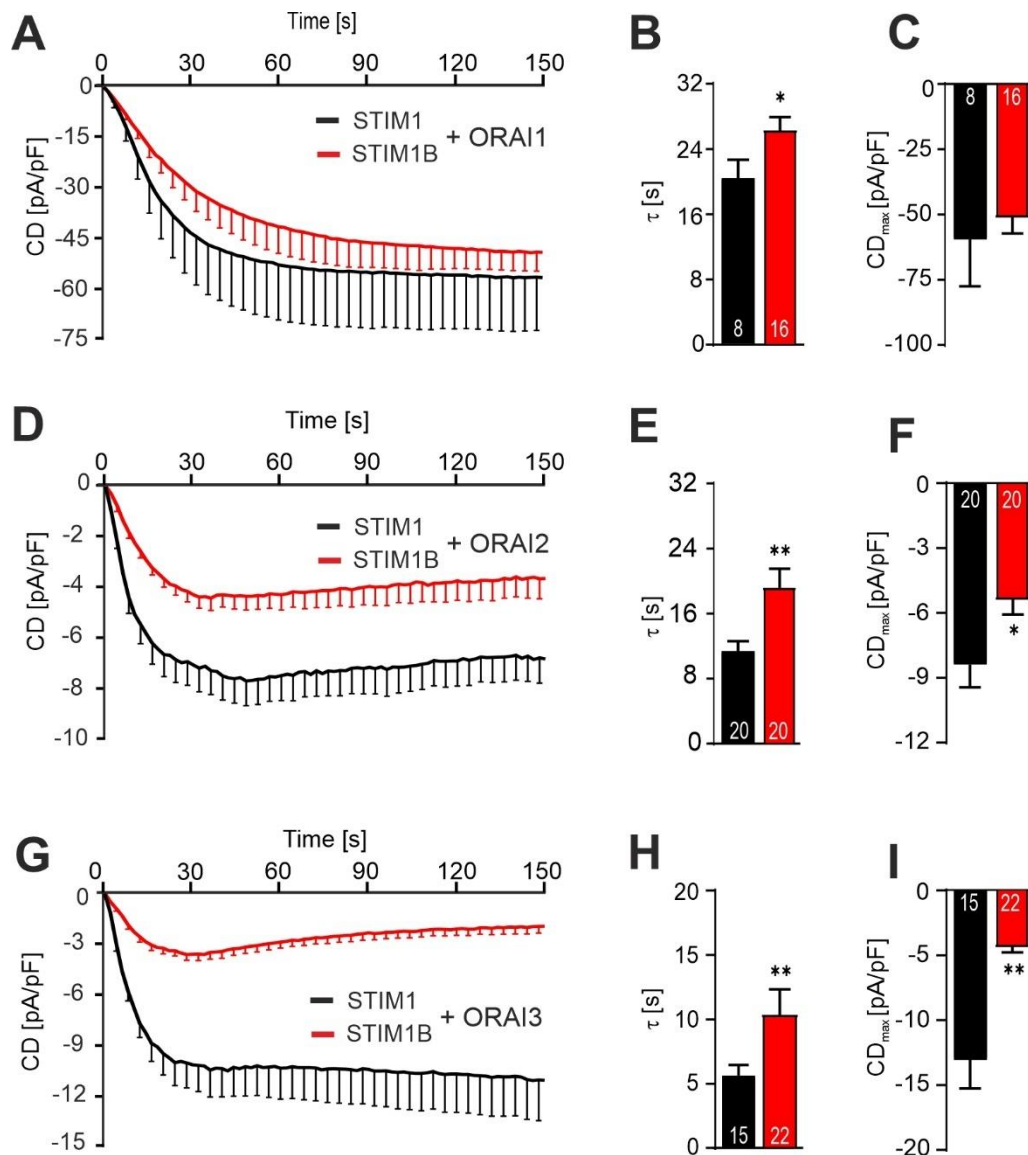


Figure 7 Overexpression of hSTIM1B attenuated hORAI2 and hORAI3 CRAC but not hORAI1 in HEK WT. (A) Average traces showing whole-cell current density (CD) over time extracted at -130mV in HEK Wt cells overexpressing hSTIM1 (black, n=8) or hSTIM1B (red, n=16) with hORAI1. (B & C) Bar graphs showing average tau and average maximal current density (CD_{max}) respectively calculated from (A). (D) Average traces showing whole-cell current density (CD) over time extracted at -130mV in HEK Wt cells overexpressing hSTIM1 (black, n=20) or hSTIM1B (red, n=20) with hORAI2. (E & F) Bar graphs showing average tau and average maximal current density (CD_{max}) respectively calculated from (D). (G) Average traces showing whole-cell current density (CD) over time extracted at -130mV in HEK Wt cells overexpressing hSTIM1 (black, n=15) or hSTIM1B (red, n=22) with hORAI3. (H & I) Bar graphs showing average tau and average maximal current density (CD_{max}) respectively calculated from (G). *p<0.05, **p<0.01, ***p<0.001 represents unpaired Student's t-test with Welch's correction. Data are represented as Mean±SEM.

Overexpression of STIM1/STIM1B with ORAI1 displayed a typical inward rectified current and led to large I_{CRAC} upon break-in. Currents were analyzed at -130mV and recorded for 150s. Tau was measured to measure the rate kinetics of activation of ORAI currents and analyzed average tau showed a slightly slower rate of activation with STIM1B overexpression with ORAI1 in comparison to STIM1 while the average maximal current density is not significantly altered as seen with average current traces (Figure 7 A-C).

To further investigate the function of activating other ORAI isoforms, STIM1 and STIM1B were co-transfected with ORAI2 or ORAI3 in HEK WT cells in a similar manner and currents were recorded 24 hours after transfection. Overexpression of STIM1B with ORAI2 displayed significantly smaller CRAC current in comparison to STIM1 overexpression with ORAI2 as seen in the average current traces in Figure 7 D. Tau analysis showed a significantly slow rate of activation of OrAI2 currents with overexpression of STIM1B in comparison to STIM1 overexpression and STIM1B's average maximal current density was significantly smaller than STIM1 as shown in Figure 7 E&F.

The co-overexpression of STIM1B with ORAI3 also resulted in significantly smaller CRAC compared to the co-overexpression of STIM1 with ORAI3. The activated currents mediated by STIM1B were slightly deactivating over the period of time, which might represent slow Ca^{2+} -dependent inactivation (SCDI) which was not seen with STIM1-mediated ORAI3 currents (Figure 7G). Average tau analysis showed that STIM1B exhibits a significantly slower rate of activation of ORAI3-mediated Ca^{2+} currents and average maximal density was strongly affected by STIM1B overexpression in comparison to STIM1 (Figure 7H, I). Although STIM1B is able to activate I_{CRAC} upon store depletion, the observed reduction of CRAC current is only seen in ORAI2 and ORAI3, but not ORAI1. The presence of endogenous STIM 1/2 and ORAI homologs in the HEK wildtype cells could be masking the phenotype of STIM1B.

In the aim of identifying the sole role of STIM1B in activating SOCE, further patch clamp experiments are performed in HEK S1/2 DKO cells. As this cell line lacks endogenous STIM1/2, measured CRAC currents will only be due to the activity of the overexpressed constructs.

STIM1 and STIM1B were co-overexpressed with ORAI1 or ORAI2 in the HEK S1/2 DKO cell line and cells were measured 24 hours after transfection. Overexpression of STIM1B with

ORAI1 displayed a slightly larger I_{CRAC} compared to STIM1 overexpression, although with a slower rate of activation of ORAI1 currents. Average maximal current density showed no differences between STIM1 and STIM1B. The current density mediated by STIM1 was approximately 14% higher in HEKS1/2DKO than HEK 293 cells and the current density mediated by overexpression of STIM1B was approximately 40% higher in HEKS1/2 DKO than in HEK293 cells. Due to the absence of STIM2, it is anticipated that overexpression of STIM1 alone can lead to increased Ca^{2+} entry. In the absence of STIM2, STIM1B overexpression led to significantly increased current density (Figure 8 A-C).

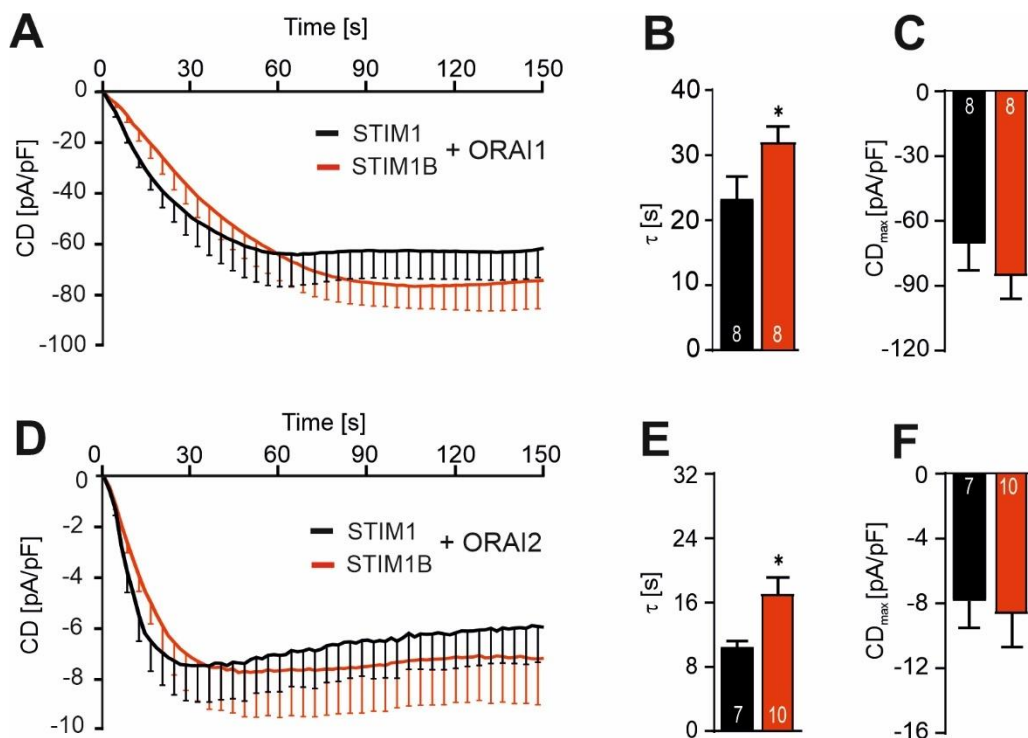


Figure 8 Overexpression of hSTIM1B did not alter the hORAI1 and hORAI2 CRAC in HEKS1/2 DKO. (A) Average traces showing whole-cell current density (CD) over time extracted at -130mV in HEK S1/S2 DKO cells overexpressing hSTIM1 (black, n=8) or hSTIM1B (red, n=8) with hORAI1. (B & C) Bar graphs showing average tau and average maximal current density (CD_{max}) respectively calculated from (A). (D) Average traces showing whole-cell current density (CD) over time extracted at -130mV in HEK S1/2 DKO cells overexpressing hSTIM1 (black, n=7) or hSTIM1B (red, n=10) with hORAI2. (E & F) Bar graphs showing average tau and average maximal current density (CD_{max}) respectively calculated from (D). *p<0.05, **p<0.01, ***p<0.001 represents unpaired Student's t-test with Welch's correction. Data are represented as Mean±SEM.

The overexpression of STIM1 and STIM1B with ORAI2 in HEKS1/2 DKO showed similar current amplitude with a tendency in the delayed activation rate of ORAI2 mediated currents as seen in Figure 8D. In contrast to the data recorded in HEK 293 cells which displayed a strong

phenotype of STIM1B over ORAI2, the analysis of currents recorded from HEKS1/2DKO cells shows that average maximal current density was relatively similar between the groups and tau analysis showed delayed activation rate kinetics of ORAI2 with STIM1B overexpression compared to STIM1 overexpression (Figure 8E, F). Unlike ORAI1, ORAI2 mediated current amplitude recorded in HEKS1/2 DKO cells was not significantly different from HEK293 cells.

4.2.2 Murine Stim1B also differentially activates Orai channels

To test the functionally active murine Stim1B variant, murine Stim1B is cloned by insertion of exon B (36bp) with primer pairs BAN1395 and BAN1396 using pMax-mSTIM1-IRES-mCherry as a template (prepared by Lukas Jarzembowski in his Bachelor Thesis, 2017). Stim1 and Stim1B were co-overexpressed with pMax-Orai1-IRES-GFP in the ratio of 3:1 in HEKS1/2 DKO cells using electroporation and cells were measured 24 hours after transfection. Cells were maintained in a bath solution containing 10mM Ca^{2+} and the patch pipette contained 20mM BAPTA and 0.05mM IP3. Currents were analyzed at -130mV and recorded for 300s. Stim1B overexpression led to a decreased rate of activation of Orai1 I_{CRAC} , however current densities at the end of 300s were similar to Stim1 mediated Orai1 currents with no significant differences in average maximal current density. In addition to that, Stim1-induced currents displayed approximately 22% rundown of the activated currents which may represent slow Ca^{2+} dependent inactivation (SCDI), while Stim1B-induced currents displayed only 4% rundown (Figure 9A-D).

The co-overexpression of Orai2 with Stim1B resulted in a significantly smaller CRAC current compared to Stim1 overexpression. Analysis of tau from current traces showed a 47% slower kinetic rate of activation of Orai2 compared to Stim1. The average maximal current density was significantly reduced by approximately 60% compared to Stim1. Stim1B-induced current displayed a significantly reduced rundown/SCDI by approximately 70% compared to those of Stim1 (Figure 9E-H).

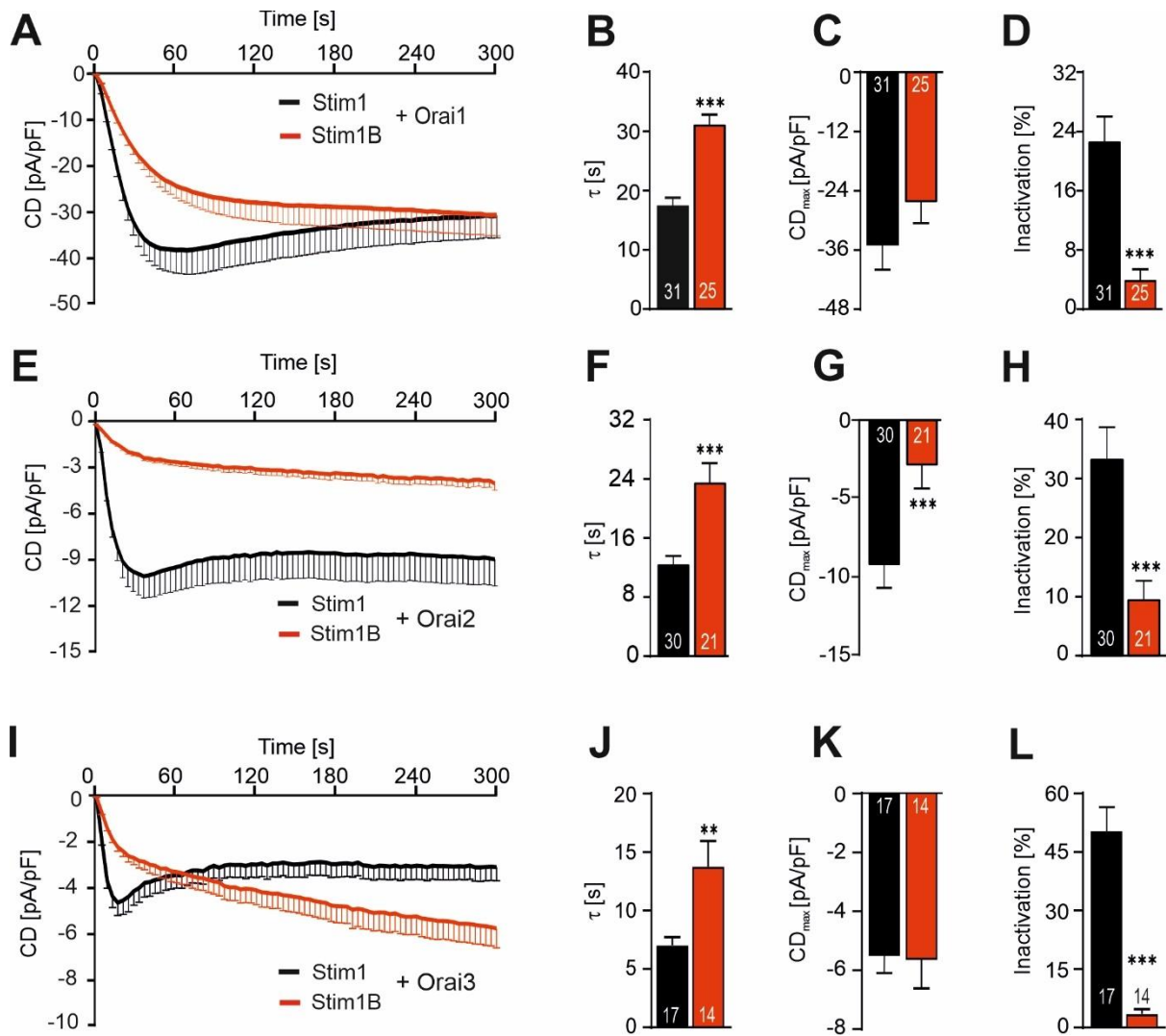


Figure 9 Overexpression of mSTIM1B differentially regulates mORAI1,2, & 3 channels at 20mM BAPTA in HEK S1/2 DKO. (A) Average traces showing whole-cell current density (CD) over time extracted at -130mV in HEK S1/2 DKO cells overexpressing mStim1 (black, n=31) or mStim1B (red, n=25) with mOrai1. (B, C, & D) Bar graphs showing average tau, average maximal current density (CD_{max}), and average % inactivation respectively calculated from individual cells measured in (A). (E) Average traces showing whole-cell current density (CD) over time extracted at -130mV in HEK S1/2 DKO cells overexpressing mStim1 (black, n=30) or mStim1B (red, n=22) with mOrai2. (F, G, & H) Bar graphs showing average tau and average maximal current density (CD_{max}) average % inactivation respectively calculated from individual cells measured in (E). (I) Average traces showing whole-cell current density (CD) over time extracted at -130mV in HEK S1/2 DKO cells overexpressing mStim1 (black, n=17) or mStim1B (red, n=14) with mOrai3. (J, K, & L) Bar graphs showing average tau and average maximal current density (CD_{max}) average % inactivation respectively calculated from individual cells measured in (I). *p<0.05, **p<0.01, ***p<0.001 represents unpaired Student's t-test with Welch's correction. Data are represented as Mean±SEM. (Ramesh et al., 2021).

Stim1 co-expression with Orai3 showed an overall faster onset of activation of I_{CRAC} compared to the other two Orai isoforms with a significantly increased SCDI/ rundown of the activated

currents over a period of ≈ 260 s. In contrast, Stim1B co-expression with Orai3 exhibited significantly slower kinetics of I_{CRAC} . The analysis from Stim1B mediated I_{CRAC} showed that the average rate kinetics of activation of Orai3 was significantly reduced by half in comparison to Stim1, the average maximal current density was relatively similar to Stim1 and most importantly Stim1B exhibited virtually no rundown/SCDI as seen in Figure 9I-L. The average tau of Stim1 mediated current was decreased in Orai2 and Orai3 when compared to Orai1; a similar pattern is observed with human STIM1 and it is congruent with the previously reported studies. A similar degree of reduction of tau is seen with Stim1B (both murine and human) and it argues for an overall similar affinity of Stim1B's CAD domain to Orai homologues.

From the data of human and murine Stim variants in HEKS1/2 DKO cells, it is notable that human STIM1 mediated ORAI1 currents were approximately 50% smaller compared to mouse Stim1 mediated Orai1 currents while Stim1B mediated Orai1 currents were 70% smaller compared to STIM1B mediated Orai1 currents. Similarly, Stim1-mediated Orai2 currents were 17% bigger compared to STIM1-mediated ORAI2 currents, while Stim1B-mediated Orai2 currents were 55% smaller compared to STIM1B-mediated ORAI2 currents.

Altogether, Stim1B is able to activate I_{CRAC} despite the truncated C-terminus, through delayed rate of activation of all Orai homologs and reduced current amplitude in Orai2 and Orai3, but not Orai1 isoform.

4.2.3 Stim1B showed significantly reduced Orai1 CRAC and does not exhibit SCDI under low buffering conditions

The slower rate of activation was observed for both murine and human Stim1B when it is co-expressed with all three Orai homologs (Figures 8&9) under strong Ca^{2+} buffering conditions. However, with a higher concentration of BAPTA in the patch pipette, measured Orai/ORAI currents mediated by Stim1/B & STIM1/B are significantly larger and might mask a physiological function; in addition, high BAPTA buffering is not ideal for observing slow or fast Ca^{2+} -dependent inactivation. Therefore, the buffering capacity during the recording is reduced by replacing the 20mM BAPTA with 2mM EGTA, a slow Ca^{2+} buffer in the intracellular solution in the patch pipette, thus larger microdomains of calcium remain around the channel pore. pMax-Stim1-IRES-mCherry /pMax-Stim1B-IRES-mCherry was co-expressed with pMax-Orai1-IRES-GFP in HEKS1/2 DKO cells in the same ratio as previously described and patch recordings were performed 24 hours after the transfection in the presence

of 2mM EGTA in the intracellular solution. After the break-in, Stim1 expressed cells led to fast activation of Orai1 current with average current density reaching approximately -40pA/pF in less than a minute and showed a prominent, steady slow Ca^{2+} dependent inactivation up to approximately 75% rundown, while Stim1B overexpression led to significantly reduced current density reaching only 22% of Stim1's average maximal current density at 300s with significantly slower activation rate kinetics, approximately 65% slower than Stim1 and significantly less inactivation with approximately 50% less than Stim1 (Figure 10A-D).

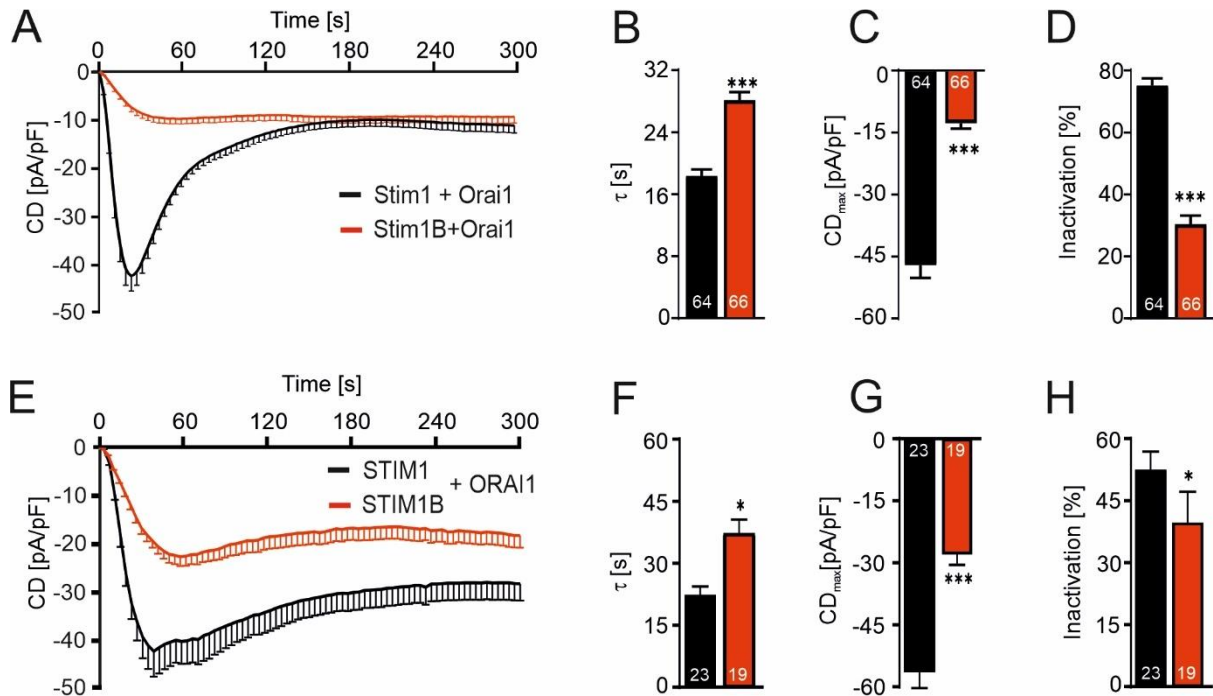


Figure 10 Overexpression of hSTIM1B/mStim1B reduced SCDI phenotype in HEK S1/2 DKO under 2mM EGTA conditions. (A) Average traces showing whole-cell current density (CD) over time extracted at -130mV in HEK S1/2 DKO cells overexpressing mStim1 (black, n=64) or mStim1B (red, n=66) with mOrai1. (B, C, & D) Bar graphs showing average tau, average maximal current density (CD_{max}), and average % inactivation respectively calculated from individual cells measured in (A). (E) Average traces showing whole-cell current density (CD) over time extracted at -130mV in HEK S1/2 DKO cells overexpressing hSTIM1 (black, n=30) or hSTIM1B (red, n=22) with hORAI1. (F, G, & H) Bar graphs showing average tau and average maximal current density (CD_{max}) average % inactivation respectively calculated from individual cells measured in (E). * $p < 0.05$, ** $p < 0.01$, *** $p < 0.001$ represents unpaired Student's t-test with Welch's correction. Data are represented as Mean \pm SEM. (Figure A-D, Ramesh et al., 2021).

4.2.4 STIM1B also significantly reduced Orai1 I_{CRAC} and reduced SCDI, but not as strong as murine Stim1B

Since STIM1B mediated ORAI1 CRAC was not significantly different with respect to current amplitude and SCDI under strong BAPTA conditions and that Stim1B uncovered its physiological phenotype under low buffering conditions, it is important to test the STIM1B

effect on the size of the current, activation kinetics and SCDI of ORAI1 under low EGTA conditions. Therefore YFP-STIM1/YFP-STIM1B were transfected with pCAGGS-ORAI1-IRES-RFP in HEKS1/2 DKO cells as previously described and patch clamp recordings were performed in the presence of 2mM EGTA with IP3 in the patch pipette. The average current density of ORAI1 mediated by STIM1 overexpression reached approximately 40pA/pF in less than a minute after the break-in, which is quite similar to Stim1 mediated Orai1 currents and showed a prominent SCDI with a rundown reaching approximately 50%, although not as significant as Stim1. In contrast to STIM1, STIM1B resulted in a significantly slower rate of activation of ORAI1 CRAC reaching only half the maximal current density of STIM1 and significantly reduced SCDI which is quite similar to Stim1B, although the current densities are approximately 2 times bigger than Stim1B (Figure 10E-H).

4.2.5 Fast Ca^{2+} dependent inactivation (FCDI) is not altered by Stim1B

To assess the potential influence of Stim1B on Fast Ca^{2+} -dependent inactivation (FCDI), a series of experiments were conducted involving Stim1 and Stim1B co-expression with Orai1 in HEKS1/2 DKO cells. Electroporation was used for transfection, and recordings were performed 24 hours post-transfection. Orai1 currents were recorded using whole-cell patch clamp configuration under two distinct conditions: in the presence of 20mM BAPTA or 2mM EGTA in the patch pipette. Additionally, a voltage pulse of -100mV was applied at the end of each recording, 30 seconds after which the plateau over peak was calculated for each experimental group.

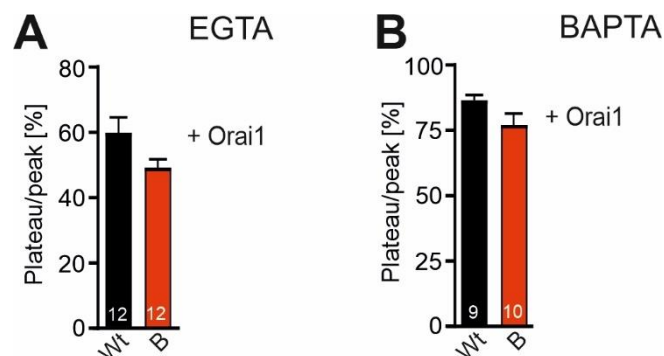


Figure 11 Analysis of Fast Ca^{2+} -dependent inactivation (FCDI). (A) Bar graph showing average % Plateau/peak ratio with Stim1 co-expressed with Orai1 (black, n=12), or Stim1B coexpressed with Orai1 (red, n=12) in HEKS1/2 DKO cells under BAPTA conditions (B) Bar graph showing average % Plateau/peak ratio with Stim1 co-expressed with Orai1 (black, n=9), or Stim1B coexpressed with Orai1 (red, n=10) in HEKS1/2 DKO cells under EGTA conditions.

Under EGTA conditions, where Ca^{2+} buffering was less pronounced, the results indicated that cells overexpressing Stim1/Orai1 displayed an inactivation to approximately 60% of the peak value, while cells overexpressing Stim1B/Orai1 exhibited inactivation to approximately 49% of the peak value (Figure 11A). Conversely, when BAPTA was used as a stronger Ca^{2+} buffer, the inactivation percentages were more pronounced. Stim1/Orai1 overexpressed cells exhibited inactivation to about 87% of the peak value, whereas Stim1B/Orai1 overexpressed cells displayed inactivation to approximately 77% of the peak value (Figure 11B). When comparing the two conditions, the strong Ca^{2+} buffering provided by BAPTA led to approximately 33% more inactivation in cells expressing Stim1, and approximately 38% more inactivation in cells expressing Stim1B. Overall, the results indicated that Stim1B did not significantly alter Fast Ca^{2+} -dependent inactivation (FCDI) when compared to Stim1.

4.3 Investigation of Molecular mechanism regulating Stim1B's phenotype

4.3.1 Reduced SCDI function mediated by STIM1B is not altered by SARAF

Slow Ca^{2+} -dependent inactivation has been previously described by several research groups and has been poorly understood on a molecular level. One potential candidate to be mediating SCDI is the protein SARAF (SOCE-associated regulatory factor). SARAF is a resident protein within the endoplasmic reticulum that engages with the C-terminal inhibitory domain (CTID) of STIM1. The CTID spans amino acids 448 to 530 and comprises two distinct segments: one from amino acids 448 to 490, which confines SARAF's interaction to the STIM-Orai Activating Region (SOAR), and another from amino acids 490 to 530, enabling SARAF to interact with the SOAR domain. This interplay between SARAF and the CTID governs the modulation of slow calcium-dependent inactivation (SCDI) of Orai1 channels, thereby influencing the regulation of SCDI facilitation or inhibition (Palty et al., 2012, Jha et al., 2013). Since the entire domain of CTID is not intact in STIM1B as the last common amino acid between STIM1 and STIM1B is aa514, potentially the SARAF docking site could be affected in STIM1B. Therefore, an extensive set of patch clamp recordings was performed to test if the altered interaction with SARAF may account for the SCDI phenotype as shown earlier. YFP-STIM1/STIM1B in pEX is co-expressed with SARAF-mCherry in HEK cells stably expressing ORAI1 and whole cell patch clamp recordings were performed in the presence of EGTA in the patch pipette.

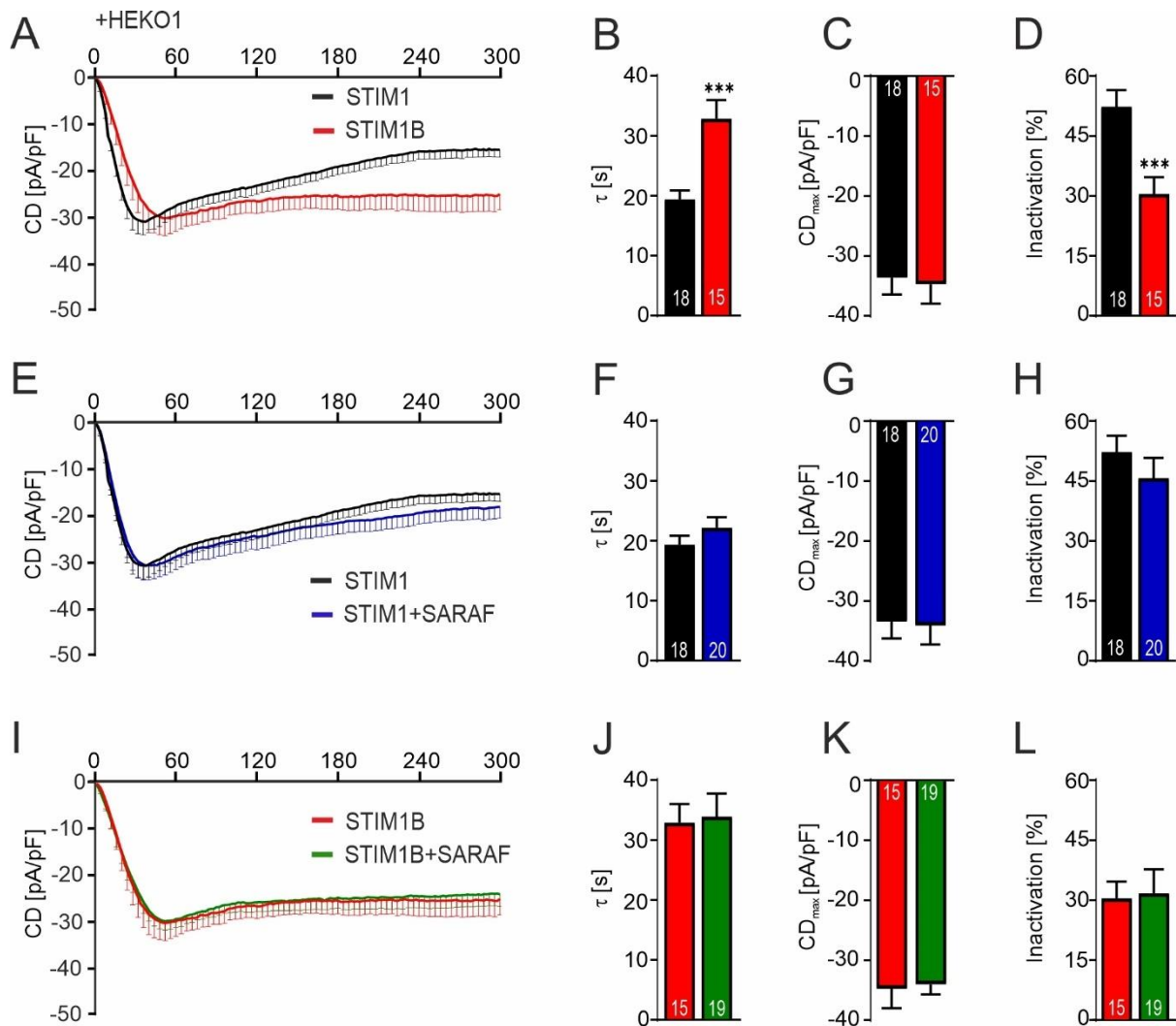


Figure 12 SARAF overexpression with STIM1B did not alter STIM1B phenotype in HEKO1 in the presence of EGTA. (A) Average traces showing whole-cell current density (CD) over time extracted at -130mV in HEKO1 cells overexpressing hSTIM1 (black, n=18) or hSTIM1B (red, n=15). (B, C, & D) Bar graphs showing average tau, average maximal current density (CD_{max}), and average % inactivation respectively calculated from individual cells measured in (A). (E) Average traces showing whole-cell current density (CD) over time extracted at -130mV in HEKO1 cells overexpressing hSTIM1 (black, n=18) or hSTIM1 with SARAF (blue, n=20). (F, G, & H) Bar graphs showing average tau and average maximal current density (CD_{max}) average % inactivation respectively calculated from individual cells measured in (E). (I) Average traces showing whole-cell current density (CD) over time extracted at -130mV in HEKO1 cells overexpressing hSTIM1B (black, n=15) or hSTIM1B with SARAF (green, n=19). (J, K, & L) Bar graphs showing average tau and average maximal current density (CD_{max}) average % inactivation respectively calculated from individual cells measured in (I). *p<0.05, **p<0.01, ***p<0.001 represents unpaired Student's t-test with Welch's correction. Data are represented as Mean±SEM.

Average current traces of ORAI1 mediated by both STIM1 and STIM1B reached approximately -34pA/pF with no significant differences in average current maximal density, although the kinetics of activation of STIM1 is approximately 40% faster than STIM1B and approximately 43% less inactivating with STIM1B mediated Orail currents in comparison to

STIM1(Figure 12A-D). In addition to that, with strong overexpression of ORAI1, kinetic differences in activation became smaller. Overexpressing with SARAF, both STIM1, and STIM1B were incomparable with respect to kinetics of activation, average maximal current density, and SCDI (Figure 12E-L). Surprisingly, no significant differential role in SARAF-mediated inhibition was detected between STIM1 and STIM1B, indicating that SARAF may not be a primary contributor to the observed SCDI phenotype.

4.3.2 Mutation of Negatively Charged Residues Modifies CDI, but the STIM1B Phenotype Remains Unchanged

As reported previously, in addition to SARAF regulation, a highly negatively charged region within the inactivation domain of STIM1 (475DDVDDMDEE483) which is conserved between human and mouse is considered a potential Ca^{2+} binding site for Ca^{2+} -dependent inactivation (Mullins et al., 2009, 2016, Lee et al., 2009, Derler et al., 2009). This particular domain is still intact in STIM1B.

Therefore, mutations of all the 7 negatively charged residues in this domain into respective Alanines (7A) were obtained and investigated if they altered the CDI phenotype within STIM1B. YFP-STIM1/STIM1B/STIM17A/STIM1B7A in pEX was co-expressed with pCAGGS-ORAI1-IRES-RFP in HEK S1/2 DKO cells using electroporation as previously described and whole cell patch clamp recordings were performed 24 hours after transfection in the presence of 2mM EGTA in the patch pipette. STIM1 and STIM1B traces and analysis (Figure 13A-D) were compared with 7A mutant current traces.

Current traces of STIM1 7A significantly slowed down in comparison to STIM1 with a significantly reduced current maximal density and indeed, the SCDI of STIM17A was significantly reduced. Added to this, it also significantly slowed down for STIM1B 7A with similar characteristics observed in STIM17A when compared to STIM1B (Figure 13 D-G). These findings summarize the fact that the negatively charged region within the inactivation domain of STIM1B, conserved in STIM1B elucidated the functional significance of this region in the context of CDI.

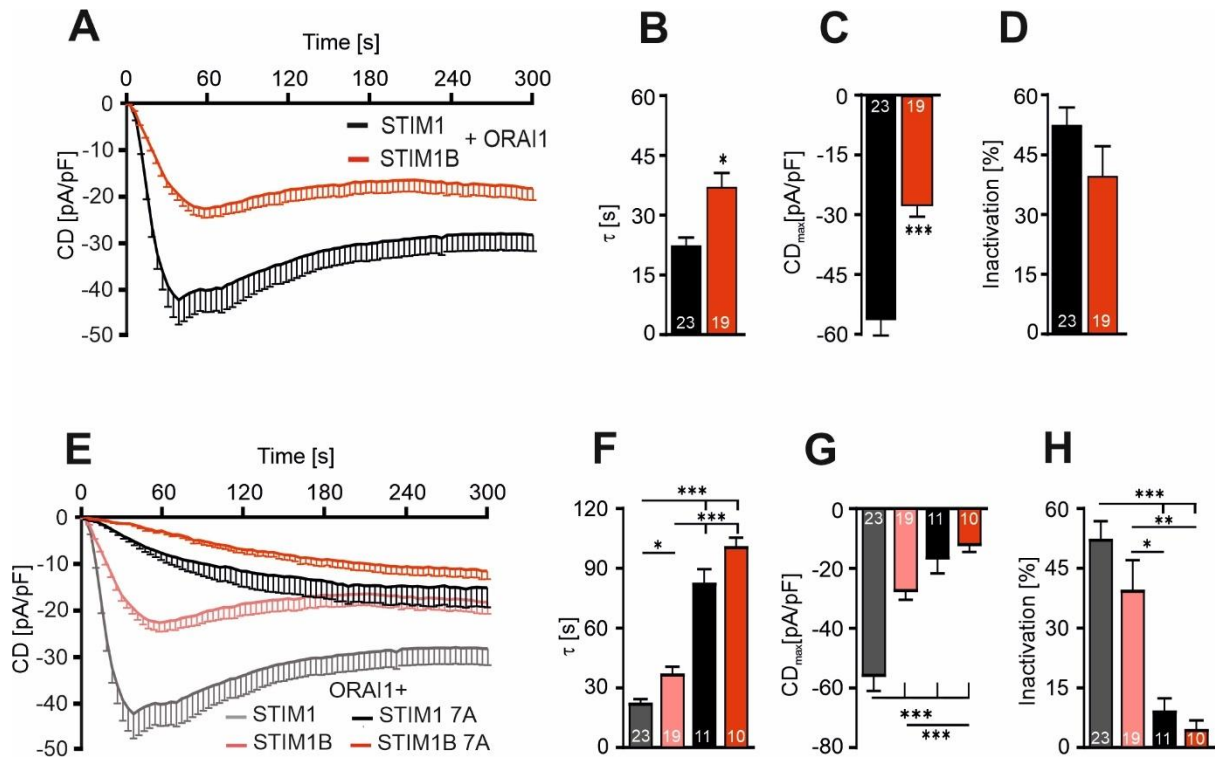


Figure 13 Mutation of STIM1B's inactivation domain (7A mutant) did not alter the CDI phenotype under EGTA conditions. (A) Average traces showing whole-cell current density (CD) over time extracted at -130mV in HEK S1/2 DKO cells overexpressing hSTIM1 (black, n=23) or hSTIM1B (red, n=19) with hORAI1. (B, C, & D) Bar graphs showing average tau, average maximal current density (CD_{max}), and average % inactivation respectively calculated from individual cells measured in (A). (E) Average traces showing whole-cell current density (CD) over time extracted at -130mV in HEK S1/2 DKO cells overexpressing hSTIM1 (grey, n=23) or hSTIM1B (pink, n=19), or hSTIM1_7A (black, n=11) or hSTIM1B_7A (red, n=10) with hROAI1. (F, G, & H) Bar graphs showing average tau and average maximal current density (CD_{max}) average % inactivation respectively calculated from individual cells measured in (E). * $p < 0.05$, ** $p < 0.01$, *** $p < 0.001$ represents unpaired Student's t-test with Welch's correction. Data are represented as Mean \pm SEM.

4.3.3 Cloning of genetically modified constructs of Stim1B

As neither the protein SARAF nor mutation of negatively charged residues in the ID domain of STIM1B failed to uncover the molecular mechanism of the SCDI phenotype, further cloning strategies were implemented using modified constructs of Stim1B/STIM1B in order to explore the reasons for the SCDI phenotype. By quick change PCR insertion method, two subsequent stop codons were incorporated after the last common amino acid of Stim1 and Stim1B, aa 514 using primer pairs BAN1498/99 for STIM1 and by PCR amplification and restriction site cloning with primer BAN 1566 for Stim1. The construct is named Stim1_514* or STIM1_514* Similarly, deletion of the Exon B stop codon via site-directed mutagenesis using primer pairs BAN1794/95 with pMax-mKate2-Stim1B as the DNA template, which shifts to the reading frame of Stim1 to retain the C terminal residues of Stim1 but now includes the B domain, thus

resulting in a slightly longer protein than Stim1. This construct is named Stim1B \emptyset * or STIM1B \emptyset * (for murine or human constructs respectively).

The above-cloned constructs, Stim1 and Stim1B in pMax-IRES-mCherry were transfected in HEK S1/2 DKO cells, and lysates were made. Equal amounts of proteins from each sample were loaded on a 7% SDS-PA Gel and after transfer to the Nitrocellulose membrane probed with an N-terminally directed Stim1 antibody and recognizes all the constructs. As shown in Figure 14B, Stim1 runs slightly higher than the 75 kDa marker band which corresponds to Stim1's estimated molecular weight (77kDa). Stim1B runs lower than 75kDa which corresponds to the Stim1B molecular weight (62kDa). Stim1_514* which lacks the 26 amino acids that correspond to the exon B, runs slightly lower than Stim1B. Since Stim1B \emptyset contains an N-terminal 26 kDa mKate2 tag, while the other three constructs are untagged, it runs above all the other three samples. The lower bands seen in all four samples could be due to Calpain/Caspase cleavage or partial degradation of the protein sample itself.

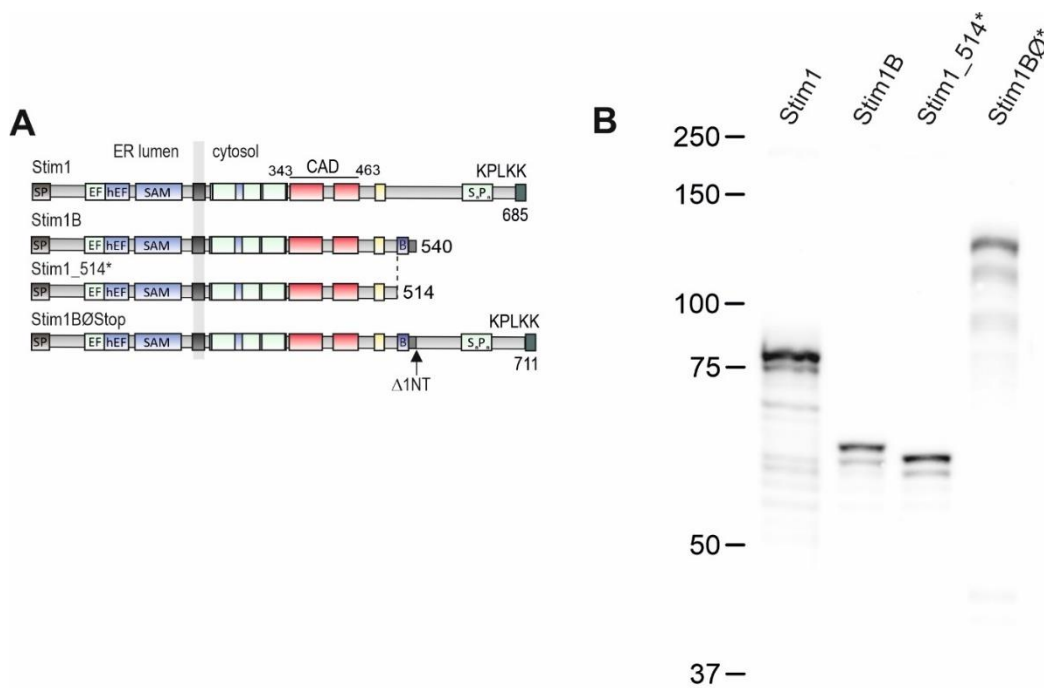


Figure 14 Screening of cloned constructs by Western blotting. (A) Schematic domain representation of Stim1, Stim1B, Stim1_514*, Stim1B \emptyset protein showing functional motives. **(B)** Western blot image showing overexpression levels of Stim1, Stim1B, Stim1_514*, Stim1B \emptyset in HEK S1/2 DKO cells.

4.3.4 Stim1 phenotype is still retained despite the missing C-terminal domain of Stim1

The functional characteristics of Stim1_514*, Stim1, and Stim1B were comprehensively investigated through co-expression with Orai1 in HEK S1/2 DKO cells, followed by patch-clamp recordings conducted 24 hours post-transfection in the presence of 2mM EGTA in the patch pipette. Upon analysis, the average current traces of Stim1_514* were found to exhibit a reduced current density, reaching approximately 60% of Stim1's average maximal current density. However, these traces were significantly larger than those of Stim1B, displaying approximately 40% more current than Stim1B. Additionally, the activation kinetics of Stim1_514* fell in between Stim1 and Stim1B, showcasing intermediate behavior. Moreover, Stim1_514* displayed a notably higher calcium-dependent inactivation (SCDI) when compared to Stim1B (Figure 15A-D). Further investigations involving Stim1_514* were conducted under conditions of 20mM BAPTA.

In this scenario, Stim1_514* mediated Orai1 currents demonstrated similar rate kinetics to Stim1, slightly larger current densities than Stim1, and an inactivation profile akin to Stim1 (Figure 15E-H). Parallel assessments were conducted using human constructs, involving the co-expression of STIM1, STIM1B, and STIM1_514* with ORAI1 in the presence of 2mM EGTA. The average current traces of STIM1_514* were characterized by activation kinetics and inactivation patterns similar to STIM1, featuring a 30% faster rate of activation compared to STIM1B. Although the average current maximal density of STIM1_514* fell between STIM1 and STIM1B (Figure 15I-L).

These detailed analyses collectively indicate that Stim1_514* did not replicate the functional characteristics observed in Stim1B. This underscores the conclusion that the absence of C-terminal residues alone does not solely account for the altered functionality observed in Stim1B, further implicating intricate molecular interactions and mechanisms underlying the distinctive properties of Stim1B-mediated calcium signaling.

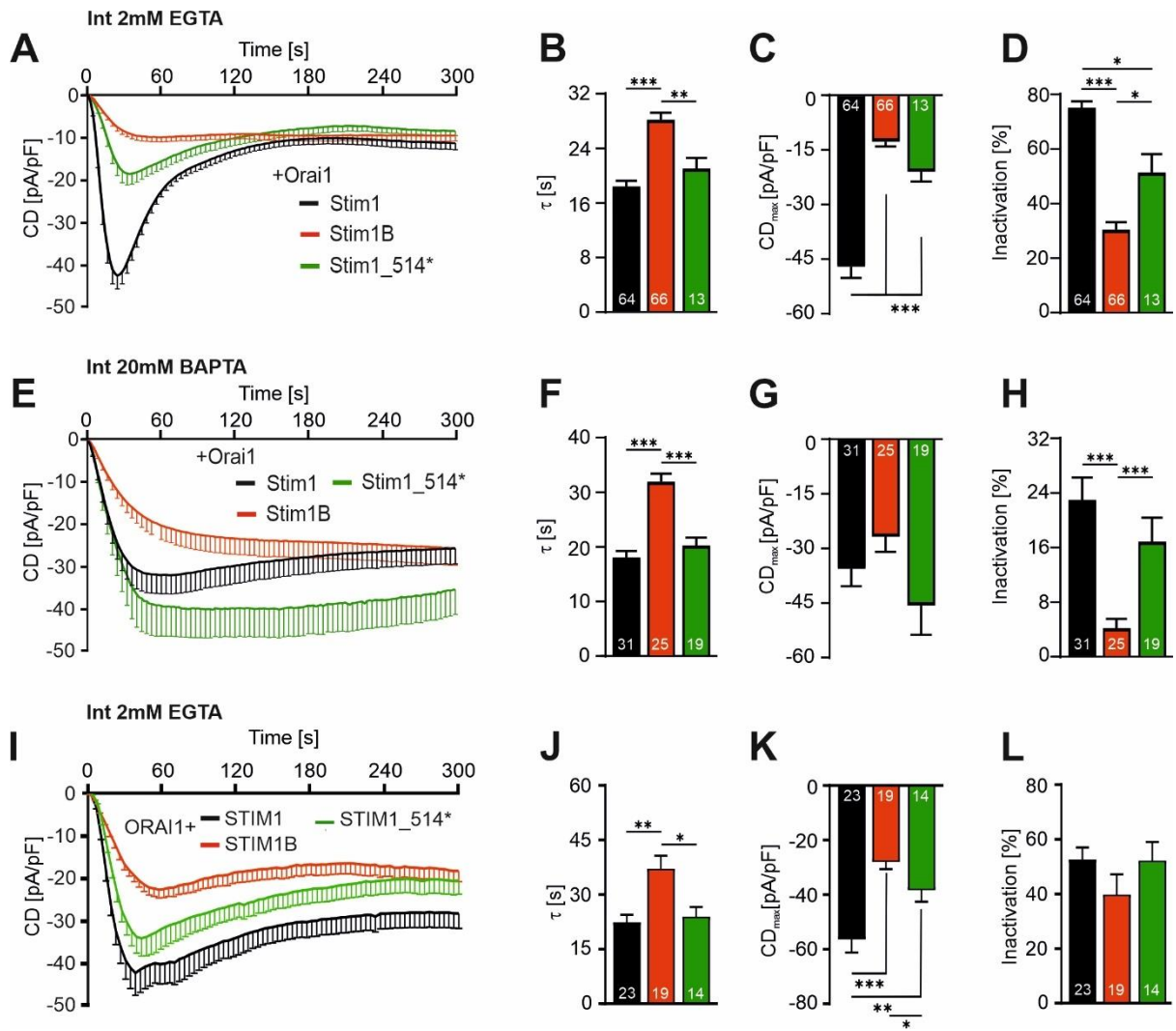


Figure 15 The absence of the C-terminal domain still retained Stim1 phenotype. (A) Average traces showing whole-cell current density (CD) over time extracted at -130mV in HEK S1/2 DKO cells overexpressing mStim1 (black, n=64) or mStim1B (red, n=66) or mStim1_514* (green, n=13) with mOrai1 under 2mM EGTA conditions. (B, C, & D) Bar graphs showing average tau, average maximal current density (CD_{max}), and average % inactivation respectively calculated from individual cells measured in (A). (E) Average traces showing whole-cell current density (CD) over time extracted at -130mV in HEK S1/2 DKO cells overexpressing mStim1 (black, n=31) or mStim1B (red, n=25) or mStim1_514* (green, n=19) with mOrai1 under 20mM BAPTA conditions. (F, G, & H) Bar graphs showing average tau and average maximal current density (CD_{max}) average % inactivation respectively calculated from individual cells measured in (E). (I) Average traces showing whole-cell current density (CD) over time extracted at -130mV in HEK S1/2 DKO cells overexpressing hSTIM1 (black, n=23) or hSTIM1B (red, n=19) or hSTIM1_514* (green, n=14) with hORAI1 under 2mM EGTA conditions. (J, K, & L) Bar graphs showing average tau and average maximal current density (CD_{max}) average % inactivation respectively calculated from individual cells measured in (I). *p<0.05, **p<0.01, ***p<0.001 represents unpaired Student's t-test with Welch's correction. Data are represented as Mean±SEM. (Ramesh et al., 2021).

4.3.5 Insertion of Domain B determines the Stim1B phenotype

The functional characteristics of Stim1BØStop, a construct involving the deletion of C-terminal residues and associated domains, were systematically explored. For this purpose, Stim1, Stim1B, and Stim1BØStop were co-expressed with Orai1 in HEK S1/2 DKO cells, followed by whole-cell patch clamp recordings conducted 24 hours post-transfection in the presence of 2mM EGTA in the patch pipette. Current traces of Stim1BØStop mediated Orai1 currents displayed a notable reduction in calcium release-activated current (CRAC) density, exhibiting a significantly reduced rate of activation by 40% and a diminished calcium-dependent inactivation (SCDI) by 60%, when compared to Stim1-mediated Orai1 currents (Figure 16A-D). Surprisingly, Stim1BØStop demonstrated kinetics and inhibition characteristics similar to Stim1B, despite harbouring the microtubule tracking EB1 attachment site (TRIP motif) and the polybasic domain (PBD). Subsequent recordings were performed in the presence of 20 mM BAPTA, revealing that Stim1BØStop mediated Orai1 currents were significantly larger, with no difference in average maximal current density. However, these currents exhibited a reduced activation kinetics by 35% compared to Stim1, and 25% compared to Stim1_514*. SCDI was also significantly reduced by 60% for Stim1 and 48% for Stim1_514*. As anticipated, Stim1BØStop displayed analogous kinetics of activation and SCDI to that of Stim1B (Figure 16E-H).

Parallel experiments involving human constructs were conducted using pEX-STIM1/STIM1B/STIM1BØStop with a YFP tag, co-expressed with pCAGGS-ORAI1-IRES-RFP in HEK S1/2 DKO cells, as previously described. Notably, STIM1BØStop mediated ORAI1 current density and kinetics did not differ from STIM1B mediated ORAI1, with a significantly reduced rate of activation by 32% compared to STIM1, and 25% compared to Stim1_514*. Similarly, SCDI was notably diminished when compared to STIM1 and STIM1_514* (Figure 16I-L). BAPTA conditions further demonstrated a substantial reduction in SCDI for all constructs and its virtual absence in Stim1B/STIM1B/ Stim1BØStop/ STIM1BØStop.

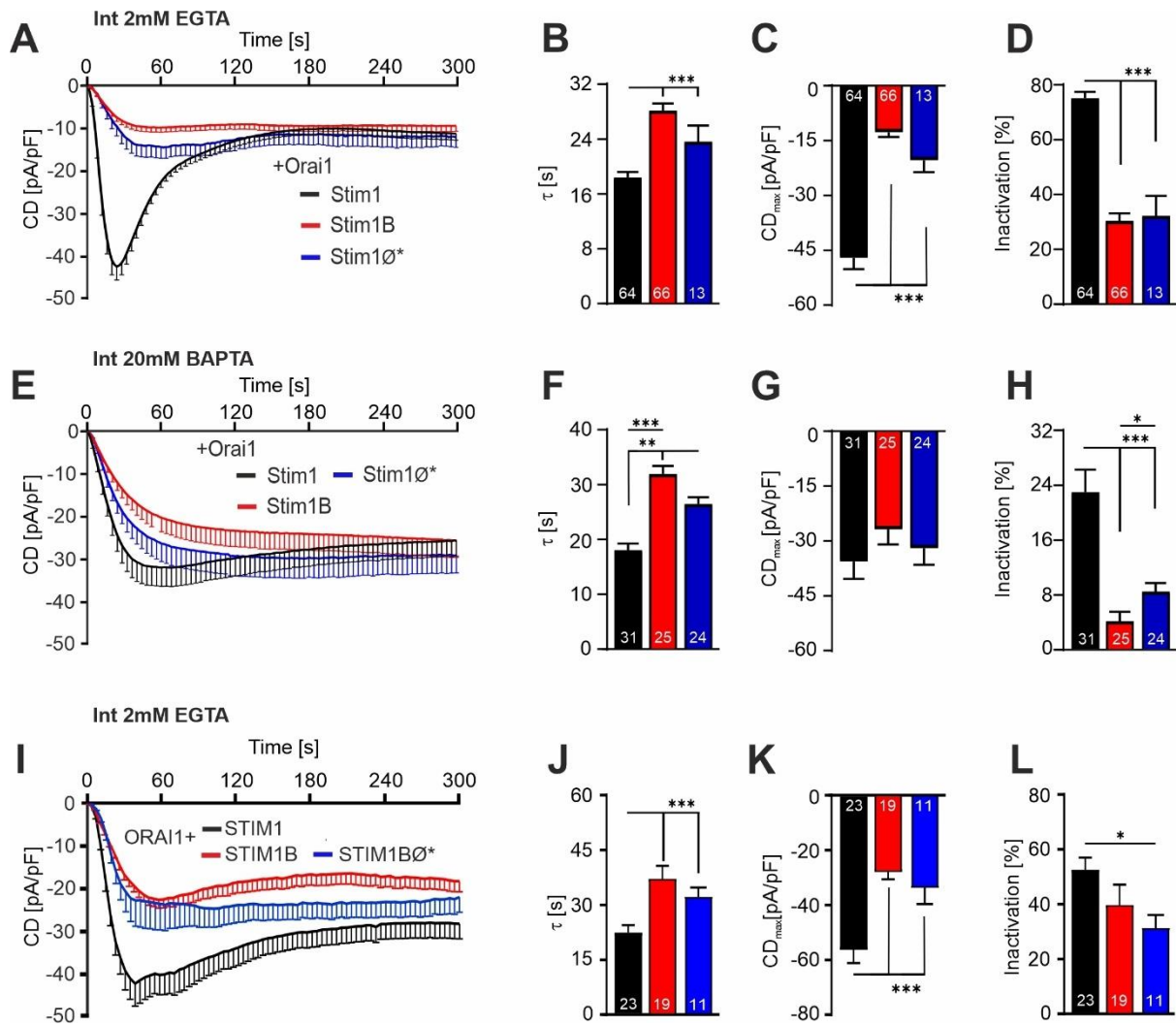


Figure 16 The insertion of Domain B in Stim1 mimics Stim1B phenotype. (A) Average traces showing whole-cell current density (CD) over time extracted at -130mV in HEK S1/2 DKO cells overexpressing mStim1 (black, n=64) or mStim1B (red, n=66) or mStim1 \emptyset^* (blue, n=13) with mOrai1 under 2mM EGTA conditions. (B, C, & D) Bar graphs showing average tau, average maximal current density (CD_{max}), and average % inactivation respectively calculated from individual cells measured in (A). (E) Average traces showing whole-cell current density (CD) over time extracted at -130mV in HEK S1/2 DKO cells overexpressing mStim1 (black, n=31) or mStim1B (red, n=25) or mStim1 \emptyset^* (blue, n=24) with mOrai1 under 20mM BAPTA conditions. (F, G, & H) Bar graphs showing average tau and average maximal current density (CD_{max}) average % inactivation respectively calculated from individual cells measured in (E). (I) Average traces showing whole-cell current density (CD) over time extracted at -130mV in HEK S1/2 DKO cells overexpressing hSTIM1 (black, n=23) or hSTIM1B (red, n=19) or hSTIM1 \emptyset^* (blue, n=11) with hORAI1 under 2mM EGTA conditions. (J, K, & L) Bar graphs showing average tau and average maximal current density (CD_{max}) average % inactivation respectively calculated from individual cells measured in (I). *p<0.05, **p<0.01, ***p<0.001 represents unpaired Student's t-test with Welch's correction. Data are represented as Mean±SEM. (Ramesh et al., 2021).

To investigate the role of domain B encoded residues or the additional 14 residues encoded by the altered reading frame encoded in the conventional exon 12, a modified construct was created named Stim1B_526*. This construct contained a Stop codon after

domain B, effectively deleting the additional 14 residues generated due to the frameshift. Stim1/Stim1B/Stim1B_526 were co-expressed with Orail, followed by patch clamp recordings. Stim1B_526* mediated Orail currents displayed reduced amplitude, slower kinetics, and inactivation when compared with Stim1. Importantly, Stim1B_526* retained the Stim1B phenotype in terms of activation kinetics and SCDI, suggesting that the additional 14 residues resulting from the frameshift are not responsible for this phenotype (Figure 17A-D). These findings solidify the notion that the insertion of domain B, and not the deletion of C-terminal residues or the additional 14 residues following domain B, confers specific functional changes.

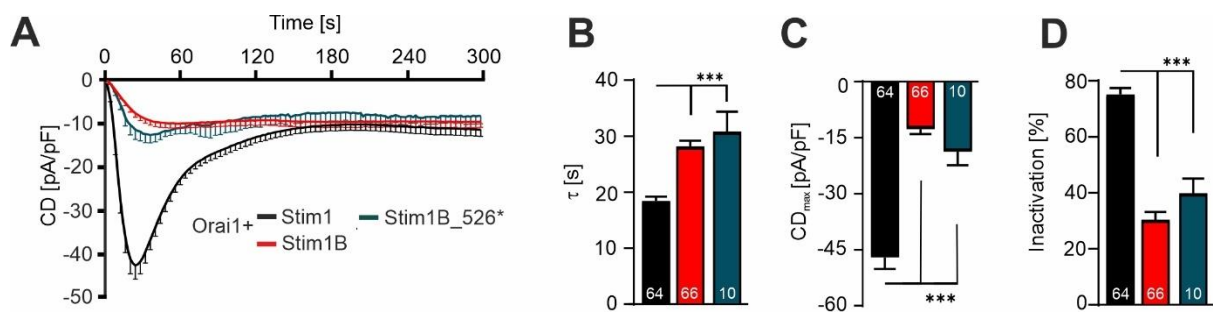


Figure 17 Deletion of additional 26 translated residues due to domain B still retained the Stim1B phenotype. (A) Average traces showing whole-cell current density (CD) over time extracted at -130mV in HEK S1/2 DKO cells overexpressing mStim1 (black, n=64) or mStim1B (red, n=66) or mStim1B_526* (blue, n=10) with mOrail under 2mM EGTA conditions. (B, C, & D) Bar graphs showing average tau, average maximal current density (CD_{max}), and average % inactivation respectively calculated from individual cells measured in (A). * $p < 0.05$, ** $p < 0.01$, *** $p < 0.001$ represents unpaired Student's t-test with Welch's correction. Data are represented as Mean \pm SEM.

4.3.6 Cloning of genetically modified constructs of Stim1B

Since the presence of domain B and not the C terminal residues determines the Stim1B's phenotype as shown from the patch clamp experiments, further cloning strategies were adapted to mutate the specific residues of domain B (GSSLKANRLSSK) to further delineate which specific motif could be responsible for this phenotype.

By quick change PCR insertion method, the first, middle, and last 4 amino acids of domain B is mutated to 4 alanine (i.e., GSSL>AAAA, KANR>AAAA, LSSK>AAAA). Using primer pairs BAN1888/89 for GSSL>AAAA, BAN1890/91 for KANR>AAAA and BAN1891/92 for LSSK>AAAA were used with Stim1B-pMAX-IRES mCherry as the DNA template. Mutations were then confirmed by DNA sequencing.

4.3.7 A specific motif in domain B determines the STIM1B phenotype

Stim1, Stim1B, Stim1B with the GSSL>AAAA mutation, and Stim1B with the KANR>AAAA mutation were co-expressed with pMax-Orai1-IRES-GFP in HEK293/2 DKO cells as per previously described methods. Whole-cell patch clamp recordings were conducted 24 hours post-transfection, using a patch pipette containing 2mM EGTA. Analysis of GSSL>AAAA-mediated Orai1 currents unveiled several noteworthy findings. These currents exhibited calcium release-activated calcium (CRAC) channel characteristics, displaying similar rate kinetics and Slow Ca²⁺-dependent inactivation (SCDI) as Stim1B. Importantly, GSSL>AAAA currents displayed larger current densities, surpassing Stim1B by approximately 40% (P=0.0276). Despite this increase, GSSL>AAAA currents fell notably short of Stim1 currents, with significantly reduced current densities by 48%, a decreased rate of activation by 44%, and attenuated SCDI by 50% (Figure 18A-D).

Conversely, KANR>AAAA-mediated Orai1 currents exhibited distinct properties. These currents demonstrated a significantly accelerated rate of activation, approximately 78% faster than Stim1B-mediated Orai1 currents. Moreover, the average maximal current density was augmented by 40%, and a stronger SCDI was evident, amplified by 46%, compared to Stim1B-mediated Orai1 currents. Most notably, KANR>AAAA mutation effectively rescued the Stim1B phenotype, as indicated by the rescue of average maximal current density, which reached around 80% of Stim1 levels. SCDI was also notably restored to approximately 85% of Stim1 levels. Importantly, the kinetic rate of activation displayed no significant difference in comparison to Stim1 (P=0.06) (Figure 18E-G).

Taken together, these findings provide compelling evidence that a specific motif within domain B, namely the KANR motif, is the key determinant responsible for the distinct phenotype observed in Stim1B. This motif appears to play a critical role in modulating current density and SCDI. Notably, the KANR>AAAA mutation significantly rescued the reduced current density and SCDI compared to Stim1 Wt that were evident in Stim1B-mediated Orai1 currents. This mechanistic insight sheds light on the functional significance of domain B and its role in regulating Orai1-mediated currents and associated calcium signaling dynamics.

Indeed, experiments performed by Dr. Yvonne Schwarz after the experimental part of my thesis was closed, also indicate a clear reversal of the Stim1B enhanced synaptic potentiation by the KANR/AAAA mutation.

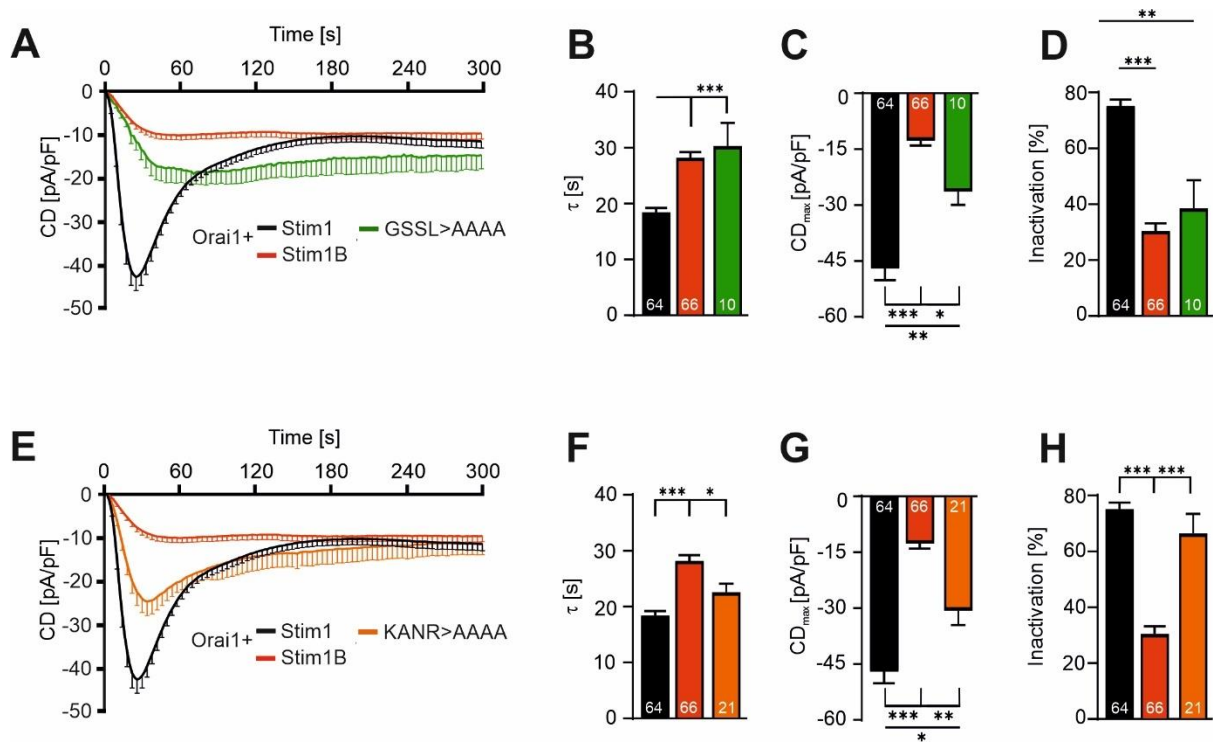


Figure 18 A Specific motif in domain B (KANR) determines the Stim1B phenotype. (A) Average traces showing whole-cell current density (CD) over time extracted at -130mV in HEK S1/2 DKO cells overexpressing mStim1 (black, n=64) or mStim1B (red, n=66) or mStim1B_GSSL>AAAA (green, n=10) with mOrai1 under 2mM EGTA conditions. (B, C, & D) Bar graphs showing average tau, average maximal current density (CDmax), and average % inactivation respectively calculated from individual cells measured in (A). (E) Average traces showing whole-cell current density (CD) over time extracted at -130mV in HEK S1/2 DKO cells overexpressing mStim1 (black, n=31) or mStim1B (red, n=25) or mStim1B_KANR>AAAA (blue, n=21) with mOrai1 under 2mM EGTA conditions. (F, G, & H) Bar graphs showing average tau and average maximal current density (CDmax) average % inactivation respectively calculated from individual cells measured in (E). * $p < 0.05$, ** $p < 0.01$, *** $p < 0.001$ represents unpaired Student's t-test with Welch's correction. Data are represented as Mean \pm SEM.

4.4. Function of Stim1B in regulating synaptic plasticity and maintaining neuronal calcium homeostasis

4.4.1 Neither quantal signaling nor basal synaptic signaling is affected by Stim1B expression

Given the robust expression of Stim1B in neurons at both mRNA and protein levels, it becomes essential to comprehend the functional implications of Stim1B in neuronal store-operated

calcium entry (SOCE). To unravel this, our collaborator, Dr. Yvonne Schwarz, conducted further experiments involving synaptic recordings and the subcellular localization of Stim1/Stim1B within neurons and aimed to discern whether Stim1 and Stim1B exert distinct roles in synaptic transmission. To facilitate the identification of the constructs upon transfection into neuronal cultures, Stim1, Stim1B, and their respective mutant variants were cloned into lentiviral vectors (pWPXL) with a mKate2 tag incorporated in the luminal region of Stim proteins.

The synaptic recordings encompassed various types of synaptic activity, starting from spontaneous activity to stimulus trains of varying frequencies, including 0.2 Hz, 20 Hz, and 40 Hz. To dissect the potential synaptic phenotype associated with Stim1B variants, the Stim1B \emptyset Stop construct, which lacks domain B, was also included for analysis. Additionally, a Stim1B mutant, named S1B_CADm, carrying two single amino acid substitutions within the Orai channel activation domain (CAD/SOAR), was generated. This mutant was previously shown to disrupt the activation of all Orai channel isoforms (Frischauf et al., 2009) and was employed to examine the impact of CAD/SOAR mutation on synaptic properties.

HEKS1/2 DKO cells were utilized to co-express Stim1B CAD mutant with Orai1, and subsequent whole-cell patch clamp recordings verified the inability of Stim1B CAD mutant to activate Orai1 currents (Figure 19, Ramesh et al., 2021).

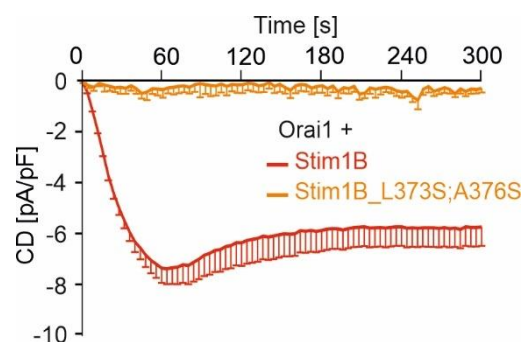


Figure 19 Mutation of Stim1B's CAD Domain abolishes Orai1 mediated I_{CRAC}. Average traces showing whole-cell current density (CD) over time extracted at -130mV in HEK S1/2 DKO cells overexpressing mStim1B (red, n=66) or mStim1B L373S, A376S (mStim1B_CADm (Orange, n=5) with mOrai1 under 2mM EGTA conditions.

Lentiviral vectors carrying Stim1, Stim1B, Stim1B \emptyset Stop, and Stim1B CADm constructs, all tagged with mKate2 luminal markers, were introduced into autaptic hippocampal cultures. The

cultures were maintained for 10-14 days to allow for construct expression, and their synaptic properties were subsequently evaluated. While much of the detailed data obtained by Dr. Yvonne Schwarz is presented in the accompanying manuscript, the salient scientific findings are outlined here, with the full publication available in the attached appendix.

Measurement of miniature excitatory postsynaptic currents (mEPSCs) revealed no alterations in frequency, amplitude, charge, rise time, or decay time of spontaneous neurotransmitter release across all Stim1 variants. Furthermore, analysis of single quantal events' kinetics remained consistent among the measured groups, indicating no impact on postsynaptic receptor machinery. Following the assessment of spontaneous activity, stimulation at a frequency of 0.2 Hz was applied, and basal action potential-evoked release was found to be unaffected by Stim1 or Stim1B expression, as indicated by the lack of changes in evoked amplitude or charge. These findings collectively demonstrate that the expression of Stim1 or Stim1B does not significantly influence basal synaptic transmission (Figure S2 E-G, Ramesh et al., 2021).

4.4.2 Stim1B but not Stim1 turns synaptic depression into short-term enhancement at high-frequency stimulation (HFS)

To evaluate the impact of Stim1B expression on synaptic efficacy, a series of experiments were conducted using hippocampal autaptic cultures. Stim1, Stim1B, Stim1B Δ Stop, and Stim1B CADm constructs were introduced into the cultures through viral transduction, and synaptic recordings were performed 14 days after transfection. High-frequency stimulations (HFS) involving 20 Hz trains were applied for a duration of 100 milliseconds.

Consistent with previous data obtained from experiments using a 0.2 Hz stimulus train, the 20 Hz stimulus did not result in any changes in the initial excitatory postsynaptic current (EPSC) amplitude within the measured groups. Additionally, the temporal progression of synaptic depletion during the 20 Hz stimulus remained unaltered, as indicated by the consistent normalized EPSCs. The ratios of AmpEPSC1/AmpEPSC2 remained unchanged, and the cumulative frequencies of AmpEPSC10/AmpEPSC1 showed no alterations, consistently reflecting a state of short-term depression (STD) across all the examined groups. Similarly, the cumulative synchronous charge component, as well as the replenishment rate reflecting vesicle replenishment, exhibited no significant differences among the groups. In order to assess the size of the readily releasable pool (RRP) of vesicles, the steady-state phase of the cumulative

synchronous charge component was extrapolated back to the initial Y-intercept, which corresponds to the initial RRP size. Notably, neither of the Stim constructs led to any modification in the RRP size (Figure S3 A-G, Ramesh et al., 2021).

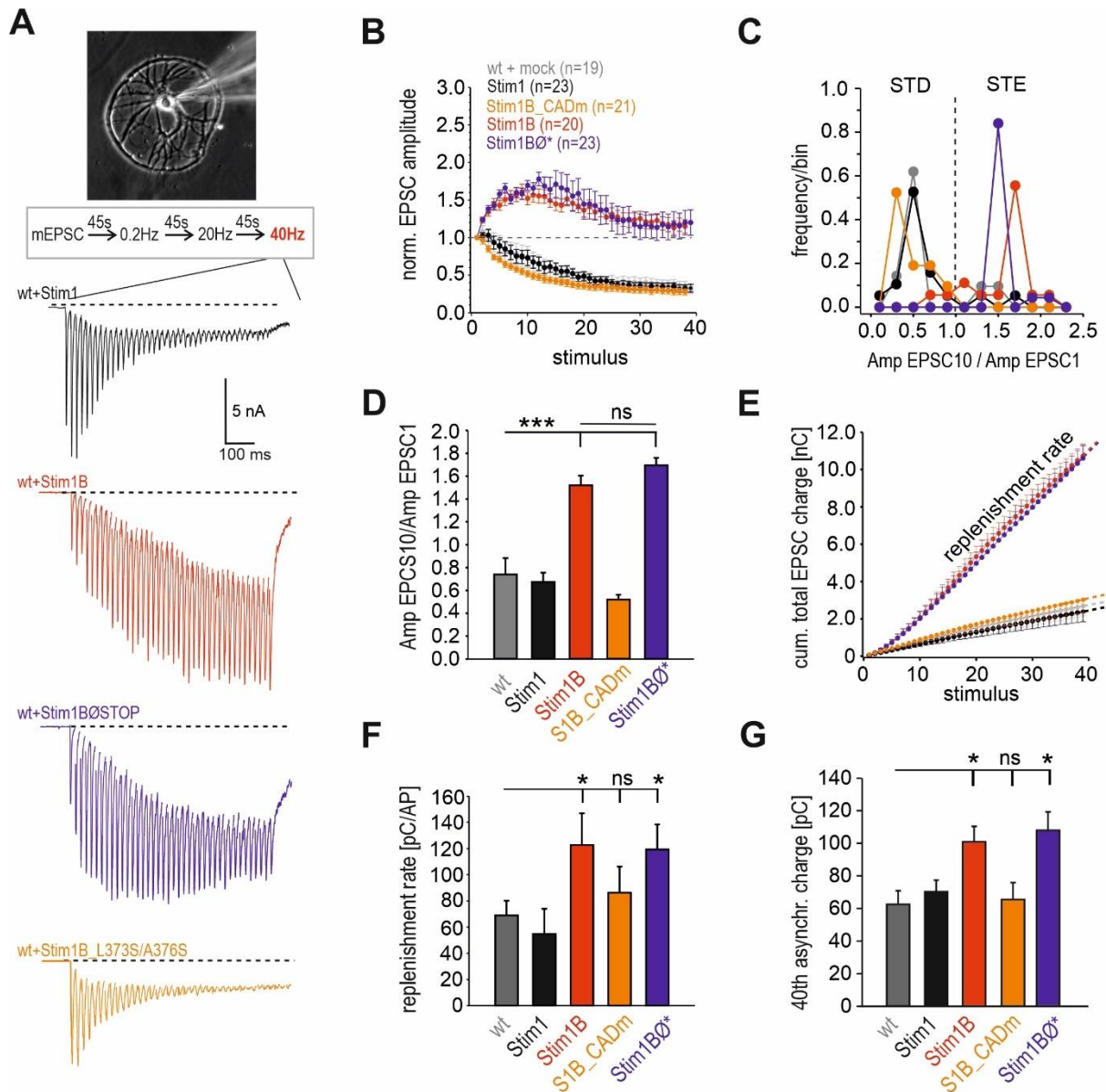


Figure 20 Stim1B promotes strong short-term enhancement (STE) of synaptic signaling. (A) Exemplanary EPSC recordings triggered by a HFS (40 Hz) of wt neurons and those expressing Stim1, Stim1B, Stim1B_L373S/A376S, and Stim1B0Stop. (B) Expression of the Stim1B and Stim1B0Stop caused STE and significantly altered the time course of synaptic depression, Data were normalized to the 1st EPSC amplitude. (C&D) Expression of StimB and Stim1B0Stop shifts the AmpEPSC10/AmpEPSC1 ratio towards STE. (E) Mean cumulative total release components during the 40 Hz train. (F) The replenishment rate is significantly enhanced in neurons expressing Stim1B or Stim1B0Stop. (G) Quantification of the 40th asynchronous charge. Data was collected from wt, n=19; wt+S1, n=23; wt+S1B, n=20; wt+ Stim1B0Stop, n=23; wt+ Stim1B_L373S/A376S, n=21. *p>0.05; **p<0.01; one-way ANOVA on ranks followed by Dunn’s post-hoc test. Figure and analysis made by Yvonne Schwarz. (Ramesh et al., 2021).

Subsequent to the 20 Hz stimulus, a 40 Hz stimulus train was administered to neurons expressing Stim1, Stim1B, Stim1B \emptyset Stop, and Stim1B CADm (Figure 20). During this high-frequency stimulation (40 Hz Stimulus), neurons expressing Stim1 displayed a classic short-term depression (STD) phenotype (Figure 20A), which closely resembled that of mock-transfected wild-type neurons. This observation was supported by comparable excitatory postsynaptic current (EPSC) amplitudes, consistent ratios of AmpEPSC10/AmpEPSC1 (Figure 20C, D), and cumulative total EPSC charge resembling the control group (Figure 20E). The replenishment rate and the asynchronous charge at the 40th stimulus was almost equivalent to those of the control, indicating the absence of an elevated presynaptic Ca²⁺ influx (Figure 20F, G).

In strong contrast, neurons expressing Stim1B exhibited a distinct response during the 40 Hz HFS train. Despite initiating with unaltered initial EPSC amplitudes in comparison to Stim1 or wild-type neurons, Stim1B-expressing neurons displayed a robust short-term enhancement (STE) phenotype (Figure 20A, B). This was evidenced by an increased AmpEPSC10/AmpEPSC1 ratio, which was notably elevated by nearly 1.5-fold compared to mock-transfected or Stim1-expressing neurons (Figure 20C, D). Statistical analysis using a one-way ANOVA on ranks confirmed the significance of this difference ($p < 0.001$). Furthermore, the total charge transfer of the evoked response and the replenishment rate, indicative of vesicle replenishment, was markedly augmented in neurons expressing Stim1B (Figure 20E, F). The enhanced asynchronous release observed upon Stim1B expression provided additional evidence of the rise in presynaptic Ca²⁺ levels within the terminal (Figure 20G).

Remarkably, the robust short-term enhancement phenotype (STE) observed in Stim1B-expressing neurons was similarly evident in neurons expressing the Stim1B \emptyset Stop mutant (Figure 20B-G). These neurons exhibited comparable AmpEPSC10/AmpEPSC1 ratios, total EPSC charge, and higher replenishment rates relative to Stim1B-expressing neurons. This agreement between the Stim1B and Stim1B \emptyset Stop phenotypes was consistent with results from patch clamp recordings performed in heterologous co-expression with Orail1 in HEK S1/2 DKO cells under low buffering conditions (2mM EGTA). These recordings demonstrated that both Stim1B and the mutant variant, Stim1B \emptyset Stop, exhibited phenotypic similarities, which

highlighted an unprecedented role for domain B rather than the absence of C-Terminal Stim1 residues in synaptic plasticity.

Surprisingly, the Stim1B CAD mutant failed to elicit the short-term enhancement (STE) phenotype characteristic of Stim1B (Figure 20A). Instead, these neurons exhibited a short-term depression (STD) phenotype, similar to mock-transfected or Stim1-expressing neurons. Notably, the frequency ratio of AmpEPSC10/AmpEPSC1 shifted towards STD, despite an accelerated rate of synaptic depression (Figure 20C, D). Furthermore, the replenishment rate and the asynchronous charge response at the 40th stimulus were similar to those observed in Stim1-expressing neurons (Figure 20E-G).

The inability of the Stim1B CAD mutant to manifest the STE phenotype observed in Stim1B-expressing neurons suggests that the rise in presynaptic Ca²⁺ influx, as indicated by the 40th asynchronous charge, could be attributed to Orai channels, either directly or indirectly. This influence of Orai channels potentially mediates the effect of Stim1B on the short-term enhancement (STE) of synaptic signaling. The combined data from these experiments on high-frequency stimulus trains strongly indicate an emerging and novel role for Stim1B in the modulation of synaptic efficacy.

4.4.3 Stim1B's STE phenotype requires a rise in presynaptic Ca²⁺ levels

In further validation of the dependency of Stim1B's short-term enhancement (STE) phenotype on an increase in presynaptic Ca²⁺, we employed EGTA-AM treatment to buffer the intracellular Ca²⁺ rise during high-frequency stimulus trains, as previously described by Otsu et al. in 2004. Remarkably, EGTA-AM treatment effectively abolished the STE phenotype mediated by Stim1B. This is evidenced by exemplary recordings from neurons co-expressing Stim1B and EGTA-AM, which exhibited a short-term depression (STD) phenotype similar to that of neurons expressing Stim1 or wild-type (Wt) constructs. Notably, there were no discernible alterations in the normalized EPSC amplitude, while the AmpEPSC10/AmpEPSC1 ratio shifted towards a short-term depression (STD) across all measured groups. The synchronous excitatory postsynaptic current (EPSC) charge and the action potential-evoked response mirrored those observed in Stim1-expressing neurons. Conversely, the elevated asynchronous charge release component observed during the high-frequency stimulus (HFS) was entirely abolished upon EGTA-AM treatment, contrasting with the profile of Stim1-

expressing neurons. This points to the effective Ca^{2+} buffering conferred by EGTA-AM treatment, underscoring the reliance of the Stim1B-mediated STE phenotype on enhanced presynaptic Ca^{2+} levels (Figure S3, A-L, Ramesh et al., 2021).

Given that EGTA-AM treatment effectively reversed the HFS stimulus-induced synaptic properties associated with Stim1B, we explored the possibility that the STE phenotype of Stim1B might be frequency-dependent or influenced by an accumulation of presynaptic calcium resulting from the preceding 20 Hz stimulus. To elucidate this, a subsequent 2x20 Hz stimulus train instead of a single 40 Hz stimulus was applied across the same groups. Strikingly, both Stim1B and Stim1B \emptyset Stop constructs displayed the STE phenotype during the second 20 Hz stimulus, in contrast to Wt, Stim1, or Stim1B CADm expressing neurons. Similar to the observations at 40 Hz HFS, the initial amplitude remained consistent across the groups. The AmpEPSC10/AmpEPSC1 ratio exhibited a shift towards STE in neurons expressing Stim1B and Stim1B \emptyset Stop compared to those expressing Stim1. Notably, both the total charge transfer of the evoked response and the replenishment rate were significantly enhanced relative to Stim1-expressing neurons. Furthermore, the 40th asynchronous charge observed in Stim1B and Stim1B \emptyset Stop expressing neurons was notably elevated compared to Stim1 expressing neurons, indicative of heightened presynaptic Ca^{2+} levels during the second 20 Hz train. In summary, the phenotypic congruence of Stim1B expression across different stimulation frequencies suggests a mechanism wherein an increase in presynaptic $[\text{Ca}^{2+}]_i$ is necessary to trigger the Stim1B-mediated STE (Figure S4, A-J, Ramesh et al., 2021). The comparative analysis of Stim1B and its mutant variants underscores the pivotal role of Stim1's domain B in modulating synaptic STE, potentially mediated by additional Ca^{2+} influx or ER Ca^{2+} release, either directly or indirectly, through the activation of synaptic Orai channels.

4.4.4 Presynaptic localization corroborates the synaptic physiology of Stim1B

As Stim1B displayed prominent neuronal expression as shown in Figure 5 and given the strong synaptic phenotype as described above, protein localization was investigated by Yvonne Schwarz using mKate2- tagged Stim1, Stim1B, and the mutant constructs Stim1B \emptyset Stop, Stim1B CADm in lenti vectors. Following the lentiviral transfection into the hippocampal mass cultures, the neurons were co-immunolabelled with anti-mKate2 antibody along the anti-Bassoon, which is presynaptic to better distinguish the localization of Stim1B. Stim1-

expressing neurons localized mainly to the ER within the soma of the neuron with fluorescence in meagre amount protruding into the larger dendritic or axonal structures and displayed very little co-localization with the presynaptic protein marker bassoon (Figure 21A). Stim1B-expressing neurons, however, displayed a clear distinct localization with minimal somatic ER localization but a much more distal punctate localization that significantly overlapped with presynaptic marker Bassoon as confirmed with Mander's co-localization coefficient (Figure 21 A&B). To investigate whether the differential localization of Stim1B was attributed to the absence of C-terminal residues and binding partners or whether the inserted residues encode a potential trafficking signal, the engineered construct with superficial B containing full-length Stim1 C terminal residues (Stim1B \emptyset Stop) was transfected in a similar manner as Stim1/Stim1B. Remarkably, immunolabeling with mKate2 antibody along with Bassoon showed that Stim1B \emptyset Stop still exhibited the differential localization when compared to Stim1 and also displayed substantial co-localization with Bassoon as Stim1B indicating that insertion of specific residues (domain B) rather than the loss of C-terminal residues governed differential localization which further confirmed that the STE phenotype observed is due to the presynaptic localization of Stim1B. Similarly, the ORAI coupling deficient Stim1B_L373S; A376S (Stim1B_CADm) expressing neurons was also immunolabelled for mKate2 and bassoon. As seen in Figure 21A, Stim1B_CADm still maintained its localization at the presynaptic sites with strong colocalization with Bassoon suggesting that the failure of STE observed with this mutant (Figure 20A –G) was not due to the altered localization.

The extent of stronger peripheral localization of Stim1B can also be directly visualized with live microscopy visualizing the mKate2 fluorescence of the patch-clamped neurons as shown in Figure 21C. To summarize, the distinct localization of Stim1B to the presynaptic terminals coupled with enhanced synaptic responsiveness at HFS offers a new dynamic role of SOCE that dynamically shapes STE during periods of high-demand synaptic activity.

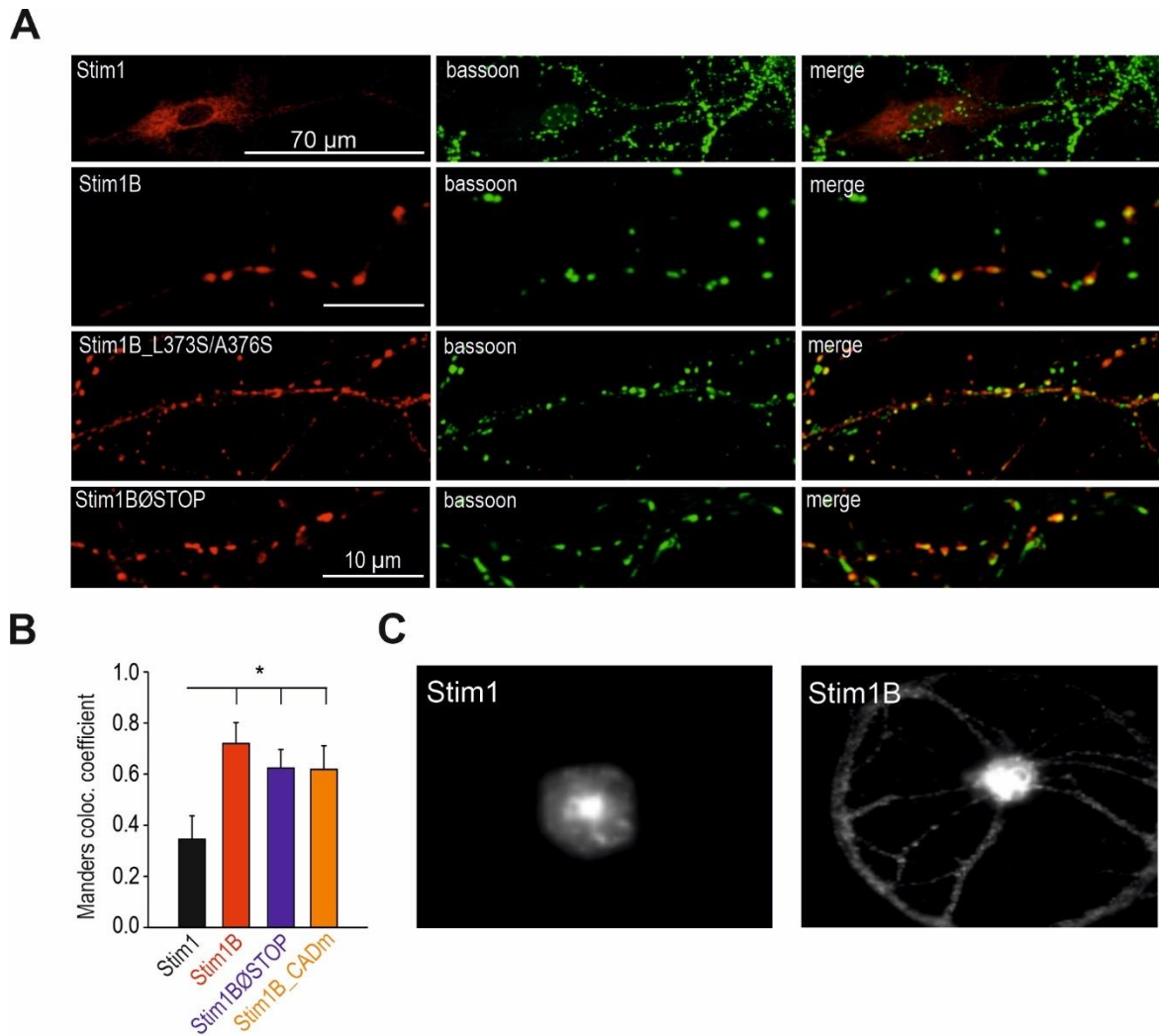


Figure 21 Stim1B is localized to presynaptic terminals. (A) Representative images of Stim1, Stim1B, Stim1B_L373S/A376S, and Stim1BØStop (left panels) co-immunolabeled with an anti-mkate2 antibody and the presynaptic marker protein bassoon (middle). Stim1 is found primarily in somatic ER regions showing little overlap with bassoon. Stim1B and derived mutants colocalize with the bassoon in varicosity-like punctate regions in soma-proximal and soma-distal axonal branches. (B) Colocalization was quantified using Manders' coefficient in thin axonal structures to avoid the contribution of somatic or dendritic signals. Data were collected from 12 Stim1, 8 Stim1B, 6 Stim1B_L373S/A376S, and 7 Stim1BØStop expressing neurons from 2 independent cultures. $p < 0.05$, one-way ANOVA on ranks followed by Dunn's post-hoc test. (C) Exemplary images showing in vivo fluorescence of mkate2-Stim1 and mkate2-Stim1B expressing neurons. Figure and analysis made by Yvonne Schwarz. (Ramesh et al., 2021).

4.5 Validation of Splice-deficient mice (10A mice)

We obtained a genetically modified mouse strain in which exons 10, 11, and 12 of Stim1 were fused and flanked by LoxP sites to replace the C-terminal genomic region with the aim of inducing recombination with a construct in which all C-terminal Serines are mutated. This parental construct disables splicing between conventional exons 10-12 (Yu et al., 2019). These mice are named 10A mice in this thesis and were kindly provided by Dr. Machaca, Cornell Weil Campus, Qatar. Cerebelli and retinas were isolated from wild-type and 10A mice of the same age group and Western blotting was performed and probed with an N-terminally directed anti-Stim1 antibody, thus able to detect both Stim1 and Stim1B variant to validate the absence of Stim1B in 10A mice. As seen in Figure 22, in both wildtype and 10A cerebellum & retina, a prominent band at approximately above 77kDa was seen which corresponds to Stim1. As expected, a band below Stim1 was detected in the wildtype group at approximately 15kDa less which corresponds to the size of Stim1B (62kDa) but is absent in the tissues derived from the 10A mice.

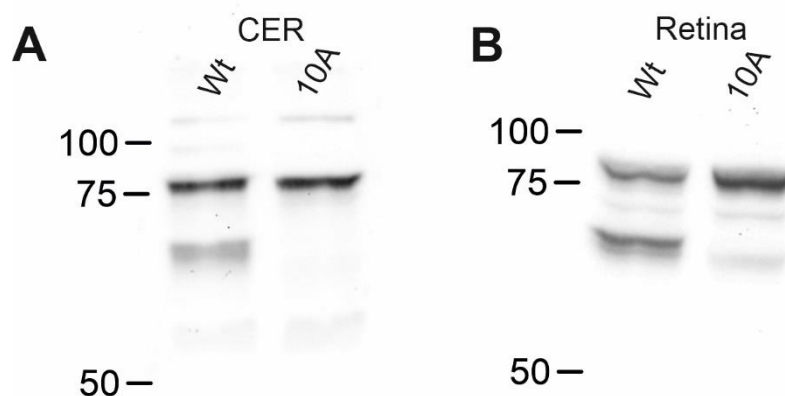


Figure 22 Screening and validation of splice-deficient mice. Western blot image showing overexpression levels of Stim1 & Stim1B in Wild type (Wt) and splice-deficient (10A) in mouse cerebellum (A) and mouse retina (B).

4.6 The absence of Stim1B suggests reduced levels of Synapsin

Synapsins constitute a prominent family of synaptic vesicle (SV) phosphoproteins that play a pivotal role in modulating SV trafficking by engaging in interactions with both actin and SVs,

thereby regulating neurotransmitter release. The intriguing observation of an augmented readily releasable pool size upon the overexpression of Stim1B in hippocampal mass cultures prompted an exploration into the potential impact of Stim1B on synapsin levels. To this end, protein lysates were extracted from cerebellum tissues of wild-type and 10A mice across different age groups (P4, P11, 5 weeks, & 20 weeks).

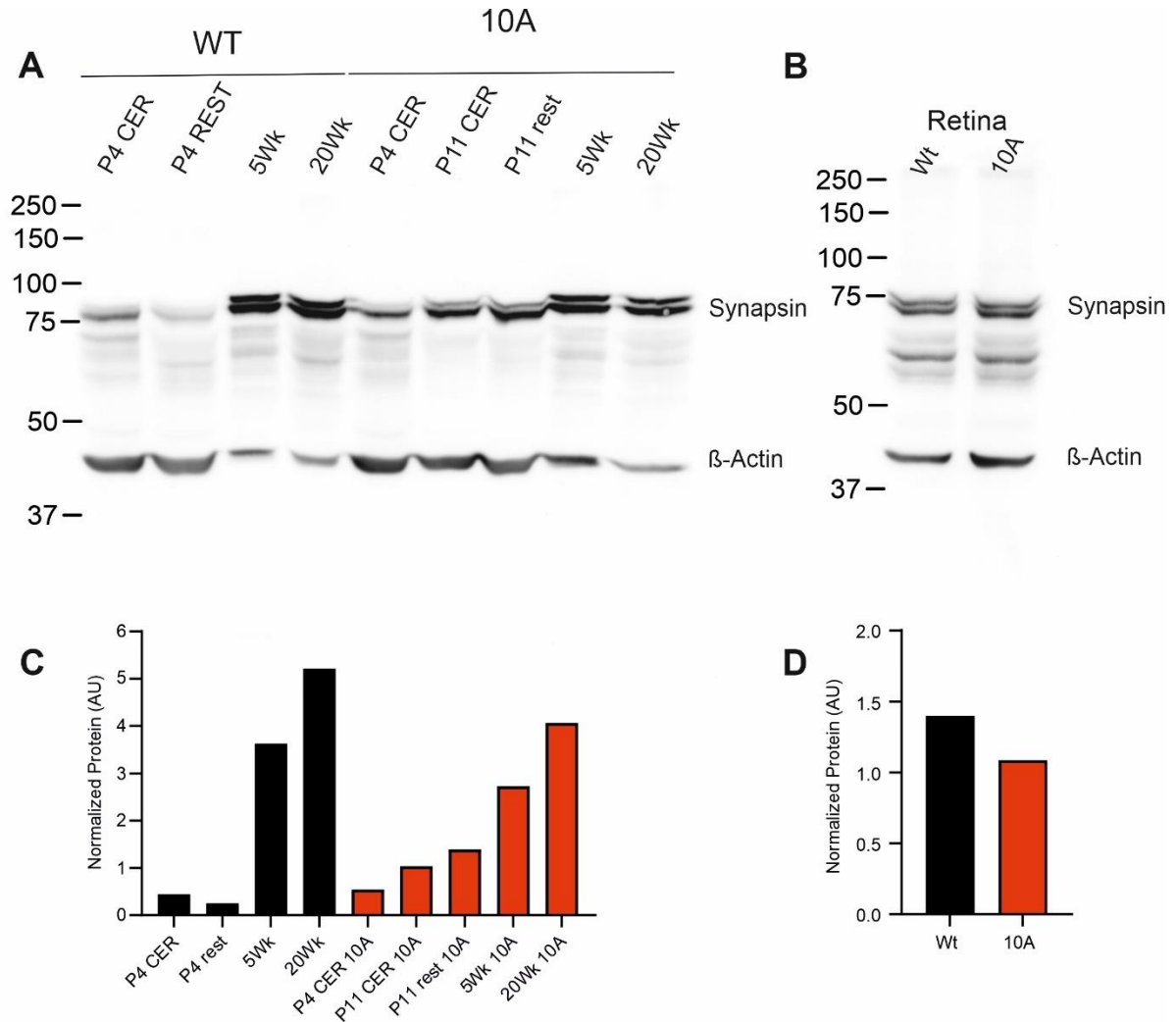


Figure 23 Analysis of expression levels of Synapsin in wild-type (Wt) and splice-deficient mice (10A). Western blot image showing expression levels of synapsin tested with lysates of Cerebellum or whole brain extracted from Wt and 10A mice of different ages (A) and from mouse retina (B). (C&D) Bar graphs showing quantification of synapsin levels normalized to beta-actin from their respective blot images.

Using the Western blotting technique, these lysates were probed with an anti-Synapsin antibody, with synapsin levels quantified through normalization to β -Actin levels. The obtained results, as illustrated in Figure 23A, revealed a progressive increase in synapsin levels with

advancing age in both wild-type and 10A groups. In comparison to the wild-type counterparts, 5-week-old and 20-week-old 10A mice exhibited a reduction in synapsin levels by approximately 25% (Figure 23C). Correspondingly, a parallel assessment of synapsin levels was performed in retina protein extracts from wildtype and 10A groups (Figure 23B). As anticipated, synapsin levels were also found to be diminished in the retinal tissue obtained from 10A mice in comparison to the wild-type control (Figure 23D).

The collective implications of these findings suggest a discernible influence of Stim1B's absence on the expression levels of synapsin. However, it is noteworthy that further comprehensive experiments are requisite to validate and elucidate the precise mechanisms underlying this observed relationship between Stim1B and synapsin expression. This multifaceted interplay between Stim1B and synapsin provides intriguing inroads for deeper exploration into the intricate mechanisms governing synaptic function and plasticity.

4.7 Behavioral studies

The aim of this chapter is to investigate the behavioral alterations due to the absence of Stim1B by evaluating motor performance, motor learning, and anxiety by performing the Erasmus ladder, Open field test, and Elevated plus maze test in splice-deficient mice and compare them with littermate controls. These experiments were performed in collaboration with the laboratory of Dr. Frank Kirchhoff. The Erasmusladder TVA (08/2021, Mausverhaltenstests und Awake Imaging)) included both sets of WT controls and 10A mice.

4.7.1 Assessment of motor performance and motor learning in mice lacking Stim1B

4.7.2 Both Motor performance and Adaptive cerebellar learning were impaired in splice-deficient mice

The Erasmus Ladder is a system to study motor performance and motor learning in rodents. Mice were allowed to run across the horizontal ladder to reach from one goal box to another. A trial is considered complete when the mouse walks across the ladder to reach the goal box and each session consists of 42 trials. Entire experimental paradigm is carried over 8 such sessions, of which first 4 sessions were the training phase and the following 4 sessions were the perturbation phase where sudden challenges were imposed on the mice such as the

conditional / unconditional / or paired stimulus which are programmed by the software in a randomized fashion. The rungs of the ladder is connected to the sensor which enables to measure the step types and duration.

Eight-week-old and sixteen-week-old mice belonging to both the control and 10A experimental groups underwent testing using the Erasmus ladder paradigm. The average proportion of high-to-high (H-H) short steps was comparable between the male control and 10A groups at the onset of the experimental paradigm (day 1). However, by the conclusion of the training phase, there was an approximate 15% reduction in this metric, as illustrated in Figure 24, Panel A. In contrast, the locomotion behavior of 10A female mice displayed a preference for a higher occurrence of H-H short steps, around 20% more in comparison to the control female mice (Figure 26, Panel A). Notably, both groups exhibited a decline in the percentage of H-H short steps by the end of the training phase (day 4), as depicted in Figure 24 & 25, Panel A.

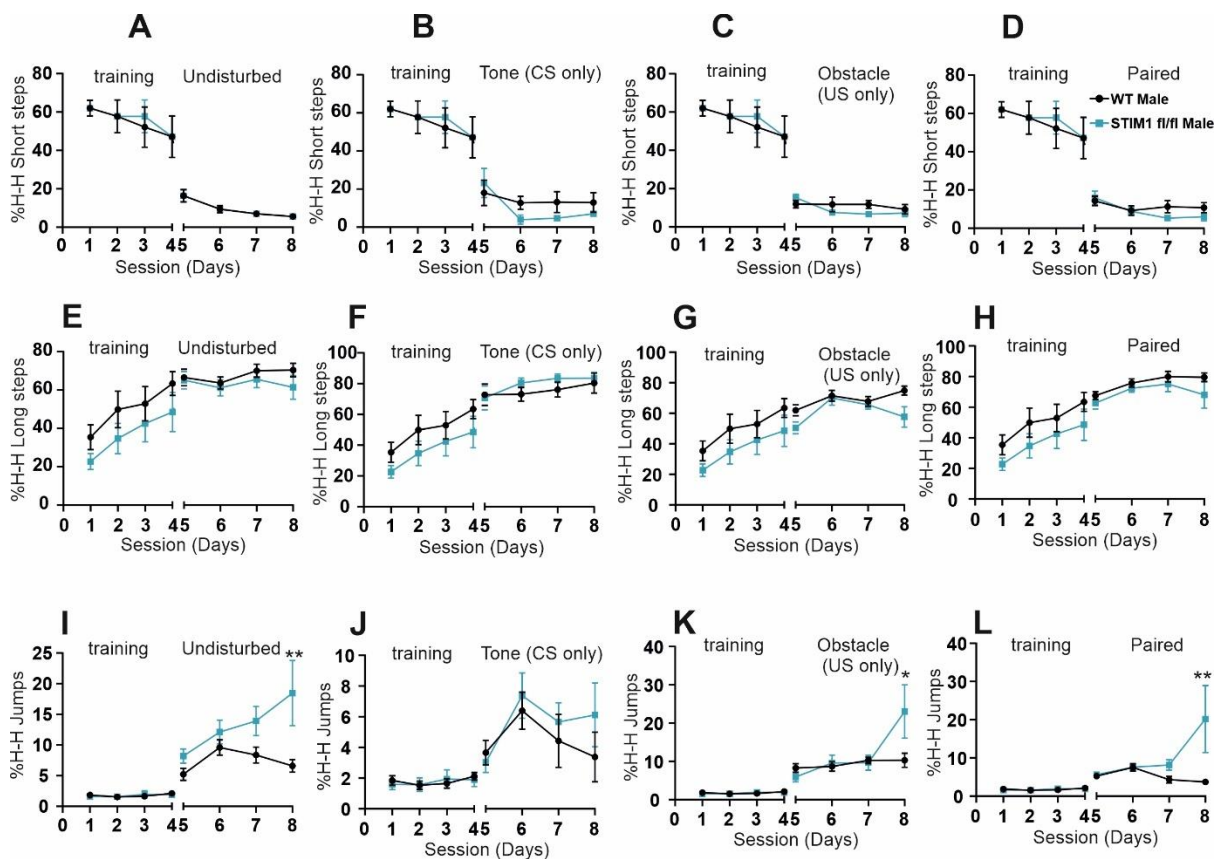


Figure 24 Erasmus ladder outcome: Analysis of locomotive behavior patterns of various step types in male splice-deficient mice. Average percentage of H-H short steps during pre- and post-perturbation phases observed in wild-type male (Wt male, black, n=17) and female splice-deficient mice (10A male, blue, n=18) during undisturbed trials (A), Conditional Stimulus (CS only) (B), Unconditional stimulus (US only) (C), and Paired (D). Average percentage of H-H long steps during pre- and post-perturbation phases observed during undisturbed trials

(E), Conditional Stimulus (CS only) (F), Unconditional stimulus (US only) (G), and Paired (H). Average percentage of H-H jumps during pre- and post-perturbation phases observed during undisturbed trials (I), Conditional Stimulus (CS only) (J), Unconditional stimulus (US only) (K), and Paired (L). * $p < 0.05$, ** $p < 0.01$, *** $p < 0.001$ represents unpaired Student's t-test with Welch's correction. Data are represented as Mean \pm SEM.

Conversely, the percentage of H-H long steps remained notably lower than that of short steps, and these long steps exhibited a gradual increase throughout the training phase, as indicated by Figure 24, Panel E, and Figure 25, Panel E. The occurrence of H-H jumps remained minimal, accounting for less than 2% during the training phase for both control and 10A groups, regardless of gender, as shown in Figure 24, Panel I, and Figure 25, Panel I. The outcomes derived from the training phase underscore that the learning process transpired within the initial four sessions for both the control and 10A mice cohorts.

During the perturbation phase, a notable reduction in the occurrence of the percentage of H-H short steps was observed in both the control and 10A experimental groups across genders, subsequent to the training phase (refer to Figure 24, Panel A, and Figure 25, Panel A). Naturally, the proportion of % H-H long steps exhibited a significant increase compared to the percentage of H-H short steps in undisturbed trials during the perturbation phase.

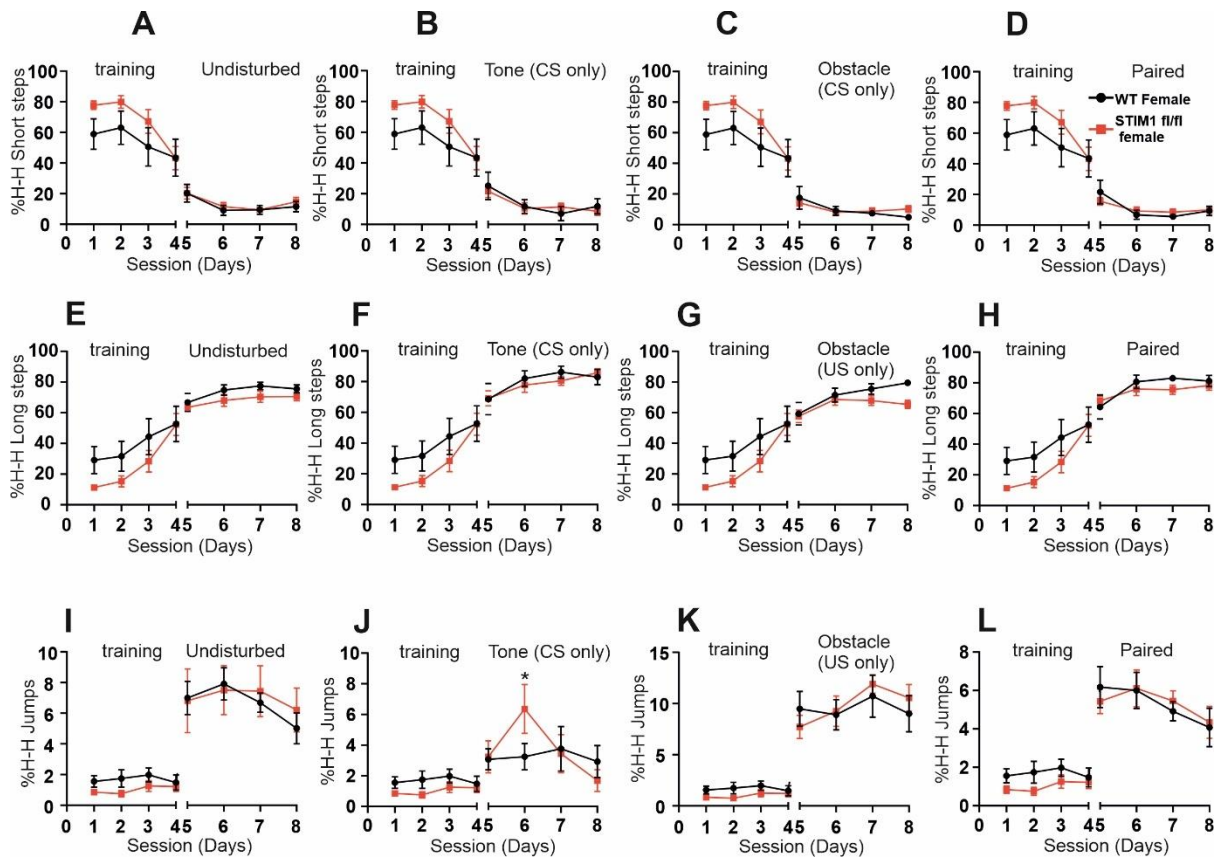


Figure 25 Erasmus ladder outcome: Analysis of locomotive behavior patterns of various step types in female splice-deficient mice. Average percentage of H-H short steps during pre- and post-perturbation phases observed in wild-type females (Wt female, black, n=14) and female splice-deficient mice (10A female, red, n=11) during undisturbed trials (A), Conditional Stimulus (CS only) (B), Unconditional stimulus (US only) (C), and Paired (D). Average percentage of H-H long steps during pre- and post-perturbation phases observed during undisturbed trials (E), Conditional Stimulus (CS only) (F), Unconditional stimulus (US only) (G), and Paired (H). Average percentage of H-H jumps during pre- and post-perturbation phases observed during undisturbed trials (I), Conditional Stimulus (CS only) (J), Unconditional stimulus (US only) (K), and Paired (L). *p<0.05, **p<0.01, ***p<0.001 represents unpaired Student's t-test with Welch's correction. Data are represented as Mean±SEM.

Particularly in the 10A male group, there was a marked increase in the percentage of H-H jumps within undisturbed trials during the perturbation phase in comparison to the control male group (Figure 24 Panel I). In contrast, both the 10A female and control female groups demonstrated significantly fewer instances of H-H jumps during undisturbed trials in comparison to males (as depicted in Figure 25, Panel I) throughout the perturbation session.

The percentage of H-H short steps observed in the 10A male and female groups closely paralleled the levels seen in the corresponding control groups when subjected to the perturbation session with a conditional stimulus (CS), as evidenced in Figure 24, Panel B and Figure 25, Panel B. Consequently, there was a steady upward trend in the proportion of H-H

long steps within both the 10A and control groups, regardless of gender, as illustrated in Figure 24, Panel F and Figure 25, Panel F. During the 5th day of the perturbation phase, both the 10A and control male groups demonstrated an equal utilization of H-H jumps. However, by the 6th day, there was an approximately 35% increase in H-H jump occurrences compared to the previous day for both groups. Intriguingly, this pattern diverged on the final day of the perturbation phase: the control males exhibited a pronounced reduction in the percentage of H-H jumps, while the 10A males experienced a significant and substantial increase relative to the control males, as depicted in Figure 24, Panel J. Similarly, at the outset of the perturbation phase with a conditional stimulus, the 10A and control female groups displayed an equivalent count of H-H jumps. However, by the 6th day of the perturbation session, the 10A female group demonstrated a notably higher utilization of H-H jumps in comparison to the control female group. Interestingly, both the 10A and control female groups exhibited a significant decline in their utilization of H-H jumps on the 7th and 8th days of the perturbation phase with the conditional stimulus only, as portrayed in Figure 25, Panel J.

Throughout the perturbation phase, when subjected to the unconditional stimulus (US, obstacle), the percentage of H-H short steps and H-H long steps within the 10A male and female groups did not exhibit any significant distinctions when contrasted with the control group. This trend is evident in Figure 24, Panels C, and G, as well as Figure 25, Panels C and G. However, with regard to H-H jumps, a distinct pattern emerges. Specifically, among the 10A male group, the percentage of H-H jumps was notably higher compared to the control male group, but this difference was only prominent on the final day of the perturbation phase, as illustrated in Figure 24, Panel K. Conversely, the 10A female group did not manifest any noteworthy variations in the percentage of H-H jumps when exposed to the perturbation phase with the unconditional stimulus, as compared to the control female group as shown in Figure 25, Panel K.

Consistent with observations from the unconditional stimulus data, there were no discernible disparities in the percentage of High-to-High (H-H) short steps and the percentage of H-H long steps within both cohorts, when juxtaposed with their respective control groups, under the influence of paired stimulus conditions throughout the perturbation phase. This consistency is evident in Figure 24, Panels D, and H, as well as Figure 25, Panels D, and H. However, a distinct trend emerged in relation to H-H jumps. Specifically, among the 10A male group, there was a marked escalation in the percentage of H-H jumps compared to their corresponding

control group. This discrepancy was particularly notable on the 8th day of the perturbation phase, in the context of paired stimulus conditions. This distinction is clearly depicted in Figure 24, Panel L. On the other hand, 10A females did not demonstrate a comparable increase in the percentage of H-H jumps when contrasted with their respective control group under the influence of paired stimulus conditions during the perturbation phase. This lack of distinction is highlighted in Figure 25, Panel L.

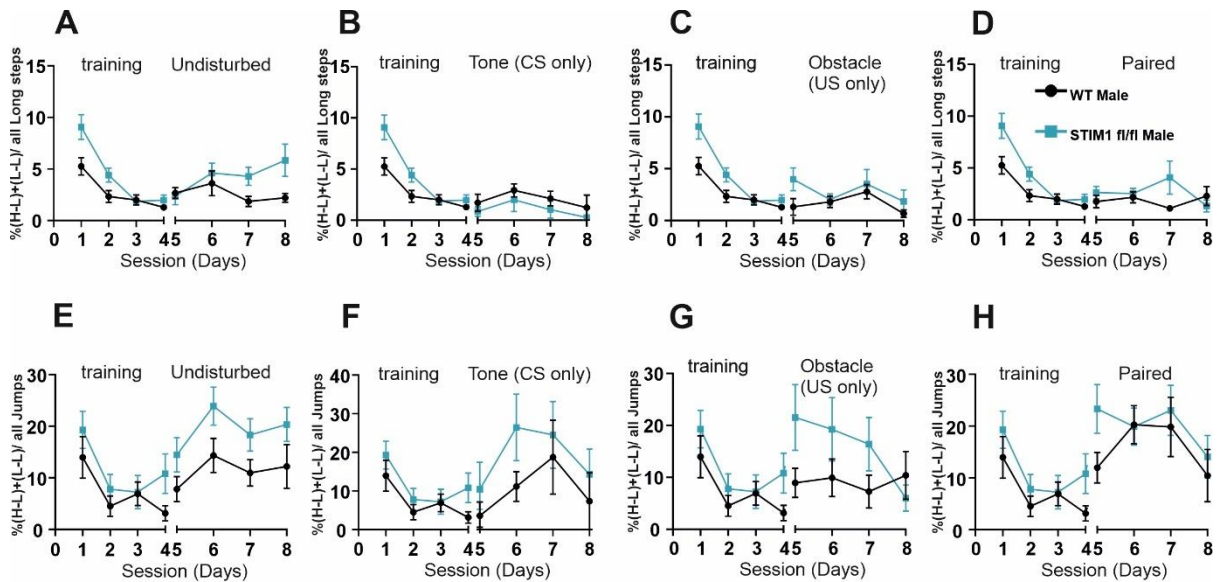


Figure 26 Erasmus ladder outcome: Analysis of locomotor performance in male splice-deficient mice. Average percentage of (H-L) + (L-L)/ all long steps during pre-and post-perturbation phases observed in wild-type male (Wt male, black, n=17) and male splice-deficient mice (10A male, blue, n=18) during undisturbed trials (A), Conditional Stimulus (CS only) (B), Unconditional stimulus (US only) (C), and Paired (D). Average percentage of (H-L) + (L-L)/ all Jumps during pre- and post-perturbation phases observed during undisturbed trials (E), Conditional Stimulus (CS only) (F), Unconditional stimulus (US only) (G), and Paired (H). * $p < 0.05$, ** $p < 0.01$, *** $p < 0.001$ represents unpaired Student's t-test with Welch's correction. Data are represented as Mean \pm SEM.

To further elucidate potential disparities in locomotion patterns and performance between the control and 10A groups, we included the locomotion pattern of H-L (High-to-Low) and L-L (Low-to-Low) long steps, along with H-L and L-L jumps, to assess the percentage of accurate steps undertaken on the higher rung during both the training and perturbation phases.

An intriguing pattern emerged in the analysis of H-L and L-L long steps. For 10A males, the cumulative percentage ratio of H-L and L-L long steps to the overall count of long steps was approximately twofold higher in comparison to control males on the initial day of the training

phase. However, this disparity diminished as the training phase progressed, as demonstrated in Figure 26, Panel A. Similarly, 10A females exhibited a parallel trend, with a higher percentage ratio of H-L and L-L long steps to all long steps on the first day compared to control females, yet this distinction became negligible by the conclusion of the training phase, as depicted in Figure 27, Panel A.

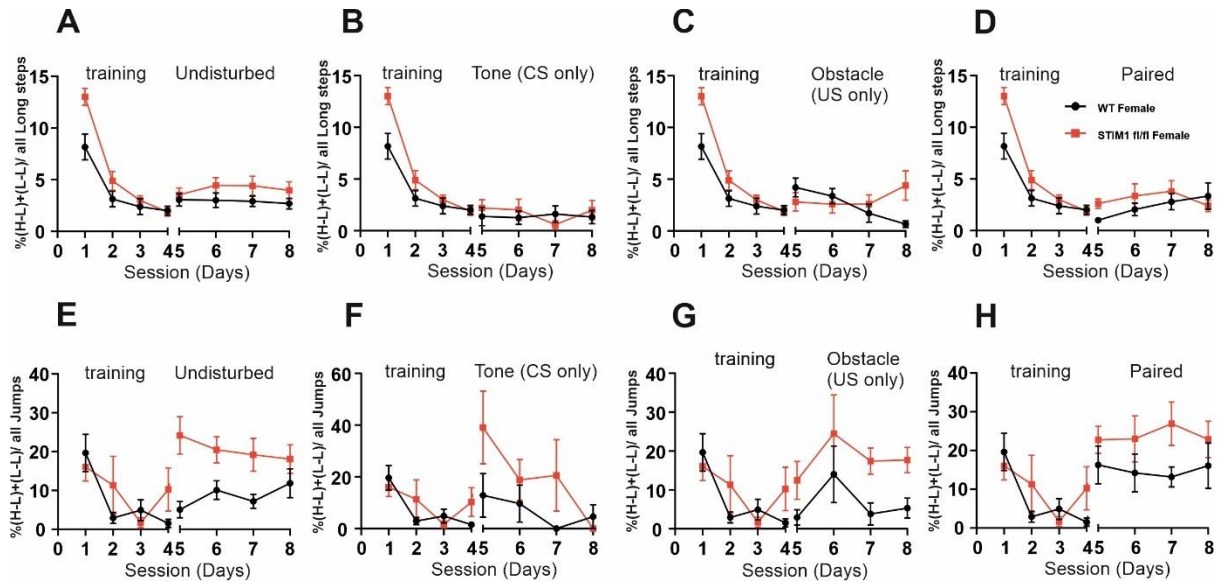


Figure 27 Erasmus ladder outcome: Analysis of locomotor performance in female splice-deficient mice. Average percentage of (H-L) + (L-L)/ all long steps during pre- and post-perturbation phases observed in wild-type female (Wt female, black, n=14) and female splice-deficient mice (10A female, red, n=11) during undisturbed trials (A), Conditional Stimulus (CS only) (B), Unconditional stimulus (US only) (C), and Paired (D). Average percentage of (H-L) + (L-L)/ all Jumps during pre- and post-perturbation phases observed during undisturbed trials (E), Conditional Stimulus (CS only) (F), Unconditional stimulus (US only) (G), and Paired (H). *p<0.05, **p<0.01, ***p<0.001 represents unpaired Student's t-test with Welch's correction. Data are represented as Mean±SEM.

During the perturbation phase, a noteworthy divergence was evident among 10A males. They displayed a greater occurrence of irregular long-step types, involving stepping onto the lower rung, during undisturbed trials. Moreover, when subjected to conditional and unconditional stimuli, as well as paired stimuli, the irregular long step types exhibited discernible differences compared to control males, as presented in Figure 26, Panels B, C, and D. Conversely, 10A females demonstrated an elevated presence of irregular long-step types when encountering obstacles (unconditional stimulus) on the last day of the perturbation phase. However, their performance in other trials did not markedly differ from control females, as depicted in Figure 27, Panels A-D.

Furthermore, the analysis of irregular jumps yielded significant findings in both gender groups. Notably, the irregular jumps in both 10A male and female groups demonstrated a considerable impact compared to their respective control groups, spanning both undisturbed and perturbation trials. This underscored a substantial effect on motor performance and associative motor learning, as elucidated in Figure 26, Panels E-H, and Figure 27, Panels E-H.

To evaluate the motor performance of 10A mice, the percentage of missteps per trial day were quantified. Among 10A male mice, there was an elevated percentage of missteps observed during the initial two days of the training phase in comparison to control males, as depicted in Figure 28, Panel A.

Transitioning to the perturbation phase, 10A males exhibited notable differences in the percentage of missteps per session. Specifically, significant differences were apparent on the 7th and 8th days during undisturbed trials, on the 6th day with an unconditional stimulus, and on the 7th day with a paired stimulus. However, there were no pronounced differences associated with the conditional stimulus, as illustrated in Figure 28, Panels B-D.

In contrast, the percentage of missteps per session within the 10A female group remained relatively unchanged throughout the training phase in comparison to the control female group. During the perturbation phase, discernible discrepancies emerged on the 6th and 7th days with undisturbed trials, as shown in Figure 29, Panel E. Additionally, minor distinctions were observed in the context of conditional and paired stimulus conditions, albeit less prominently, as displayed in Figure 28, Panels F, and H. Notably, the 10A female group exhibited a significant increase in missteps on the 8th day during unconditional stimulus trials, compared to the control group, as presented in Figure 28, Panel G.

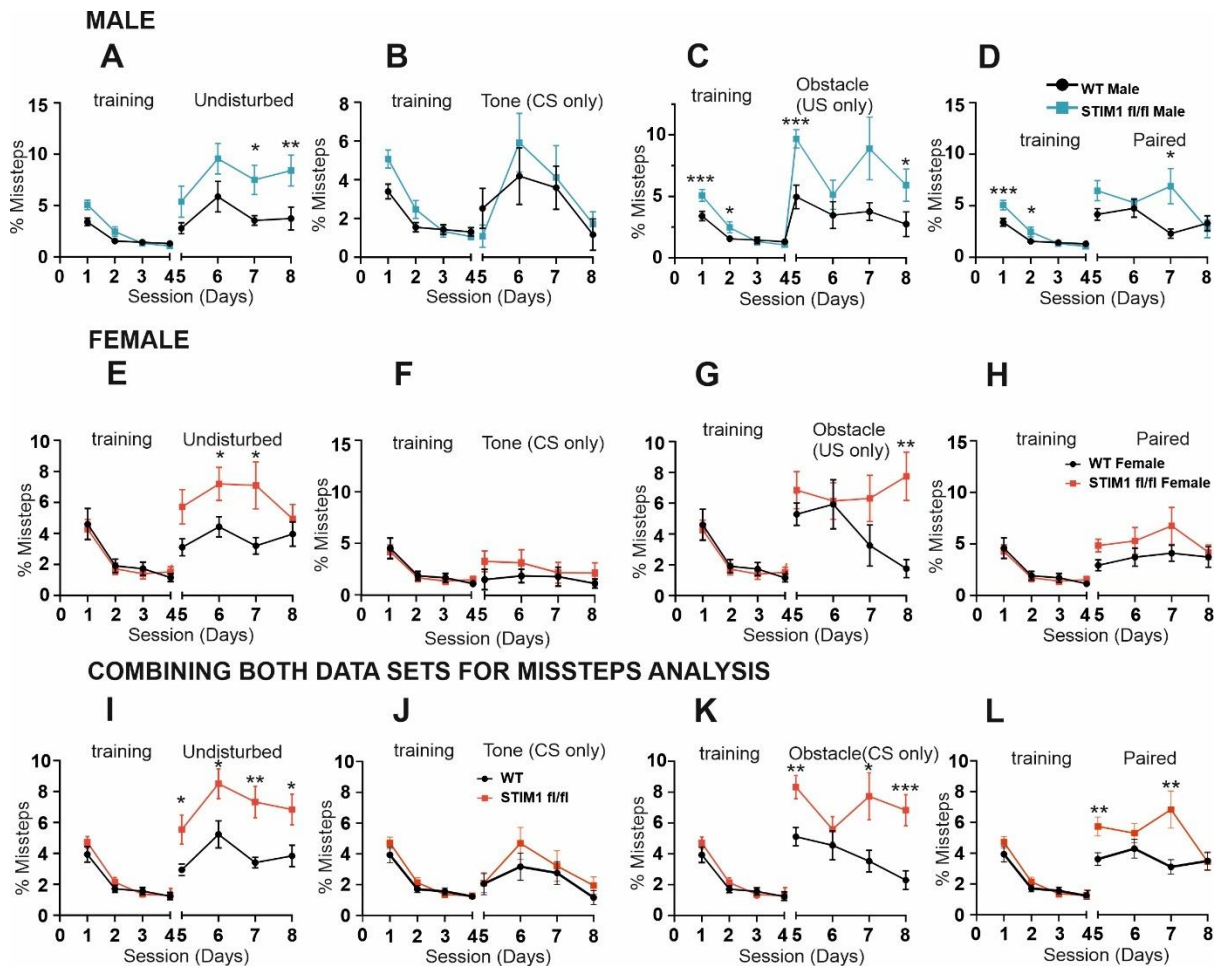


Figure 28 Erasmus ladder outcome: Adaptive cerebellar learning deficits in splice-deficient mice. Average percentage of missteps analyzed from various step types during pre- and post-perturbation phases observed in wild-type males (Wt male, black, n=17) and male splice-deficient mice (10A male, blue, n=18) during undisturbed trials (A), Conditional Stimulus (CS only) (B), Unconditional stimulus (US only) (C), and Paired (D). Average percentage of missteps analyzed from various step types observed during pre- and post-perturbation phases observed in wild-type females (Wt female, black, n=14) and female splice-deficient mice (10A female, red, n=11) during undisturbed trials (E), Conditional Stimulus (CS only) (F), Unconditional stimulus (US only) (G), and Paired (H). Average percentage of missteps analyzed from various step types during pre- and post-perturbation phases combining both the gender data sets (Wt in black, splice-deficient group (10A) in red) during undisturbed trials (I), Conditional Stimulus (CS only) (J), Unconditional stimulus (US only) (K), and Paired (L). *p<0.05, **p<0.01, ***p<0.001 represents unpaired Student's t-test with Welch's correction. Data are represented as Mean±SEM.

Combining data from both genders underscored significant disparities in the percentage of missteps during the perturbation phase with undisturbed trials and obstacle trials. This collective evidence strongly indicates an impairment in motor performance and a deficit in adaptive cerebellar learning among splice-deficient mice, as emphasized in Figure 28, Panels I-L.

4.7.3 Assessment of anxiety behavior in mice lacking Stim1B

The elevated plus maze (EPM) and Open field test (OF) were performed to investigate if there were any anxiety-related behavioral changes. These tests are based on the natural aversion of mice to open and elevated areas as well as their spontaneous exploratory behavior in novel environments.

4.7.4 Anxiety-related behavior was unaffected in splice-deficient mice

4.7.4.1 Elevated plus maze

Mice aged 8 weeks and 16 weeks, originating from both the 10A and control groups, were subjected to exploration within an elevated plus apparatus (EPM), characterized by two open arms and two closed arms. During this process, the mice were given the freedom to explore the arms, and their behavior was recorded through video recording. Subsequently, their movement trajectories were analyzed using video tracking software. The analysis of these recorded behaviors led to noteworthy observations. Specifically, in the case of the 8-week-old 10A mice, their exploratory behavior was on par with the control group. Additionally, the number of entries into the open arms closely resembled that of the control group, as illustrated in Figures 29A and B.

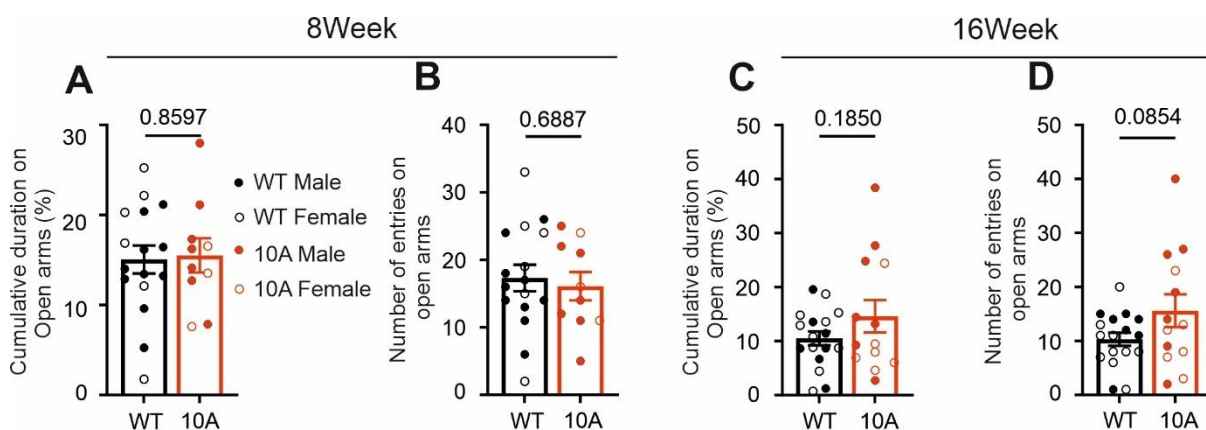


Figure 29 Elevated plus maze outcomes: Assessment of anxiety and impulse behavior in splice-deficient mice. Bar graphs showing (A) percentage of cumulative duration in open arms and (B) the number of entries in open arms observed with 8-week-old splice-deficient mice (male wt, n=10 (black solid), female wt, n=6 (round black), 10A male, n=7 (red solid), 10A female, n=3 (round red)) and (C) percentage of cumulative duration in open arms and (D) number of entries in open arms observed with 16-week-old splice-deficient mice (male wt, n=7 (black solid), female wt, n=10 (round black), 10A male, n=7 (red solid), 10A female, n=6 (round red)). * $p < 0.05$, ** $p < 0.01$, *** $p < 0.001$ represents unpaired Student's t-test with Welch's correction. Data are represented as Mean \pm SEM.

Similarly, the 16-week-old 10A mice did not exhibit signs of anxiety-related behavior. Their exploratory behavior included spending more time in open arms as compared to the control group. Furthermore, the frequency of entries into the open arms remained unaffected within the 10A group, as depicted in Figures 29C and D.

Based on these findings, it is evident that both 8-week-old and 16-week-old 10A mice displayed exploratory behavior and open-arm entries in a manner that did not suggest the presence of anxiety symptoms. This underscores the absence of open space-induced anxiety in mice lacking the Stim1B splice variant, as evidenced by the outcomes from the elevated plus apparatus exploration.

4.7.4.2 Open field test

Mice aged 8 weeks and 16 weeks, belonging to both the 10A and control groups, were introduced to an open-box environment for exploration. During this phase, video recordings were made to capture the mice's locomotion and exploration behaviors. Subsequently, these recordings were subjected to analysis using video tracking software, with a focus on assessing anxiety-related behaviors.

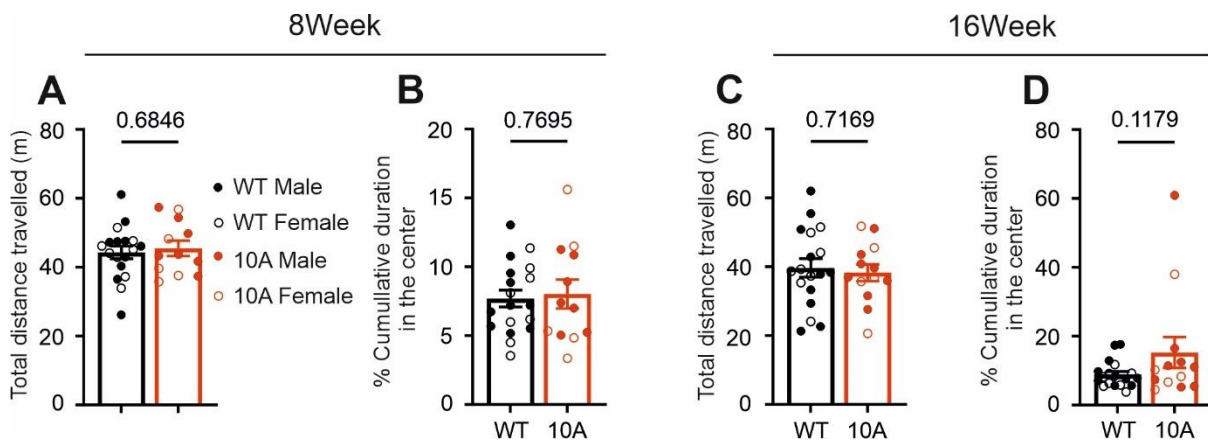


Figure 30 Open field maze outcomes: Assessment of anxiety and impulse behavior in splice-deficient mice. Bar graphs showing (A) total distance traveled and (B) average percentage of cumulative duration in the center observed with 8-week-old old splice-deficient mice (male wt, n=10 (black solid), female wt, n=8 (round black), 10A male n=7 (red solid), 10A female, n=5 (round red)) and (C) total distance traveled and (D) average percentage of cumulative duration in the center observed with 16-week old splice-deficient mice (male wt, n=7 (black solid), female wt, n=10 (round black), 10A male, n=7 (red solid), 10A female, n=6 (round red)). * $p < 0.05$, ** $p < 0.01$, *** $p < 0.001$ represents unpaired Student's t-test with Welch's correction. Data are represented as Mean \pm SEM.

Upon analyzing the tracking data, noteworthy findings emerged. Specifically, the total distance covered by the 8-week-old 10A mice and the percentage of time spent in the center of the open maze were comparable to those of the control group, as depicted in Figures 30A and B. Similarly, the 16-week-old 10A mice exhibited exploratory behavior over an equivalent distance to the control group when inside the open box. Moreover, the duration of time spent in the center of the open maze was also comparable to that of the control group, as illustrated in Figures 30C and D. Based on these observations, it is evident that mice lacking the Stim1B splice variant did not exhibit anxiety-related behaviors within the experimental context. These findings suggest a lack of development of anxiety-related behaviors in mice without Stim1B.

4.8 Proteomics

4.8.1 To identify potential interacting partners of Stim1B – Mass spectrometry approach

A Splice specific antibody – Stim1B antibody was developed with the help of Dr. Martin Jung, Department of Biochemistry. Results from immunoprecipitation of Stim1 NT showed that Stim1B is precipitated along with Stim1 (Figure 31A) although immunoprecipitation with Stim1CT did not show any successful precipitation of the proteins (both variants). This could be due to the unsuccessful binding of dynaG beads to the antibody-protein complex or due to protein degradation or it could be the fact that Stim1B prefers to dimerize with itself or with Stim2. Immunoprecipitation with Stim1B antibody has precipitated Stim1B only to some extent, as the input lane still showed a strong band corresponding to Stim1B. This could be due to the poor efficacy of Stim1B's antibody to precipitate Stim1B protein. Similarly, immunoprecipitation was performed in cerebellar lysates by incubating with Stim2 antibody and eluates were probed with Stim1 antibody with N terminal epitope. Figure 31B shows that Stim2 is able to pull both the variants, Stim1 and Stim1B.

To confirm this result, the reverse experiment was done by performing immunoprecipitation with Stim1B and probed the eluates with Stim2 polyclonal antibody. Figure 31C confirmed that Stim1B also pulled Stim2, thus Stim2 is clearly one interaction partner of Stim1B. To identify potential interacting partners of Stim1B, immunoprecipitation was performed with Stim1 polyclonal antibody with N – terminal epitope or Stim1 monoclonal antibody with C

terminal epitope in freshly extracted lysates from MEF S1/2 DKO cells and cerebellar extracts. IP eluates were run on SDS PAGE and the coomassie stained gel were excised based on molecular weights fractions corresponding to the protein standard (Figure 31D). Probes 1, 5, 9, 13 corresponds to proteins that were approximately above 250kDa, Probes 2, 6, 10, 14 corresponds to proteins with molecular weight between 60-200kDa, Probes 3, 7, 11, 15 corresponds to proteins with molecular weight between 40-60kDa, Probes 4, 8, 12, 16 corresponds to proteins with molecular weight between 20-40kDa. The samples were sent to Dr. Vera Jakowski, Aachen, who performed the MS analysis. Table 29 shows the protein hits from the corresponding probe with MASCOT score, and that did not show up in the extracts of MEF S1/2 DKO cells (Probes 5-8 & 13-16). The MASCOT scoring system takes into account various parameters such as the number of matched peptide sequences, the quality of the matches, the mass accuracy of the observed peptides, and other factors. The higher the MASCOT Score, the more reliable the identification of the protein. If the protein with a high MASCOT score was found in probes 1-8, but not seen in samples 9-16, we could have tracked down the potential interacting partner specific for Stim1B.

Table 29 Potential protein interaction hits from Mass Spectrometry

Name of the protein	Gene Name	Probe	MASCOT Score
Paralemmin	PALM	4	70
Serine/Threonine Kinase 25	STK25	3	64
Potassium Channel, Inwardly Rectifying Subfamily J Member 15	KCNJ15	3&7	72
Microtubule Associated Protein RP/EB Family Member 3	MAPRE3	4	21
Microtubule Associated Protein RP/EB Family Member 3	MAPRE3	12	63

Although several hits with high MASCOT score was observed, such as Paralemmin (PALM) in probe 4 with a MASCOT score of 70, STK25 with a MASCOT score of 64 in probe 3 and KCNJ15 detected with a score of 72, they were seen in both groups of samples pulled by Stim1 antibodies. MAPRE3 was detectable with a score of 21 in probe 4, but a significant score of 63 in probe 12 (See in Table 29). With the MS analysis, we could not find a potential interacting partner specific to Stim1B.

Similarly, IP experiments were conducted with cerebellar extracts and retinal extracts from both wildtype and 10A mouse which lacks Stim1B and are immune precipitated using Stim1 antibody (N terminal epitope). The eluates were run on 10% SDS gel and silver staining was performed and the gel was cut following staining (Figure 3 1E). The respective samples were sent for MS analysis as explained earlier. Analysis of these samples was not promising as they did not show any potential hits that came for wild type alone or in 10A only, and the potential reason could be that the protein in the IP eluates would be too little to detect in MS. Following the MS analysis, Paralemmin was tested for Co-IP with tagged Paralemmin constructs, but without positive results.

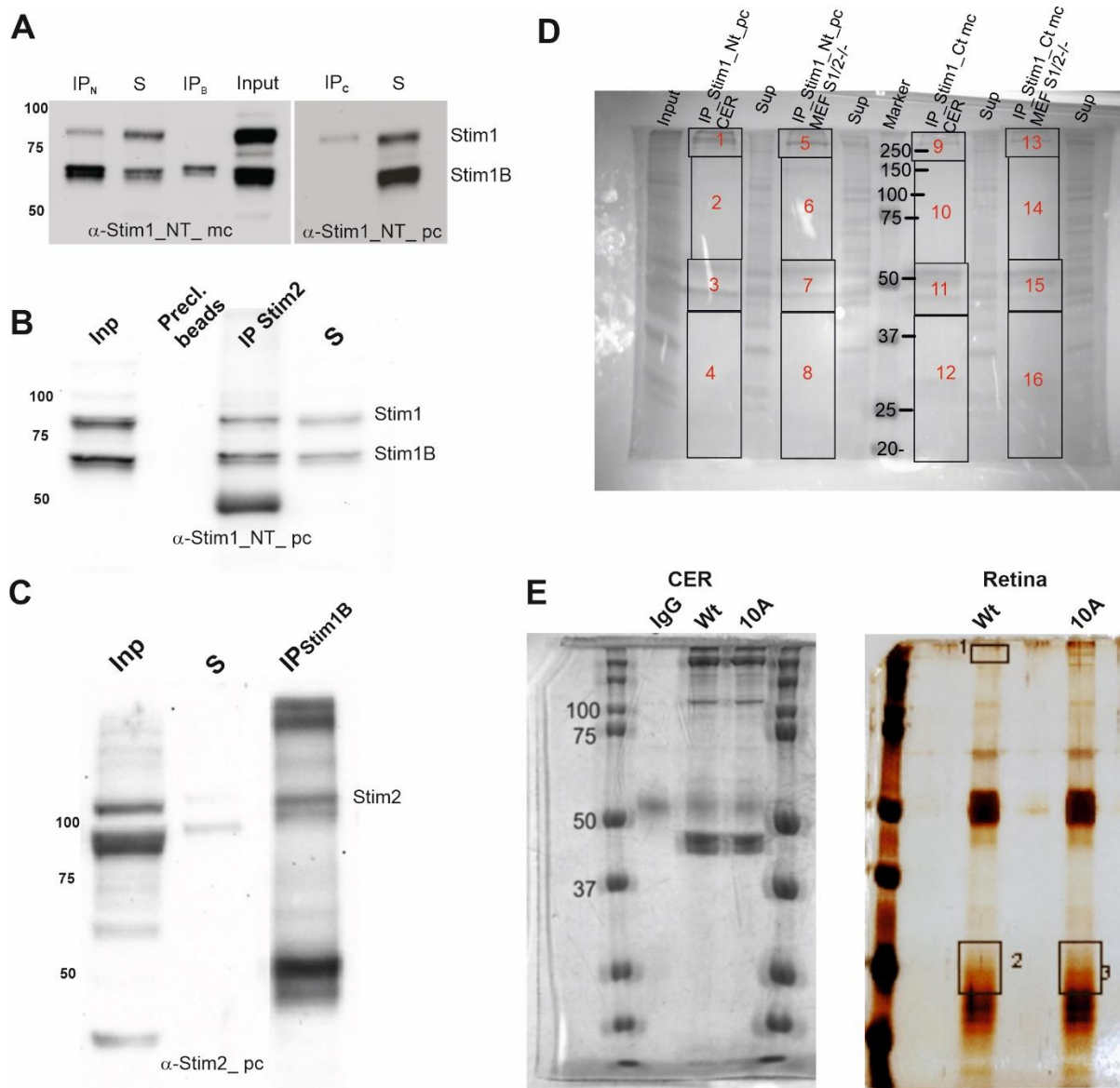


Figure 31 Investigation of Interacting partners of Stim1B. (A) Immunoprecipitation of Stim1 and Stim1B with Stim1 N terminal monoclonal antibody (right) & Stim1 N terminal polyclonal antibody (left). (B) Immunoprecipitation of Stim1 and Stim1B with Stim2 polyclonal antibody. (C) Immunoprecipitation of Stim2 with Stim1B polyclonal antibody (self-made). (D) Immunoprecipitated eluates from mouse cerebellar lysates and MEF S1/S2 ^{-/-} with Stim1 polyclonal antibody with N terminal epitope or Stim1 monoclonal antibody with C terminal epitope on SDS PAGE gel stained with Coomassie dye. (E) Immunoprecipitation of cerebellar lysates from wild-type and 10A mice (Left) and retinal lysates from wild-type and 10A mice with Stim1 polyclonal antibody with N terminal epitope. MS analysis performed by Dr. Vera Jankowski, Aachen.

5. Discussion

5.1 Splice variants of Stim1

5.1.1 Stim1B is a new Stim1 splice variant

The human genome consists of approximately 20,600 protein-coding genes, which seems to be surprisingly low for the proteomic complexity in tissues, but with an average of 6.3 alternatively spliced transcripts (3.9 different protein-coding transcripts) per locus (The ENCODE project consortium, 2012). Previously in 2011, a splice variant of Stim1, Stim1L was found to be expressed in several mammalian cell types allowing for rapid replenishment of intracellular Ca^{2+} stores and generation of repetitive cytosolic Ca^{2+} signals by interacting with Actin (Darbellay et al., 2011, Saüc et al., 2015, Dyrda et al., 2020). In addition to this splice variant of Stim1, database mining predictions yielded yet other splice variants of Stim1: Stim1B, Stim1A, and Stim1AB. All the identified splice variants of Stim1 arose due to alternative splice in the region around exon 12-14, which indicates a high hot spot for splicing this region. Alina Gilson was able to provide the first evidence of newly predicted Stim1 splice variants through a diagnostic PCR method during her Bachelor thesis (2016). The existence of Stim1B was confirmed by diagnostic PCR in different regions of the brain, viz. cortex, cerebellum, hippocampus, and thalamus, and also in human post-mortem brain tissue (UdS Bachelor thesis of Alina Gilson, 2016). These detections were further confirmed by quantitative real-time PCR with splice-specific primers (Performed by Getrud Schwär and Kathrin Förderer). Added to this, qPCR data from human post-mortem brain tissue regions along with stimulated CD^{4+} and CD^{8+} provided concrete evidence that Stim1B is expressed only in the brain. While abundant in several investigated brain regions, exon B and the corresponding Stim1B protein is the dominant Stim1 isoform in cerebellum but also contributes to approximately 40% of Stim1 protein in hippocampus, cortex, and olfactory bulb (Figure 5G). The regional differences between Stim1 and Stim1B at the protein level followed a consistent trend as seen with diagnostic PCR and qRT-PCR data (Figure 5C-E). Previous studies have indicated a notably high expression of Stim1 in the cerebellum relative to other regions of the brain, as reported by Kleijman et al. (2009) and Skibinska-Kijek et al. (2009). However, it is worth noting that in Kleijman et al.'s research, an intriguing lower band below Stim1 was consistently observed in the cerebellum. Surprisingly, this lower band's characteristics and significance were neither elucidated nor discussed in their study. This lower band could

correspond to the newly identified Stim1B splice variant in this work. Glycosylation is a post-translational modification process in which sugar molecules are attached to specific amino acid residues of a protein. Two N-linked glycosylation sites have been identified in Stim1 at the N terminal within the SAM domain, one at Asn 13 preceding the initial alpha helix of SAM domain and other at Asn 171 within the SAM domain region which remains endoH sensitive (Williams et al., 2002). Stim1B, along with Stim1 was also partially glycosylated in cerebellum (Figure 5H) which was confirmed by treating the cerebellar lysate extracts with PNGase. Earlier studies have shown that mutation of the two glycosylation sites to glutamine resulted in impaired SOCE through reduced Stim1 function (Custora et al., 2008), or unaltered endogenous Stim1 levels or the endogenous SOCE (Mignen et al., 2007). In contrast to earlier research, a study from Kilch et al., 2013 showed that double mutation of glycosylation sites of Stim1 does not negatively impact the Stim1's functional ability, a rather specific mutant combination of the two glycosylation sites to Aspartic acid and glutamine (N131D/N171Q) displayed a strong gain of function. The other splice variant of Stim1, Stim1A was clearly identified in astrocytes and testes (Knapp et al., 2022) while Stim1B was clearly absent in astrocytic cultures (Figure 5D) which indicated that Stim1B is neuronal specific. Overall, of several predicted splice variants of the Stim1 gene, one particular variant, which we termed Stim1B, is highly enriched in the CNS. The evolutionary analysis also revealed that exon B represents a mammalian-specific event which is highly conserved (Ramesh et al., 2021, Figure S1B) and the high neuronal expression could suggest a selective advantage correlated with mammalian brain function.

5.2 STIM1B is a differential activator of SOCE with distinct characteristics

Functional characterization of the newly identified splice variant of Stim1 was not reported elsewhere. Therefore, following the successful detection of Stim1B in the brain and cloning of the Stim1B in a bicistronic vector system, it was tested if Stim1B is able to activate SOCE in the overexpression system in comparison to the conventional variant Stim1. Immunostaining of Stim1 showed ER localization and formed puncta-like clusters along the ER extensions upon the addition of Tg as described in several reports (Li et al., 2007, Muik et al., 2008, Park et al., 2009, McNally et al., 2013). In the same way, Stim1B was also seen localized in ER and formed clusters upon the addition of Tg and strongly colocalized with Stim1 which indicated Stim1B's ability to form heterodimers with Stim1 (Figure 6A-D). Functionally, when Stim1B was

overexpressed alongside endogenous Stim1 in HEK293 cells or in cells lacking endogenous Stim1/2 (HEKS1/2 DKO), the result was a deceleration in the activation kinetics of I_{CRAC} (Calcium-Release Activated Calcium Current) without any significant alteration in its amplitude, as illustrated in Figure 7-9 (Ramesh et al., 2021). However, when Stim1B was co-expressed with Orai2, it led to a weaker activation of Orai2 currents compared to Stim1, resulting in reduced CRAC current amplitude and slower kinetics, as depicted in Figure 9E-H. Interestingly, the interaction of Stim1B with Orai3 produced a unique outcome, where there was a continuous increase in I_{CRAC} mediated by Stim1B, in contrast to the continuous decrease observed with the co-expression of Stim1 (Figure 9I-L). This effect was not replicated with ORAI3, which was only weakly activated by STIM1B, as shown in Figure 7G-I. Furthermore, the activation of Store-Operated Calcium Entry (SOCE) by both Stim1 and Stim1B exhibited maximal current amplitudes for Orai2 and Orai3 that were approximately three times smaller than the corresponding current amplitude observed for Orai1. This finding fits with previous studies that suggested Orai1 as the dominant homolog among the three Orai homologs in augmenting store-operated calcium entry (SOCE). (Mercer et al., 2006, Lis et al., 2007, Gross et al., 2007). Ca^{2+} imaging data also confirmed that STIM1B overexpressed in SHSY5Y S1/2 DKO cells only partially rescued SOCE, and displayed decreased rate, peak, and plateau of SOCE (Data by Lukas Jarzembowski). Also, the addition of STIM1B in the SHSY5Y DKO background led to increased basal Ca^{2+} , which was not observed in the presence of STIM2 (Ramesh et al., 2021). The translated Stim1B protein due to the insertion of exon B led to a frameshift and has a premature stop codon, which makes Stim1B a shortened variant lacking 146 amino acids at the C-terminal which contains the serine-proline rich and a C-terminal polybasic domain. The importance of the C terminal region of Stim1 in the attachment of Plasma Membrane and the regulation of SOCE has been previously discussed, although controversial. The polybasic domain at the C terminal tail of Stim1 is crucial for SOCE function (Huang et al., 2006, Baba et al., 2006, Jardin et al., 2013). On the other hand, another report suggests that the polybasic domain of Stim1 mediates Stim1 targeting to PM but not essential for CRAC channel activation (Li et al., 2007, Park et al., 2009, Yuan et al., 2009, Bhardwaj et al., 2013). Stim1 lacking C terminal polybasic domain resulted in decreased Stim1 translocation to the ER-PM junction but did not fail to oligomerize upon store depletion (Park et al., 2009) which is contrasting to previous studies which showed that delayed translocation leads to a failure in puncta formation which is the first step in SOCE activation (Huang et al.,

2006, Liou et al., 2007). The failure of puncta formation of Stim1 upon store depletion did not persist when expressed together with Orai1 and it suggests that the polybasic domain of Stim1 is required for targeting Stim1 to ER-PM junctions independent of Orai1 and that the CAD domain is required for channel activation (Park et al., 2009, Kawasaki et al., 2009, Yuan et al., 2009). The C terminal polybasic domain of Stim1 interacts with phospholipids of the plasma membrane and functions as an anchor to attach Stim1 to the inner leaflet phospholipids of PM (Ercan et al., 2009, Yuan et al., 2009, Zhou et al., 2013), the lack of this domain could therefore affect the recruitment of Stim1B to the ER-PM junction and formation of clusters. However, the TIRFM experimental data showed that expression of STIM1B in HEK cells lacking endogenous Orai proteins showed ER distribution at rest and cluster formation after Tg treatment (Figure 2F from Ramesh et al., 2021). The TRIP motif (aa 642-645) of Stim1 is the interacting region for EB1 (End binding protein) which helps Stim1 to attach to the microtubuli (MT) plus ends enabling Stim1 to extend along cortical ER structures. EB1 binding also acts as a regulatory feedback mechanism by delaying Stim1 translocation to the ER-PM junction upon store depletion, thereby preventing excess SOCE and ER Ca^{2+} overload (Chang et al., 2018, Orci et al., 2009). Stim1B, lacking also this binding motif could alter the regulation of SOCE. This led us to perform TIRF imaging experiments to understand its kinetics of activation. STIM1 overexpressed in HEK S1/2 DKO cells showed initial translocation towards the PM along the longitudinal tracks (MTs) (Ramesh et al., 2021, video S1) as previously reported by Chang et al., 2018, while STIM1B which lacks the TRIP displayed delayed translocation lacking MT tracking but eventually formed clusters at the TIRF plane (Ramesh et al., 2021, Video S2). The analysis of TIRF images showed that Stim1B delayed cluster formation and developed smaller clusters (Ramesh et al., 2021). In our study involving HEK cells devoid of endogenous Orais, we observed clear endoplasmic reticulum (ER) distribution at rest and the formation of clusters following treatment with Thapsigargin (Tg) for Stim1, Stim1B, and Stim1_514* (as shown in Figure 2F & S1I from Ramesh et al., 2021). Notably, Stim1B and Stim1_514* induced the formation of smaller clusters compared to Stim1. Furthermore, patch clamp experiments conducted in the absence of Stim2 unequivocally demonstrated the formation of I_{CRAC} for all the examined constructs. These findings strongly indicate that neither Stim2, the polybasic domain (PBD), nor the presence of Orai homologs plays a central role in the initial formation of ER-plasma membrane (PM) clusters. Instead, their significance becomes evident in facilitating the expansion of cluster sizes. These

observations unequivocally emphasize that the involvement of Stim2, the polybasic domain, or Orai homologs primarily influences the amplification of ER-PM clusters rather than their initial formation (Zheng et al., 2018). Several functional studies have identified differing roles for C terminal and N terminal sites of Orai homologs in gating and activation of Stim1. Deletion of C terminal residues of Orai1 between aa254-301 has been shown to completely eliminate the binding to Stim1 and CRAC channel activation following the store depletion using FRET, pull-down assays, and crystallography experiments (Li et al., 2007, Muik et al., 2008, Navarro-Borelly et al., 2008, Muik et al., 2009, Park et al., 2009, Yuan et al., 2009). These results have highlighted the significance of Stim1CT-Orai1CT coupling in channel activation. In addition to that, another interaction site of Orai1 is the later part of the N terminal region (aa 65-91) is crucial for its interaction with Stim1 CT (Park et al., 2009, Zhou et al., 2010, Zhou et al., 2016). Unlike the C terminal deletion of Orai1, functional studies have revealed that deletion of the N terminal region of Orai1 has abrogated SOCE; however physical binding of Orai1 to Stim1 is still retained (Li et al., 2007, Lis et al., 2010, Muik et al., 2008). Report from McNally et al., 2013 suggests that the N terminal region of Orai1 contributed to the overall stability of Stim1-Orai1 binding; however, both N terminal and C terminal binding sites are crucial for CRAC channel function. Studies have clearly demonstrated the ability of Orai homologs to interact with each other to form a multimeric composition with each Orais depending on the stoichiometry, although the latter part is discussed controversially (Gwack et al., 2007, Lis et al., 2007, Zhou et al., 2010, Reviewed in Prakriya, 2013, Alansary et al., 2015). With respect to Orai2, mouse Orai2 gives rise to two splice isoforms due to splicing at the N terminal site of Orai2 – Orai2s and Orai2l only differing in their N terminus with 14 amino acids longer in Orai2L than Orai2s (Gross et al., 2007). The pronounced effect of Stim1B on Orai2 cannot be solely based on N terminal splicing of Orai2 as patch clamp experiments on co-expressing Stim1B and Orai2L also displayed similar observations (data not included in the thesis). The previous report also suggests that both N terminal and C terminal sites are crucial for gating Stim1. Therefore, a clear mechanism could not be illustrated on why Stim1B has a more profound effect on Orai2, unlike Orai1. A report from Alansary et al., 2015 showed that endogenous Orai1 amplifies Orai3 currents and that Orai1 mediates the facilitation of Orai3 targeting. It could be argued that STIM1B might be blocking the ORAI1 in the facilitation of ORAI3 targeting via an unknown mechanism. The Orai3 subunit stoichiometry was suggested to be in closed and open states and varies between dimer and tetramer based on its activating

conditions (Demuro et al., 2011). However, why the run-down phenotype of Orai3 currents activated by Stim1B was observed is unclear. It is known that phenotype is dependent on its gene expression. Western blotting quantification upon expressing Stim1 or Stim1B in HEK cells showed equal expression (Figure 1F from Ramesh et al., 2021). In addition, the functionality of SOCE depends on the stoichiometry of the Stim1:Orai1 ratio at the ER-PM junctions. The CRAC current and the Ca^{2+} -dependent inactivation were reported to be drastically reduced if the Stim1:Orai1 protein ratio fell below 2 (Hoover et al., 2011, Li et al., 2011, Kilch et al., 2013, Yen et al., 2018), although the number of CRAC channels bound to Stim1 appears to be non-linear with Stim1 concentration. Therefore, in this work, we transfected the Stim/Orai DNA in the ratio of 3:1 for the patch clamp experiments to avoid the experimental glitch.

5.2 Calcium-dependent inactivation (CDI) is significantly altered by Stim1B

Slow and fast Ca^{2+} -dependent inactivation are two different mechanisms by which calcium ion (Ca^{2+}) influx through calcium channels is regulated. Slow Ca^{2+} -dependent inactivation (SCDI) occurs relatively over longer timescales ranging from milli to tenth of seconds, which is mediated by Ca^{2+} binding proteins to the regulatory site of a protein, while fast Ca^{2+} -dependent inactivation occurs rapidly within microseconds and mainly mediated by the interaction between Ca^{2+} ions and intracellular proteins leading to rapid closure of the channel. Over the years, several reports have demonstrated how CRAC channels are turned off once activated, although the precise mechanism is still under debate with Orai homologs differing in CDI characteristics with Orai1 exhibiting strong SCDI while Orai3 exhibiting strong FCDI (Lis et al., 2007). Native CRAC currents experience fast Ca^{2+} dependent inactivation (FCDI) which occurs in the millisecond range close to the inner mouth of the channel pore due to local calcium feedback causing the channel to inactivate (Zweifach & Lewis, 1995a, Fierro & Parekh, 1999, Rychkov, 2018). The feedback mechanism to regulate Ca^{2+} influx is also mediated by slow calcium-dependent inactivation (SCDI) which ranges over tens of seconds and may involve interacting proteins such as SARAF (Palty et al., 2012, Jha et al., 2013, Albarran et al., 2016) and Calmodulin (Singh et al., 2002, Litjens et al., 2004, Mullins et al., 2009, Li et al., 2017) to modulate its regulation. SCDI accounts for up to approximately 70% of total inactivation and appears to be the dominant inhibitory mechanism that shapes the Ca^{2+}

signal (Lis et al., 2007, Zweifach & Lewis, 1995b, Parekh 1998, Naraghi & Neher, 1997, Reviewed in Parekh et al., 2005, Muallem, 2007). When the channel undergoes slow inactivation, the presence of BAPTA as an intracellular chelator might more effectively control the local calcium levels around the calcium channel allowing for a faster recovery, enabling the channel to return to its active state more rapidly compared to the presence of EGTA as an intracellular chelator (Hoth & Penner, 1992, Parekh, 1998), arguing also for local effects close to the pore. The effects seen in patch clamp experiments with overexpression of Orai1 and with strong buffering by 20mM BAPTA displayed a near normal gating of Orai1 and might be masking the physiological phenotype exhibited by Stim1B. Therefore, patch clamp recordings were performed in the presence of 2mM EGTA as the calcium chelator. EGTA is a weak calcium chelator compared to BAPTA, primarily due to differences in their K_d (dissociation constant) values. BAPTA has a significantly lower K_d of $0.17\mu\text{M}$ allowing it to buffer calcium efficiently even at lower concentrations. Moreover, the buffering is not limited by Mg^{2+} concentration and low affinity for protons. In contrast, EGTA possesses a relatively higher K_d value of $2.5 \times 10^{-5}\mu\text{M}$ which is several folds higher than BAPTA making it less efficient in buffering calcium ions. The key observation is that during the transient phase of calcium elevation, the slower binding of EGTA to Ca^{2+} ions at a given $[\text{Ca}^{2+}]_{\text{ext}}$ results in a lower amount of calcium being bound by EGTA compared to a steady state equilibrium (Naraghi & Neher, 1997, Naraghi, 1997, Reviewed in Eisner et al., 2023). This property makes EGTA a suitable choice where slow calcium buffering is advantageous for unraveling both fast and slow Ca^{2+} -dependent inactivation dynamics despite its weaker calcium binding affinity compared to BAPTA. In the presence of EGTA in the patch pipette, FCDI measured by applying voltage pulses to -100mV for 100ms was not significantly affected by Stim1B (Figure 11 A, B), arguing that direct channel gating is unlikely to be altered by Stim1B. Strikingly, Stim1/Orai1 I_{CRAC} recorded with 2mM EGTA showed prominent (70%) slow Ca^{2+} dependent inactivation while Stim1B/Orai1 I_{CRAC} displayed significantly reduced I_{CRAC} with slower kinetics and significantly less inactivation (Figure 10A-D). The slow inactivation is dependent on the Ca^{2+} entry into the cell (Zweifach & Lewis, 1995, Parekh, 1998). To facilitate a better data interpretation, a normalization approach was employed where the data obtained from BAPTA experiments were standardized with respect to average responses observed under EGTA conditions. Notably, the rate of CRAC current activation in the presence of IP₃ was found to be independent of extracellular Ca^{2+} concentration. Surprisingly, we noted that the choice of

buffering agent did not exert a significant influence on the maximal current densities generated by Stim1, although other variants including Stim1B, Stim1514*, and Stim1BØ* displayed a significant difference in modulating maximal current densities based on the choice of buffer. Additionally, SCDI exhibited a substantial reduction in the presence of BAPTA across all examined constructs, and intriguingly, Stim1B displayed a virtual absence of SCDI (Figure S2C, Ramesh et al., 2021). These findings collectively suggest that Stim1B's reduced susceptibility to SCDI is likely the consequence of attenuated CRAC current and slower activation kinetics when subjected to EGTA conditions.

Slow Calcium-dependent inactivation has been widely discussed in earlier reports and has not been well understood on a molecular basis. One potential protein candidate that is reported to mediate SCDI is SARAF. SOCE-associated regulatory factor (SARAF) is an ER membrane protein that associates Stim1 to facilitate SCDI of Orai1 mediated currents via interaction with two binding motifs within the CTID region of Stim1 (aa 448-490, aa 490-530), with former lobe (aa 448-490) restricts and the latter part of CTID (aa 490-530) direct the access of SARAF to SOAR. SARAF also interacts with Orai within the PIP2-rich microdomain, which is independent of Stim1 (Palty et al., 2012, Jha et al., 2013, Albarran et al., 2016a, 2016b, Reviewed in Jardín et al., 2018,). In addition, SARAF also interacts with TRPC1 which is Stim1 independent. As the CTID domain ranges from aa 448-530 which is not entirely intact for Stim1B with the last common amino acid between Stim1 and Stim1B being aa514, thus the variant could potentially affect the SARAF docking site. Therefore, we tried to detect differences in SARAF regulation of STIM1 or STIM1B mediated function using SARAF overexpression in HEK cells stably expressing ORAI1 (HEKO1). However, we were unable to detect any differential SARAF-mediated effects between STIM1 and STIM1B at 2mM EGTA buffering conditions (Figure 12). To note that with strong overexpression of ORAI1, kinetic differences in activation became smaller. This is due to the synergistic effect of stable expression of Orai1 which surpasses the expression level of the other two ORAI homologs and resulted in larger currents than usual overexpression. None of the data shown in Figure 12 indicated a differential role in SARAF-mediated inhibition.

The region 470HFIMTDDVDDMDEEIV485 within the Inhibitory Domain (ID) of Stim1 is noteworthy for its high-density negatively charged region, and it has been previously linked to both fast and slow Ca^{2+} -dependent inactivation (CDI). Neutralizing all the acidic residues

within this region effectively eliminates CDI, as reported by Derler et al. (2009), Lee et al. (2009), Mullins et al. (2009), and Mullins et al. (2016). Recent studies have proposed that the ID domain of Stim1 interacts with the Orai1 pore, facilitating CDI. In light of these findings, we carried out experiments in which we neutralized the seven acidic residues within the ID domain of both Stim1 and Stim1B by mutating them to Alanine (referred to as STIM1_7A and STIM1B_7A). Our aim was to investigate whether this mutation affected the distinct behavior of Stim1B.

The results revealed that the 7A mutant not only exerted a dominant influence on STIM1 function, as previously reported by Mullins et al. (2016), but also had a notable impact on STIM1B, although the ID domain and B domain have independent effects. These findings underscore the critical role of the ID domain in shaping the functional properties of both Stim1 and Stim1B in the context of Ca²⁺ regulation and CDI. (Figure 13E-H).

5.3 Insertion of Domain B and not the missing C terminal determines the Stim1B phenotype

Previous reports have highlighted the significance of the C terminal region of Stim1 in the gating and coupling of Orai homologs. The slower kinetics, reduced CRAC amplitude, and inactivation of Stim1B as shown in patch clamp experiments, TIRFM, and Ca²⁺ imaging has led to the hypothesis that either the missing C-terminal residues or domain B-specific residues or the additional translated residues due to inserted domain B are responsible for this phenotype. This led to the cloning of three different genetically modified constructs (Stim1_514*, Stim1BØ*, Stim1_526*) to test these possibilities. Patch clamp data with Stim1_514*, where C terminal residues of Stim1 were deleted by site-directed mutagenesis did not fully phenocopy Stim1B as seen from patch clamp electrophysiology experimental data. (Figure 15). In addition, TIRFM analysis with co-expression of Stim1_514* in HEK TKO resulted in smaller clusters as seen with Stim1B (Ramesh et al., 2021, Figure S1) which corresponds well with data published by Zheng et al., 2018 where they show delayed but increased FRET when Stim1(1-442) is co-expressed with PM localized Orai1 FRET donor. In contrast, FRET was completely absent upon expressing Stim1ΔK (only PBD). These data confirm the evidence provided by Chang et al., 2018 where the PBD domain facilitates the detachment of Stim1 from microtubules that are bound via Stim1's EB1 binding motif - aa641TRIPaa646. This binding motif is absent in Stim1 (1-442) (Zheng et al., 2018),

Stim1_514*, or Stim1B which still has the capacity to reach PM better than Stim1 Δ K likely because they lack retention by the MT, however, they cannot expand the junctional ER and result in smaller clusters as shown for Stim1B (Figure 2I from Ramesh et al., 2021). Patch clamp data with co-expression of Stim1_514* with Orai1 under EGTA conditions displayed decreased CD's compared to wt, however, significantly larger and more rapidly activating than those of Stim1B (Figure 15A-D), indicating an additional function of the B-specific residues. Interestingly, patch-clamp recordings with BAPTA and co-expressing Stim1_514* with Orai1 displayed rapid activation and showed similar CD's as Stim1, while Stim1B remained slower and showed more SCDI, also confirming additional domain B-specific effects (Figure 15E-H). These shreds of evidence clearly argue for the fact that the lack of C-terminal residues was not the sole reason for the altered function. Insertion of specific and conserved residues (GSSLKANRLSSK) into the full length of Stim1 with an additional 26 residues and a single nucleotide deletion to retain the wild-type reading frame results in a construct named Stim1B \emptyset *. The translated protein contains both MT tracking EB1 attachment site (TRIP) and the PBD in addition to the added B-specific residues quite strikingly displayed slow kinetics and inhibited CRAC comparable to Stim1B (Figure 16A-D). Patch data of Stim1B \emptyset * co-expressed with Orai1 recorded with BAPTA showed slower activation kinetics and less inactivation than Stim1B (Figure 16E-H). In addition, normalizing BAPTA values to average EGTA responses revealed that current activation kinetics with IP₃ is Ca²⁺ independent (Figure S2C from Ramesh et al., 2021). Additional patch clamp experiments with Stim1_526*, missing the additional translated residues (GFDPFRFGVLPPHE) due to the frameshift with exon 13 (B) insertion (GSSLKANRLSSK) still retained the phenotype of Stim1B or Stim1B \emptyset * which argues for the fact that indeed the exon 13 encoded residues are responsible for most of Stim1B's phenotype (Figure 17A-D). These results clearly indicate that the insertion of domain B and not the deletion of C terminal residues per se confer the majority of the observed changes in channel physiology.

5.4 Domain B-specific motif KANR is responsible for Stim1B's phenotype

Domain B contains 12 highly conserved amino acid residues among various species, although longer variants are predicted in *Bos taurus* and *Equus* species as seen in the evolutionary analysis (Ramesh et al., 2021). Mutating stretches of four of the 12 residues of domain B by neutralizing them to Alanines has provided additional evidence of Stim1B's phenotype in

regulating SOCE. Mutation of the specific motif of the B domain (KANR) has indeed reverted a large degree of Stim1B's phenotype of SCDI to a significant extent as seen with Stim1, (Figure 18 E-H). In contrast, mutation of GSSL to AAAA while also showing a slight rescue of maximal current density, did not rescue the Stim1B phenotype as effectively as the KANR/AAAA exchange, especially regarding activation and inactivation kinetics (Figure 18A-D). These findings put forth compelling evidence that a specific motif of B domain – KANR potentially contributed to Stim1B's phenotype.

5.5 Presynaptic localization of Stim1B, but not Stim1 reinforced the synaptic physiology of Stim1B

Neuronal expression of both Stim1 and Stim1B in hippocampal neurons revealed a striking difference in localization with only Stim1B, but not Stim1 targeting Stim1B to presynaptic sites and strongly co-localized with bassoon, a well-known presynaptic marker (Figure 21A). The finding that not all synapses show co-localization may indicate distinct categories of synapses. In addition, Stim1B localization was also dependent on the 26 specific residues and not due to the lack of C-terminal residues as Stim1B Δ Stop expressed in hippocampal neurons also co-localized with bassoon at presynaptic sites (Figure 21A). Since non-neuronal cells do not display differential localization, domain B likely encodes a neuron (synapse) specific zip code. Using EM microscopy, Wu et al. 2017 generated 3D reconstructions of intracellular organelles and their membrane appositions involving ER and observed that at synaptic varicosities the ER formed a system of anastomosed tubules that branched or expanded into small cisternae and also included networks of tubules physically disconnected from the ER network (Wu et al., 2017). Thin cortical ER seems to be concentrated with STIM1, but not in thicker regions of ER which highlighted the involvement of thin ER in SOCE. Since thin ER is predominantly present in cell bodies, SOCE was thought to play a vital part in the soma of the neuronal cell (Orci et al., 2009, Wu et al., 2017). Interestingly, ER formed contacts with clusters of synaptic vesicles including vesicles or vacuoles larger than synaptic vesicles (bulk endosomes), potentially representing organelles generated by bulk/ultrafast endocytosis (Wu et al., 2014, Watanabe et al., 2013). Functionally, the introduction of Stim1B into hippocampal neurons resulted in pronounced and notably altered synaptic transmission patterns, particularly evident during high-frequency stimulation at 40 Hz, but not during low-frequency stimulation at 20 Hz (Figure20). In contrast, neurons expressing Stim1 exhibited a characteristic short-term

depression response to both 20 Hz and 40 Hz depolarizations, similar to the control group. This indicates that Stim1 did not significantly impact synaptic transmission dynamics at these frequencies. Remarkably, when Stim1B was introduced, it induced distinct short-term facilitation of synaptic signaling, primarily attributable to an enhanced rate of synaptic vesicle replenishment. Strikingly the 20 Hz stimulation preceded by a prior 20 Hz stimulation also led to significantly altered synaptic transmission (FigureS4, Ramesh et al., 2021). This strong enhancement was also observed with Stim1B Δ Stop expressing neurons, suggesting that either the spliced-in residues confer this specific synaptic function, or that the function might be mediated by Stim1 if efficiently localized to presynaptic ER. Treatment with EGTA-AM abolished Stim1B-mediated STE, suggesting that Stim1B-mediated STE phenotype required an increase in cytosolic Ca²⁺ (Figure S3, Ramesh et al., 2021). Ca²⁺ entry through Voltage-gated calcium channels (VGCC) in neurons is primarily responsible for initiating synaptic transmission in most conventional synapses (Catterall et al., 2008). Thus, Ca²⁺ influx through VGCC (during initial stimulus train) and subsequent increase in [Ca²⁺]_i is likely a prerequisite for Stim1B mediated STE of synaptic signaling. Inhibition of postsynaptic VGCC by Stim1 led to the growth of spine ER content and also attenuated NFAT translocation pointing towards Stim1's role in postsynaptic structural plasticity (Dittmer et al., 2017). Here in our study, a direct inhibition of presynaptic VGCC by Stim1B is unlikely given that we did not observe changes in the initial EPSC amplitude and RRP size (mini size and frequency), as both the parameters would be reduced in case of VGCC inhibition (Catterall & Few, 2008). In contrast, Stim1B facilitated release during the second stimulus train. Stim1 is reported to inhibit the depolarization-induced opening of Cav1.2 via interaction between C terminal region of Cav1.2 and SOAR region of Stim1, the same domain that couples Orail and controls this channel via Store depletion (Park et al., 2010, Wang et al., 2010), although recent report from Erdogmus et al., 2022 suggests that regulation of T cell function by Cav β 1 is independent of functional VGCC activity. In contrast to these reports, presynaptic AP evoked Ca²⁺ signals are insensitive towards L-type calcium channel inhibitor isradipine or to the Cav2 channel blockers agatoxin or conotoxin (de Juan-Sanz et al., 2017, Reviewed in Eggermann et al., 2011). Previous research has demonstrated that SH-SY5Y cell lines express functional Voltage-Gated Calcium Channels (VGCCs) (Sousa et al., 2013). In our Ca²⁺ imaging experiments involving SH-SY5Y cells devoid of endogenous Stim1/Stim2, we employed a brief depolarizing pulse induced by high extracellular potassium concentration ([K⁺]_o), followed by a Store-Operated Calcium

Entry (SOCE) re-addition protocol. Surprisingly, the results showed that neither Stim1 nor Stim1B had a significant impact on K^+ -induced Ca^{2+} entry (Figure 2A-C from Ramesh et al., 2021). VGCCs are well-established as the primary mediators of calcium entry in response to membrane depolarization, particularly in scenarios involving high extracellular K^+ (Miyachi et al., 1990; Hall et al., 2000). However, our findings clearly indicate that neither Stim1 nor Stim1B directly modulates VGCC activity in SH-SY5Y cells. This suggests that the observed lack of influence on K^+ -induced Ca^{2+} entry does not result from VGCC modulation by Stim1 or Stim1B, highlighting that Stim1 and Stim1B may not directly modulate VGCC activity. De Juan-Sanz et al. also show that hippocampal synapses display a wide heterogeneity in axonal ER Ca^{2+} concentrations which control local Ca^{2+} influx and exocytosis in a feedback loop mediated by Stim1 and postulate that presynaptic function correlates with ER Ca^{2+} -content in a temperature-dependent manner, with the ER acting as a sink, not a source of Ca^{2+} . In their hands, Stim1 enrichment at nerve terminals inhibits Ca^{2+} influx at low-frequency stimulations by disabling stores from acting as a Ca^{2+} sink. In our hands, the expression of conventional Stim1 did not alter synaptic signaling, regardless of the stimulation frequency used (Figures 21 & Figure 4, S3 & S4 from Ramesh et al., 2021). A significant increase in the refilling rate of RRP without affecting the size of RRP was reported with increased temperature (physiological temperature, $37^\circ C$) during spontaneous and action potential evoked release. Moreover, this impacted the degree and time course of synaptic depression during HFS at higher temperatures highlighting the temperature-dependent variations. Therefore, we purposefully did not record at physiological temperature ($37^\circ C$), as we wanted to avoid the well-known off-target temperature effects on synaptic transmission (Pyott & Rosenmund, 2002). Interestingly, Stim1 can also be activated by temperatures above $35^\circ C$ which is independent of ER Ca^{2+} stores and this mechanism requires PBD of Stim1. This heat stimulation blocks the functional STIM1/ORAI1 coupling thereby modulating STIM1-dependent gene expression in Jurkat T cells (Xiao et al., 2011). Since Stim1B lacks the C terminal tail of Stim1 which contains this heat sensing domain, its functional regulation is likely independent of temperature. We also did not observe major evidence for differential inhibition of VGCE by STIM1 or STIM1B in SH-SY5Y cells (Ramesh et al., 2021), although genetic deletion of STIM1 leads to an upregulation of CACNA1C gene expression in SH-SY5Y cells resulting in cell death (Pascual-Caro et al., 2018).

The increase in the replenishment rate, as well as in the asynchronous release is observed with Stim1B. To test involvement of Stim1B coupling to Orai channels the L373S; A376S mutation was introduced within the Orai channel activating domain (CAD) of Stim1B, completely abrogating Stim1B induced I_{CRAC} (Figure 19) and STE (Figure 20F), pointing to a *bona fide* role for Stim1B mediated SOCE by functionally coupling to Orai channels providing an additional Ca^{2+} entry pathway (into cytosol/ER) required for vesicle replenishment and/or recruitment during protracted stimulation in being able to support or trigger STE at high frequencies. A considerable disparity in the time course of I_{CRAC} activation observed during heterologous overexpression, in comparison to EPSCs measurement (Figure S2 E-H, Ramesh et al., 2021) suggests several intriguing possibilities regarding the role of Stim1B in neurons. It is conceivable that in neurons, Stim1B may have a pre-established association with Orai1/2/3 channels at specific presynaptic contact sites. This notion aligns with the postulation put forth by Maneshi et al. in 2020, which proposed a similar pre-coupling phenomenon for Orai1 in dendritic spines. This association could facilitate rapid calcium influx upon stimulation. Alternatively, it is plausible that Stim1B-mediated Store-Operated Calcium Entry (SOCE) is essential to maintain actively charged Endoplasmic Reticulum (ER) stores within close proximity to presynaptic terminals. This scenario suggests that high-frequency stimulation (HFS) induces Calcium-Induced Calcium Release (CICR) locally, relying on well-charged ER stores as a source. This process could account for the slower time course observed in I_{CRAC} activation during heterologous expression. Another hypothesis to consider is that Stim1B prevents presynaptic ER stores from acting as calcium "sinks." This idea is consistent with the proposal by de Juan-Sanz et al. in 2017, which suggests that the presynaptic ER primarily absorbs calcium ions rather than releasing them. In this context, Stim1B could play a crucial role in maintaining ER stores in a charged state, preventing them from depleting calcium ions. Single channel conductance measurements of receptor-induced Ca^{2+} from Sarcoplasmic Ca^{2+} channels in artificial membranes showed higher channel conductance of RyR or IP3R (~125 pS for RyR1) and single channel conductance studies of IP3R ion channel in *Xenopus* oocytes exhibited multiple conductance states ranging from 113pS at 0mV to ~300pS at 60mV (Smith et al., 1986, Mak et al., 1997). In comparison to those, assessment of the single channel conductance through changes in current variance suggested that the conductance of I_{CRAC} was significantly below 1pS, in the fS range (Hoth & Penner, 1992 &1993) which argues for CICR supporting STE. Apart from Store Operated Ca^{2+} channels, a family of TRP protein superfamily

(TRPC1-7) forming hetero-multimers at the plasma membrane, initiates the release of intracellular Ca^{2+} stores and subsequent entry of Ca^{2+} via TRPC channels which is regulated by DAG and Protein kinase C (PKC) (Venkatachalam et al., 2003, Liao et al., 2008, Reviewed in Lopez et al., 2020, & Bacsá et al., 2020). The interaction between TRPC1 and STIM1 has been reported to be between the two negatively charged Aspartates at the C terminal region of TRPC1 and two positively charged lysine residues at the PBD of STIM1 which is regulated by intermolecular electrostatic interaction (Zeng et al., 2008) and same extent with similar gating mechanism with TRPC3 has been shown. In addition, the deletion of the lysine-rich domain of Stim1 did not affect the gating of Orai1 but prevented the action of TRPC1 (Zeng et al., 2008). Another report from Sun et al., 2017 showed the interaction between TRPC1-STIM1-Cav1.3 during ER Ca^{2+} store depletion and that the TRPC1-STIM1 complex promotes the survival of dopaminergic neurons by inhibiting L-type Ca^{2+} channels (Cav1.3 activity). This report puts into an argument that the absence of the C terminal region in Stim1B could affect its interaction with TRPC1. TRPC1 expression has been identified in the mammalian brain and forms a heteromeric complex with TRPC5 whose activation is independent of store depletion (Strübling et al., 2001). Voltage-gated Calcium entry at the active zone can rapidly trigger additional Ca^{2+} influx through different sources of Ca^{2+} activated channels like TRPC1/5 (Schwarz et al., 2019), which could enhance CICR and induce SOCE to mobilize more distantly localized synaptic vesicles in order to maintain STE of synaptic signaling. The TRPC1/5 activity has been shown to exhibit strong STE at HFS promoting short-term plasticity at the presynaptic sites and their knockdown is implicated in replenishment rate and readily releasable pool of vesicles (Schwarz et al., 2019). The finding that neither basal transmission, nor the synaptic response to an initial 20 Hz stimulation train was altered by Stim1B expression suggests that Stim1B is selectively engaged to support vesicle replenishment in “high demand” situations. Using pharmacological manipulation, pre and postsynaptic recordings showed the potential contribution of CICR in the recruitment of synaptic vesicles in rapidly firing auditory hair cell ribbon synapses during protracted stimulation which is independent of voltage-gated calcium entry (Castellano-Munoz et al., 2016). High-frequency synapses are also seen in the cerebellum, in particular in Purkinje cells (PCs) where the total Stim1 knockout in PCs (which also lacks Stim1B) showed aberration in neural plasticity in vestibular nucleus neurons and impacted in motor memory consolidation of the rapid vestibule-ocular reflex (VOR) memory (Jang et al., 2020). While frequency dependent changes in synaptic strength are important for

gain control and sensory adaptation (Abbott & Regehr, 2004), continued activation of synapses from Purkinje cells to deep cerebellar nuclei and vestibular nuclei led to initial depression, followed by steady-state and are frequency invariant and that Synaptotagmin-7, the Ca^{2+} sensor for STE supporting facilitation with increased firing frequencies to counteract the depression (Jackman et al., 2016, Turecek et al., 2017). A recent report from Fujii et al., 2021 suggests that Syt-7 converts depression to facilitation by suppressing synaptic transmission without acting as a Ca^{2+} sensor to sense the residual Ca^{2+} . These synapses have not been taken under consideration in the Ryu et al., 2017 report, where measurement of spike firing properties of Purkinje Cell-specific STIM1 KO was performed by blocking both excitatory and inhibitory synapses present in the medial part of the flocculus using 2,3-Dihydroxy-6-nitro-7-benzo(F)quinoxaline and picrotoxin respectively, thus potentially missing the contribution of Stim1B. In another study from Hartman et al., 2014, PN-specific deletion of STIM1 influenced the mGluR1-dependent synaptic transmission, thus affecting IP3-dependent ER Ca^{2+} store refilling and TRPC3-mediated post-synaptic responses and these alterations are impacted in cerebellar motor coordination. Arguably, if Stim1B is needed to maintain high firing rates of cerebellar granule cell (GC) synapses onto Purkinje neurons (PN), a potential phenotype would be missed in Purkinje cell-specific deletion of total Stim1 (Ryu et al., 2017; Hartmann et al., 2014). Indeed, a study investigating GC-PN synapses has shown segregation of the readily releasable pool (RRP) into sub-pools that are differentially poised for exocytosis and may shape short-term plasticity; the first sub-pool being silenced leading to complete blockage of synaptic transmission and a second pool can be differentially recruited upon ultrafast changes in stimulation frequency, the underlying molecular mechanism of STE being poorly understood (Doussau et al., 2017). At neuromuscular junction synapses in *Drosophila*, two distinct vesicle pools have been identified, one being responsible for exo / endocytosis mediated recycling which maintains synaptic transmission and the other being the reserve pool of vesicles that take part in synaptic transmission only during tetanic stimulation and is refilled after cessation of tetanus by a process mediated by Ca^{2+} -released from internal stores (Kuromi et al., 2002). Interestingly, the single STIM isoform in *Drosophila* is shorter than conventional mammalian STIM1 and thereby more closely resembles Stim1B. Stim1B's delayed activation and reduced basal coupling to Orai channels in the plasma membrane seen in heterologous expression may prevent unnecessary SOCE activation in low-demand situations, while the reduced SCDI and continuous current run-up with Orai3 (higher expression than Orai1 in the brain) may guarantee

steady and continuous Ca^{2+} entry and store replenishment needed to support the reserve pool of vesicles during HFS.

5.6 Stim1B expression might promote the facilitation through enhanced Synapsin levels

Synapsins are a family of synaptic vesicle-associated phosphoproteins, abundantly expressed in brain regions mostly at the pre-synaptic terminals play a vital role in the regulation of neurotransmitter release (Matsubara et al., 1996, Hosaka et al., 1999). Synapsin proteins contribute to the regulation and maintenance of the reserve pool and recruitment of synaptic vesicles from the reserve pool to a readily releasable pool by means of changes due to phosphorylation mediated by cAMP-dependent protein kinase (PKA), CaM Kinase I, and cyclin-dependent kinase 5 (Cdk5) (Hosaka et al., 1999, Matsubara et al., 1996, Bonanomi et al., 2004, Sun et al., 2006, Menegon et al., 2006, Verstegen et al., 2014). In addition, vesicle mobilization is regulated by phosphorylation of Synapsin I mediated by CaM kinases at LFS while MAP kinase or Calcineurin site-directed phosphorylation takes part in both LFS and HFS (Chi et al., 2003, Reviewed in Tarasova et al., 2018). Phosphorylation of Synapsin at Serine-9 promotes the dissociation of synaptic vesicles from the reserve pool and ready for release at the presynaptic terminals thereby increasing the RRP thereby controlling the SV-dynamics via neuromodulators in the cAMP-dependent signaling pathway (Patzke et al., 2019). The absence of Stim1B in 10A mice has indicated a reduced level of Synapsin as observed in brain and retinal lysates (Figure 23) and the expression level of phosphorylated Synapsin was also reduced, however, further experiments have to be performed to concrete this finding. The data argue the contribution of phosphorylated Synapsin in Stim1B's synaptic phenotype as observed with increased replenishment rate and RRP pool size during high-demand situations.

5.7 Stim1B's absence leads to an impairment in motor performance and adaptive cerebellar learning

Few studies have reported the importance of Stim1 and Orai1 in cerebellar motor coordination and learning memory. Recent studies from Maneshi et al., 2020 have highlighted the importance of Orai1, where they show that loss of Orai1 in excitatory pyramidal neurons, but not in inhibitory neurons led to impairment of learning memory and working memory. Purkinje cell-specific deletion of Stim1 is implicated in cerebellar motor behavior (Hartmann et al., 2014) and showed deficits in memory consolidation without affecting memory acquisition (Ryu

et al., 2017). Overexpression of Stim1 led to impairment of long-term depression although it showed improved contextual learning and significantly reduced anxiety behavior (Majewski et al., 2017). Overexpression of Orai1 in female mice but not in males increased seizure-like symptoms (Maciag et al., 2019). In contrast, mice lacking Orai1 displayed strong seizures in response to chemoconvulsants like kainic acid and pilocarpine (Hori et al., 2020). Therefore, any alterations in SOCE genes (overexpression/deletion) have majorly affected normal behavior.

In our study, we conducted Erasmus ladder experiments to comprehensively evaluate cerebellar motor performance and motor learning, drawing on established methodologies (Gallinano et al., 2013, Vinueza Veloz et al., 2015). To investigate the role of Stim1B, we used a genetically modified mouse model developed by Yu et al. in 2019. In this model, the disabling of C-terminal splicing led to the absence of Stim1B, and we subsequently referred to these mice as "10A mice."

Our findings unveiled a significant impairment in motor performance and a conspicuous deficit in adaptive cerebellar learning when comparing the 10A mice to the control group. This was particularly evident through a notable disparity in missteps during the perturbation phase, observed both in undisturbed trials and obstacle trials, as represented in Figure 28. These results underscore the critical involvement of Stim1B in optimizing cerebellar motor skills and highlight its potential relevance to motor-related neurological conditions.

In addition to assessing motor performance and learning, we explored the aspect of anxiety-associated learning through open field tests and elevated plus maze experiments. Intriguingly, our investigations did not reveal any discernible differences in anxiety-related learning between the 10A mice and the control group, as depicted in Figures 29 and 30.

In summary, our study underscores the pivotal role of Stim1B in cerebellar motor function and adaptive learning, as evidenced by the pronounced deficits observed in 10A mice. However, it's noteworthy that anxiety-related learning does not appear to be significantly influenced by the absence of Stim1B. These findings require further exploration into the specific mechanisms underlying these observed deficits and may hold implications for understanding and potentially addressing motor-related neurological disorders.

5.8 Identification of interacting partner of new splice variant - Stim1B

The results from immunoprecipitation (IP) experiments provided intriguing insights into the interactions of Stim1B with Stim2 and Stim1. Notably, Stim1B exhibited a strong binding affinity for Stim2, while its interaction with Stim1 was comparatively weaker. These findings suggest that Stim1B has the capacity to form heteromultimers with Stim2 or potentially dimerize with itself rather than primarily associating with Stim1, as visually represented in Figure 31A-C.

In the context of neuronal function, Stim1 and Stim2 play distinct roles in maintaining calcium (Ca^{2+}) homeostasis. STIM1 is recognized for its pivotal role in initiating Store-Operated Calcium Entry (SOCE) and contributing to the development of dendritic spines or filopodia in developing neurons. In contrast, STIM2 primarily regulates resting Ca^{2+} levels, as documented in studies by Biegala et al. in 2011 and Kushnireva et al. in 2021.

Furthermore, recent research by Chanaday et al. in 2021 has revealed that STIM2, in conjunction with synaptotagmin-7, contributes to elevated presynaptic Ca^{2+} levels and enhanced glutamate release upon acute depletion of endoplasmic reticulum (ER) Ca^{2+} stores. These observations extend to situations involving acute ER stress, unveiling a novel role for Stim2 in the regulation of presynaptic SOCE.

Consequently, it can be postulated that Stim1B may potentially recruit endogenous conventional Stim1 or Stim2 to the presynaptic ER, thus influencing presynaptic Ca^{2+} dynamics. Notably, our attempts at immunoprecipitation experiments to identify potential interacting partners may not have yielded the expected results due to various factors. These factors could include transient interactions during activated conditions, weak protein-protein bonding, or the choice of elution buffers.

As alternatives, promising approaches such as cross-linking or labeling the protein with stable isotopes (SILAC) in combination with mass spectrometry (MS) analysis could possibly identify intricate protein interactions involving Stim1B and shedding light on its roles in calcium signaling and neuronal function.

5.9 Outlook:

In addition to other characterized splice variants of Stim1 & Stim2 in regulating SOCE, the identification and characterization of a newly identified splice variant of Stim1-Stim1B has further enhanced our understanding on the mechanism of Ca^{2+} regulation. Despite having some unanswered questions regarding the exact molecular machinery involved in Stim1B'S phenotype, this study employed patch clamp electrophysiology, combined with other microscopic techniques such as TIRFM, confocal microscopy, and Ca^{2+} imaging allowed us to uncover the role of Stim1B in regulating neuronal SOCE and modulating synaptic plasticity.

Patch clamp electrophysiology experiments with Stim1B KANR>AAAA mutant significantly rescued the reduced current density and SCDI which was quite evident in Stim1B mediated Orai1 currents and Stim1BØStop was able to display Stim1B's unique properties. Based on this finding, it will be interesting to generate another construct where inserting the KANR mutant into Stim1BØStop and performing a patch clamp electrophysiology experiment would further validate the observed finding.

Neuronal patch-clamp recordings showed clear evidence that Stim1B altered the synaptic dynamics under high-frequency stimulation which is mediated by Ca^{2+} influx or through Orai1 mediated ER Ca^{2+} release. Therefore further investigations should be performed to assess presynaptic calcium levels by using genetic calcium indicators like jGCaMP7f which will answer whether Stim1B increases presynaptic Ca^{2+} levels at high frequency stimulation.

Proteome investigation of Stim1B was not successful during this work. Therefore additional experiments for protein interaction studies should be performed involving the generation of Stable cell lines expressing Stim1, Stim1B, and another mutant construct (Stim1BØStop) in SH-SY5Y cell line background and FISH with corresponding antibody. Alternatively, cross-linking or labeling the protein with stable isotopes (SILAC) with extracted cerebellar lysates from wild-type and 10A mice and mass spectrometry analysis would possibly identify potential protein interaction with Stim1B. Behavioral data from the Erasmus ladder collectively indicated an impairment in motor performance and adaptive cerebellar learning with mice lacking Stim1B. Additional experiments have to be followed up to investigate if it is implicated in any neurological conditions.

References

- Abbott, L.F., and Regehr, W.G. (2004). Synaptic computation. *Nature* 431, 796–803. <https://doi.org/10.1038/nature03010>
- Alansary, D., Bogeski, I. und Niemeyer, B. A. (2015). Facilitation of Orai3 targeting and store operated function by Orai1. *Biochim Biophys Acta*.1853.7, 15411550. doi: 10.1016/j.bbamcr.2015.03.007.
- Alansary, D., Schmidt, B., Dörr, K., Bogeski, I., Rieger, H., Kless, A. et al. (2016). Thiol-dependent intramolecular locking of Orai1 channels. *Sci Rep.* 6-3347. <https://doi.org/10.1038/srep33347>
- Albarran, L., Lopez, J. J., Amor, N. Ben, Martin-Cano, F. E., Berna-Erro, A., Smani, T., Salido, G. M., & Rosado, J. A. (2016). Dynamic interaction of SARAF with STIM1 and Orai1 to modulate store-operated calcium entry. *Scientific Reports*, 6. <https://doi.org/10.1038/srep24452>
- Antebi, A. und Fink, G. R. (1992). The yeast Ca(2+)-ATPase homologue, PMR1, is required for normal Golgi function and localizes in a novel Golgi-like distribution. *Mol Biol Cell*. 3.6, 633654. doi: 10.1091/mbc.3.6.633.
- Ay, A.S., Benzerdjerdj, N., Sevestre, H., Ahidouch, A., Ouadid-Ahidouch, H. (2013) Orai3 Constitutes a Native Store-Operated Calcium Entry That Regulates Non Small Cell Lung Adenocarcinoma Cell Proliferation. *PLoS ONE* 8(9): e72889. <https://doi.org/10.1371/journal.pone.0072889>
- Baba, Y., Hayashi, K., Fujii, Y., Mizushima, A., Watarai, H., Wakamori, M., Numaga, T., Mori, Y., Iino, M., Hikida, M., & Kurosaki, T. (2006). Coupling of STIM1 to store-operated Ca²⁺ entry through its constitutive and inducible movement in the endoplasmic reticulum. *Proceedings of the National Academy of Sciences of the United States of America*, 103(45), 16704–16709. <https://doi.org/10.1073/pnas.0608358103>
- Bacaj, T., Wu, D., Yang, X., Morishita, W., Zhou, P., Xu, W., Malenka, R.C., Südhof, T.C. (2013). Synaptotagmin-1 and synaptotagmin-7 trigger synchronous and asynchronous phases of neurotransmitter release. *Neuron*. 80(4):947-59. doi: 10.1016/j.neuron.2013.10.026.
- Bacsa, B., Tiapko, O., Stockner, T., Groschner, K. (2020). Mechanisms and significance of Ca²⁺ entry through TRPC channels. *Curr Opin Physiol.* Oct;17:25-33. doi:10.1016/j.cophys.2020.06.005
- Bandyopadhyay, B.C., Pingle, S.C., Ahern, G.P. (2011). Store-operated Ca²⁺ signaling in dendritic cells occurs independently of STIM1. *J Leukoc Biol.* Jan;89(1):57-62. doi:10.1189/jlb.0610381

- Bergmeier, W., & Stefanini, L. (2009). Novel molecules in calcium signaling in platelets. *J Thromb Haemost*;7(Suppl. 1): 187–90 doi: 10.1111/j.1538-7836.2009.03379.x
- Berna-Erro, A., Braun, A., Kraft, R., Kleinschnitz, C., Schuhmann, M. K., Stegner, D., et al. (2009). STIM2 Regulates Capacitive Ca²⁺ Entry in Neurons and Plays a Key Role in Hypoxic Neuronal Cell Death. *Science Signaling*, 2(93), 1–11. doi:10.1126/scisignal.2000522
- Berna-Erro, A., Jardin, I., Salido, G.M., Rosado, J.A. (2017). Role of STIM2 in cell function and physiopathology. *J Physiol*. 2017 May 15;595(10):3111-3128. doi: 10.1113/JP273889.
- Berridge, M., Irvine, R. (1984). Inositol trisphosphate, a novel second messenger in cellular signal transduction. *Nature* 312, 315–321. doi: <https://doi.org/10.1038/312315a0>
- Berridge, M. J. (1993). Inositol trisphosphate and calcium signaling. *Nature* 361.6410, 315-325.
- Berridge MJ. (1995). Capacitative calcium entry. *Biochem J*. Nov 15;312 (Pt 1)(Pt 1):1-11. doi: 10.1042/bj3120001
- Berridge, M. J. (1998). Neuronal Calcium Signaling. *Neuron* 21.1, 13-26
- Berridge, M.J. (2002). The endoplasmic reticulum: a multifunctional signaling organelle. *Cell Calcium*. Vol.32, 5–6, 235-249. Doi: <https://doi.org/10.1016/S0143416002001823>.
- Bhardwaj, R., Mueller, H.-M., Nickel, W. und Seedorf, M. (2013). Oligomerization and Calcium calmodulin control binding of the ER Calcium-sensors STIM1 and STIM2 to plasma membrane lipids. *Biosci Rep*. 33.5, e00077. doi: 10.1042/BSR20130089.
- Bogeski, I., Kummerow, C., Al-Ansary, D., Schwarz, E. C., Koehler, R., Kozai, D. et al. (2010). Differential redox regulation of ORAI ion channels: a mechanism to tune cellular calcium signaling. *Sci Signal*. 3 (115). doi: 10.1126/scisignal.2000672.
- Böhm, J., Bulla, M., Urquhart, J.E., Malfatti, E., Williams, S.G., O'Sullivan, J., Szlauer, A., Koch, C., Baranello, G., Mora, M., Ripolone, M., Violano, R., Moggio, M., Kingston, H., Dawson, T., DeGoede, C.G., Nixon, J., Boland, A., Deleuze, J.-F., Romero, N., Newman, W.G., Demareux, N. and Laporte, J. (2017). ORAI1 Mutations with Distinct Channel Gating Defects in Tubular Aggregate Myopathy. *Human Mutation*, 38: 426-438. <https://doi.org/10.1002/humu.23172>
- Bonanomi, D., Menegon, A., Miccio, A., Ferrari, G., Corradi, A., Kao, H-T., Benfenati, F., Valtorta, F. (2005). Phosphorylation of Synapsin I by cAMP-Dependent Protein Kinase Controls Synaptic Vesicle Dynamics in Developing Neurons. *The Journal of Neuroscience*, 25(32):7299 –7308. DOI : <https://doi.org/10.1523/JNEUROSCI.1573-05.2005>

- Brandman, O., Liou, J., Park, W. S. und Meyer, T. (2007). STIM2 is a feedback regulator that stabilizes basal cytosolic and endoplasmic reticulum Ca²⁺ levels. *Cell* 131 (7), 1327-39. doi: 10.1016/j.cell.2007.11.039.
- Braun, A., Varga-Szabo, D., Kleinschnitz, C., Pleines, I., Bender, M., Austinat, M., Bösl, M., Stoll, G., Nieswandt, B. (2009). Orai1 (CRACM1) is the platelet SOC channel and essential for pathological thrombus formation. *Blood*, 113 (9): 2056–2063. doi: <https://doi.org/10.1182/blood-2008-07-171611>
- Brini, M. und Carafoli, E. (2009). Calcium Pumps in Health and Disease. *Physiological Reviews*. 89.4, 1341-1378. doi: 10.1152/physrev.00032.2008.
- Cai, X. (2007). Molecular Evolution and Structural Analysis of the Ca²⁺ Release-Activated Ca²⁺ Channel Subunit, Orai. *Journal of Molecular Biology*, Vol.368, Issue 5, p1284-1291, <https://doi.org/10.1016/j.jmb.2007.03.022>.
- Cai, X., Zhou, Y., Nwokonko, R. M., Loktionova, N. A., Wang, X., Xin, P. (2016). The Orai1 Store-operated Calcium Channel Functions as a Hexamer. *Journal of Biological Chemistry*. Vol. 291, Issue 50, p. 25764-25775. Doi: <https://doi.org/10.1074/jbc.M116.758813>
- Carafoli, E. (1982). The Regulation of Intracellular Calcium. *Advances in Experimental Medicine and Biology*, vol 151. Springer, Boston, MA. Doi: https://doi.org/10.1007/978-1-4684-4259-5_51
- Carafoli, E. (1987). Intracellular calcium homeostasis. *Annu Rev Biochem*, 56:395-433. doi: 10.1146/annurev.bi.56.070187.002143
- Carafoli, E., Santella, L., Branca, D., Brini, M. (2001). Generation, control, and processing of cellular calcium signals. *Crit Rev Biochem Mol Biol*. 36 (2): 107-260. doi: 10.1080/20014091074183
- Carafoli, E., Krebs, J. (2016). Why Calcium? How Calcium Became the Best Communicator. *J Biol Chem*. 30;291(40):20849-20857. doi: 10.1074/jbc.R116.735894.
- Carter, A.G., Vogt, K.E., Foster, K.A., and Regehr, W.G. (2002). Assessing the role of calcium-induced calcium release in short-term presynaptic plasticity at excitatory central synapses. *J. Neurosci*. 22, 21–28. doi: 10.1523/JNEUROSCI.22-01-00021.2002.
- Catterall, W.A., and Few, A.P. (2008). Calcium channel regulation and presynaptic plasticity. *Neuron* 59, 882–901. doi: 10.1016/j.neuron.2008.09.005.
- Cassina, P., Cassina, A., Pehar, M., Castellanos, R., Gandelman, M., de León, A., Robinson, K.M., Mason, R.P., Beckman, J.S., Barbeito, L., Radi, R. (2008). Mitochondrial dysfunction in SOD1G93A-bearing astrocytes promotes motor neuron degeneration: prevention by mitochondrial-targeted antioxidants. *J Neurosci*. 28(16):4115-22. doi: 10.1523/JNEUROSCI.5308-07.2008.

- Castellano-Muñoz, M., Schnee, M.E., Ricci, A.J. (2016). Calcium-induced calcium release supports recruitment of synaptic vesicles in auditory hair cells. *J Neurophysiol.* 115(1):226-39. doi: 10.1152/jn.00559.2015
- Chamlali, M., Kouba, S., Rodat-Despoix, L., Todesca, L.M., Pethö, Z., Schwab, A., Ouadid-Ahidouch, H. (2021). Orai3 Calcium Channel Regulates Breast Cancer Cell Migration through Calcium-Dependent and -Independent Mechanisms. *Cells*, 10, 3487. <https://doi.org/10.3390/cells10123487>
- Chanaday, N.L., Nosyreva, E., Shin, O.H., Zhang, H., Aklan, I., Atasoy, D., Bezprozvanny, I., Kavalali, E.T. (2021). Presynaptic store-operated Ca^{2+} entry drives excitatory spontaneous neurotransmission and augments endoplasmic reticulum stress. *Neuron*. 21;109(8):1314-1332.e5. doi: 10.1016/j.neuron.2021.02.023
- Chang, C.L., Chen, Y.J., Quintanilla, C.G., Hsieh, T.S., and Liou, J. (2018). EB1 binding restricts STIM1 translocation to ER-PM junctions and regulates store-operated Ca^{2+} entry. *J. Cell Biol.* 217, 2047–2058. doi: 10.1083/jcb.201711151.
- Chen-Engerer, H.J., Hartmann, J., Karl, R.M., Yang, J., Feske, S., and Konnerth, A. (2019). Two types of functionally distinct Ca^{2+} stores in hippocampal neurons. *Nat. Commun.* 10, 3223. doi: 10.1038/s41467-019-11207-8.
- Chi, P., Greengard, P., Ryan, T.A. (2003). Synaptic vesicle mobilization is regulated by distinct synapsin I phosphorylation pathways at different frequencies. *Neuron*. 10;38(1):69-78. doi: 10.1016/s0896-6273(03)00151-x.
- Clapham, D. E. (2007). Calcium Signaling. *Cell* 131.6, 1047-1058.
- Courtney, N.A., Bao, H., Briguglio, J.S., Chapman, E.R. (2019). Synaptotagmin 1 clamps synaptic vesicle fusion in mammalian neurons independent of complexin. *Nat Commun.* 10(1):4076. doi: 10.1038/s41467-019-12015-w.
- Covington, E. D., Wu, M. M., Lewis, R. S. (2010). Essential Role for the CRAC Activation Domain in Store-dependent Oligomerization of STIM1. *Molecular Biology of the Cell* 21.11, 1897-1907.
- Csutora, P., Peter, K., Kilic, H., Park, K. M., Zarayskiy, V., Gwozdz, T. et al. (2008). Novel Role for STIM1 as a Trigger for Calcium Influx Factor Production. *J Biol Chem.* 283.21, 14524-14531. doi: 10.1074/jbc.M709575200.
- Darbellay, B., Arnaudeau, S., Bader, C. R., König, S., Bernheim, L. (2011). STIM1L is a new actin-binding splice variant involved in fast repetitive Ca^{2+} release. *The Journal of Cell Biology* 194.2, 335-346.
- Déliot, N., Constantin, B. (2015). Plasma membrane calcium channels in cancer: Alterations and consequences for cell proliferation and migration. *Biochim Biophys Acta.* 1848(10 Pt B):2512-22. doi: 10.1016/j.bbamem.2015.06.009.

- Demuro, A., Penna, A., Safrina, O., Yeromin, A.V., Amcheslavsky, A., Cahalan, M.D., Parker, I. (2011). Subunit stoichiometry of human Orai1 and Orai3 channels in closed and open states. *Proc Natl Acad Sci.* 25;108(43):17832-7. doi: 10.1073/pnas.1114814108
- Derler, I., Fahrner, M., Muik, M., Lackner, B., Schindl, R., Groschner, K., Romanin, C. (2009). A Ca^{2+} release-activated Ca^{2+} (CRAC) modulatory domain (CMD) within STIM1 mediates fast Ca^{2+} -dependent inactivation of ORAI1 channels. *J Biol Chem.* 11;284(37):24933-8. doi: 10.1074/jbc.C109.024083
- Derler, I., Plenk, P., Fahrner, M., Muik, M., Jardin, I., Schindl, R., Gruber, H. J., Groschner, K., & Romanin, C. (2013). The extended transmembrane orai1 N-terminal (ETON) region combines binding interface and gate for orai1 activation by STIM1. *Journal of Biological Chemistry*, 288(40), 29025–29034. <https://doi.org/10.1074/jbc.M113.501510>
- Derler, I., Jardin, I., Romanin, C. (2016). Molecular mechanisms of STIM/Orai communication. *Am J Physiol Cell Physiol.* 310(8):C643-62. doi: 10.1152/ajpcell.00007.2016.
- de Juan-Sanz, J., Holt, G.T., Schreiter, E.R., de Juan, F., Kim, D.S., and Ryan, T.A. (2017). Axonal Endoplasmic Reticulum Ca^{2+} Content Controls Release Probability in CNS Nerve Terminals. *Neuron* 93, 867–881.e6. doi: 10.1016/j.neuron.2017.01.010.
- Dhitavat, J., Fairclough, R.J., Hovnanian, A., Burge, S.M. (2004). Calcium pumps and keratinocytes: lessons from Darier's disease and Hailey-Hailey disease. *Br J Dermatol.* 2004 May;150(5):821-8. doi: 10.1111/j.1365-2133.2004.05904.x.
- De Stefani, D., Raffaello, A., Teardo, E., Szabò, I., Rizzuto, R. (2011). A forty-kilodalton protein of the inner membrane is the mitochondrial calcium uniporter. *Nature.* 476(7360):336-40. doi: 10.1038/nature10230.
- Dittmer, P. J., Wild, A. R., Dell'Acqua, M. L., Sather, W. A. (2017). STIM1 Ca^{2+} sensor control of L-type Ca^{2+} channel-dependent dendritic spine structural plasticity and nuclear signaling. *Cell reports* 19.2, 321-334. doi: 10.1016/j.celrep.2017.03.056.
- Dörr, K., Kilch, T., Kappel, S., Alansary, D., Schwar, G., Niemeyer, B. A. et al. (2016). Cell type-specific glycosylation of Orai1 modulates store-operated Ca^{2+} entry. *Sci Signal.* 9 (418). doi: 10.1126/scisignal.aaa9913.
- Doussau, F., Schmidt, H., Dorgans, K., Valera, A.M., Poulain, B., Isope, P. (2017). Frequency-dependent mobilization of heterogeneous pools of synaptic vesicles shapes presynaptic plasticity. *eLife.* 6:e28935. doi: 10.7554/eLife.28935.
- Dubois, C., Vanden, A.F., Lehen'kyi, V., Gkika, D., Guarmit, B., Lepage, G., Slomianny, C., Borowiec, A.S., Bidaux, G., Benahmed, M., Shuba, Y., Prevarskaya, N. (2014). Remodeling of channel-forming ORAI proteins determines an oncogenic switch in prostate cancer. *Cancer Cell.* 26(1):19-32. doi: 10.1016/j.ccr.2014.04.025.

- Dyrda, A., Koenig, S., Frieden, M. (2020). STIM1 long and STIM1 gate differently TRPC1 during store-operated calcium entry. *Cell Calcium*. 86:102134. doi: 10.1016/j.ceca.2019.102134
- Ebashi, F., Ebashi, S. (1962). Removal of calcium and relaxation in actomyosin systems. *Nature*. 194:378-9. doi: 10.1038/194378a0
- Eisner, D., Neher, E., Taschenberger, H., Smith, G. (2023). Physiology of intracellular calcium buffering. *Physiol Reviews*. 103:4, 2767-2845. Doi: doi.org/10.1152/physrev.00042.2022
- Eggermann, E., Bucurenciu, I., Goswami, S.P., Jonas, P. (2011). Nanodomain coupling between Ca²⁺ channels and sensors of exocytosis at fast mammalian synapses. *Nat Rev Neurosci*. 13(1):7-21. doi: 10.1038/nrn3125.
- Emptage, N. J., Reid, C. A., Fine, A. (2001). Calcium Stores in Hippocampal Synaptic Boutons Mediate Short-Term Plasticity, Store-Operated Calcium Entry, and Spontaneous Transmitter Release. *Neuron* 29.1, 197-208. doi: 10.1016/s0896-6273(01)00190-8.
- Endo, Y., Noguchi, S., Hara, Y., Hayashi, Y.K., Motomura, K., Miyatake, S., Murakami, N., Tanaka, S., Yamashita, S., Kizu, R., Bamba, M., Goto, Y., Matsumoto, N., Nonaka, I., Nishino, I. (2015). Dominant mutations in ORAI1 cause tubular aggregate myopathy with hypocalcemia via constitutive activation of store-operated Ca²⁺ channels. *Hum Mol Genet*. 24(3):637-48. doi: 10.1093/hmg/ddu477.
- Enyedi, A., Flura, M., Sarkadi, B., Gardos, G., Carafoli, E. (1987). The maximal velocity and the calcium affinity of the red cell calcium pump may be regulated independently. *Journal of Biological Chemistry* 262.13, 6425-6430.
- Ercan, E., Momburg, F., Engel, U., Temmerman, K., Nickel, W. Seedorf, M. (2009). A conserved, lipid-mediated sorting mechanism of yeast Ist2 and mammalian STIM proteins to the peripheral ER. *Traffic* 10 (12), 1802-18. doi: 10.1111/j.1600-0854.2009.00995.x
- Erdogmus, S., Concepcion, A.R., Yamashita, M. (2022). Cavβ1 regulates T cell expansion and apoptosis independently of voltage-gated Ca²⁺ channel function. *Nat Commun* 13, 2033. <https://doi.org/10.1038/s41467-022-29725-3>
- Fahrner, M., Muik, M., Schindl, R., Butorac, C., Stathopoulos, P., Zheng, L., Jardi, I., Ikura, M., & Romanin, C. (2014). A coiled-coil clamp controls both conformation and clustering of stromal interaction molecule 1 (STIM1). *Journal of Biological Chemistry*, 289(48), 33231–33244. <https://doi.org/10.1074/jbc.M114.610022>
- Fahrner, M., Schindl, R., Romanin, C. (2018). Studies of Structure-Function and Subunit Composition of Orai/STIM Channel. In: Kozak JA, Putney JW Jr, editors. *Calcium Entry Channels in Non-Excitable Cells*. Boca Raton (FL): CRC Press/Taylor & Francis; Chapter 2.

- Fairclough, R.J., Dode, L., Vanoevelen, J., Andersen, J.P., Missiaen, L., Raeymaekers, L., Wuytack, F., Hovnanian, A. (2003). Effect of Hailey-Hailey Disease mutations on the function of a new variant of human secretory pathway $\text{Ca}^{2+}/\text{Mn}^{2+}$ -ATPase (hSPCA1). *J Biol Chem.* 278(27):24721-30. doi: 10.1074/jbc.M300509200.
- Fasolato, C., Pizzo, P., Pozzan, T. (1998). Delayed activation of the store-operated calcium current induced by calreticulin overexpression in RBL-1 cells. *Mol Biol Cell.* 9(6):1513-22. doi: 10.1091/mbc.9.6.1513.
- Feske, S., Giltnane, J., Dolmetsch, R., Staudt, L.M., Rao, A. (2001). Gene regulation mediated by calcium signals in T lymphocytes. *Nat Immunol.* 2(4):316-24. doi: 10.1038/86318.
- Feske, S., Prakriya, M., Rao, A., Lewis, R.S. (2005). A severe defect in CRAC Ca^{2+} channel activation and altered K^{+} channel gating in T cells from immunodeficient patients. *J Exp Med.* 202(5):651-62. doi: 10.1084/jem.20050687
- Feske, S., Gwack, Y., Prakriya, M., Srikanth, S., Puppel, S.-H., Tanasa, B. (2006). A mutation in Orai1 causes immune deficiency by abrogating CRAC channel function. *Nature* 441, 179-85. Doi: <https://doi.org/10.1038/nature04702>
- Fierro, L., Parekh, A.B. (1999). Fast calcium-dependent inactivation of calcium release-activated calcium current (CRAC) in RBL-1 cells. *J Membr Biol.* 168(1):9-17. doi: 10.1007/s002329900493.
- Frischauf, I., Schindl, R., Derler, I., Bergsmann, J., Fahrner, M., Romanin, C. (2008). The STIM/Orai coupling machinery. *Channels (Austin, Tex.)* 2 (4), 261-8. doi: 10.4161/chan.2.4.6705
- Frischauf, I., Zayats, V., Deix, M., Hochreiter, A., Jardin, I., Muik, M., Lackner, B., Svobodová, B., Pammer, T., Litviňuková, M., Sridhar, A.A., Derler, I., Bogeski, I., Romanin, C., Etrich, R.H., Schindl, R. (2015). A calcium-accumulating region, CAR, in the channel Orai1 enhances Ca^{2+} permeation and SOCE-induced gene transcription. *Sci Signal.* 8(408):ra131. doi: 10.1126/scisignal.aab1901.
- Fujii, T., Sakurai, A., Littleton, J.T., Yoshihara, M. (2021). Synaptotagmin 7 switches short-term synaptic plasticity from depression to facilitation by suppressing synaptic transmission. *Sci Rep.* 11(1):4059. doi: 10.1038/s41598-021-83397-5.
- Galliano, E., Gao, Z., Schonewille, M., Todorov, B., Simons, E., Pop, A.S., D'Angelo, E., van den Maagdenberg, M.J.M., Hoebeek, F.E., De Zeeuw, C.I. (2013). Silencing the Majority of Cerebellar Granule Cells Uncovers Their Essential Role in Motor Learning and Consolidation. *Cell Reports.* Vol.3;1239-1251. Doi: <https://doi.org/10.1016/j.celrep.2013.03.023>.
- Garcia-Alvarez, G., Shetty, M.S., Lu, B., Yap, K.A., Oh-Hora, M., Sajikumar, S., Bichler, Z., and Fivaz, M. (2015). Impaired spatial memory and enhanced long-term potentiation in

- mice with forebrain-specific ablation of the Stim genes. *Front. Behav. Neurosci.* 9, 180. doi: 10.3389/fnbeh.2015.00180.
- Garibaldi, M., Fattori, F., Riva, B., Labasse, C., Brochier, G., Ottaviani, P., Sacconi, S., Vizzaccaro, E., Laschena, F., Romero, N.B., Genazzani, A., Bertini, E., Antonini, G. (2017). A novel gain-of-function mutation in ORAI1 causes late-onset tubular aggregate myopathy and congenital miosis. *Clin Genet.* 91(5):780-786. doi: 10.1111/cge.12888.
- Gilson, A. (2016). Identification of new STIM splice variants and expression in the mouse brain during healthy aging. UdS Bachelor Thesis.
- Gross, S. A., Wissenbach, U., Philipp, S. E., Freichel, M., Cavalié, A., & Flockerzi, V. (2007). Murine ORAI2 splice variants form functional Ca²⁺ release-activated Ca²⁺ (CRAC) channels. *Journal of Biological Chemistry*, 282(27), 19375–19384. <https://doi.org/10.1074/jbc.M701962200>
- Grosse, J., Braun, A., Varga-Szabo, D., Beyersdorf, N., Schneider, B., Zeitlmann, L., Hanke, P., Schropp, P., Mühlstedt, S., Zorn, C., Huber, M., Schmittwolf, C., Jagla, W., Yu, P., Kerkau, T., Schulze, H., Nehls, M., Nieswandt, B. (2007). An EF hand mutation in Stim1 causes premature platelet activation and bleeding in mice. *J Clin Invest.* 117(11):3540-50. doi: 10.1172/JCI32312.
- Gruszczynska-Biegala, J., Pomorski, P., Wisniewska, M.B., Kuznicki, J. (2011). Differential roles for STIM1 and STIM2 in store-operated calcium entry in rat neurons. *PLoS One.* 6(4):e19285. doi: 10.1371/journal.pone.0019285.
- Grynkiewicz, G., Poenie, M., Tsien, R. Y. (1985). A new generation of Ca²⁺ indicators with greatly improved fluorescence properties. *The Journal of Biological Chemistry* 260 (6), 3440-50.
- Guerini, D., García-Martin, E., Gerber, A., Volbracht, C., Leist, M., Merino, C.G., Carafoli, E. (1999). The expression of plasma membrane Ca²⁺ pump isoforms in cerebellar granule neurons is modulated by Ca²⁺. *J Biol Chem.* 274(3):1667-76. doi: 10.1074/jbc.274.3.1667
- Gwack, Y., Srikanth, S., Feske, S., Cruz-Guilloty, F., Oh-hora, M., Neems, D. S., Hogan, P. G., & Rao, A. (2007). Biochemical and functional characterization of orai proteins. *Journal of Biological Chemistry*, 282(22), 16232–16243. <https://doi.org/10.1074/jbc.M609630200>
- Gwack, Y., Feske, S., Srikanth, S., Hogan, P. G., Rao, A. (2007a). Signalling to transcription: Store-operated Ca²⁺ entry and NFAT activation in lymphocytes. *Cell Calcium* 42 (2), 145-56. Doi: 10.1016/j.ceca.2007.03.007.
- Hajnóczky, G., Hager, R., Thomas, A. P. (1999). Mitochondria Suppress Local Feedback Activation of Inositol 1,4,5-Trisphosphate Receptors by Ca²⁺. *Journal of Biological Chemistry*, 274.20, 14157-14162. doi: 10.1074/jbc.274.20.14157

- Hall, D.A., Carmines, P.K., Sansom, S.C. (2000). Dihydropyridine-sensitive Ca²⁺ channels in human glomerular mesangial cells. *Am. J. Physiol. Renal Physiol.* 278: F97–F103. Doi: 10.1152/ajprenal.2000.278.1.F97
- Hartmann, J., Karl, R. M., Alexander, R. P. D., Adelsberger, H., Brill, M. S., Rühlmann, C. (2014). STIM1 Controls Neuronal Calcium Signaling, mGluR1-Dependent Synaptic Transmission, and Cerebellar Motor Behavior. *Neuron* 82.3, 635-644. doi: 10.1016/j.neuron.2014.03.027.
- Hawkins, B.J., Irrinki, K.M., Mallilankaraman, K., Lien, Y.C., Wang, Y., Bhanumathy, C.D., Subbiah, R., Ritchie, M.F., Soboloff, J., Baba, Y. (2010). S-glutathionylation activates STIM1 and alters mitochondrial homeostasis. *J. Cell Biol.* 190, 391–405. doi: 10.1083/jcb.201004152.
- Hilgemann, D. W., Yaradanakul, A., Wang, Y., & Fuster, D. (2006). Molecular control of cardiac sodium homeostasis in health and disease. *Journal of Cardiovascular Electrophysiology*, 17: 47–56. Doi: <https://doi.org/10.1111/j.1540-8167.2006.00383.x>
- Holzmann, C., Kilch, T., Kappel, S., Armbrüster, A., Jung, V., Stöckle, M., Bogeski, I., Schwarz, E.C., Peinelt, C. (2013). I_{CRAC} controls the rapid androgen response in human primary prostate epithelial cells and is altered in prostate cancer. *Oncotarget*. 4(11):2096-107. doi: 10.18632/oncotarget.1483.
- Hooper, R., Samakai, E., Kedra, J., & Soboloff, J. (2013). Multifaceted roles of STIM proteins. *Pflügers Archiv European Journal of Physiology*, 465(10), 1383–1396. <https://doi.org/10.1007/s00424-013-1270-8>
- Hoover, P. J. & Lewis, R. S. (2011). Stoichiometric requirements for trapping and gating of Ca²⁺ release-activated Ca²⁺ (CRAC) channels by stromal interaction molecule 1 (STIM1). *Proc Natl Acad Sci U S A.* 108(32):13299-304. doi: 10.1073/pnas.1101664108.
- Hori, K., Tsujikawa, S., Novakovic, M.M., Yamashita, M., Prakriya, M. (2020). Regulation of chemoconvulsant-induced seizures by store-operated Orai1 channels. *J Physiol.* 598(23):5391-5409. doi: 10.1113/JP280119.
- Horinouchi, T., Higashi, T., Higa, T., Terada, K., Mai, Y., Aoyagi, H., Hatate, C., Nepal, P., Horiguchi, M., Harada, T., Miwa, S. (2012). Different binding property of STIM1 and its novel splice variant STIM1L to Orai1, TRPC3, and TRPC6 channels. *Biochem Biophys Res Commun.* 428(2):252-8. doi: 10.1016/j.bbrc.2012.10.034
- Hosaka, M., Hammer, R.E., Südhof, T.C. (1999). A phospho-switch controls the dynamic association of synapsins with synaptic vesicles. *Neuron.* 24(2):377-87. doi: 10.1016/s0896-6273(00)80851-x.
- Hoth, M. & Penner, R. (1992). Depletion of intracellular calcium stores activates a calcium current in mast cells. *Nature* 355 (6358), 353-356. doi: 10.1038/355353a0

- Hoth, M. & Penner, R. (1993). Calcium release-activated calcium current in rat mast cells. *J Physiol.* 465:359-86. doi: 10.1113/jphysiol.1993.sp019681.
- Hou, X., Pedi, L., Diver, M. M., Long, S. B. (2012). Crystal structure of the calcium release-activated calcium channel Orai. *Science* 338.6112, 1308-1313.
- Huang, G.N., Zeng, W., Kim, J.Y., Yuan, J.P., Han, L., Muallem, S., Worley, P.F. (2006). STIM1 carboxyl-terminus activates native SOC, I(crac) and TRPC1 channels. *Nat Cell Biol.* 8(9):1003-10. doi: 10.1038/ncb1454.
- Humer, C., Romanin, C., Höglinger, C. (2022). Highlighting the Multifaceted Role of Orai1 N-Terminal- and Loop Regions for Proper CRAC Channel Functions. *Cells.* 11, 371. Doi:<https://doi.org/10.3390/cells11030371>
- Jackman, S.L., Turecek, J., Belinsky, J.E., Regehr, W.G. (2016). The calcium sensor synaptotagmin 7 is required for synaptic facilitation. *Nature.* 529(7584):88-91. doi: 10.1038/nature16507.
- Jang, D.C., Shim, H.G., Kim, S.J. (2020). Intrinsic plasticity of cerebellar Purkinje cells contributes to motor memory consolidation. *J. Neurosci.* 40, 4145–4157. doi: 10.1523/JNEUROSCI.1651-19.2020.
- Jardín, I., López, J.J., Redondo, P.C., Salido, G.M., Rosado, J.A. (2009). Store-operated Ca²⁺ entry is sensitive to the extracellular Ca²⁺ concentration through plasma membrane STIM1. *Biochim Biophys Acta.* 1793(10):1614-22. doi: 10.1016/j.bbamcr.2009.07.003.
- Jardin, I., Dionisio, N., Frischauf, I., Berna-Erro, A., Woodard, G.E., López, J.J., Salido, G.M., Rosado, J.A. (2013). The polybasic lysine-rich domain of plasma membrane-resident STIM1 is essential for the modulation of store-operated divalent cation entry by extracellular calcium. *Cell Signal.* 25(5):1328-37. doi: 10.1016/j.cellsig.2013.01.025.
- Jardín, I., Albarran, L., Salido, G.M., López, J.J., Sage, S.O., Rosado, J.A. (2018). Fine-tuning of store-operated calcium entry by fast and slow Ca²⁺-dependent inactivation: Involvement of SARAF. *Biochim Biophys Acta Mol Cell Res.* 1865(3):463-469. doi: 10.1016/j.bbamcr.2017.12.001.
- Jha, A., Ahuja, M., Maléth, J., Moreno, C.M., Yuan, J.P., Kim, M.S., Muallem, S. (2013). The STIM1 CTID domain determines access of SARAF to SOAR to regulate Orai1 channel function. *J Cell Biol.* 202(1):71-9. doi: 10.1083/jcb.201301148.
- Karch, C.M., Goate, A.M. (2015). Alzheimer's disease risk genes and mechanisms of disease pathogenesis. *Biol Psychiatry.* 77(1):43-51. doi: 10.1016/j.biopsych.2014.05.006.
- Kar, P., Bakowski, D., Di Capite, J., Nelson, C., Parekh, A.B. (2012). Different agonists recruit different stromal interaction molecule proteins to support cytoplasmic Ca²⁺ oscillations and gene expression. *Proc Natl Acad Sci U S A.* 109(18):6969-74. doi: 10.1073/pnas.1201204109.

- Kawamata, H., Ng, S.K., Diaz, N., Burstein, S., Morel, L., Osgood, A., Sider, B., Higashimori, H., Haydon, P.G., Manfredi, G., Yang, Y. (2014). Abnormal intracellular calcium signaling and SNARE-dependent exocytosis contributes to SOD1G93A astrocyte-mediated toxicity in amyotrophic lateral sclerosis. *J Neurosci.* 34(6):2331-48. doi: 10.1523/JNEUROSCI.2689-13.2014.
- Kawasaki, T., Lange, I., Feske, S. (2009). A minimal regulatory domain in the C terminus of STIM1 binds to and activates ORAI1 CRAC channels. *Biochem Biophys Res Commun.* 385(1):49-54. doi: 10.1016/j.bbrc.2009.05.020.
- Kilch, T., Alansary, D., Peglow, M., Dörr, K., Rychkov, G., Rieger, H. (2013). Mutations of the Ca²⁺-sensing Stromal Interaction Molecule STIM1 Regulate Ca²⁺ Influx by Altered Oligomerization of STIM1 and by Destabilization of the Ca²⁺ Channel Orai1. *J Biol Chem.* 288(3):1653-64. doi: 10.1074/jbc.M112.417246.
- Klejman, M. E., Gruszczynska-Biegala, J., Skibinska-Kijek, A., Wisniewska, M. B., Misztal, K., Blazejczyk, M. (2009). Expression of STIM1 in brain and puncta-like co-localization of STIM1 and ORAI1 upon depletion of Ca²⁺ store in neurons. *Neurochem Int.* 54(1):49-55. doi: 10.1016/j.neuint.2008.10.005.
- Knapp, M.L., Alansary, D., Poth, V., Förderer, K., Sommer, F., Zimmer, D., Schwarz, Y., Künzel, N., Kless, A., Machaca, K., Helms, V., Mühlhaus, T., Schroda, M., Lis, A., Niemeyer, B.A. (2022). A longer isoform of Stim1 is a negative SOCE regulator but increases cAMP-modulated NFAT signaling. *EMBO Rep.* 23(3):e53135. doi: 10.15252/embr.202153135.
- Kuromi, H., Kidokoro, Y. (2002). Selective replenishment of two vesicle pools depends on the source of Ca²⁺ at the Drosophila synapse. *Neuron.* 35(2):333-43. doi: 10.1016/s0896-6273(02)00777-8.
- Korkotian, E., Segal, M. (2017). Orai1 regulates calcium entry into dendritic spines. *Channels (Austin).* 11(2):99-100. doi: 10.1080/19336950.2016.1247528.
- Kraft, R. (2015). STIM and ORAI proteins in the nervous system. *Channels*, 9(5), 244– 252. doi:10.1080/19336950.2015.1071747
- Kushnireva, L., Korkotian, E., Segal, M. (2021). Calcium Sensors STIM1 and STIM2 Regulate Different Calcium Functions in Cultured Hippocampal Neurons. *Front Synaptic Neurosci.* 12:573714. doi: 10.3389/fnsyn.2020.573714.
- Lacruz, R. S. und Feske, S. (2015). Diseases caused by mutations in ORAI1 and STIM1. *Ann N Y Acad Sci.* 1356(1):45-79. doi: 10.1111/nyas.12938.
- Lalonde, J., Saia, G., Gill, G. (2014). Store-operated calcium entry promotes the degradation of the transcription factor Sp4 in resting neurons. *Sci Signal.* 7(328):ra51. doi: 10.1126/scisignal.2005242.

- Li, Z., Lu, J., Xu, P., Xie, X., Chen, L., & Xu, T. (2007). Mapping the interacting domains of STIM1 and Orai1 in Ca^{2+} release-activated Ca^{2+} channel activation. *Journal of Biological Chemistry*, 282(40), 29448–29456. <https://doi.org/10.1074/jbc.M703573200>
- Li, Z., Liu, L., Deng, Y., Ji, W., Du, W., Xu, P., Chen, L., Xu, T. (2011). Graded activation of CRAC channel by binding of different numbers of STIM1 to Orai1 subunits. *Cell Res*. 21(2):305-15. doi: 10.1038/cr.2010.131
- Li, X., Wu, G., Yang, Y., Fu, S., Liu, X., Kang, H., Yang, X., Su, X.C., Shen, Y. (2017). Calmodulin dissociates the STIM1-Orai1 complex and STIM1 oligomers. *Nat Commun*. 8(1):1042. doi: 10.1038/s41467-017-01135-w.
- Liao, Y., Erxleben, C., Abramowitz, J., Flockerzi, V., Zhu, M.X., Armstrong, D.L., Birnbaumer, L. (2008). Functional interactions among Orai1, TRPCs, and STIM1 suggest a STIM-regulated heteromeric Orai/TRPC model for SOCE/ I_{CRAC} channels. *Proc Natl Acad Sci U S A*. 105(8):2895-900. doi: 10.1073/pnas.0712288105.
- Liou, J., Fivaz, M., Inoue, T., Meyer, T. (2007). Live-cell imaging reveals sequential oligomerization and local plasma membrane targeting of stromal interaction molecule 1 after Ca^{2+} store depletion. *Proc Natl Acad Sci U S A*. 104(22):9301-6. doi: 10.1073/pnas.0702866104.
- Liou, J., Kim, M., Heo, W., Jones, J., Myers, J., Ferrell, J. J., & Meyer, T. (2005). STIM is a Ca^{2+} sensor essential for Ca^{2+} -store-depletion-triggered Ca^{2+} influx. *Curr Biol*, 136:15(13), 1235–1241. <https://doi.org/10.1016/j.cub.2005.05.055>.
- Lis, A., Peinelt, C., Beck, A., Parvez, S., Monteilh-Zoller, M., Fleig, A. et al. (2007). CRACM1, CRACM2, and CRACM3 Are Store-Operated Ca^{2+} Channels with Distinct Functional Properties. *Curr Biol*. 17(9):794-800. doi: 10.1016/j.cub.2007.03.065.
- Lis, A., Zierler, S., Peinelt, C., Fleig, A., Penner, R. (2010). A single lysine in the N-terminal region of store-operated channels is critical for STIM1-mediated gating. *J Gen Physiol*. 136(6):673-86. doi: 10.1085/jgp.201010484.
- Litjens, T., Harland, M.L., Roberts, M.L., Barritt, G.J., Rychkov, G.Y. (2004). Fast Ca^{2+} -dependent inactivation of the store-operated Ca^{2+} current (ISOC) in liver cells: a role for calmodulin. *J Physiol*. 558(Pt 1):85-97. doi: 10.1113/jphysiol.2004.065870.
- Liu, H., Bai, H., Hui, E., Yang, L., Evans, C.S., Wang, Z., Kwon, S.E., Chapman, E.R. (2014). Synaptotagmin 7 functions as a Ca^{2+} -sensor for synaptic vesicle replenishment. *Elife*. 3:e01524. doi: 10.7554/eLife.01524.
- Llano, I., González, J., Caputo, C., Lai, F.A., Blayney, L.M., Tan, Y.P., Marty, A. (2000). Presynaptic calcium stores underlie large-amplitude miniature IPSCs and spontaneous calcium transients. *Nat Neurosci*. 3(12):1256-65. doi: 10.1038/81781

- Lopez, J.J., Jardin, I., Sanchez-Collado, J., Salido, G.M., Smani, T., Rosado, J.A. (2020). TRPC Channels in the SOCE Scenario. *Cells*. 9(1):126. doi: 10.3390/cells9010126.
- Luik, R. M., Wu, M. M., Buchanan, J., Lewis, R. S. (2006). The elementary unit of store-operated Ca^{2+} entry: local activation of CRAC channels by STIM1 at ER-plasma membrane junctions. *J Cell Biol*. 174(6):815-25. doi: 10.1083/jcb.200604015.
- Ma, G., Wei, M., He, L., Liu, C., Wu, B., Zhang, S. L. (2015). Inside-out Ca^{2+} signaling prompted by STIM1 conformational switch. *Nat Commun*. 6:7826. doi: 10.1038/ncomms8826.
- Maciąg, F., Majewski, Ł., Boguszewski, P.M., Gupta, R.K., Wasilewska, I., Wojtaś, B., Kuznicki, J. (2019). Behavioral and electrophysiological changes in female mice overexpressing ORAI1 in neurons. *Biochim Biophys Acta Mol Cell Res*. 1866(7):1137-1150. doi: 10.1016/j.bbamcr.2019.01.007.
- Majewski, L., Filip, M., Boguszewski, P. M., Wasilewska, I., Wiera, G., Wojtowicz, T. (2017). Overexpression of STIM1 in neurons in mouse brain improves contextual learning and impairs long-term depression. *Biochim Biophys Acta Mol Cell Res*. 1864(6):1071-1087. doi: 10.1016/j.bbamcr.2016.11.025.
- Mak, D.O., Foskett, J.K. (1997). Single-channel kinetics, inactivation, and spatial distribution of inositol trisphosphate (IP₃) receptors in *Xenopus* oocyte nucleus. *J Gen Physiol*. 109(5):571-87. doi: 10.1085/jgp.109.5.571.
- Malli, R., Naghdi, S., Romanin, C., Graier, W.F. (2008). Cytosolic Ca^{2+} prevents the subplasmalemmal clustering of STIM1: an intrinsic mechanism to avoid Ca^{2+} overload. *J Cell Sci*. 121(Pt 19):3133-9. doi: 10.1242/jcs.034496.
- Maneshi, M.M., Toth, A.B., Ishii, T., Hori, K., Tsujikawa, S., Shum, A.K., Shrestha, N., Yamashita, M., Miller, R.J., Radulovic, J., Swanson, G.T., Prakriya, M. (2020). Orai1 Channels Are Essential for Amplification of Glutamate-Evoked Ca^{2+} Signals in Dendritic Spines to Regulate Working and Associative Memory. *Cell Rep*. 33(9):108464. doi: 10.1016/j.celrep.2020.108464.
- Matsubara, M., Kusubata, M., Ishiguro, K., Uchida, T., Titani, K., Taniguchi, H. (1997). Site-specific phosphorylation of synapsin I by mitogen-activated protein kinase and Cdk5 and its effects on physiological functions. *J Biol Chem*. 271:21108–21113. doi: 10.1074/jbc.271.35.21108.
- Maus, M., Jairaman, A., Stathopoulos, P.B., Muik, M., Fahrner, M., Weidinger, C., Benson, M., Fuchs, S., Ehl, S., Romanin, C., Ikura, M., Prakriya, M., Feske, S. (2015). Missense mutation in immunodeficient patients shows the multifunctional roles of coiled-coil domain 3 (CC3) in STIM1 activation. *Proc Natl Acad Sci U S A*. 112(19):6206-11. doi: 10.1073/pnas.1418852112.

- McCarl, C.A., Picard, C., Khalil, S., Kawasaki, T., Röther, J., Papolos, A. (2009). ORAI1 deficiency and lack of store-operated Ca^{2+} entry cause immunodeficiency, myopathy, and ectodermal dysplasia. *J Allergy Clin Immunol.* 124(6):1311-1318.e7. doi: 10.1016/j.jaci.2009.10.007.
- McNally, B.A., Yamashita, M., Engh, A., Prakriya, M. (2009). Structural determinants of ion permeation in CRAC channels. *Proc Natl Acad Sci U S A.* 106(52):22516-21. doi: 10.1073/pnas.0909574106.
- McNally, B. A., Somasundaram, A., Jairaman, A., Yamashita, M., Prakriya, M. (2013). The C- and N-terminal STIM1 binding sites on Orai1 are required for both trapping and gating CRAC channels. *J Physiol.* 591(11):2833-50. doi: 10.1113/jphysiol.2012.250456.
- Mercer, J. C., DeHaven, W. I., Smyth, J. T., Wedel, B., Boyles, R. R., Bird, G. S. (2006). Large store-operated calcium-selective currents due to coexpression of Orai1 or Orai2 with the intracellular calcium sensor, Stim1. *J Biol Chem.* 281(34):24979-90. doi: 10.1074/jbc.M604589200.
- Miederer, A.M., Alansary, D., Schwar, G., Lee, P.-H., Jung, M., Helms, V. (2015). A STIM2 splice variant negatively regulates store-operated calcium entry. *Nat Commun.* 6:6899. doi: 10.1038/ncomms7899.
- Menegon, A., Bonanomi, D., Albertinazzi, C., Lotti, F., Ferrari, G., Kao, H.T., Benfenati, F., Baldelli, P., Valtorta, F. (2006). Protein kinase A-mediated synapsin I phosphorylation is a central modulator of Ca^{2+} -dependent synaptic activity. *J Neurosci.* 26(45):11670-81. doi: 10.1523/JNEUROSCI.3321-06.2006.
- Mignen, O., Thompson, J. L., Shuttleworth, T. J. (2007). STIM1 regulates Ca^{2+} entry via arachidonate-regulated Ca^{2+} -selective (ARC) channels without store depletion or translocation to the plasma membrane. *J Physiol.* 2007 Mar 15;579(Pt 3):703-15. doi: 10.1113/jphysiol.2006.122432.
- Missiaen, L., Dode, L., Vanoevelen, J., Raeymaekers, L., Wuytack, F. (2007). Calcium in the Golgi apparatus. *Cell Calcium* 41(5): 405-416. doi: 10.1016/j.ceca.2006.11.001.
- Miyauchi, A., Hruska, K.A., Greenfield, E.M., Duncan, R., Alvarez, J., Barattolo, R., Colucci, S., Zamboni-Zallone, A., Teitelbaum, S.L., Teti, A. (1990). Osteoclast cytosolic calcium, regulated by voltage-gated calcium channels and extracellular calcium, controls podosome assembly and bone resorption. *J Cell Biol.* 111(6 Pt 1):2543-52. doi: 10.1083/jcb.111.6.2543.
- Motiani, R.K., Abdullaev, I.F., Trebak, M. (2010). A novel native store-operated calcium channel encoded by Orai3: selective requirement of Orai3 versus Orai1 in estrogen receptor-positive versus estrogen receptor-negative breast cancer cells. *J Biol Chem.* 285(25):19173-83. doi: 10.1074/jbc.M110.102582.

- Muallem S. (2007). Calcium signaling: pyruvate and CRAC meet at the crossroads. *Curr Biol.* 17(14):R549-51. doi: 10.1016/j.cub.2007.05.037
- Muik, M., Frischauf, I., Derler, I., Fahrner, M., Bergsmann, J., Eder, P. (2008). Dynamic Coupling of the Putative Coiled-Coil Domain of ORAI1 with STIM1 Mediates ORAI1 Channel activation. *Journal of Biological Chemistry* 283.12, 8014-8022.
- Muik, M., Fahrner, M., Derler, I., Schindl, R., Bergsmann, J., Frischauf, I., Groschner, K., Romanin, C. (2009). A Cytosolic Homomerization and a Modulatory Domain within STIM1 C Terminus Determine Coupling to ORAI1 Channels. *J Biol Chem.* 27;284(13):8421-6. doi: 10.1074/jbc.C800229200.
- Mullins, F. M., Chan, Y. P., Dolmetsch, R. E., & Lewis, R. S. (2009). STIM1 and calmodulin interact with Orai1 to induce Ca^{2+} - dependent inactivation of CRAC channels. *Proceedings of the National Academy of Sciences of the United States of America*, 106(36), 15495–15500. Doi: <https://doi.org/10.1073/pnas.0906781106>
- Mullins, F. M., & Lewis, R. S. (2016). The inactivation domain of STIM1 is functionally coupled with the Orai1 pore to enable Ca^{2+} -dependent inactivation. *Journal of General Physiology*, 147(2), 153–164. <https://doi.org/10.1085/jgp.201511438>
- Münzer, P., Borst, O. (2022). CRACking the Molecular Regulatory Mechanism of SOCE during Platelet Activation in Thrombo-Occlusive Diseases. *Cells* 2022, 11, 619. Doi: <https://doi.org/10.3390/cells11040619>
- Naraghi M, Neher E. Linearized buffered Ca^{2+} diffusion in microdomains and its implications for calculation of $[Ca^{2+}]$ at the mouth of a calcium channel. *J Neurosci.* 1997 Sep 15;17(18):6961-73. doi: 10.1523/JNEUROSCI.17-18-06961.1997.
- Naraghi M. (1997). T-jump study of calcium binding kinetics of calcium chelators. *Cell Calcium.* 22(4):255-68. doi: 10.1016/s0143-4160(97)90064-6.
- Navarro-Borelly, L., Somasundaram, A., Yamashita, M., Ren, D., Miller, R.J., Prakriya, M. (2008). STIM1-Orai1 interactions and Orai1 conformational changes revealed by live-cell FRET microscopy. *J Physiol.* 586(22):5383-401. doi: 10.1113/jphysiol.2008.162503.
- Nesin, V., Wiley, G., Kousi, M., Ong, E.C., Lehmann, T., Nicholl, D.J., Suri, M., Shahrizaila, N., Katsanis, N., Gaffney, P.M., Wierenga, K.J., Tsiokas, L. (2014). Activating mutations in STIM1 and ORAI1 cause overlapping syndromes of tubular myopathy and congenital miosis. *Proc Natl Acad Sci U S A.* 111(11):4197-202. doi: 10.1073/pnas.1312520111.
- Nguyen, N.T., Ma, G., Lin, E., D'Souza, B., Jing, J., He, L., Huang, Y., Zhou, Y. (2018). CRAC channel-based optogenetics. *Cell Calcium.* 75:79-88. doi: 10.1016/j.ceca.2018.08.007.
- Nilsen, T. W. & Graveley, B. R. (2010). Expansion of the eukaryotic proteome by alternative splicing. *Nature* 463.7280, 457-463. doi: 10.1038/nature08909.

- Oh-Hora, M., Yamashita, M., Hogan, P.G., Sharma, S., Lamperti, E., Chung, W., Prakriya, M., Feske, S., Rao, A. (2008). Dual functions for the endoplasmic reticulum calcium sensors STIM1 and STIM2 in T cell activation and tolerance. *Nat Immunol.* 9(4):432-43. doi: 10.1038/ni1574.
- Orci, L., Ravazzola, M., Le Coadic, M., Shen, W.W., Demaurex, N., Cosson, P. (2009). From the Cover: STIM1-induced precortical and cortical subdomains of the endoplasmic reticulum. *Proc Natl Acad Sci U S A.* 106(46):19358-62. doi: 10.1073/pnas.0911280106. Orci et al., 2009
- Palty, R., Silverman, W.F., Hershfinkel, M., Caporale, T., Sensi, S.L., Parnis, J., Nolte, C., Fishman, D., Shoshan-Barmatz, V., Herrmann, S., Khananshvil, D., Sekler, I. (2010). NCLX is an essential component of mitochondrial Na⁺/Ca²⁺ exchange. *Proc Natl Acad Sci U S A.* 107(1):436-41. doi: 10.1073/pnas.0908099107.
- Palty, R., Raveh, A., Kaminsky, I., Meller, R., & Reuveny, E. (2012). SARAF inactivates the store operated calcium entry machinery to prevent excess calcium refilling. *Cell*, 149(2), 425–438. <https://doi.org/10.1016/j.cell.2012.01.055>
- Palty, R., Stanley, C., Isacoff, E.Y. (2015). Critical role for Orai1 C-terminal domain and TM4 in CRAC channel gating. *Cell Res.* 25(8):963-80. doi: 10.1038/cr.2015.80.
- Parekh, A.B., & Putney, J.W. Jr. (2005). Store-operated calcium channels. *Physiol Rev.* 85(2):757-810. doi: 10.1152/physrev.00057.2003.
- Parekh, A.B. Store-operated CRAC channels: function in health and disease. *Nat Rev Drug Discov.* 2010 May;9(5):399-410. doi: 10.1038/nrd3136.
- Park, C. Y., Hoover, P. J., Mullins, F. M., Bachhawat, P., Covington, D., Raunser, S., Walz, T., Garcia, K. C., E, R., & Lewis, R. S. (2009). STIM1 Clusters and Activates CRAC Channels via Direct Binding of a Cytosolic Domain to Orai1. *Direct*, 136(5), 876–890. <https://doi.org/10.1016/j.cell.2009.02.014.STIM1>
- Park, C. Y., Shcheglovitov, A., Dolmetsch, R. (2010). The CRAC Channel Activator STIM1 Binds and Inhibits L-Type Voltage-Gated Calcium Channels. *Science* 330.6000, 101-5. doi: 10.1126/science.1191027.
- Pathak, T., Agrawal, T., Richhariya, S., Sadaf, S., Hasan, G. (2015). Store-Operated Calcium Entry through Orai Is Required for Transcriptional Maturation of the Flight Circuit in *Drosophila*. *J Neurosci.* 35(40):13784-99. doi: 10.1523/JNEUROSCI.1680-15.2015.
- Patzke, C., Brockmann, M.M., Dai, J., Gan, K.J., Grauel, M.K., Fenske, P., Liu, Y., Acuna, C., Rosenmund, C., Südhof, T.C. (2019). Neuromodulator Signaling Bidirectionally Controls Vesicle Numbers in Human Synapses. *Cell.* 179(2):498-513.e22. doi: 10.1016/j.cell.2019.09.011.

- Penna, A., Demuro, A., Yeromin, A.V., Zhang, S.L., Safrina, O., Parker, I., Cahalan, M.D. (2008). The CRAC channel consists of a tetramer formed by Stim-induced dimerization of Orai dimers. *Nature*. 456(7218):116-20. doi: 10.1038/nature07338.
- Picard, C., McCarl, C.A., Papolos, A., Khalil, S., Lüthy, K., Hivroz, C., LeDeist, F., Rieux-Laucat, F., Rechavi, G., Rao, A., Fischer, A., Feske, S. (2009). STIM1 mutation associated with a syndrome of immunodeficiency and autoimmunity. *N Engl J Med*. 360(19):1971-80. doi: 10.1056/NEJMoa0900082.
- Pozo-Guisado, E., Martin-Romero, F.J. (2013). The regulation of STIM1 by phosphorylation. *Commun Integr Biol*. 6(6):e26283. doi: 10.4161/cib.26283
- Poth, V., Knapp, M. L., & Niemeyer, B. A. (2020). STIM proteins at the intersection of signaling pathways. *Current Opinion in Physiology*, 17, 63–73. <https://doi.org/10.1016/j.cophys.2020.07.007>
- Prakriya, M., Feske, S., Gwack, Y., Srikanth, S., Rao, A., Hogan, P. G. (2006). Orai1 is an essential pore subunit of the CRAC channel. *Nature* 443 (7108), 230-3. doi: 10.1038/nature05122.
- Prakriya, M. (2013). Store-operated Orai channels: structure and function. *Curr Top Membr*. 71:1-32. doi: 10.1016/B978-0-12-407870-3.00001-9.
- Prakriya, M., & Lewis, R. S. (2015). Store-Operated Calcium Channels. *Physiological Reviews*, 95(4), 1383–1436. <https://doi.org/10.1152/physrev.00020.2014>
- Putney, J. W. (1986). A model for receptor-regulated calcium entry. *Cell Calcium*, 7(1), 1–12. [https://doi.org/10.1016/0143-4160\(86\)90026-6](https://doi.org/10.1016/0143-4160(86)90026-6)
- Pyott, S.J., Rosenmund, C. (2002). The effects of temperature on vesicular supply and release in autaptic cultures of rat and mouse hippocampal neurons. *J Physiol*. 539(Pt 2):523-35. doi: 10.1113/jphysiol.2001.013277.
- Ramesh, G., Jarzembowski, L., Schwarz, Y., Alansary, D., Bruns, D., Correspondence, B. A. N., Poth, V., Konrad, M., Knapp, M. L., Schwär, G., Lauer, A. A., Grimm, M. O. W., & Niemeyer, B. A. (2021). A short isoform of STIM1 confers frequency-dependent synaptic enhancement. *CellReports*, 34, 108844. <https://doi.org/10.1016/j.celrep.2021.108844>
- Ramos, B., Gaudillière, B., Bonni, A., Gill, G. (2007). Transcription factor Sp4 regulates dendritic patterning during cerebellar maturation. *Proc Natl Acad Sci U S A*. 104(23):9882-7. doi: 10.1073/pnas.0701946104.
- Rana, A., Yen, M., Sadaghiani, A. M., Malmersjö, S., Park, C. Y., Dolmetsch, R. E. (2015). Alternative splicing converts STIM2 from an activator to an inhibitor of store-operated calcium channels. *The Journal of Cell Biology* 209.5, 653-670.

- Rebecchi, M.J., Pentylala, S.N. (2000). Structure, function, and control of phosphoinositide-specific phospholipase C. *Physiol Rev.* 80(4):1291-335. doi: 10.1152/physrev.2000.80.4.1291.
- Rizzuto, R., Pinton, P., Carrington, W., Fay, F. S., Fogarty, K. E., Lifshitz, L. M. (1998). Close Contacts with the Endoplasmic Reticulum as Determinants of Mitochondrial Ca²⁺ Responses. *Science* 280.5370, 1763-1766. doi: 10.1126/science.280.5370.1763.
- Rizzuto, R., Pozzan, T. (2006). Microdomains of intracellular Ca²⁺: molecular determinants and functional consequences. *Physiol Rev.* 86(1):369-408. doi: 10.1152/physrev.00004.2005.
- Rizzuto, R., Marchi, S., Bonora, M., Aguiari, P., Bononi, A., De Stefani, D., Giorgi, C., Leo, S., Rimessi, A., Siviero, R., Zecchini, E., Pinton, P. (2009). Ca(2+) transfer from the ER to mitochondria: when, how and why. *Biochim Biophys Acta.* 1787(11):1342-51. doi: 10.1016/j.bbabi.2009.03.015.
- Roos, J., DiGregorio, P. J., Yeromin, A. V., Ohlsen, K., Lioudyno, M., Zhang, S. (2005). STIM1, an essential and conserved component of store-operated Ca²⁺ channel function. *The Journal of Cell Biology* 169 (3), 435-45. doi: 10.1083/jcb.200502019.
- Rosado, J. A., Diez, R., Smani, T., & Jardín, I. (2016). STIM and orai1 variants in store-operated calcium entry. *Frontiers in Pharmacology*, 6(JAN), 1–9. <https://doi.org/10.3389/fphar.2015.00325>
- Rothberg, B.S., Wang, Y., Gill, D.L. (2013). Orai channel pore properties and gating by STIM: implications from the Orai crystal structure. *Sci Signal.* 6(267):pe9. doi: 10.1126/scisignal.2003971.
- Rychkov GY. (2018). Measurement of the CRAC Channel Fast Ca²⁺-Dependent Inactivation (FCDI). *Methods Mol Biol.* 1843:167-173. doi: 10.1007/978-1-4939-8704-7_14.
- Ryu, C., Jang, D. C., Jung, D., Kim, Y. G., Shim, H. G., Ryu, H.H. (2017). STIM1 regulates somatic Ca²⁺ signals and intrinsic firing properties of cerebellar Purkinje neurons. *Journal of Neuroscience.* 37: 8876–8894. doi: 10.1523/JNEUROSCI.3973-16.2017.
- Sathyanesan, A., Gallo, V. (2019). Cerebellar contribution to locomotor behavior: A neurodevelopmental perspective. *Neurobiol Learn Mem.* 165:106861. doi: 10.1016/j.nlm.2018.04.016.
- Saić, S., Bulla, M., Nunes, P., Orci, L., Marchetti, A., Antigny, F., Bernheim, L., Cosson, P., Frieden, M., Demaurex, N. (2015). STIM1L traps and gates Orai1 channels without remodeling the cortical ER. *J Cell Sci.* 2015 Apr 15;128(8):1568-79. doi: 10.1242/jcs.164228.
- Saul, S., Gibhardt, C.S., Schmidt, B., Lis, A., Pasieka, B., Conrad, D., Jung, P., Gaupp, R., Wonnenberg, B., Diler, E., Stanisiz, H., Vogt, T., Schwarz, E.C., Bischoff, M., Herrmann,

- M., Tschernig, T., Kappl, R., Rieger, H., Niemeyer, B.A., Bogeski, I. (2016). A calcium-redox feedback loop controls human monocyte immune responses: The role of ORAI Ca²⁺ channels. *Sci Signal*. 9(418):ra26. doi: 10.1126/scisignal.aaf1639.
- Scharff, O., Foder, B., Skibsted, U. (1983). Hysteretic activation of the Ca²⁺ pump revealed by calcium transients in human red cells. *Biochim Biophys Acta*. 730(2):295-305. doi: 10.1016/0005-2736(83)90346-2.
- Secondo, A., Bagetta, G., Amantea, D. (2018). On the Role of Store-Operated Calcium Entry in Acute and Chronic Neurodegenerative Diseases. *Front Mol Neurosci*. 11:87. doi: 10.3389/fnmol.2018.00087
- Selvaraj, S., Sun, Y., Watt, J.A., Wang, S., Lei, S., Birnbaumer, L., Singh, B.B. (2012). Neurotoxin-induced ER stress in mouse dopaminergic neurons involves downregulation of TRPC1 and inhibition of AKT/mTOR signaling. *J Clin Invest*. 2012 Apr;122(4):1354-67. doi: 10.1172/JCI61332.
- Serwach, K., & Gruszczynska-Biegala, J. (2020). Target Molecules of STIM Proteins in the Central Nervous System. *Front Mol Neurosci*. 13:617422. doi: 10.3389/fnmol.2020.617422.
- Singh, B.B., Liu, X., Tang, J., Zhu, M.X., Ambudkar, I.S. (2002). Calmodulin regulates Ca(2+)-dependent feedback inhibition of store-operated Ca(2+) influx by interaction with a site in the C terminus of TrpC1. *Mol Cell*. 739-50. doi: 10.1016/s1097-2765(02)00506-3.
- Skibinska-Kijek, A., Wisniewska, M. B., Gruszczynska-Biegala, J., Methner, A., Kuznicki, J. (2009). Immunolocalization of STIM1 in the mouse brain. *Acta Neurobiol Exp*. 69(4):413-28
- Smith, J.S., Coronado, R., Meissner, G. (1986). Single-channel calcium and barium currents of large and small conductance from sarcoplasmic reticulum. *Biophys J*. 50(5):921-8. doi: 10.1016/S0006-3495(86)83533-0.
- Schwarz, Y., Oleinikov, K., Schindeldecker, B., Wyatt, A., Weißgerber, P., Flockerzi, V., Boehm, U., Freichel, M., and Bruns, D. (2019). TRPC channels regulate Ca²⁺-signaling and short-term plasticity of fast glutamatergic synapses. *PLoS Biol*. 2019 Sep 19;17(9):e3000445. doi: 10.1371/journal.pbio.3000445.
- Soboloff, J., Rothberg, B. S., Madesh, M., & Gill, D. L. (2012). STIM proteins: Dynamic calcium signal transducers. *Nat Rev Mol Cell Biol*. 13(9):549-65. doi: 10.1038/nrm3414.
- Spassova, M.A., Soboloff, J., He, L.P., Xu, W., Dziadek, M.A., Gill, D.L. (2006). STIM1 has a plasma membrane role in the activation of store-operated Ca(2+) channels. *Proc Natl Acad Sci U S A*. 103(11):4040-5. doi: 10.1073/pnas.0510050103.
- Srikanth, S., Woo, J.S., Wu, B., El-Sherbiny, Y.M., Leung, J., Chupradit, K., Rice, L., Seo, G.J., Calmettes, G., Ramakrishna, C., Cantin, E., An, D.S., Sun, R., Wu, T.T., Jung, J.U., Savic,

- S., Gwack, Y. (2019). The Ca²⁺ sensor STIM1 regulates the type I interferon response by retaining the signaling adaptor STING at the endoplasmic reticulum. *Nat Immunol.* 20(2):152-162. doi: 10.1038/s41590-018-0287-8.
- Stegner, D., Hofmann, S., Schuhmann, M.K., Kraft, P., Herrmann, A.M., Popp, S., Höhn, M., Popp, M., Klaus, V., Post, A. (2019). Loss of Orai2-Mediated Capacitative Ca²⁺ Entry Is Neuroprotective in Acute Ischemic Stroke. *Stroke* 50, 3238–3245. doi: 10.1161/STROKEAHA.119.025357.
- Steinbeck, J.A., Henke, N., Opatz, J., Gruszczynska-Biegala, J., Schneider, L., Theiss, S., Hamacher, N., Steinfarz, B., Golz, S., Brüstle, O., Kuznicki, J., Methner, A. (2011). Store-operated calcium entry modulates neuronal network activity in a model of chronic epilepsy. *Exp Neurol.* 2011 Dec;232(2):185-94. doi: 10.1016/j.expneurol.2011.08.022.
- Strübing, C., Krapivinsky, G., Krapivinsky, L., Clapham, D. E. (2001). TRPC1 and TRPC5 Form a Novel Cation Channel in Mammalian Brain. *Neuron* 29.3, 645-655. doi: 10.1016/s0896-6273(01)00240-9.
- Stathopoulos, P. B., Li, G.-Y., Plevin, M. J., Ames, J. B., Ikura, M. (2006). Stored Ca²⁺ Depletion-induced Oligomerization of Stromal Interaction Molecule 1 (STIM1) via the EF-SAM Region: An initiation mechanism for capacitative Ca²⁺ entry. *J Biol Chem.* 281.47, 35855-62. doi: 10.1074/jbc.M608247200.
- Stathopoulos, P. B., Schindl, R., Fahrner, M., Zheng, L., Gasmi-Seabrook, G. M., Muik, M. (2013). STIM1/Orai1 coiled-coil interplay in the regulation of store-operated calcium entry. *Nat Commun.* 4:2963. doi: 10.1038/ncomms3963.
- Stathopoulos, P. B., Zheng, L., Li, G.-Y., Plevin, M. J., Ikura, M. (2008). Structural and mechanistic insights into STIM1-mediated initiation of store-operated calcium entry. *Cell* 135 (1), 110-22. doi: 10.1016/j.cell.2008.08.006.
- Stathopoulos, P. B., & Ikura, M. (2013). Structural aspects of calcium-release activated calcium channel function. *Channels* 7.5, 344-353. doi: 10.4161/chan.26734.
- Streb, H., Irvine, R. F., Berridge, M. J., Schulz, I. (1983). Release of Ca²⁺ from a nonmitochondrial intracellular store in pancreatic acinar cells by inositol-1,4,5-trisphosphate. *Nature* 306 (5938), 67-9. doi: 10.1038/306067a0.
- Sun. J., Bronk, P., Liu, X., Han, W., Südhof, T.C. (2006). Synapsins regulate use-dependent synaptic plasticity in the calyx of Held by a Ca²⁺/calmodulin-dependent pathway. *Proc Natl Acad Sci U S A.* 103(8):2880-5. doi: 10.1073/pnas.0511300103.
- Sun, S., Zhang, H., Liu, J., Popugaeva, E., Xu, N.J., Feske, S. (2014). Reduced Synaptic STIM2 Expression and Impaired Store-Operated Calcium Entry Cause Destabilization of Mature Spines in Mutant Presenilin Mice. *Neuron* 82.1, 79-93. doi: 10.1016/j.neuron.2014.02.019.

- Sun, Y., Zhang, H., Selvaraj, S., Sukumaran, P., Lei, S., Birnbaumer, L., Singh, B.B. (2017). Inhibition of L-Type Ca^{2+} Channels by TRPC1-STIM1 Complex Is Essential for the Protection of Dopaminergic Neurons. *J Neurosci.* 37(12):3364-3377. doi: 10.1523/JNEUROSCI.3010-16.2017.
- Tagliatti, E., Bello, O.D., Mendonça, P.R.F., Kotzadimitriou, D., Nicholson, E., Coleman, J., Timofeeva, Y., Rothman, J.E., Krishnakumar, S.S., Volynski, K.E. (2020). Synaptotagmin 1 oligomers clamp and regulate different modes of neurotransmitter release. *Proc Natl Acad Sci U S A.* 117(7):3819-3827. doi: 10.1073/pnas.1920403117.
- The ENCODE Project Consortium, 2012
- Tarasova, E.O., Gaydukov, A.E., Balezina, O.P. (2018). Calcineurin and Its Role in Synaptic Transmission. *Biochemistry (Mosc.)* 2018 Jun;83(6):674-689. doi: 10.1134/S0006297918060056.
- Tedeschi, V., La Russa, D., Franco, C., Vinciguerra, A., Amantea, D., Secondo, A. (2021). Plasma Membrane and Organellar Targets of STIM1 for Intracellular Calcium Handling in Health and Neurodegenerative Diseases. *Cells.* 10, 2518. <https://doi.org/10.3390/cells10102518>
- Tiffner, A., Maltan, L., Weiß, S., Derler, I. (2021). The Orai Pore Opening Mechanism. *Int. J. Mol. Sci.* 22, 533. <https://doi.org/10.3390/ijms22020533>
- Toyoshima, C., Nakasako, M., Nomura, H., Ogawa, H. (2000). Crystal structure of the calcium pump of sarcoplasmic reticulum at 2.6 angstrom resolution. *Nature* 405.6787, 647-655.
- Thorn, P., Lawrie, A.M., Smith, P.M., Gallacher, D.V., Petersen, O.H. (1993). Local and global cytosolic Ca^{2+} oscillations in exocrine cells evoked by agonists and inositol trisphosphate. *Cell.* 74(4):661-8. doi: 10.1016/0092-8674(93)90513-p.
- Thastrup, O., Cullen, P. J., Drobak, B. K., Hanley, M. R., Dawson, A. P. (1990). Thapsigargin, a tumor promoter, discharges intracellular Ca^{2+} stores by specific inhibition of the endoplasmic reticulum Ca^{2+} -ATPase. *Proceedings of the National Academy of Sciences* 87.7, 2466-2470.
- Turecek, J., Jackman, S. & Regehr, W. (2017). Synaptotagmin 7 confers frequency invariance onto specialized depressing synapses. *Nature* 551, 503–506. <https://doi.org/10.1038/nature24474>
- Uhlén. M., Fagerberg, L., Hallström, B.M., Lindskog, C., Oksvold, P., Mardinoglu, A., Sivertsson, Å., Kampf, C., Sjöstedt, E., Asplund, A., Olsson, I., Edlund, K., Lundberg, E., Navani, S., Szigartyo, C.A., Odeberg, J., Djureinovic, D., Takanen, J.O., Hober, S., Alm, T., Edqvist, P.H., Berling, H., Tegel, H., Mulder, J., Rockberg, J., Nilsson, P., Schwenk, J.M., Hamsten, M., von Feilitzen, K., Forsberg, M., Persson, L., Johansson, F., Zwahlen, M., von Heijne, G., Nielsen, J., Pontén, F. (2015). Proteomics. Tissue-based

map of the human proteome. *Science*. 347(6220):1260419. doi: 10.1126/science.1260419.

- Venkatachalam, K., Zheng, F., Gill, D.L. (2003). Regulation of canonical transient receptor potential (TRPC) channel function by diacylglycerol and protein kinase C. *J Biol Chem*. 278(31):29031-40. doi: 10.1074/jbc.M302751200.
- Varga-Szabo, D., Pleines, I., Nieswandt, B. (2008). Cell adhesion mechanisms in platelets. *Arterioscler Thromb Vasc Biol*. 28(3):403-12. doi: 10.1161/ATVBAHA.107.150474.
- Verstegen, A.M., Tagliatti, E., Lignani, G., Marte, A., Stoloro, T., Atias, M., Corradi, A., Valtorta, F., Gitler, D., Onofri, F., Fassio, A., Benfenati, F. (2014). Phosphorylation of synapsin I by cyclin-dependent kinase-5 sets the ratio between the resting and recycling pools of synaptic vesicles at hippocampal synapses. *J Neurosci*. 34(21):7266-80. doi: 10.1523/JNEUROSCI.3973-13.2014.
- Vig, M., Beck, A., Billingsley, J. M., Lis, A., Parvez, S., Peinelt, C. (2006). CRACM1 Multimers Form the Ion-Selective Pore of the CRAC Channel. *Curr Biol*. 2006 Oct 24;16(20):2073-9. doi: 10.1016/j.cub.2006.08.085.
- Vinueza Veloz, M.F., Zhou, K., Bosman, L.W., Potters, J.W., Negrello, M., Seepers, R.M., Strydis, C., Koekkoek, S.K., De Zeeuw, C.I. (2015). Cerebellar control of gait and interlimb coordination. *Brain Struct Funct*. 220(6):3513-36. doi: 10.1007/s00429-014-0870-1.
- Wang, Y., Deng, X., Mancarella, S., Hendron, E., Eguchi, S., Soboloff, J. (2010). The Calcium Store Sensor, STIM1, Reciprocally Controls Orai and Ca(V)1.2 Channels. *Science* 330.6000, 105-109. doi: 10.1126/science.1191086.
- Wang, X., Wang, Y., Zhou, Y., Hendron, E., Mancarella, S., Andrade, M.D., Rothberg, B.S., Soboloff, J., Gill, D.L. (2014). Distinct Orai-coupling domains in STIM1 and STIM2 define the Orai-activating site. *Nat Commun*. 5:3183. doi: 10.1038/ncomms4183.
- Wang, Q.C., Wang, X., Tang, T.S. (2018). EB1 traps STIM1 and regulates local store-operated Ca²⁺ entry. *J Cell Biol*. 217(6):1899-1900. doi: 10.1083/jcb.201805037.
- Watanabe, S., Rost, B.R., Camacho-Pérez, M., Davis, M.W., Söhl-Kielczynski, B., Rosenmund, C., Jorgensen, E.M. (2013). Ultrafast endocytosis at mouse hippocampal synapses. *Nature*. 504(7479):242-247. doi: 10.1038/nature12809.
- White, C. (2017). The Regulation of Tumor Cell Invasion and Metastasis by Endoplasmic Reticulum-to-Mitochondrial Ca²⁺ Transfer. *Front Oncol*. 7:171. doi: 10.3389/fonc.2017.00171.
- Williams, R. T., Senior, P. V., Van Stekelenburg, L., Layton, J. E., Smith, P. J., Dziadek, M. A. (2002). Stromal interaction molecule 1 (STIM1), a transmembrane protein with growth suppressor activity, contains an extracellular SAM domain modified by N-linked

- glycosylation. *Biochim Biophys Acta*. 1596(1):131-7. doi: 10.1016/s0167-4838(02)00211-x.
- Wu, M. M., Buchanan, J., Luik, R. M., Lewis, R. S. (2006). Ca^{2+} store depletion causes STIM1 to accumulate in ER regions closely associated with the plasma membrane. *J Cell Biol*. 174(6):803-13. doi: 10.1083/jcb.200604014.
- Wu, J., Shih, H.P., Vigont, V., Hrdlicka, L., Diggins, L., Singh, C., Mahoney, M., Chesworth, R., Shapiro, G., Zimina, O., Chen, X., Wu, Q., Glushankova, L., Ahlijanian, M., Koenig, G., Mozhayeva, G.N., Kaznacheyeva, E., Bezprozvanny, I. (2011). Neuronal store-operated calcium entry pathway as a novel therapeutic target for Huntington's disease treatment. *Chem Biol*. 18(6):777-93. doi: 10.1016/j.chembiol.2011.04.012.
- Wu, J., Ryskamp, D.A., Liang, X., Egorova, P., Zakharova, O., Hung, G., Bezprozvanny, I. (2016). Enhanced Store-Operated Calcium Entry Leads to Striatal Synaptic Loss in a Huntington's Disease Mouse Model. *J Neurosci*. 36(1):125-41. doi: 10.1523/JNEUROSCI.1038-15.2016.
- Wu, M. M., Covington, E. D., Lewis, R. S. (2014). Single-molecule analysis of diffusion and trapping of STIM1 and Orai1 at endoplasmic reticulum-plasma membrane junctions. *Molecular biology of the cell* 25 (22), 3672-85.
- Wu, Y., Whiteus, C., Xu, C.S., Hayworth, K.J., Weinberg, R.J., Hess, H.F., De Camilli, P. (2017). Contacts between the endoplasmic reticulum and other membranes in neurons. *Proc Natl Acad Sci U S A*. 114(24):E4859-E4867. doi: 10.1073/pnas.1701078114.
- Xiao, B., Coste, B., Mathur, J., Patapoutian, A. (2011). Temperature-dependent STIM1 activation induces Ca^{2+} influx and modulates gene expression. *Nat Chem Biol*. 7(6):351-8. doi: 10.1038/nchembio.558.
- Xu, J., Pang, Z.P., Shin, O.H., Südhof, T.C. (2009). Synaptotagmin-1 functions as a Ca^{2+} sensor for spontaneous release. *Nat Neurosci*. 12(6):759-66. doi: 10.1038/nn.2320.
- Yang, S., Zhang, J. J., Huang, X.-Y. (2009). Orai1 and STIM1 Are Critical for Breast Tumor Cell Migration and Metastasis. *Cancer Cell* 15.2, 124-34. doi: 10.1016/j.ccr.2008.12.019
- Yang, X., Jin, H., Cai, X., Li, S., Shen, Y. (2012). Structural and mechanistic insights into the activation of Stromal interaction molecule 1 (STIM1). *Proc Natl Acad Sci U S A*. 109(15):5657-62. doi: 10.1073/pnas.1118947109.
- Yap, K. A. F., Shetty, M. S., Garcia-Alvarez, G., Lu, B., Alagappan, D., Oh-Hora, M. (2017). STIM2 regulates AMPA receptor trafficking and plasticity at hippocampal synapses. *Neurobiology of Learning and Memory*, 138, 54–61. doi:10.1016/J.NLM.2016.08.007
- Yen, M., Lewis, R.S. (2018). Physiological CRAC channel activation and pore properties require STIM1 binding to all six Orai1 subunits. *J Gen Physiol*. 150(10):1373-1385. doi: 10.1085/jgp.201711985.

- Yuan, J. P., Zeng, W., Dorwart, M. R., Choi, Y., Paul, F., & Muallem, S. (2009). SOAR and the polybasic STIM1 domains gate and regulate the Orai channels. *Nat Cell Biol.* 11(3), 337–343. doi:10.1038/ncb1842.SOAR
- Yeung, P.S., Yamashita, M., Prakriya, M. (2020). Molecular basis of allosteric Orai1 channel activation by STIM1. *J Physiol.* 598(9):1707-1723. doi: 10.1113/JP276550.
- Zbidi, H., Jardin, I., Woodard, G.E., Lopez, J.J., Berna-Erro, A., Salido, G.M., Rosado, J.A. (2011). STIM1 and STIM2 are located in the acidic Ca²⁺ stores and associates with Orai1 upon depletion of the acidic stores in human platelets. *J Biol Chem.* 286(14):12257-70. doi: 10.1074/jbc.M110.190694.
- Zhang, H., Sun, S., Wu, L., Pchitskaya, E., Zakharova, O., Fon Tacer, K., Bezprozvanny, I. (2016). Store-Operated Calcium Channel Complex in Postsynaptic Spines: A New Therapeutic Target for Alzheimer's Disease Treatment. *J Neurosci.* 36(47):11837-11850. doi: 10.1523/JNEUROSCI.1188-16.2016.
- Zhang, H., Wu, L., Pchitskaya, E., Zakharova, O., Saito, T., Saido, T., Bezprozvanny, I. (2015). Neuronal Store-Operated Calcium Entry and Mushroom Spine Loss in Amyloid Precursor Protein Knock-In Mouse Model of Alzheimer's Disease. *J Neurosci.* 35(39):13275-86. doi: 10.1523/JNEUROSCI.1034-15.2015.
- Zhang, S.L., Yu, Y., Roos, J., Kozak, J.A., Deerinck, T.J., Ellisman, M.H., Stauderman, K.A., Cahalan, M.D. (2005). STIM1 is a Ca²⁺ sensor that activates CRAC channels and migrates from the Ca²⁺ store to the plasma membrane. *Nature.* 437(7060):902-5. doi: 10.1038/nature04147.
- Zhang, S. L., Yeromin, A. V, Zhang, X. H.-F., Yu, Y., Safrina, O., Penna, A., et al. (2006). Genome-wide RNAi screen of Ca(2+) influx identifies genes that regulate Ca(2+) release-activated Ca(2+) channel activity. *Proc Natl Acad Sci U S A.* 103(24), 9357–9362. doi:10.1073/pnas.0603161103
- Zeng, W., Yuan, J.P., Kim, M.S., Choi, Y.J., Huang, G.N., Worley, P.F., Muallem, S. (2008). STIM1 gates TRPC channels, but not Orai1, by electrostatic interaction. *Mol Cell.* 32(3):439-48. doi: 10.1016/j.molcel.2008.09.020.
- Zheng, L., Stathopoulos, P. B., Li, G.-Y., Ikura, M. (2008). Biophysical characterization of the EF-hand and SAM domain-containing Ca²⁺ sensory region of STIM1 and STIM2. *Biochem Biophys Res Commun.* 2008 Apr 25;369(1):240-6. doi: 10.1016/j.bbrc.2007.12.129.
- Zheng, L., Stathopoulos, P. B., Schindl, R., Li, G.-Y., Romanin, C., Ikura, M. (2011). Autoinhibitory role of the EF-SAM domain of STIM proteins in store-operated calcium entry. *Proc Natl Acad Sci U S A.* 2011 Jan 25;108(4):1337-42. doi: 10.1073/pnas.1015125108.

- Zheng, S., Zhou, L., Ma, G., Zhang, T., Liu, J., Li, J., Nguyen, N.T., Zhang, X., Li, W., Nwokonko, R., Zhou, Y., Zhao, F., Liu, J., Huang, Y., Gill, D.L., Wang, Y. (2018). Calcium store refilling and STIM activation in STIM- and Orai-deficient cell lines. *Pflugers Arch.* 470(10):1555-1567. doi: 10.1007/s00424-018-2165-5.
- Zhou, X., Qyang, Y., Kelsoe, J.R., Masliah, E., Geyer, M.A. (2007). Impaired postnatal development of hippocampal dentate gyrus in Sp4 null mutant mice. *Genes Brain Behav.* 6(3):269-76. doi: 10.1111/j.1601-183X.2006.00256.x.
- Zhou, Y., Meraner, P., Kwon, H.T., Machnes, D., Oh-hora, M., Zimmer, J., Huang, Y., Stura, A., Rao, A., Hogan, P.G. (2010). STIM1 gates the store-operated calcium channel ORAI1 in vitro. *Nat Struct Mol Biol.* 17(1):112-6. doi: 10.1038/nsmb.1724.
- Zhou, Y., Srinivasan, P., Razavi, S., Seymour, S., Meraner, P., Gudlur, A. (2013). Initial activation of STIM1, the regulator of store-operated calcium entry. *Nat Struct Mol Biol* 20.8, 973-981. doi: 10.1038/nsmb.2625.
- Zhou, Y., Cai, X., Loktionova, N. A., Wang, X., Nwokonko, R. M., Wang, X., et al. (2016). The STIM1-binding site nexus remotely controls Orai1 channel gating. *Nat Commun.* 7, 13725. doi:10.1038/ncomms13725
- Zweifach, A. & Lewis, R. S. (1993). Mitogen-regulated Ca^{2+} current of T lymphocytes is activated by depletion of intracellular Ca^{2+} stores. *Proc Natl Acad Sci USA.* 1993 Jul 1;90(13):6295-9. doi: 10.1073/pnas.90.13.6295.
- Zweifach, A., & Lewis, R.S. (1995a). Rapid inactivation of depletion-activated calcium current (I_{CRAC}) due to local calcium feedback. *J Gen Physiol.* 105(2):209-26. doi: 10.1085/jgp.105.2.209.
- Zweifach, A., & Lewis, R.S. (1995b). Slow calcium-dependent inactivation of depletion-activated calcium current. Store-dependent and -independent mechanisms. *J Biol Chem.* 270(24):14445-51. doi: 10.1074/jbc.270.24.14445.

Publications & Conferences

Publications

Ramesh, G., Jarzembowski, L., Schwarz, Y., Alansary, D., Bruns, D., Correspondence, B. A. N., Poth, V., Konrad, M., Knapp, M. L., Schwär, G., Lauer, A. A., Grimm, M. O. W., & Niemeyer, B. A. (2021). A short isoform of STIM1 confers frequency-dependent synaptic enhancement. *CellReports*, 34, 108844. <https://doi.org/10.1016/j.celrep.2021.108844>

Conferences & Presentations

Girish Ramesh, Barbara A. Niemeyer. Store Operated Calcium entry (SOCE): Identification of new key players. **SFB 1027 Summer retreat, 2017**, Tagungshotel Hohenwart Forum, Pforzheim, Germany.

Girish Ramesh, Lukas Jarzembowski, Maik Konrad, Dalia Alansary, Alina Gilson, Annette Lis, Barbara A. Niemeyer. Store Operated Calcium entry (SOCE): Identification of new key players. **Cell Physics 2017**, Universität des Saarlandes, Saarbrücken, Germany.

Girish Ramesh, Lukas Jarzembowski, Yvonne Schwarz, Maik Konrad, Vanessa Poth, Dalia Alansary, Dieter Bruns, Barbara A. Niemeyer. Alternative splicing of STIM1 creates a differential SOCE regulator. **FASEB Science research conference on Calcium and cell function, 2018**, Tahoe, California, USA.

Girish Ramesh, Lukas Jarzembowski, Yvonne Schwarz, Maik Konrad, Vanessa Poth, Dalia Alansary, Dieter Bruns, Barbara A. Niemeyer. A neuron-specific alternative STIM1 splice variant differentially influences SOCE and synaptic plasticity. **Cell Physics 2019**, Universität des Saarlandes, Saarbrücken, Germany.

Abbreviations

AMPA	α -amino-3-hydroxy-5-methyl-4-isoxazolepropionic acid
AMPA	AMPA Receptor
APP	Amyloid Precursor Protein
ATP	Adenosine Tri Phosphate
BAPTA	1,2-bis(o-aminophenoxy)ethane-N,N,N',N'-tetraacetic acid
CCE	Capacitative Ca ²⁺ Entry
CC	Coiled coil region
CPA	cyclopiazonic acid
CAD	Channel activation domain
Ca ²⁺	Calcium
CaM	Calmodulin
CaMKI	Ca ²⁺ /calmodulin-dependent kinase I
CaMKII	Ca ²⁺ /calmodulin-dependent kinase II
CRAC	Ca ²⁺ release activated Ca ²⁺
Cdk5	Cyclic dependent kinase 5
DAG	diacyl glycerol
DNA	Deoxyribonucleic acid
dNTP	Deoxynucleoside triphosphate
EB	End binding protien
EGTA	ethylene glycol-bis (β -aminoethyl ether)-N,N,N',N'-tetraacetic acid
ER	Endoplasmic Reticulum
EPSC	Excitatory Post Synaptic Current
FCDI	Fast Ca ²⁺ dependent inactivation
FCS	Fetal Calf Serum
GC	Granular cells
GPCR	G Protein-Coupled Receptor
GoF	Gain of function
GFP	Green Fluorescent Protein
GluA1	Glutamate receptor A1
HFS	High Frequency Stimulation
IP ³	1,4,5-inositol triphosphate
IP ³ R	IP3 Receptor
ID	Inactivation domain
Ifn	Interferon
IPSC	inhibitory postsynaptic currents
K ⁺	Potassium
LFS	Low Frequency Stimulation
LoF	Loss of function
LTP	Long term Potentiation
LTD	Long term depression
Mn ²⁺	Manganese
mGluR	metabotropic glutamate receptor
Mg ²⁺	Magnesium
MCU	Mitochondrial Ca ²⁺ Uniporter

MS	Mass Spectrometry
NMDA	N methyl-D-Aspartate
NMDAR	NMDA Receptor
Na ⁺	Sodium
nM	Nanomolar
NCLX	Na ⁺ -Ca ²⁺ /Li ⁺ exchangers
NCX	Na ⁺ /Ca ²⁺ exchanger
NCKX	Na ⁺ -Ca ²⁺ /K ⁺ exchangers
NFAT	nuclear factor of activated T cells
PAGE	Polyacryl amide gel electrophoresis
PBS	Phosphate buffered Saline
PDE	Phospho Diesterase
PBD	Polybasic domain
PMCA	Plasma Membrane Ca ²⁺ ATPase
PM	Plasma Membrane
PIP2	phosphatidylinositol 4,5 bisphosphate
PKA	Protein Kinase A
PKC	Protein Kinase C
PLC	Phospholipase C
PN	Purkinje Neuron
qRT-PCR	quantitative real -time PCR
RyR	Ryanodine Receptor
RNA	Ribonucleic Acid
RRP	Readily Releasable Pool
SERCA	Sarco/Endoplasmic Reticulum Ca ²⁺ ATPase
SR	Sarcoplasmic Reticulum
SPCA	Secretory Pathway Ca ²⁺ - ATPases
SOCE	Store Operated Ca ²⁺ Entry
SCID	severe combined immune deficiency
SAM	sterile alpha motif
SOAP	Stim1-Orai1 Association pocket
SOAR	STIM1 ORAI activating region
SCDI	Slow Ca ²⁺ dependent inactivation
STE	Short term enhancement
Syt	Synaptotagmin
SDS	Sodium dodecyl sulphate
TBP	TATA box binding protein
Tg	Thapsigargin
TM	Transmembrane
TRPC	transient receptor potential cation channels
TIRFM	Total Internal Reflection Microscopy
VGCC	Voltage-Gated- Calcium Channels
YFP	Yellow Fluorescent Protein

Appendix

List of Tables

Table 1 List of Chemical reagents used in this study	25
Table 2 List of commercial kits used in this study	26
Table 3 List of Primary antibodies	27
Table 4 List of Secondary antibodies	27
Table 5 List of Bacterial competent cells used in this study	28
Table 6 List of Protein markers / Standards	28
Table 7 List of modified enzymes used in this study	32
Table 8 List of restriction enzymes used in this study	32
Table 9 List of Primers used for this study	33
Table 10 List of plasmid constructs used in this study	34
Table 11 List of media used for cell culture	35
Table 12 List of different cell lines & primary cells used in this study	35
Table 13 List of Transfection kits used in this study	36
Table 14 Animal model used in this study	36
Table 15 List of different software tools used for data analysis	36
Table 16 Pipetting Scheme for PCR reaction	37
Table 17 Reaction program of PCR amplification	37
Table 18 Pipetting scheme for analytical PCR	38
Table 19 Reaction program for analytical PCR	38
Table 20 Pipetting scheme for PCR with Phusion DNA polymerase	39
Table 21 PCR reaction program with DpnI reaction	39
Table 22 Pipetting scheme for cloning reaction	40
Table 23 Pipetting scheme for dephosphorylation reaction	40
Table 24 Pipetting scheme for ligation reaction	41
Table 25 Pipetting scheme for colony PCR reaction	43
Table 26 PCR reaction program for colony PCR	43
Table 27 Pipetting scheme for sequencing	43
Table 28 Composition of stacking & separating gel for western blot	47
Table 29 Potential protein interaction hits from Mass Spectrometry	103

List of Figures

Figure 1 Intracellular Ca ²⁺ Homeostasis	7
Figure 2 Store-Operated Ca ²⁺ Entry (SOCE) activation process	10
Figure 3 Schematic representation of the exon and domain structure of the STIM1 and its splice variants	16
Figure 4 Cerebellar motor learning behavioral analysis using Erasmus Ladder.....	52
Figure 5 Expression of the alternative Stim1 exon 13B splice variant	56
Figure 6 Colocalization analysis of Stim1B.....	60
Figure 7 Overexpression of hSTIM1B attenuated hORAI2 and hORAI3 CRAC but not hORAI1 in HEK WT.....	61
Figure 8 Overexpression of hSTIM1B did not alter the hORAI1 and hORAI2 CRAC in HEKS1/2 DKO	63
Figure 9 Overexpression of mSTIM1B differentially regulates mORAI1,2, & 3 channels at 20mM BAPTA in HEKS1/2 DKO.....	65
Figure 10 Overexpression of hSTIM1B/mStim1B reduced SCDI phenotype in HEK S1/2 DKO under 2mM EGTA conditions.....	67
Figure 11 Analysis of Fast Ca ²⁺ -dependent inactivation (FCDI).....	68
Figure 12 SARAF overexpression with STIM1B did not alter STIM1B phenotype in HEKO1 in the presence of EGTA.....	70
Figure 13 Mutation of STIM1B's inactivation domain (7A mutant) did not alter the CDI phenotype under EGTA conditions.....	72
Figure 14 Screening of cloned constructs by Western blotting.....	73
Figure 15 The absence of the C-terminal domain still retained Stim1 phenotype	75
Figure 16 The insertion of Domain B in Stim1 mimics Stim1B phenotype	77
Figure 17 Deletion of additional 26 translated residues due to domain B still retained the Stim1B phenotype	78
Figure 18 A Specific motif in domain B (KANR) determines the Stim1B phenotype	80
Figure 19 Mutation of Stim1B's CAD Domain abolishes Orail mediated I _{CRAC}	81
Figure 20 Stim1B promotes strong short-term enhancement (STE) of synaptic signaling.....	83
Figure 21 Stim1B is localized to presynaptic terminals	88
Figure 22 Screening and validation of splice-deficient mice.....	89

Figure 23 Analysis of expression levels of Synapsin in wild-type (Wt) and splice-deficient mice (10A)	90
Figure 24 Erasmus ladder outcome: Analysis of locomotive behavior patterns of various step types in male splice-deficient mice	92
Figure 25 Erasmus ladder outcome: Analysis of locomotive behavior patterns of various step types in female splice-deficient mice	94
Figure 26 Erasmus ladder outcome: Analysis of locomotor performance in male splice-deficient mice	96
Figure 27 Erasmus ladder outcome: Analysis of locomotor performance in female splice-deficient mice	97
Figure 28 Erasmus ladder outcome: Adaptive cerebellar learning deficits in splice-deficient mice....	99
Figure 29 Elevated plus maze outcomes: Assessment of anxiety and impulse behavior in splice-deficient mice.	100
Figure 30 Open field maze outcomes: Assessment of anxiety and impulse behavior in splice-deficient mice	101
Figure 31 Investigation of Interacting partners of Stim1B	105

Acknowledgments

I would first like to express my deepest and highest gratitude to my supervisor Prof. Dr. Barbara. A. Niemeyer, for giving me the opportunity to initiate my Doctoral thesis under her guidance. Without her encouragement and motivation, I would have not been able to successfully complete my thesis. I will always be grateful to her for being such a great advisor, mentor, and most importantly a wonderful person.

I would like to extend my thanks to Dr. Dalia Alansary, and Dr. Maik Konrad, for their support and guidance during new experiments, particularly at the beginning of my Ph.D.

I would like to thank Dr. Yvonne Schwarz for her support in performing neuronal experiments.

I sincerely thank Dr. Wenhui Huang for his support during behavioral experiments and I would like to thank Christopher for his extended support in the Erasmus ladder experiment.

I sincerely thank our collaborators Prof. Dr. Dieter Burns, Prof. Frank Kirchoff, and Prof. Dr. Frank Schmitz and all his group members for helping me with experiments at their laboratory during the course of my Ph.D.

I also thank Prof. Markus Hoth and their group members for giving constant inputs during the seminars and in general discussions.

I would like to thank all SFB1027 members for the great scientific discussions during the scientific meetings.

I thank all my friends and lab members for their excellent company including Lukas, Mona, Maryam, and Maylin for their extended support in the lab and for being such good friends who made my stay in Germany more comfortable. I extend my thanks to Kathrin, Gertrud, Carmen, Andrea, Cora, and Sandra for their excellent technical support throughout the work.

I sincerely thank my first supervisor Dr. Saravana Babu in India for giving me an opportunity in his lab that started my scientific career.

Finally and most importantly, I would like to thank my family, my beloved wife Akshaya Sankaran for her lovely support and motivation throughout my journey and gave her fullest support to finish my Ph.D.

Curriculum Vitae

Aus datenschutzrechtlichen Gründen wird der Lebenslauf in der elektronischen Fassung der Dissertation nicht veröffentlicht